Multifunctional self-stratified polyurethane-polyurea nanosystems for smart drug delivery

Pau Rocas Alonso

Programa de Doctorat de Nanociències

Multifunctional Self-stratified Polyurethane-polyurea Nanosystems for Smart Drug Delivery

Pau Rocas Alonso

Barcelona, Desembre 2015

Dirigida i Revisada per:

Prof. Fernando Albericio Palomera

Universitat de Barcelona

A la meva família i amics,
és un plaer créixer amb vosaltres.

La diferència entre l'alegria i la felicitat és que l'alegria és un líquid i la felicitat, un sòlid.

J. D. Salinger, *Nou contes*

Index

Annexes

Annex 1. Reactive species:

1. Building blocks:

Isocyanates		
IPDI: Isophorone diisocyanate	5-isocyanato-1-(isocyanatomethyl)-1,3,3-trimethylcyclohexane	
B3100: Bayhydur 3100 (Polyether modified hexamethylene diisocyanate isocyanurate trimer)	2,5,8,11,14,17-hexaoxanonadecan-19-yl (6-(3,5-bis(6-isocyanatohexyl)-2,4,6-trioxo-1,3,5-triazinan-1-yl)hexyl)carbamate	

Polyamines		
LAP 100D:	N-dodecyl-1,3-propylenediamine	
TAP 100D:	N-octadecyl-1,3-propylenediamine	
Priamine 1074	9-nonyl-10-octylnonadecane-1,19-diamine	
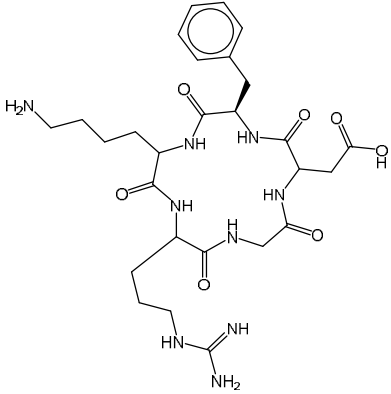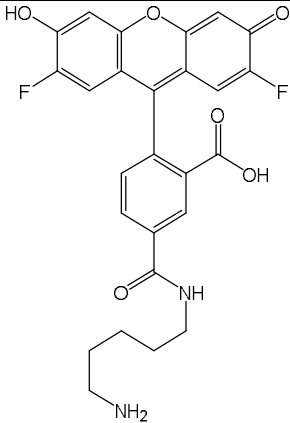
Polyols		
YMER™ N120: Linear polyethylene glycol monomethyl ether	2-ethyl-2-(2,5,8,11,14,17,20,23,26,29, 32,35,38,41,44,47,50,53,56-nonadecaoxaheptapentacontyl)propane-1,3-diol	
DEDS:	2-Hydroxyethyl disulfide	
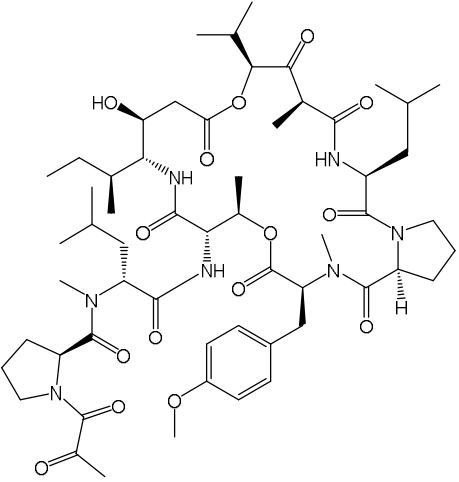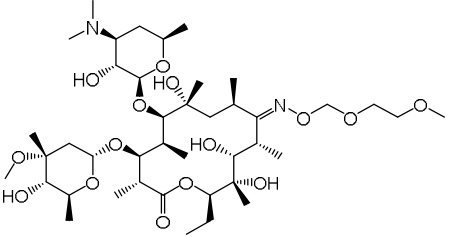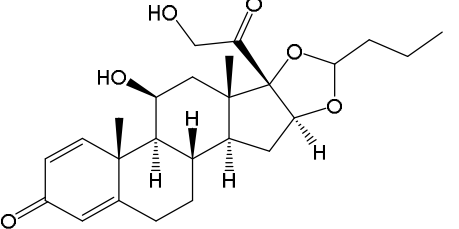
2. Crosslinkers

DETA:	Diethylenetriamine	
EDA:	Ethylenediamine	
Lys:	L- Lysine	
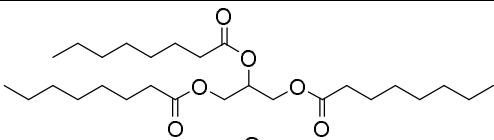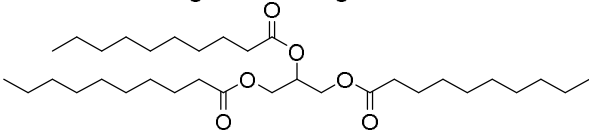
3. Conjugated molecules
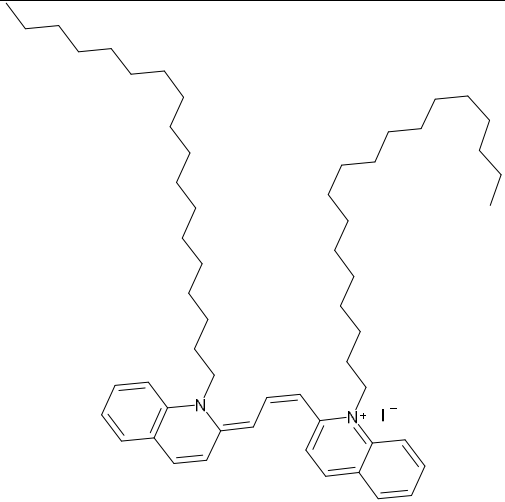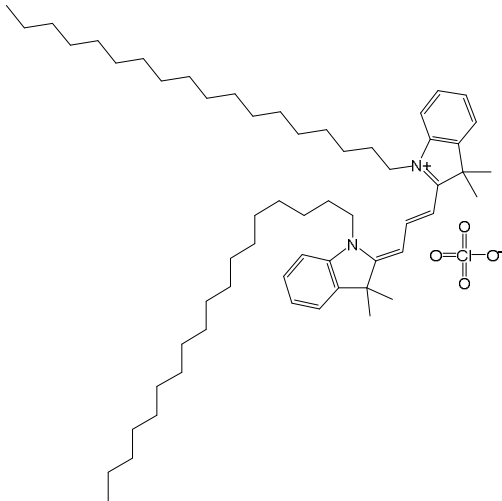
RGD peptide		
cRGDfK:	2-((5R)-8-(4-aminobutyl)-5-benzyl-11-(3-guanidinopropyl)-3,6,9,12,15-pentaoxo-1,4,7,10,13-pentaazacyclopentadecan-2-yl)acetic acid	
Fluorophore		
Oregon Green® 488 cadaverine	5-((5-aminopentyl)carbamoyl)-2-(2,7-difluoro-6-hydroxy-3-oxo-3H-xanthen-9-yl)benzoic acid	

Annex 2. Encapsulated molecules:

Drugs		
PLI: Plitidepsin	(S)-N-((R)-1-(((3S,6R,7S,10R,11S,15S,17S,20S,25aS)-10-((S)-sec-butyl)-11-hydroxy-20-isobutyl-15-isopropyl-3-(4-methoxybenzyl)-2,6,17-trimethyl-1,4,8,13,16,18,21-heptaoxodocosahydro-1H-pyrrolo[2,1-f][1,15,4,7,10,20]dioxatetraazacyclotricosin-7-yl)amino)-4-methyl-1-oxopentan-2-yl)-N-methyl-1-(2-oxopropanoyl)pyrrolidine-2-carboxamide	
RX: Roxithromycin	(3R,4S,5S,6R,7R,9R,11S,12R,13S,14R)-6-{[(2S,3R,4S,6R)-4-(Dimethylamino)-3-hydroxy-6-methyloxan-2-yl]oxy}-14-ethyl-7,12,13-trihydroxy-4-{[(2R,4R,5S,6S)-5-hydroxy-4-methoxy-4,6-dimethyloxan-2-yl]oxy}-3,5,7,9,11,13-hexamethyl-10-(2,4,7-trioxa-1-azaoctan-1-ylidene)-1-oxacyclotetradecan-2-one	
BDS: Budesonide	(11beta,16alpha)-16,17-(Butylidenebis(oxy))-11,21-dihydroxypregna-1,4-diene-3,20-dione	

Oil		
Crodamol GTCC/ Capric caprylic triglyceride	propane-1,2,3-triyl trioctanoate, propane-1,2,3-triyl tris(decanoate) (1:1)	

Fluorophores		
DiR	1-octadecyl-2-((1E,3Z)-3-(1-octadecylquinolin-2(1H)-ylidene)prop-1-enyl)quinolinium iodide	
DiI	(2Z)-2-[(E)-3-(3,3-dimethyl-1-octadecylindol-1-ium-2-yl)prop-2-enylidene]-3,3-dimethyl-1-octadecylindole perchlorate	

| DiO | 3-octadecyl-2-((1E,3E)-3-(3-octadecylbenzo[d]oxazol-2(3H)-ylidene)prop-1-en-1-yl)benzo[d]oxazol-3-ium perchlorate | |
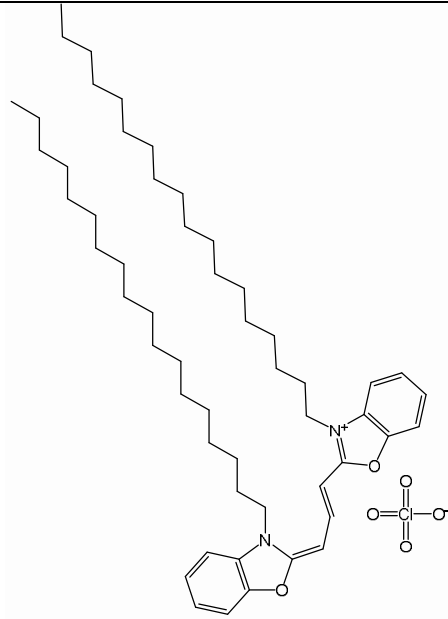
Annex 3. Abbreviations

AFM	Atomic Force Microscopy
Amphil	Amphiphilic prepolymer
APTES	(3-Aminopropyl)triethoxysilane
CTP	Cell Targeting Peptide
DDS	Drug Delivery System
DLS	Dynamic Light Scattering
DSC	Differential Scanning Calorimetry
EPR	Enhanced Permeation Retention
FRET	Förster Resonance Energy Transfer
FT-IR	Fourier Transform Infrared Spectroscopy
GSH	Glutathione
HLB	Hydrophilic-Lipophilic Balance
HPLC	High-Performance Liquid Chromatography
Hyfob	Hydrophobic Prepolymer
IR	Infrared Spectroscopy
NMR	Nuclear Magnetic Resonance
o/w	Oil-in-Water emulsion
PAA	Poly(acrylic acid)
PAAm	Polyacrylamide
PAS	Proline-Alanine-Serine Polypeptide
PCL	Polycaprolactone
PDEAEMA	Poly(2-diethylaminoethyl methacrylate)
PDMAEMA	Poly(2-dimethylaminoethyl methacrylate)
PEG	Poly(ethylene glycol)
PEO	Poly(ethylene oxide)
PHEMA	Poly(2-hydroxyethyl methacrylate)
PGA	Poly(γ-glutamic acid)
PLA	Poly(lactic acid)
PLGA	Poly(lactide-co-glycolide)
PMA	Poly(methyl acrylate)
PMAA	Poly(methacrylic acid)
PU	Polyurethane
PUUa	Polyurethane-polyurea polymer
PVA	Poly(vinyl alcohol)
QDs	Quantum Dots

RES	Reticuloendothelial System
RGD	L-arginine-Glycine-L-aspartic acid sequence containing peptide
SDS	Sodium Dodecyl Sulfate
SEM	Scanning Electron Microscopy
TEM	Transmission Electron Microscopy
TGA	Thermogravimetric Analysis
Zpot	Zeta Potential

Annex 4. List of Publications

Publication I. P. Rocas Alonso, J. Rocas Sorolla, Method for producing a microencapsulate and corresponding reactive amphiphilic compound, microencapsulate and composition, WO2014114838A3, 2014.

Publication II. P. Rocas, Y. Fernández, S. Schwartz, I. Abasolo, J. Rocas, F. Albericio, Multifunctionalized polyurethane–polyurea nanoparticles: hydrophobically driven self-stratification at the o/w interface modulates encapsulation stability, J. Mater. Chem. B. 3, 2015, 7604–7613. doi:10.1039/C5TB90134K.

Publication III. P. Rocas, Y. Fernández, S. Schwartz Jr., P. Calvo, P. Avilés, M. J. Guillén, J. Rocas, F. Albericio, I. Abasolo. Improved Pharmacokinetic Profile of Lipophilic Anti-Cancer Drugs Using αvβ3-targeted Polyurethane-Polyurea Nanoparticles, In preparation.

Publication IV. P. Rocas, M. Hoyos-Nogués, J. Rocas, J.M. Manero, J. Gil, F. Albericio, C. Mas-Moruno, Installing Multifunctionality on Titanium with RGD-Decorated Polyurethane-Polyurea Roxithromycin Loaded Nanoparticles: Toward New Osseointegrative Therapies., Adv. Healthc. Mater. 4, 2015, 1956–60. doi:10.1002/adhm.201500245.

Publication V. G. Flórez-grau, P. Rocas, R. Cabezón, C. España, J. Panés, J. Rocas, F. Albericio, D. Benítez-Ribas, Nanoencapsulation of Budesonide in Self-Stratified Polyurethane-Polyurea Nanoparticles Induces Powerful Human Tolerogenic Dendritic Cells, Submitted.

Annexes

Thesis Outline

Thesis outline

This thesis is structured as a compendium of publications, being organized around a methodological synthetic patent and four internationally peer reviewed publications on the chemical and bio-applicability of the US and EU patented inventions.

Thus, this manuscript is divided into a *General Introduction* to drug delivery with polyurethane-polyurea nanosystems and three chapters, which include the publications as *Results and Discussion* and their introductions as *Introduction* of each chapter.

Chapter 1 is focused on the synthetic methodology to produce a novel kind of self-stratified multifunctional polyurethane-polyurea nanoparticles for cancer nanotherapy. The *Introduction* of this chapter deals with the key characteristics of drug delivery nanosystems and presents the basis of self-stratification by hydrophobic effects. This chapter contains a methodological patent that breaks down multiple examples of nanoparticles formed by easy-tunable polyurethane-polyurea biocompatible and biodegradable polymers bearing multifunctionalities that are applied to cancer therapy and imaging. In addition, here we include a publication containing the *in vitro* proof-of-principle of the stratified nature, high encapsulation stability and selective targeting to cancer cells of the nanosystem. Finally, this chapter also contains a publication with the *in vivo* proof-of-concept for αvβ3 integrin targeted cancer therapy and imaging of polyurethane-polyurea nanoparticles encapsulating plitidepsin as antiangiogenic drug. This research is the consequence of a fruitful collaboration in the framework of a INNPACTO national project (Polysfera, IPT-090000-2010-1) with Dr. P. Calvo, Dr. P. Avilés and Dr. M. J. Guillén in PharmaMar SA; Dr. I. Abasolo, Dr. Y. Fernandez and Dr. S. Schwartz in Vall d'Hebron Institut de Recerca and Dr. J. Rocas in Ecopol Tech SL.

Chapter 2 arises from the encouraging results obtained from Chapter 1 in novel synthetic methods of polymer nanoparticles with shell stratification capacity. The *Introduction* of this chapter presents the current concerns with titanium implants, the outcome of nanoparticle-coated biomaterials and the perspectives in multifunctional nanomaterials. In this regard, a fantastic collaboration with Dr. C. Mas-Moruno of the BiBiTE group in the UPC lead taking profit of the cell targeting high specificity and great encapsulation capacity of PUUa NPs to develop new generation nanobiomaterials for the enhancement of titanium implants osseointegration and bacterial infection prevention. Titanium implants were innovatively coated by interfacial functionalization with RGD-decorated and roxithromycin-loaded PUUa NPs. This methodology resulted in an outstanding improvement of osteoblastic cells adhesion as well as a dramatic reduction of *S.*

Sanguinis bacteria adhesion onto titanium, which is of great interest to improve the outcome of metallic implants for regenerative medicine.

In **Chapter 3**, we explore another segment of application of PUUa NPs, this is immunotherapy. In collaboration with G. Flórez-Canals, Dr. D. Benitez-Ribas and Dr. J. Panés in IDIBAPS and Hospital Clínic of Barcelona we applied PUUa NPs encapsulating budesonide (BDS) corticosteroid for the improvement of BDS efficacy to induce tolerogenicity to dendritic cells (DCs). The *Introduction* deals with the current therapies used to treat autoimmune diseases as well as recent strategies to target dendritic cells *in vivo* using smart nanoparticles encapsulating immunosuppressive drugs. Herein we found that when PUUa NPs loaded with BDS were incubated with mature DCs, those differentiated into tolerogenic dendritic cells in a much more efficient manner than DCs incubated with free BDS. As shown in the included publication, levels of costimulatory molecules were enhanced and IL-10 immunosuppressive cytokine was largely secreted. Even more interestingly, fluorescently labeled PUUa NPs proved their DCs targeted behavior in a multi-cellular environment.

Objectives

Objectives

Objectives

The overall goal of this thesis is to synthesize multifunctional polyurethane-polyurea polymers with the ability to form self-stratified nanostructures in the oil-water interface to provide a more stable encapsulation of lipophilic molecules. As well as apply such nanotechnology in cancer therapy, tissue regeneration and immunotherapy fields. The specific objectives of this thesis are:

- Development of new methodological tools for the synthesis of polyurethane-polyurea nanoparticles (PUUa NPs) with biodegradable self-stratified core/shell nanostructures (Chapter 1)

- Development of a straightforward chemical strategy to functionalize PUUa NPs with amino-containing cyclic RGD peptides via urea bond formation (Chapter 1)

- *In vitro* and *in vivo* evaluation of αvβ3 integrin-targeted PUUa NPs loaded with Plitidepsin antiangiogenic drug as system to treat cancer (Chapter 1)

- Synthesis, characterization and in vitro evaluation of functionalized titanium surfaces with αvβ3 integrin-targeted PUUa NPs loaded with Roxithromycin antibacterial drug to enhance osseointegration and prevent bacterial infection (Chapter 2)

- *In vitro* evaluation of PUUa NPs loaded with budesonide immunosuppressive drug to treat autoimmune diseases (Chapter 3)

Objectives

General Introduction

General Introduction. Polyurethane-polyurea nanosystems for smart drug delivery

1. Nanoparticle biomedical systems

1.1. Introduction

The use of nanoparticle (NP) systems in biomedicine has evolved from being a mere promise of future benefits to being a reality. As evidence of this, a search for the term "nanoparticle" in Pubmed reveals that half of the 106,000 articles found have been published since 2012. Equally relevant is the impetus being given by the European Commission under the Horizon 2020 research and innovation framework, which is providing nearly €80 billion of funding over 7 years (2014 to 2020), in addition to private investment in this field.

The market is the indisputable judge of today's progress, and in this regard nanomedicine is no exception. It is clear that there is a need to advance in the development of novel therapeutic solutions with true scalability and using good manufacturing practices. Many large pharmaceutical companies have made significant investments in buying IP rights of small companies in order to better position themselves to respond to present and future demands. Most efforts have been channeled into nanosystems with a high level of biocompatibility, biodegradability, and ease of industrialization. Understandably, as generally occurs with cutting-edge technologies, regulatory issues limit the application of nanosystems or slow them down.

Therefore, the most clinically advanced polymeric NPs currently available are those made of biodegradable and biocompatible polymers such as PLA, PGA, PLGA, and PCL[1]. Regulatory bodies have approved these systems as therapeutically safe, thus leading to wider use of polymeric NPs. However, biodegradability must be balanced with stability *in vivo*, otherwise the NP breaks up before accumulating in the target diseased tissue. In addition, due to the incomplete reaction of poly(amino acid) NPs, the synthetic procedures of these molecules involve high amounts of organic solvents and purification steps, thus leading to high production costs and environmental issues. In this regard, the demanding field of nanomedicine requires industrially viable polymers with a greener chemistry and an adequate cost.

In this context, due to their chemical versatility, scalability and biocompatibility, polyurethane-polyurea polymers (PUUa) will play a crucial role in the very near future. In the last decade, PUUa with a broad range of chemical variations and good biocompatibility have been developed for tissue engineering and drug delivery

purposes[2–7]. They have proved to exhibit outstandingly flexible physicochemical properties, enabling the introduction of specific block copolymers into the polymer backbone to convey special functionalities to PUUa themselves. These developments have led PUUa to figure among the biomaterials of choice in various clinical applications[8].

1.2. Chemistry of polyurethanes and polyureas

Polyurethanes (PUs) were discovered in 1937 by Bayer and co-workers during the reaction of polyester diol with a diisocyanate (Figure 1a). This reaction converted diisocyanates (discovered almost one century earlier) into one of the most produced chemicals in the world. The power of the PU market lies in the versatility of the chemistry of these materials—from apparently simple isocyanate precursors a wide spectra of polymers with predicted molecular weight, purity and linearity can be synthesized. For example depending on the functionality (f) of the precursors used, either diisocyanates or polyisocyanates with diols or polyols or any combination of their respective functionalities, linear or crosslinked structures are quantitatively obtained. Depending on which structures are formed, thermoplastic or thermostable resins are achieved. The large range of phenotypical properties of such materials is determined mainly by three factors, namely separation between hard and soft segments, carbamate group with hydrogen-bonding capacity (urethane bonds), hydrophobic effects and electrostatic interactions. Another important advantage of the chemistry of PUs is the high reactivity of their isocyanate counterparts and the quantitativeness of polymerization even in solvent-free and catalyst-free conditions and at low temperature. However, one major drawback is the toxicity of isocyanate monomers. In an attempt to roll back the ghost of toxicity, many studies have shown that the toxicity of aliphatic and aromatic isocyanates differs, the former being less toxic but not negligible[9,10]. Preliminary studies have shown that the inherent respiratory tract and pulmonary toxicity of isocyanate monomers is removed when these molecules are polymerized into higher molecular weight species. This process leads to a decrease in monomer volatility and conversion of toxic isocyanates into stable urethanes and ureas[10]. However, for biomedical applications, although some research has shown the rapid elimination of the amino metabolites of aliphatic diisocyanates (PU degradation products) via the urinary tract[9], the increasing interest in urethanes for biomedical use calls for more in-depth studies.

Polyurea is the combination product of isocyanates or polyisocyanates with amines or polyamines (Figure 1b). Initially, polyureas were found to be a typical side reaction in PU chemistry due to moisture content in the reaction mixture. Concretely, side-reacted polyureas form by the reaction of an isocyanate with water, which produces the amino product of the isocyanate and carbon dioxide (Figure 1c). The amino product then further reacts with available isocyanate groups to form a polyurea foam, which is caused by carbon dioxide emission. The exothermic character of the reaction rapidly increases the reaction rate and foaming. Polyureas have long been used as high-performance coatings for multiple surfaces exposed to degradative external conditions such as water, sun, and temperature. Polyureas have the advantage that they offer higher chemical stability, longer shelf-life and higher reactivity of their precursors, even at low temperatures (compared to polyurethane precursors), thus making them the material of choice for many industrial applications[11].
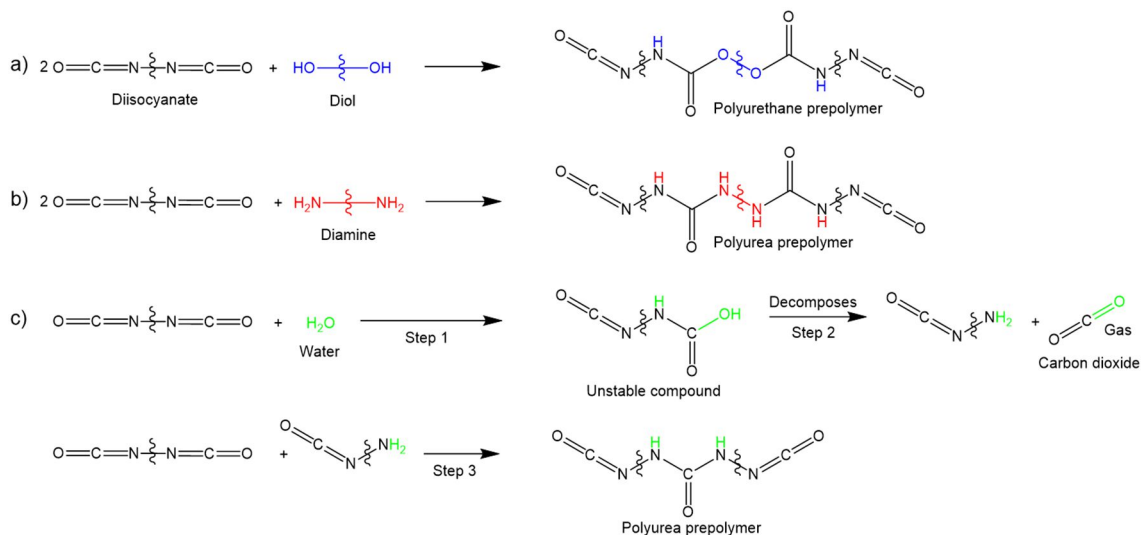
Figure 1. Schematic synthetic process of a) polyurethane from a stoichiometric excess of diisocyanate. b) Polyurea from a stoichiometric excess of diisocyanate. c) Polyurea from the side reaction of an excess of diisocyanates with water.

In addition, the combination of PU and polyurea prepolymers through a diamine or diol chain extender leads to hybrid polyurethane-polyurea polymers (PUUa), which allow even greater chemical tunability for multiple purposes and a reduction in the final cost compared to pure polyurea systems.

2. Polyurethane and polyurea carrier systems in nanomedicine

First conceived in 1950s, polymer NPs have evolved from very simple nanostructures to clinically tested smart nanosystems for multiple purposes. Although most are still limited to research activities, some have either entered the market or are in different phases of clinical trials. Given the chemical versatility and straightforward synthetic methodology of PUs, nanomedicines based on these materials are currently one of the most promising systems for drug delivery. Here we focus on several examples of recently developed PU and/or polyurea carriers, including those based on saccharide-PU, micelles, dendrimers, nanogels, as well as NPs made of various inorganic hybrid materials. In addition, we pay special attention to stratified nanostructures, which we believe represent the near future of all-in-one nanomedicines.

2.1. Polyurethane nanoparticles

PU NPs are gaining in interest as a standard of robustness and tunablility among carrier systems for drug delivery. PU NPs are commonly classified into two kinds, namely nanospheres and nanocapsules (Figure 2). The former comprise a dense whole volume exhibiting low and diffuse differences in composition between the core and the outer part of the shell. Due to their large shell-core ratio, encapsulated molecules are randomly located all around the shell, thereby facilitating a burst release of more superficially adsorbed molecules and a low release rate of those trapped internally. Nanocapsules can be differentiated from nanospheres on the basis of their core-shell structure. In this regard, they typically exhibit an oily core where hydrophobic cargos are located and a surrounding amphiphilic shell that ensures greater encapsulation efficiency and a tunable release rate.

This section will discuss only amphiphilic and biodegradable PU or PUUa NPs. The greatest advantage of these synthetic polymers is that their properties, such as molecular weight, hydrophobicity, biodegradability, tunability, can all be easily and rapidly varied in a controllable fashion in situ with few purification steps for further tailored functionalization.
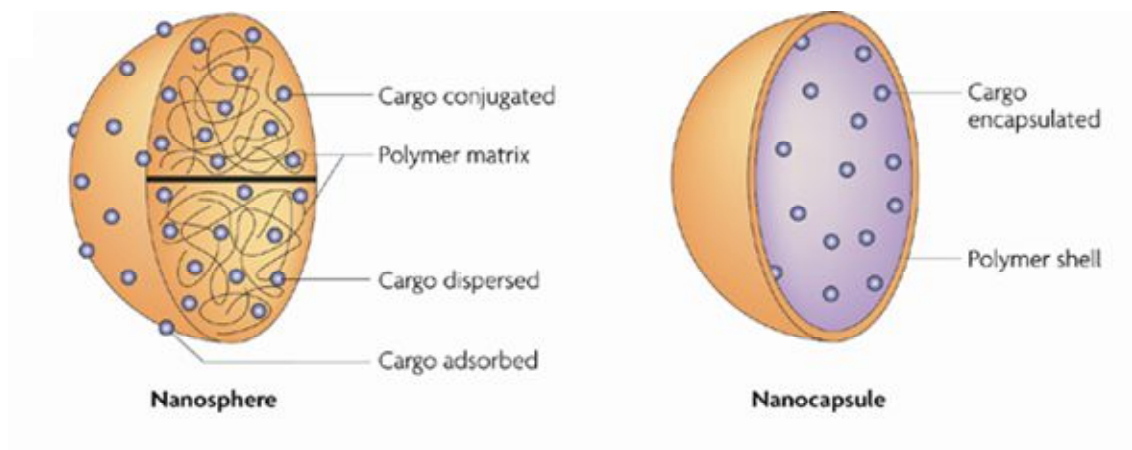
Figure 2. Schematic representation of typical structure of nanospheres (dense polymer interior) and nanocapsules (hermetic core-shell structure). Adapted from Reference[12] with permission from Macmillan Publishers Ltd.

The fabrication of this kind of NP has been achieved by diverse methods, including emulsification, coacervation, and nanoprecipitation[13,14]. This versatility is supported by a more environmentally friendly chemistry (solvent-free, low temperatures, few residues) compared to other techniques that use huge amounts of solvents and involve costly purification steps due to incomplete couplings[15]. The encapsulation of drugs, when possible, tends to be easier and highly efficient as the hydrophilic-lipophilic balance (HLB) of polymers can be tuned quantitatively. Hydrophobic drugs can be directly dissolved in the solvent, together with the prepolymer, prior to NP formation, and hydrophilic drugs can be encapsulated using multiple methods: 1) in the same manner as for hydrophobic drugs, but suspended in the solvent; 2) with techniques such as double emulsions to produce hollow NPs with hydrophilic drugs trapped in the core; and 3) with loading onto the surface of NPs after fabrication. However, as PUs are relatively new as drug delivery systems, deeper studies on their biodegradation kinetics are required in order to accurately predict the release of drugs. In fact, Ma's group developed a biodegradable class of amphiphilic poly(ether urethane) NPs with a tunable redox and temperature triggered release of doxorubicin. Depending on the length of PEG chains and ratio of DEDS the physicochemical properties were adequately tuned for controlled doxorubicin release[16]. Hsu's group studied the different swelling behavior in water of biodegradable PU NPs as well as the sol-to-gel transition temperatures upon heating. PU NPs synthesized from varying amounts of oligodiols (PCL and PLA) as soft segments, showed different hydrogen bonding capacities and cristallinity which directly

affected their sol-to-gel transition at 37 ºC to smartly delivery cells and/or drugs near body temperature[17].

2.2. Polyurethane nanomicelles

This alternative to PU NPs aims to combine the advantages of the shell flexibility of liposome and the chemical tunability of polymers. Block-by-block polymerization allows the obtention of polymers with adjusted molecular weight, HLB values, overall charge, degradation rates, and functionality (e.g. targeting properties, fluorescence). As these systems self-assemble and their stability is driven by physical interactions (they are not crosslinked), there is a true need to achieve a greater control over the molecular structure and polydispersion of polymers in order to ensure later aqueous stability. In this regard, isocyanate chemistry is a potent tool, as coupling reactions are quantitative and highly predictable. Once formed, end-capped polymers are typically emulsified in water. However, surfactants are sometimes crucial to control their size and stability. Sadly, as recently studied, the flexibility gained by avoiding crosslinking steps can jeopardize the *in vivo* stability, degradation, and release profile of these molecules. Similarly to liposomes, when self-assembled in oil-in-water systems, the polymer self-stabilizes by locating hydrophobic regions oriented to the core and hydrophilic regions to the surrounding media. This leads to a star-like structure where hydrophobic cargos and contrast agents can be physically entrapped in the core, and hydrophilic targeting molecules, fluorescent labels or biosensors are located on the surface of the assembled structure (Figure 3).
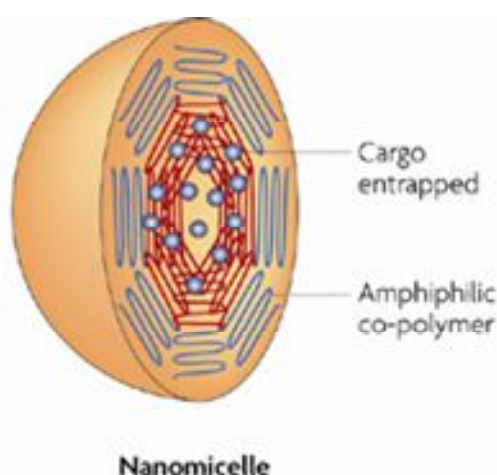
Figure 3. Typical schematic view of nanomicelles structure. Adapted from Reference[12] with permission from Macmillan Publishers Ltd.

Recently, scientists reported on the use of PU co-polymer nanomicelles with multiple functionalities to achieve controlled intracellular drug release and cell internalization[18–21]. Moreover, using mice, Tan's group was able to enhance the biodistribution and antitumor efficacy of the actively targeted PU nanomicelles encapsulating paclitaxel, compared to non-targeted nanomicelles[22].

2.3. Polyurea nanoparticles

Polyurea polymers show greater chemical resistance and mechanical strength than their PU counterparts, mainly because of increased hydrolytic stability. In addition, polyureas offer synthetic advantages. Due to the high reactivity of isocyanates with amines, polyureas can be produced at low temperature, without catalysts, and in the presence of water, obtaining almost quantitative yields. Therefore, polyurea NPs have emerged as a viable alternative to PU NPs for drug delivery. Like PUs, polyureas show magnificent biocompatibility[23] but reduced biodegradability. In order to increase biodegradability, polyurea NPs can be specifically functionalized with soft polymer segments or specific biodegradable monomers[24]. Until now, polyureas have been used mainly as industrial high-performance coatings and adhesives[25,26]. In medicine, they have found commercial application as biomaterials for catheters, stents, etc. However, polyureas in nanomedicine have been virtually overlooked by the scientific community because they are used mostly in the industrial sector. In the last decade, only a small number of scientists have intensified their research into the application of biocompatible polyureas as drug delivery vehicles for diseases treated with nanomedicines[23,27–29]. Concretely, García-Celma's group have developed a huge number of hybrid polyurea NPs from IPDI, PEG (M_w 400), L-Lysine and non-ionic surfactants for its application as targeted theranostics for cancer[27,30]. Furthermore, Bhaumik's group developed porous polyurea nanofibers from 2,4,6-Triaminopyrimidine and 1,4-phenylene diisocyanate with light-emitting, biosensing and drug delivery properties for cancer theranostics[31].

2.4. Dendrimers

Dendrimers are tree-like spherical macromolecules with many branches extending from a central core (Figure 4).
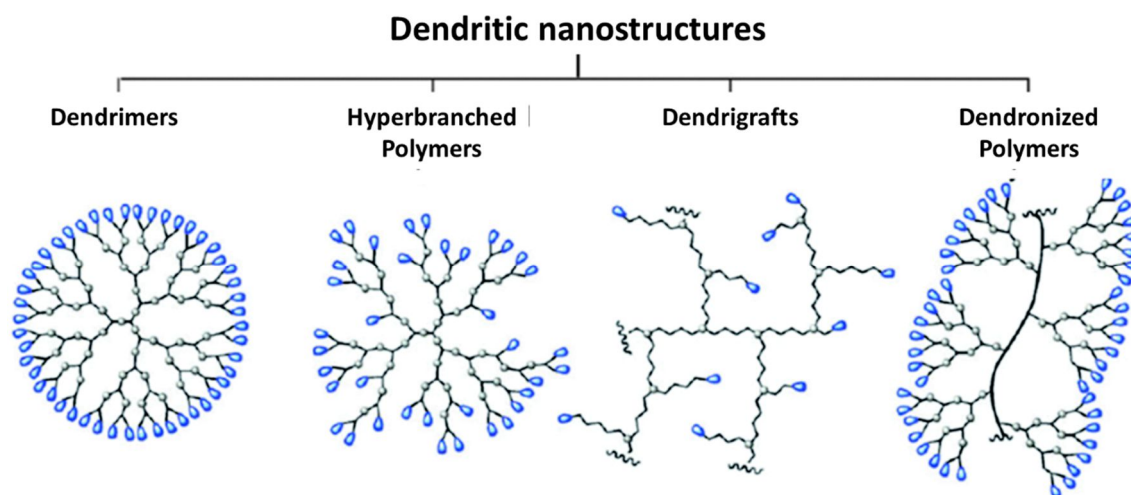
Figure 4. Different dendritic nanostructures obtained from synthetic precursors. Adapted from Reference[32] with permission from The Royal Society of Chemistry.

These structures are synthesized in a step-by-step fashion starting either from the core (divergent) or from the outer shell (convergent), resulting in narrow polydispersity (1-1.1), together with tunability over both size and branching degree. The control over branching degree makes dendrimers unique with respect to other polymers exhibiting randomly crosslinked polymer networks. The chemical control achieved by the step-by-step synthesis, the rationale of the selection of the central core, and the repeated units are crucial as they determine the molecular weight, size, branch density, flexibility, water solubility, and versatility of the final functionalization of dendrimers. However, dendrimers still face some challenges with respect to final performance and synthetic process. Their entrapment efficiency is considerably lower than that of NP-like systems, therefore host–guest interactions (e.g., drug loading, contrast agents) are not that profitable. In addition, their *in vivo* performance is mostly insufficient, as their small size often results in undesired rapid renal excretion. The synthesis of dendrimers can be time-consuming and low-yielding and therefore expensive and difficult to scale up efficiently. Therefore, PUs and polyureas could make a significant contribution to dendrimer synthesis. In later steps where steric hindrance would stop any other growing dendrimeric generation, the use of isocyanates conveniently combined with an alcohol or more conveniently with an amine or diol can greatly promote the construction of highly sterically hindered dendrimers, thereby also enhancing their entrapment efficiency and presumably their *in vivo* stability. However, the production of PUUa dendrimers is hampered by narrow polydispersity, as polyisocyanates should be selected with very high purity and low polydispersity. Various studies have used selective blocking and deblocking of isocyanates in order to control the synthetic growth of dendrimers[33–35]. Specifically,

Nasar's group developed polyurethane dendrimers with heating-sensitive isocyanate protected groups that could be accordingly tuned for drug delivery applications[33,34]. Takagishi's group engineered polyamidoamine dendrimers functionalized with variable weight PEG chains via urethane bonds at the third or fourth generation to increase encapsulation ability of drug molecules[36].

2.5. Hydrogel nanoparticles

Hydrogel nanoparticles are three-dimensional, highly crosslinked networks of hydrophilic (water-soluble) polymers, capable of retaining water or physiological fluids in large amounts, thereby promoting ordered gelification into nanometrical bodies without the need of chemical crosslinking (Figure 5).
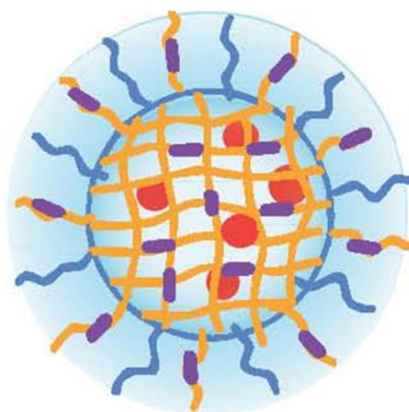
Figure 5. Schematic structure of multifunctional hydrogel nanoparticle with randomly located fluorescent tags and physically entrapped hydrophobic drug molecules in the interior. Adapted from reference[37] with permission from the Royal Society of Chemistry.

PU hydrogels have gained ground in the last decade as they exhibit high chemical tunability and therefore multiple functionalities. These water-soluble polymers are rendered gelified (partially insoluble) by physically or chemically induced crosslinking. Compared with other formulations, hydrogels have several unique advantages. Their high water content makes them physicochemically similar to biological tissues, thus reducing interfacial tension with biological fluids and promoting biocompatibility. The porosity of a hydrogel can be tuned by controlling the density of crosslinking in the gel matrix, which strongly affects drug loading and later drug release. In addition, in order to achieve a bio-triggered degradation, PU hydrogels can be easily functionalized with enzymatic, hydrolytic, and stimulus-responsive moieties. Wu's group developed biodegradable multi-sensitive poly(ether-urethane)s through a simple one-pot

polyaddition of PEG, DEDS, N-methyldiethanolamine, and hexamethylene diisocyanate. They studied the sol-to-gel phase transition with increasing temperature and pH at physiological conditions to create in situ injectable PU Hydrogels[38]. Recently, Hsu's group, engineered biodegradable PUUa NPs from IPDI, oligodiols and ethylenediamine that formed a gel upon heating to 37 ºC. This strategy allowed them to embed neural stem cells into PUUa NPs hydrogels to treat traumatic brain injury in zebrafish models[39].

2.6. Polyurethane–polysaccharide Hybrid Nanoparticles

A recurrent issue when NPs are tested *in vivo* is the formation of a physisorbed protein corona on their surfaces. Some researchers have evidenced the unwanted effect that this phenomenon has on the targeted delivery of drugs. Protein corona formation translates into crucial changes in nanocarrier size, morphology, and surface charge, and targeting ligand camouflage (Figure 6).
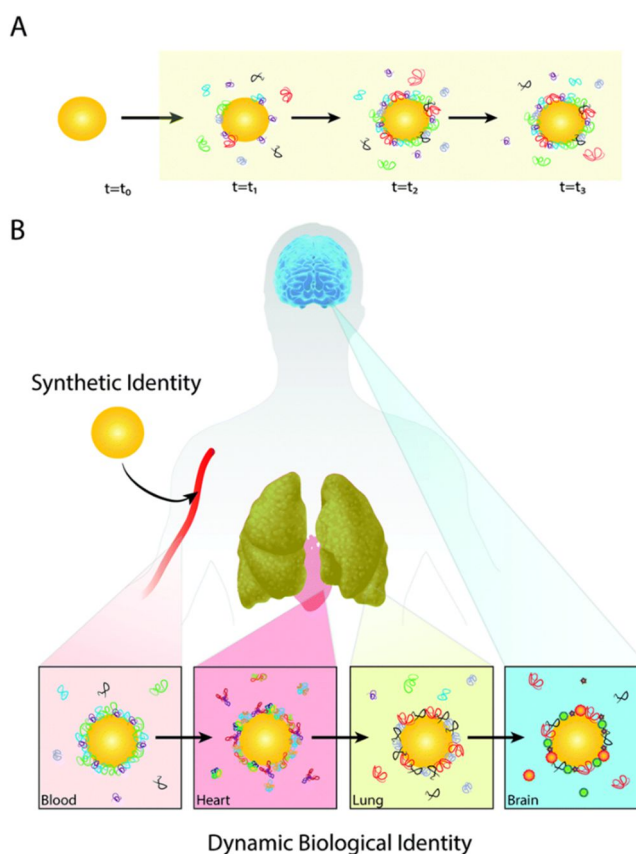
Figure 6. a) Polymer nanoparticles change their superficial morphology upon interaction with blood circulating proteins. b) The type of protein corona depends on the site and route of administration. Adapted from reference[40] with permission from the Royal Society of Chemistry.

It is widely accepted that the latter results in poor blood circulation, rapid clearance, and unspecific accumulation. Polysaccharides, as hydrophilic moieties on the NP surface, have proved efficient in diminishing circulating protein-particle interactions and thereby go unnoticed by the RES. In this regard, hybrid hydroxyethyl starch-PU NPs have recently been used to minimize plasma protein interactions in Landfester's group. In addition, after shell functionalization with a PEG-mannose conjugate via urethane bonds, efficient stealth and targeting behavior was ensured[41]. Dufresne's group developed cellulose nanoparticles and modified them superficially by anchoring a hydrophobic monoisocyanate via urethane bonds. Thus, amphiphilic cellulose-urethane nanoparticles were obtained with a wider solubility range[42]. This technology could have multiple applications in drug delivery in order to simply obtain biofunctionalized biocompatible cellulose nanoparticles using isocyanate linkers.

2.7. Polyurethane Inorganic-hybrid Nanoparticles

Generally speaking, the polymeric parts of the hybrid NP have structural functions and enhance the mechanical aspects and synthetic tunability of the materials (targeting, biodegradation, biocompatibility, etc.), while the inorganic parts can introduce more specific functionalities such as catalysis properties, traceability, magnetism, etc. and confer other specific features like mechanical strength and thermal properties to the polymer. Inorganic-hybrid NPs comprise a very important category of drug delivery systems as they ensure precision in size/shape control, excellent physicochemical properties, and multifunctionality. However, their inability to totally biodegrade has somewhat limited their fields of application and use as nanomedicines.

Recently, the combination of polyurethane nanocapsules encapsulating gold nanoparticles was used as a traceable system for multiple purposes such as diagnostics, imaging and electron microscopy. Concretely, Bernard's group engineered a simple and precise method to obtain multifunctional nanocapsules coated with either gold or iron oxide nanoparticles and crosslinked with IPDI to stabilize their nanostructure and allow their further shell functionalization via isocyanate chemistry[43]. Hsu's group used biodegradable PU NPs from IPDI and PCL to encapsulate superparamagnetic iron oxide NPs (SPIO NPs) and tested them as thermo-responsive biocompatible drug delivery vehicles.

2.8. Stratified nanostructures

Even though stratification in macromolecular structures has been long ago accepted[44–46], its importance has not been recognized until the oil-in-water interfacial properties driven by the dynamics of its constituting agents proved to allow prediction of structure-properties relations[47,48]. The acquired understanding of interfacial molecule-molecule interactions of the last decade bring significant advances that have led to the development of a new generation of multifunctional polymeric materials in general, and colloidal nanomaterials in particular. Electrostatic and hydrophobic interactions are crucial in native and externally acquired functions of biological systems. Those can be found in colloids and are starting to be rationally applied to every day materials with technological applications[49,50]. Recent advances in the development of stimuli sensitive colloidal materials with stratifying capacities will be discussed in the following section, putting a special focus on the use of hydrophobic and electrostatic interactions to get control over nanostructural morphology and performance of nanosystems.

2.8.1. Hydrophobic effects.

Hydrophobic forces are capable of forming structures that are compact and also flexible enough to allow the required fluidity in cellular and sub-cellular membranes of live organisms. Although nature uses the hydrophobic force to create compartments, the connectors between them is not an arbitrary choice. It has been demonstrated that the self-assembly of amphiphilic molecules, and more specifically polymers, is under thermodynamic control, meaning that self-stratified structures result simply from the search of each molecule for its position of lowest chemical potential, or in other words, larger thermodynamic stability. It can be assumed that what occurs in vesicle formation, e.g. phospholipid vesicles, where the polar head tends to segregate and the hydrophobic tail drives the subsequent nanostructuration, would also occur in amphiphilic polymers with hydrophilic and hydrophobic segments as it has been observed in our experiments. This implies that, over a critical micelle concentration (c.m.c), the opposing thermodynamic preferences of the two ends of an amphiphilic molecule are mostly accommodated by self-association to form an aggregate with the hydrocarbon chains in the middle, avoiding contact with water as much as possible, and the hydrophilic polar groups at the surface[51]. Of note, the c.m.c decreases as the length of the hydrophobic chain increases, being approximately 1 molar for hexyl chains and even 10^{-9} for C36 biological phospholipids[45]. The size and shape of amphiphilic nanostructures is determined both by geometric and thermodynamic factors. One of the geometric factors is the surface/volume ratio, which decreases as size increases; in other words, if the number of hydrophobic chains in the core increases, the surface area per chain decreases. Therefore, by using less hydrophobic chains but increasing their length in an

amphiphilic polymer, the size of the resulting nanostructure should decrease[52]. The second and no less important geometric factor is that the core cannot be smaller than two hydrophobic chains, each one coming from the opposite side of the shell. However, that would translate into very small structures with too large spaces between the polar heads, thus promoting contact between hydrophobic tails and water, which would translate into destabilization and coalescence of nanoassemblies. In order to solve that thermodynamic problem, longer polar groups, such as PEG-like and PAS-like chains would increase thermodynamic stability as a result of the intrinsic flexible behavior of hydrophilic chains which leads to formation of brush or mushroom configurations[53]. Hydrophilic flexible chains would self-accommodate at the oil-in-water interface (polyethylene oxide polymers are partially amphiphilic) and cause a decrease in hydrophobic tail-water interactions[53]. In this regard, we have observed during our recent studies that a specific kind of linear difunctional polyethylene glycol monomethyl ether containing both alcohols in proximity to each other (YMER™ N120) would translate into better polymerization yields, a highly packed molecular structure, and improved barrier effect by preventing diffusion of entrapped cargoes, thus making encapsulations more stable per se. To create self-stratified polymer nanostructures by hydrophobic effects, hydrophobic and hydrophilic segments of an amphiphilic polymer need to be specifically designed in order to maximize hydrophobic-hydrophilic interactions and therefore increase thermodynamic and geometric stability. In order to reduce the energetic barrier and thus achieve the formation of stratified polymeric structures, geometrical factors such as the length of hydrophobic and hydrophilic segments and their position in the main polymeric chain (either in the main chain or sideways from it) can be accurately addressed. Concretely, the hydrophilic monomers PEG and YMER™ N120 (both 1000 M_w approx.) are hydrophilic and have almost equivalent reactivity (Figure 7a and 7b) but when polymerized they show distinct morphology in water. In house data supports that when these hydrophilic diols are covalently attached to the backbone of an amphiphilic polymer, they self-orient toward the aqueous phase in different ways. When emulsified, YMER™ N120, with its closely positioned diol reactive groups and "two-headed serpent" structure with a long polyethoxylenated chain, decreases the energy needed to be solvated and enhances the formation of colloidal systems (Figure 7c). In contrast, PEG 1000 which contains the two hydroxyl groups separated by the whole polyethoxylenated chain, requires a morphological constriction of the hydrophilic chain to display it through the water phase, sideways the main chain. In addition, the resulting twisted hydrophilic polyethoxylenated chains would be repelled from each other. Therefore, this rearrangement would be less thermodynamically favored and the colloidal systems formed would be less stable[52] (Figure 7d).
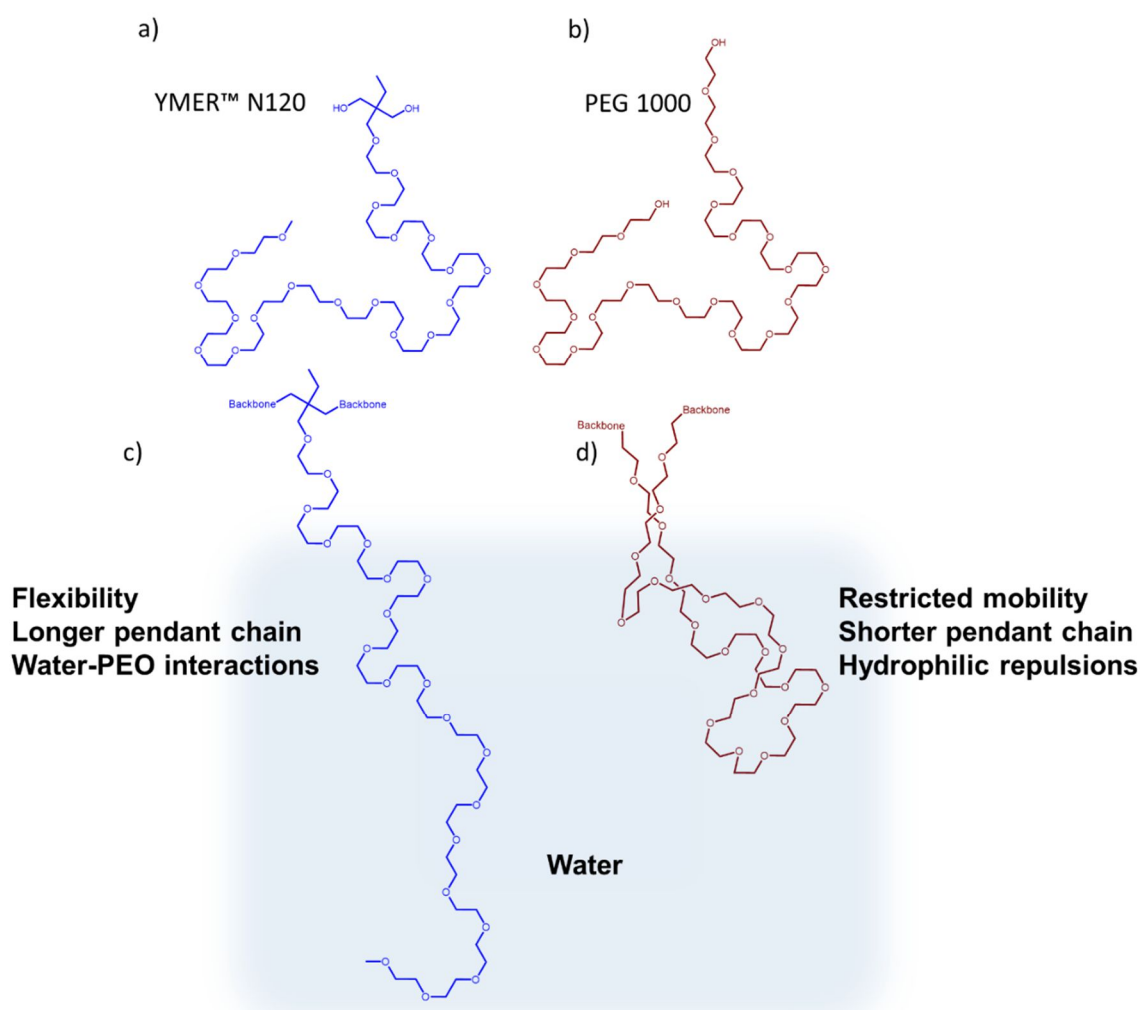
Figure 7. a), b) Ideal chemical structures of YMER™ N120 and PEG 1000, c) Adopted morphology of polymerized YMER™ N120 towards the aqueous phase of an oil-in-water emulsion, d) Representation of the adopted morphology of polymerized PEG 1000 towards the aqueous phase of an oil-in-water emulsion.

A similar behavior is observed in the hydrophobic monomers that constitute the hydrophobic segments of an amphiphilic polymer. We have noticed that the hydrophobic interactions are much more thermodynamically favored if they are sideways on to the main polymeric chain. This phenomenon gains relevance when the formation of stratified nanostructures is sought. Of note is that energetic constraints between hydrophobically stratified polymers will be less important when long hydrophobic pendant chains are responsible for this stratification. As explained before, hydrophobic "naturally pendant" chains will facilitate interactions of an amphiphilic polymer with a hydrophobic one through superposition of hydrophobic chains (Figure 8). Non-pendant hydrophobic chains will be geometrically restricted to self-orienting towards the oily phase and

thermodynamically unstable due to their energetically unfavored proximity to hydrophilic water molecules, which induces NP aggregation in water. (Figure 8).
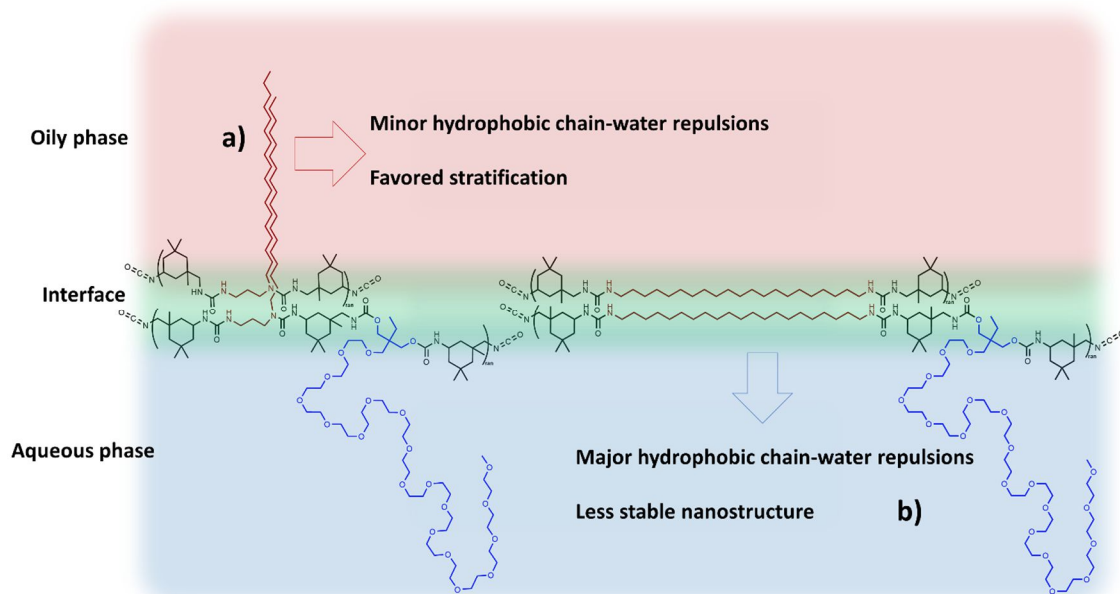
Figure 8. Ideal structures of amphiphilic prepolymers at the oil-in-water interface. a) Hydrophobic pendant chains are easily self-accomodated toward the oily phase (nanoparticle core). Hyfob and Amphil hydrophobic chains stabilize by hydrophobic effects the stratified nanostructure of a nanoparticle polymeric shell. b) Hydrophobic non-pendant chains are more restricted to self-allocate toward the oily phase as they need to constrict the whole amphiphilic prepolymer to adopt a pendant structure. Hyfob and Amphil hydrophobic chains remain close to the aqueous environment, in contact with water molecules, which is thermodynamically unfavored and destabilizes the oil-in-water interface.

Hydrophobic interactions are usually strong enough to remain stable in pure water or ionic aqueous media. However, when amphiphilic molecules come into play, some structural rearrangements might occur in order to reach thermodynamic stability again. Accordingly, amphiphilic and hydrophobic moieties have proved to be able to disrupt hydrophobically stratified entities both in *in vitro* and *in vivo* experiments[54,55]. In drug delivery with polymer nanoparticles, the stability of a nanovehicle is intended to remain unchanged during blood circulation until reaching the site of interest inside the body. If this were not so, the cargo would be unspecifically delivered and ineffective. In this regard, the chemical crosslinking would be an interesting approach to avoid destabilization of stratified nanostructures by external amphiphilic molecules that would jeopardize the specific delivery of the encapsulated cargo. Thus, chemical crosslinking of isocyanate reactive stratified nanostructures with small highly reactive polyamines would maintain preformed stratified nanostructures, increase the stability against

amphiphilic and hydrophobic molecules (e.g. phospholipids, colesterol, proteins, etc.) and eliminate toxicity issues related to isocyanate functional groups[56,57] (Figure 9).
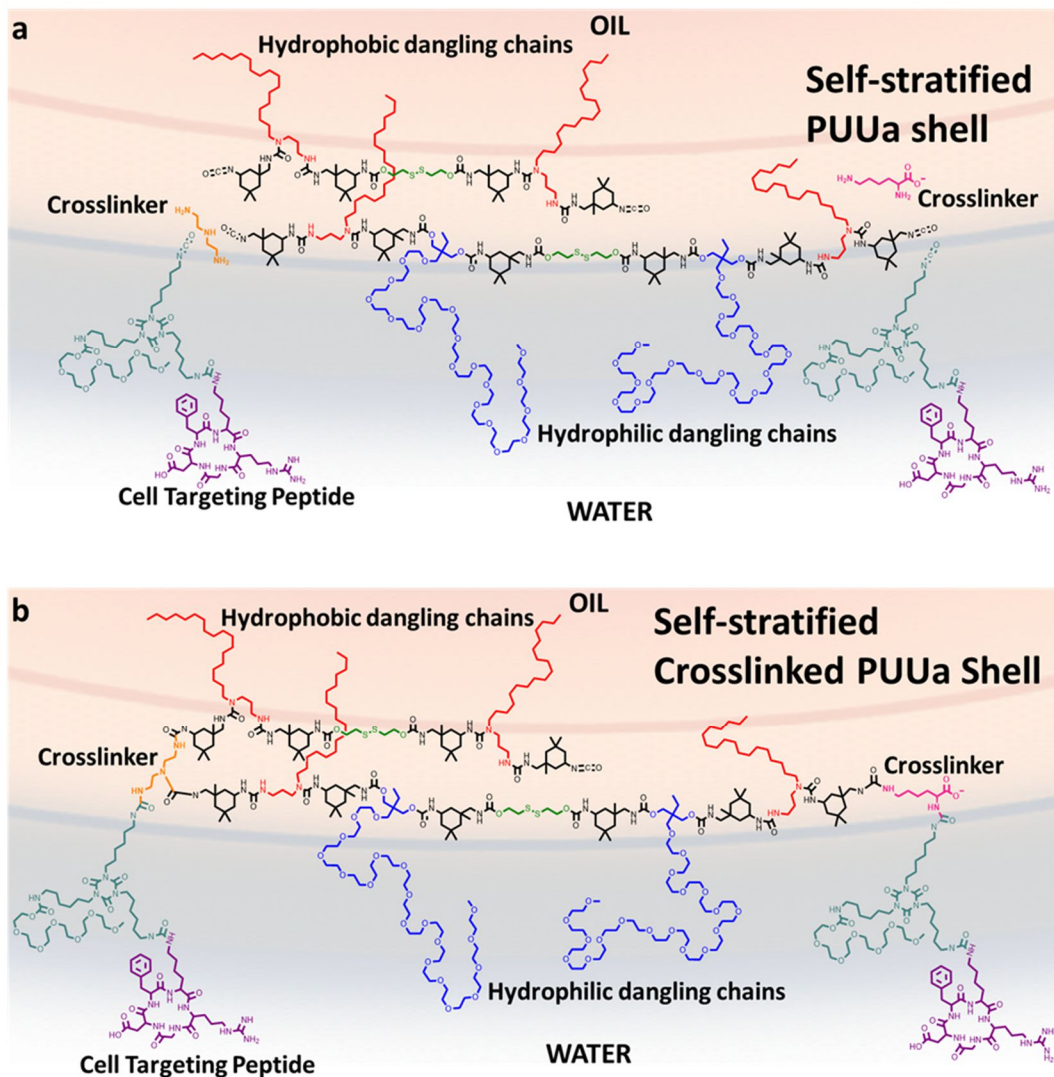
Figure 9. Ideal structures of reactive PUUa prepolymers at the oil-in-water interface a) before and b) after crosslinking via urea bonds with polyamines.

2.8.2. Electrostatic interactions. Layer-by-Layer technique.

The basic principle behind the well-established layer-by-layer (LbL) technique is the alternate immersion of a template in solutions of two oppositely charged compounds that will form the multilayer assembly. Normally, the template is washed after each immersion step in order to obtain stable multilayer coatings, thus avoiding weakly bound films. The wide interest in this technique is explained by the huge number of macromolecular structures that can be used, these ranging from polymers, synthetics and naturals, even nanoassemblies (e.g. micelles, polymersomes), to metal-frameworks, viruses and liposomes. LbL assembly properties, such as width, stability, permeability, etc., can be

effectively tuned during the self-assembly by varying concentrations, solvents, temperature, pH, etc.[58–60]
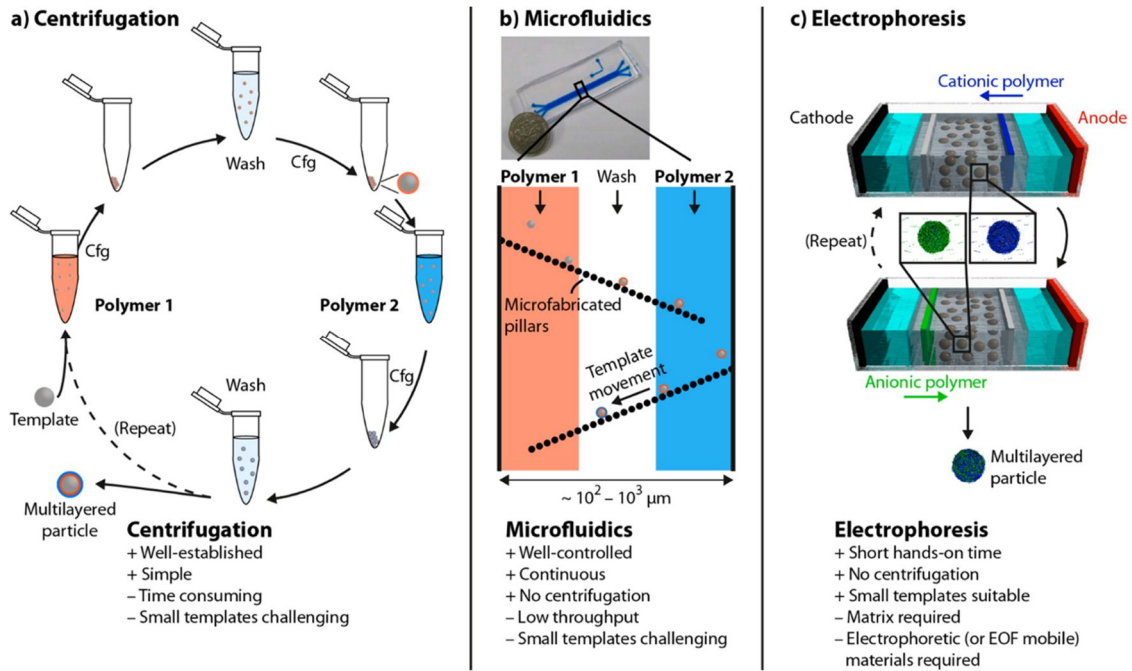
Figure 10. Different methods used to obtain multilayered particles by the LbL technique. + symbol indicates pros and – symbol cons. Reproduced from Reference[61]

3. Release methods

In many clinical situations the steady release of drugs for the treatment of diseases of difficult access is not enough and complex methods are required. Recent chrono-pharmacology studies indicate that the focus of certain diseases, such as tumor early stages and progression of cancer, have a strong circadian influence[62]. Treatment of these diseases requires an accurate and predictable control of the release of drugs in response to *in vivo* physiological conditions or external stimuli (Figure 10). Depending on the incorporated degradable functional group in the polymeric backbone of the nanosystem, the drug release can be achieved specifically upon activation by variable conditions. With respect to the biological environment, the stimuli that triggers the release of a drug can be classified as internal (for example, changes in pH value or the concentrations of ions, small molecules such reducing agents and enzymes)[63–65] or external (e.g. light, ultrasound, electric field, magnetic field, and the heating) which are also commonly known as physical stimuli[66–68]. In principle, the rapid response of a drug delivery system for a stimulus can be used for real-time control of drug release and achievement of the drug demand[69]. In the following sections, the focus will be put on

various stimuli response polyurethane-urea systems used mainly in the therapy of cancer.
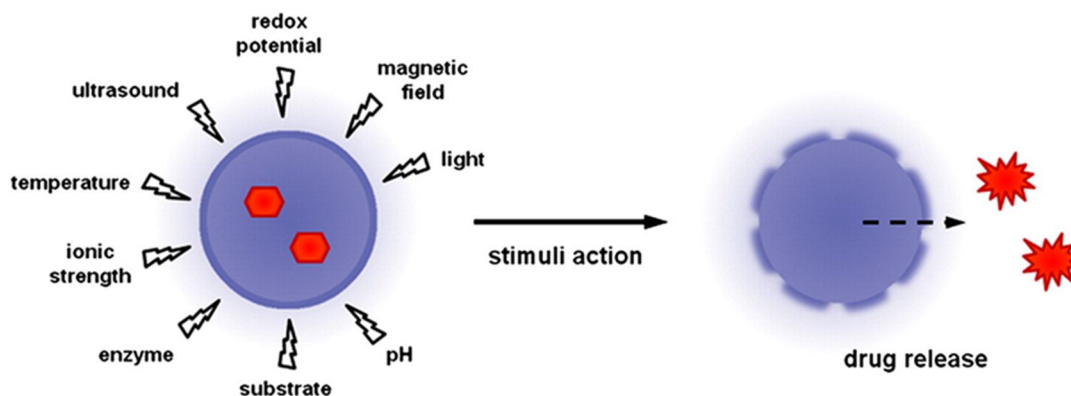
Figure 10. Most commonly used drug release mechanisms in polymeric nanoparticles. Reproduced from reference[67] with permission from Elsevier.

3.1. Glutathione-Sensitive Release

Glutathione (GSH) is the tripeptide responsible of the high reductive potential inside all living cells. Recently, it has been accurately proved *in vitro* and *in vivo* in yeast cells that the GSH:GSSG ratio is 10000:1 inside the cytosol being 13 mM for GSH and 4 µM for GSSG[70]. However, in blood and extracellular matrix, GSH levels are almost a thousand times lower (approximately 2–20 µM). More interestingly for cancer therapy, the GSH concentration in tumor cells has been reported to be four times higher than in normal cells (approximately 4 µM g^{-1} vs. 1 µM g^{-1}). In addition endo/lysosome also exhibits an important reductive potential modulated by gamma interferon-induced lysosomal thiol reductase (GILT) in the co-presence of L-cysteine. The crucial differences in reducing properties between intracellular and the extracellular environments, as well as between inside tumor and normal cells facilitates the use of redox-sensitive DDS for cancer therapy. While DDS are stable in the extracellular environment, they rapidly and efficiently release the drug in the intracellular environment upon endocytosis due to their reductive biodegradable characteristics. In fact, the high reducing potential of the intracellular environment has been extensively applied as a stimulus for the degradation of PU NPs to achieve specific and controlled drug release in cancer cells. Chen's group have developed PU NPs bearing a whole crosslinked hydrophobic core via disulfide bonds. They have proved under *in vitro* and *in vivo* conditions the selective degradation and subsequent release of doxorubicin anticancer drug from disulfide-rich PU NPs to enhance their antitumor efficacy[21]. Very interestingly, Zhang's group developed PU nanomicelles with diselenide bonds in its amphiphilic structure for both disruptive

properties in reductive and oxidative environments to ensure total biodegradation of the nanocarrier[71].

3.2. pH-Sensitive Release

The pH variations associated with a pathological condition such as cancer or inflammation have been extensively exploited to trigger drug release into a specific environment (e.g. gastrointestinal tract or vagina) or into an intracellular compartment (for example, endosome/lysosome). Many nanosystems used to administer anti-angiogenic drugs take advantage of the difference in pH values between healthy tissues (approx. 7.4) and the environment of extracellular tumor cells (6.5 - 6.8). One of the most widely used methods involves polymers with functional groups that can promote a burst of drug release from NP carriers in response to a change in pH. In some examples found in the literature, PU polymers are hybridized with polyacrylate polymers to achieve a pH dependent release. These hybrid polymers can be used to alter the structure and hydrophobicity of the NP carriers through protonation or deprotonation[66,72,73]. Another approach is to incorporate cleavable bonds into the NP carrier. These bonds can be broken to directly release the drug molecules conjugated to or encapsulated in the carrier. pH-sensitive linkages such as hydrazone, hydrazide, and acetal are among some of the most used approaches in cancer nanomedicine. Concreteley, Tan's group developed a kind of biocompatible amphiphilic and zwitterionic PU nanomicelles with hydrazone bonds in its structure for endo-lysosome low pH triggered release, subsequently, they proved the pH dependent release of paclitaxel as well as the enhanced *in vivo* performance[22]. Zhong's group introduced acetal moieties into the urethane backbone and proved the total degradation of nanomicelles into unimers and the consequent quantitative specific delivery of doxorubicin inside the cytoplasm[74]. Muñoz-Espí's group synthesized PUUa-silica hybrid nanocapsules that broke up in basic media to release encapsulated hydrophilic moieties. In addition the tailorability of the release rate was successfully accomplished by varying the PUUa:silica ratio in the precursor[75].

3.3. Enzyme-Sensitive Release

Enzymes perform an enormous range of crucial genesis and lysis functions in our bodies. They are involved in coupling biopolymer chains to generate macromolecular structures. They can also specifically break down bonds, causing the disassembly or destruction of macrostructures. Most conveniently, enzymatic reactions can be used to trigger the

release of a drug when the disease target area is associated with the overexpression of a specific enzyme.

An enzyme-triggered release system includes either a polymeric scaffold or a conjugate (carrier-linker-drug) that is susceptible to degradation by a specific enzyme. Hydrolases are the most widely used enzymes for such applications. These enzymes can break covalent bonds or modify certain chemical groups by altering the balance between electrostatic, hydrophobic, and van der Waals forces, π–π interactions, or hydrogen bonding. For example, proteases can induce the release of a drug linked to a carrier through a peptide bond; glycosidases can trigger drug release from a polysaccharide-based carrier; lipases can facilitate drug release by hydrolyzing the phospholipid building blocks in a liposome; and hydrolases can be used to maneuver the assembly and disassembly of inorganic nanoparticles, as well as the degradation of a gatekeeping material that blocks the pores of a carrier. In addition, kinases and phosphatases have been used to reversibly break/form covalent bonds, thereby achieving the release of a drug in an "on–off" manner. Jin-Wook's group developed a difunctional pH and enzyme biodegradable PU NP for drug delivery to inflamed colon. Drug release was achieved at pH > 7.4 and in presence of rat cecal contents with azo-reductase enzyme. In this conditions, burst release was achieved both *in vitro* and *in vivo,* enhancing the accumulation of the drug in the inflamed colon of rats[76]. Fu's group proved that PU nanomicelles containing PCL and hydrazone bonds in their structure biodegraded in the presence of acidic pH as well as in lipase enzyme. In 6 days, their PU nanomicelles lost between 25-35 % of initial polymer weight depending on the amount of incorporated PCL[19].

3.4. Thermoresponsive release

Thermoresponsive release is one of the most widely studied strategies for smart drug delivery because it can take advantage of the local temperature increase caused by the pathological condition (e.g., tumor, inflammation, or infection). Thermoresponsive release relies on a sharp change in the physical properties of a temperature-sensitive material. This sharp response can trigger drug release in the event of variation in the local temperature around the carrier. The range of temperatures within which the drug delivery system is activated should be kept between 37 and 42°C, as temperatures beyond this range will cause protein denaturation or disruption of function.

Thermoresponsive drug delivery systems are usually based on polymer NPs composed of a thermosensitive polymer that undergoes conformational/structural changes associated with the constituent lipids that induce variations on the permeability of the

shell. Sosnik and Cohn's group studied the degradation kinetics of PU nanomicelles containing varying ratios of lactide and caprolactone oligoesthers units. They studied the M_w loss over time by incubating their PU nanomicelles in water at 37 ºC. Lactide containing PU's degraded totally in 2 months, while caprolactone-rich PU's degraded partially after 8 months which was used to tune the *in vitro* release profile of RG-13577 anti-restenosis agent[77,78].
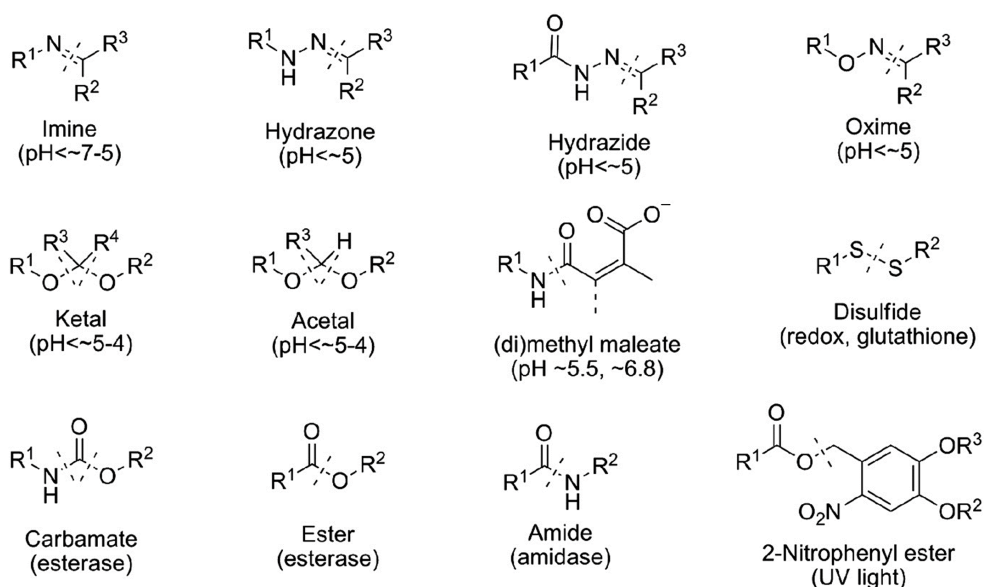
Figure 11. Commonly used chemical structures to achieve a stimuli-responsive drug release and/or biodegradation. Dashed lines indicate the bond that will be broken upon exposure to the stimulus between parentheses. Reproduced from reference[67] with permission from Elsevier.

3.5. Photosensitive release

The use of light as a stimulus to trigger drug release has been actively explored owing to its convenience for remote control and its potential for high spatiotemporal resolution. Photosensitivity is often introduced into NPs through functional groups that can change their conformations or other properties upon irradiation by light of a certain wavelength. Only few light-sensitive nanoformulations have been engineered in the last years, mainly due to the questionable biodegradability and subsequent cytotoxicity of the degradation products of common photosensitive moieties such as Au–Ag, gold nanorods, azobenzene and o-nitro benzyl derivatives. Regarding the polyurethanes segment, Landfester's group developed a multivalent kind of PU nanocapsules from toluene diisocyanate and an azo-containing diol that released an encapsulated sulforhodamine dye via pH changes, UV-light or temperature increase[66]. Tang's group developed 2-nitrophenylethylene glycol-containing PU nanomicelles as photosensitive

moiety for the specific release of Tagalsin-G drug. They observed the selective cell death upon UV-light irradiation of cells incubated with Tagalsin-G-loaded PU nanomicelles[79].

4. Types of drugs

It is generally accepted that anticancer drugs can be classified into two major groups, namely hydrophobic and hydrophilic. Alternatively, depending on their their electrostatic properties they can also be classified as highly charged (either cationic or anionic) or neutral drugs. Behind the selection or/and design of the NPs employed as carriers of a specific type of drug, it is vital to know the physicochemical properties and mechanism of action of the drug in order to achieve the required encapsulation efficiency, the desired release profile and consequent pharmacological efficacy. In this part we include different formulation strategies used to circumvent the challenges implied the delivery of hydrophobic, hydrophilic and highly charged drugs.

4.1. Hydrophobic drugs

Most anticancer drugs used in clinical practice, including paclitaxel, docetaxel, and rapamycin, are hydrophobic. The way in which to efficiently administer a drug to its target has always been a challenge and the focus of intense research efforts. The difficulty resides in the fact that hydrophobic molecules are not soluble enough to cross the aqueous-rich media (for example, the body and organ fluids *in vivo*) that surrounds a cell or to penetrate the cell membrane and specific intracellular aqueous-surrounded organelles. Moreover, hydrophobic molecules exhibit a strong tendency to aggregate after intravenous administration which in turn is the main responsible of embolisms, local toxicity, and immunological responses.

In order to overcome the poor water solubility of hydrophobic drugs two approaches have arised to change their pharmacokinetics and biodistribution, these are conjugation in an amphiphilic polymer to form a nanocarrier, or encapsulation in a nano-based carrier. If conjugated, the corresponding prodrug-like nanoconjugate should keep the pharmacological activity of the drug, or be cleaved at certain biological conditions to release the free drug. In this regard, Mahkam's group conjugated 1,4-diaminocubane and morphine to either polyurethane or polyetherurethane polymers and studied their release by hydrolysis of the polyurethane segments. The polyetherurethane drug conjugates showed accelerated release profiles due to an increased hydrophilicity of the polymeric chain that increased urethane bonds susceptibility to hydrolisis[80]. When

encapsulated, the carrier should ensure high loading capacity for the hydrophobic drug. Normally, this feature is accomplished by the use of an amphiphilic nanomaterial that displays a hydrophobic core and a hydrophilic surface. Recent investigations have shown the multiple PU or PUUa nanosystems that can be used to encapsulate hydrophobic drugs for improved cancer therapy[21,22,56,81–83].

4.2. Hydrophilic drugs

Although hydrophilic drugs are obviously highly soluble in aqueous media, their utilization in many diseases is hindered by a number of important issues. For example, their large hydrophilicity translates into poor spontaneous cell internalization due to their intrinsic inability to cross lipid-rich membranes. In addition, hydrophilic behavior also translates into rapid blood clearance through kidney filtration and low stability against enzymes like protease, lipases, etc. Hydrophilic agents, including large biomolecules (e.g., proteins, peptides, and nucleic acids) and small molecules (like cisplatin, gemcitabine, etc.), are also currently used for cancer therapy.

To circumvent the abovementioned obstacles, NPs have been actively explored as carriers to encapsulate and deliver hydrophilic drugs. Differently to hydrophobic drugs, loading efficiency is a major issue to consider because the hydrophilic drug or biocompound tends to easily diffuse from the core to the aqueous dispersion medium. Usually, most of the materials used in drug delivery are hydrophobic or at least amphiphilic. Thus, the loading in aqueous media of hydrophilic cargos inside the hydrophobic core of a polymeric nanocarrier is not easily accomplished due to their incompatible miscibility. To this end, a number of approaches have been developed to improve the loading efficiency of a hydrophilic drug. Inverse miniemulsion technique using PU NPs developed by Landfester and coworkers is one the most generally applied approach to solve this problem[84–89]. This process consists on the water-in-oil emulsification of PU NPs, followed by a crosslinking at the interface and transference to an aqueous phase using external SDS surfactant, thereby creating a water-in-oil-in-water emulsion of hydrophilic core PU NPs for encapsulation of water soluble cargos.

Table 1. Nanoformulations in clinical use or in clinical trials as anticancer nanomedicines. Reproduced from Reference[90]

Trade name	Formulation	Drug	Company	Application	Phase of development
Abraxane	albumin-bound nanoparticle	paclitaxel	Abraxis Bioscience, Inc.	metastatic breast cancer[10]	approved
Caelyx	PEGylated liposome	doxorubicin	Schering-Plough	metastatic breast and ovarian cancer, Kaposi sarcoma[11]	approved
DaunoXome	liposome	daunorubicin	Galen Ltd	Kaposi sarcoma[12]	approved
DepoCyt	lipodome	cytarabine	Pacira Pharmaceuticals, Inc.	lymphoma[13]	approved
Doxil	liposome	doxorubicin	Sequus Pharmaceuticals, Inc.	Kaposi sarcoma[14]	approved
Genexol-PM	polymeric micellar nanoparticle	paclitaxel	Samyang Biopharmaceuticals	breast cancer[15]	approved
Marqibo	liposome	vincristine sulfate	Talon Therapeutics, Inc.	lymphoblastic leukemia[16]	approved
Myocet	liposome	doxorubicin	Zeneus Pharma Ltd	metastatic breast cancer[17]	approved
Oncaspar	PEGylated asparaginase	asparaginase	Enzon Pharmaceuticals, Inc.	acute lymphoblastic leukemia[18]	approved
Zinostatin stimalamer	poly(styrene-co-maleic acid)-conjugated neocarzinostatin	neocarzinostatin	Astellas Pharma, Inc.	hepatocellular carcinoma[19]	approved
NK105	micellar nanoparticle	paclitaxel	Nippon Kayaku Co., Ltd	breast cancer[20]	phase III
BIND-014	polymer matrix	docetaxel	BIND Therapeutics, Inc.	prostate cancer[21]	phase II
Genexol-PM	methoxy PEG-PLA	paclitaxel	Samyang Biopharmaceuticals	ovarian and lung cancer[22]	phase II
CRLX101	cylodextrin-PEG micelle	camptothecin	Cerulean Pharma, Inc.	ovarian/tubal/peritoneal cancer, rectal cancer[23]	phase I/II
CYT-6091	gold nanoparticle	tumor necrosis factor α	Cytimmune Sciences, Inc.	pancreatic cancer, melanoma, soft-tissue sarcoma, ovarian, and breast cancer[24]	phase I/II
L-Annamycin	liposome	annamycin	Callisto Pharmaceuticals, Inc.	acute lymphocytic leukemia, acute myelogenous leukemia[25]	phase I/II
NL CPT-11	liposome	irinotecan	University of California, San Francisco	solid tumor[26]	phase I/II
Rexin-G	pathotropic nanoparticle	dominant negative cyclin G1 construct	Epeius Biotechnologies	breast cancer, osteosarcoma[27]	phase I/II
Anti-EGFR immunoliposome	liposome	doxorubicin	University Hospital, Switzerland	solid tumor[28]	phase I
AuroLase	gold nanoparticle		Nanospectra Biosciences, Inc.	lung cancer, head and neck cancer[29]	phase I
BikDD nanoparticle	liposome	proapoptotic Bik gene (BikDD)	National Cancer Institute	pancreatic cancer[30]	phase I
CALAA-01	cyclodextrin-containing polymer	siRNA	Calando Pharmaceuticals, Inc.	solid tumor[31]	phase I
CRLX301	cyclodextrin-based polymer	docetaxel	Cerulean Pharma, Inc.	solid tumor[32]	phase I
DEP™-Docetaxel	dendrimer	docetaxel	Starpharma Holdings, Ltd	breast, prostate, lung, and ovarian cancer[33]	phase I
Docetaxel-PNP	polymeric nanoparticle	docetaxel	Samyang Biopharmaceuticals	advanced solid malignancies[34]	phase I
TKM-080301	lipid nanoparticle	siRNA	National Institutes of Health Clinical Center	liver cancer[35]	phase I
C-dots	PEG-coated SiO_2		C-dots Development	melanoma[36]	IND approved

4.3. Highly charged drugs

Highly charged drugs, namely DNA, siRNA and microRNA have devoted an important attention by the scientific community just over the past few decades and are expected to serve as a powerful molecular therapy for the treatment of various diseases. These gene therapeutic species are a special class of hydrophilic drugs characterized by their high

densities of charges. These agents have all the previously mentioned characteristics of a hydrophilic drug. In addition, systemic administration of these therapeutics is difficulted by biological barriers such as rapid clearance by the RES and accumulation at filtration organs. Until now, is important to say that sadly, there has been no clinical success in gene therapy. In this regard, in order to get the best of gene therapeutics there is still a lot of work to do in the design of the adequate nanocarriers. The loading and delivery of gene drugs currently rely on preclinical studies using electrostatic interactions and encapsulation in charged carriers and hydrophilic nanocontainers, respectively. As nucleic acids are usually negatively charged under physiological conditions, loading efficiency is usually accomplished by using positively charged carriers, with cationic shells that allow the selective release by pH changes upon cell internalization and efficient transfection[91–96].

5. Intracellular delivery

Understanding the *in vitro* delivery of NPs is a critical initial step toward their successful application. On the one hand, to serve as a drug carrier, NPs must be first evaluated *in vitro* at the cellular level before further testing *in vivo* at the tissue, organ, and body levels. On the other hand, only with sufficient knowledge of NP–cell interactions can the properties of NPs be engineered for optimal delivery *in vivo* and effective cancer therapy[97].

Whenever a NP encounters a cell, it is rapidly internalized through endocytosis. Afterwards, it is transferred to various organelles, including endosomes, lysosomes, Golgi apparatus, mitochondria, endoplasmic reticulum (ER), and nucleus. During intracellular transport, the PU NP has to be degraded or disassembled to allow for quick release of its cargo[18,74,98]. Here we focus only on the major steps involved in the *in vitro* delivery of a polymeric NPs.

5.1. Endocytosis

To drive a NP into an intracellular target and produce a therapeutic effect, it must first cross the amphiphilic cell membrane. This movement is a partly thermodynamic process and is produced by the internalization of the system by engulfment. This internalization can be achieved selectively, whereby a cell-interacting moiety is located at the surface of the NP shell, or non-selectively, whereby internalization is achieved by diffusion. In addition, the following internalization routes have been described on the basis of NP

size: 1) clathrin-mediated endocytosis (also known as receptor-mediated endocytosis), which involves the self-cave-in of the cell membrane region containing the receptors specific to the cargos being internalized in order to form vesicles (about 100 nm in size)[99]; 2) caveolae-mediated endocytosis, which drives extracellular compounds into the cell after binding to specific receptors in caveolae, which are flask-shaped pits (ca. 50 nm in size) in the cell membrane that are present on the surface of many, but not all, types of cells[100]; 3) pinocytosis (also known as cell drinking), a process that begins with the formation of a pocket through the erosion of the cell membrane in a irregular region; the pocket is subsequently englobed into the cell to generate a vesicle (0.5–5 μm in size) that is non-specifically filled with a large volume of extracellular fluid, together with substances and small particles present in the fluid; and 4) phagocytosis, a process by which cells actively bind to and internalize particles larger than about 250 nm in diameter, such as small dust particles, cell debris, microorganisms, and even apoptotic cells. The last two processes involve the uptake of much larger areas of cell membrane than the clathrin- and caveolae-mediated pathways. While pinocytosis can occur in all types of cells, phagocytosis can be performed only by a small set of specialized mammalian cells, such as macrophages, monocytes, and neutrophils.

The internalization pathway of NPs in a specific cell type, is largely determined size and surface properties (HLB, morphology, the sign/density of charge, and the amount of a ligand). While large particles are internalized through phagocytosis and pinocytosis, small particles rely on clathrin- and caveolae-mediated (or occasionally, independent of clathrin and caveolae) pathways (Figure 12). The geometry or aspect of NPs is another factor affecting the mode of cellular uptake.
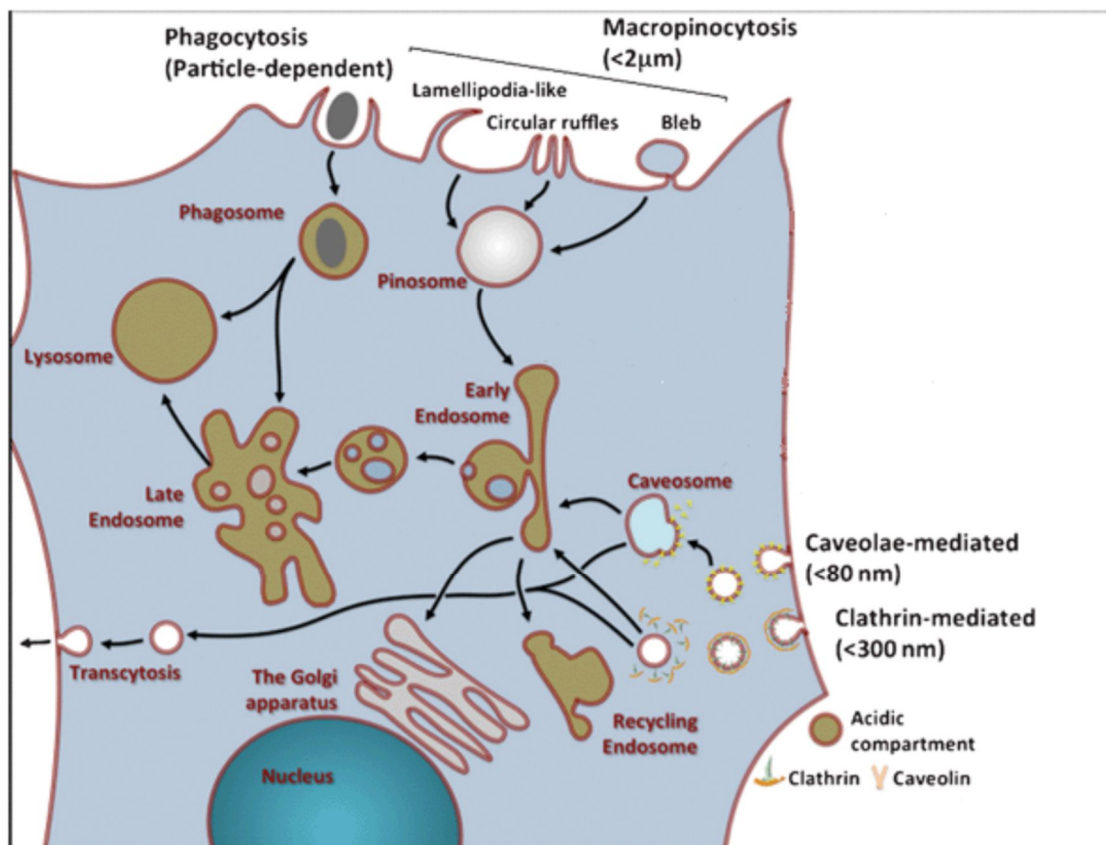
Figure 12. Typical endocytic internalization pathways of nanoparticles. Adapted from reference[101] with permission from The Royal Society of Chemistry.

5.2. Intracellular Transport

After endocytosis, the NPs enveloped by different types of vesicles are transported by the endolysosomal process to other organelles or sometimes are even exocytosed (excretion from the cell). The intracellular trafficking of NPs is a highly complex process that involves motor proteins and the microtubule network that drive the NP all along cell organelles and determine the therapeutic efficiency of the embedded drug or biomolecule (Figure 13). In order to achieve the desired efficiency of a nanocarried bioactive agent, a part from increasing the overall cellular uptake, an interesting approach would be to better drive the uptaken NP into the desired intracellular target. In this regard few work has been reported on enhancement of the intracellular transport to its intracellular target[102,103]. In our group great efforts have been put to ensure the receptor mediated endocytosis of PUUa NPs via integrin receptors and the subsequent endolysosomal localization and escape to deliver the fluorescent encapsulated molecules inside the cytosol[57,104].
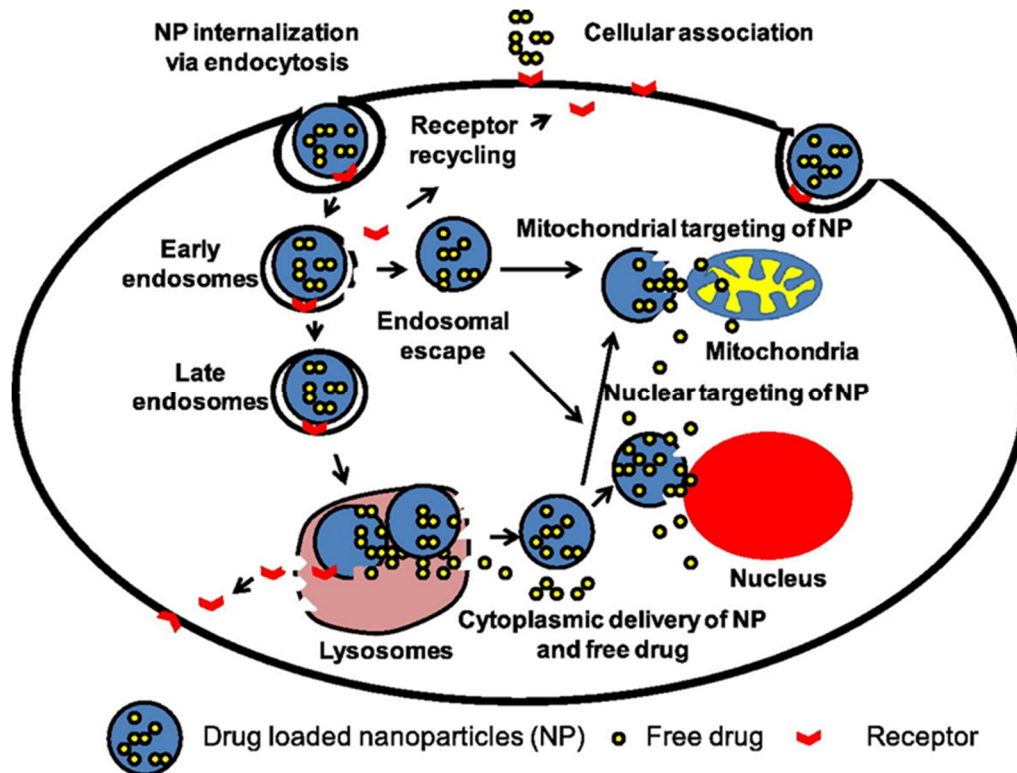
Figure 13. Receptor mediated endocytosis and intracellular transport of cell-targeted NPs. Reprinted from Biswas *et al.*[105], with permission from Elsevier

5.3. Intracellular Escape and Degradation of Nanoparticles

To achieve the delivery of therapeutic agents, NPs must also be designed with an ability to escape the endolysosomal network, to enter the cytosol, which is the typical site of action for most drugs, and to escape from the cell. Multiple methodologies have been applied to achieve this. For example, Cherng's group developed a cationic a poly(ester–co–urethane) bearing short chain polyethyleneimine nanomicelles which showed low cytotoxicity, high biodegradability, and high efficiency to deliver DNA to the cell nucleous as seen from their large transfecting efficiency of COS-7 cells[95]. The same group reported the effect of smaller particle size, hydrophilicity, cytotoxicity and degradability, on the transfection ability of PU nanomicelles bearing different amine-rich side-chains. They observed that the side-chain bearing a tertiary amino group was the best balanced in terms of cytotoxicity, transfection ability and hydrophilicity[92]. It has been reported that polymers containing free amine groups exhibit buffering capacity between pH 5.2–7.0 that facilitates endosomal escape through the "proton-sponge effect". Usually, once contained in the low pH endolysosomal compartment, the amino groups work as proton-sequestering agents from the cytosol through the proton pump, leading to accumulation of water molecules inside the compartment. This accumulation inside the endolysosme

is likely to result into the rupture of the endolysosome. Although the endocytosis process and mechanisms of nanoparticles has been deeply studied by many research groups, the exocytosis mechanisms involving polymeric nanoparticles has been much more superficially explored (Figure 14). It is very likely that the toxicity issues, accumulation in filtration organs and further systemic elimination of nanoparticles upon administration are closely related with the exocytosis process of NPs from MPS. Therefore, to achieve more reliable results to confidently move from *in vitro to* preclinical phases and clinical trials a considerable amount of investigations are still lacking in this aspect. In this regard, Fréchet's group performed a series of experiments to prove not only the exocytosis a fully intracellularly acid-degradable microparticles as vaccines but also the non-cytotoxic behavior of the degradation monomers in macrophages[106,107].
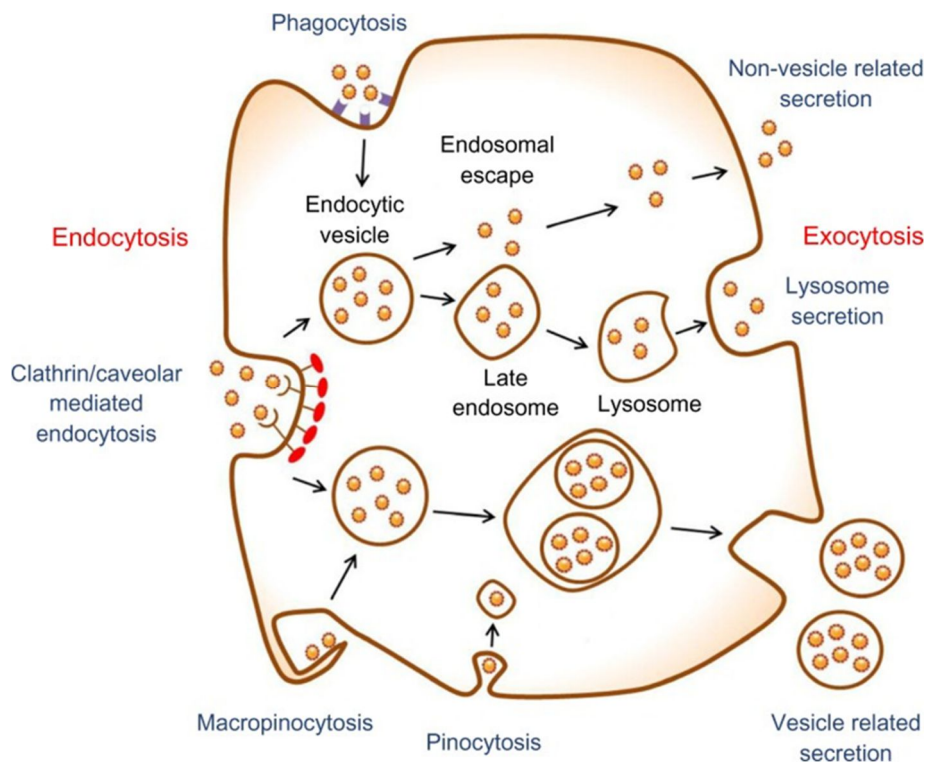
Figure 14. Exocytosis mechanisms from the diverse endocytic pathways. Adapted with permission from reference[108].

6. Passive and active targeting

6.1. Passive targeting

Over 30 years ago, some researchers envisaged that certain macromolecules accumulate preferentially in tumor tissues, as shown for poly(Styrene-*co*-Maleic Acid)-

NeoCarzinoStatin (SMANCS). This preferential distribution in tumors was rationally explained by the leaky tumor blood vessels and by the poor lymphatic drainage in the tissue. These two phenomena lead to the well-known enhanced permeation and retention effect (EPR). Since then, many scientists have used the EPR effect to achieve the efficient delivery of anticancer drugs to tumors, either using polymer prodrugs, micelles, or NPs.

The EPR effect enables NP drug carriers to extravasate from the hyperpermeable tumor blood vessels and accumulate within the tumor tissues[109,110]. Hence, long blood circulating nanocarriers have a greater chance of reaching the tumor site. Subsequently, they accumulate predominantly in the tumors than in healthy tissues, thereby releasing larger amounts of their cargo specifically into cancer cells, thus allowing a more efficient anticancer therapy with minimum drug toxicity. However, the EPR effect has been shown to be variable and specific for each type of cancer. Therefore, the designation of the EPR as a simple extrapolable phenomenon for all tumor microenvironments should be updated accordingly[40].

6.1.1. The EPR effect basis

When a solid tumor reaches 150-200 µm, the normal vasculature surrounding it is not able to provide all the oxygen needed for its growth. Thus, cells start to die, expressing and further secreting growth factors that promote the biosynthesis of new blood vessels from close capillaries. This process, known as angiogenesis, leads to new, irregular blood vessels that present fenestrations in the epithelium and lack the basal membrane of normal vascular structures. Depending on the tumor, the resulting fenestrations can range from 0.2 to 2 µm. Therefore, when any macromolecule larger than 4 nm reaches these abnormal vessels, the fenestrations offer little resistance to extravasation to the tumor interstitium. This feature represents the enhanced permeation component of the EPR effect[109].

In addition, in tumors, the lymphatic function is defective, resulting in minimal uptake of the interstitial fluid. This scenario implies minimal drainage and the accumulation of extravasated compounds. Although molecules smaller than 4 nm are able to drain and return to blood circulation, the recirculation of NPs over 4 nm is hindered by their larger hydrodynamic radius. Therefore, NPs that have reached the interstititum are not cleared efficiently and they accumulate in the tumor interstitium. This feature represents the enhanced retention component of the EPR effect[109].

Current understanding of the EPR effect is much greater than that of Matsumura and Maeda in the mid-1980s[111–113]. This effect has been studied in depth and unraveled using multiple tumor types and animal models. For example, it is now recognized that

lymphatic drainage is not homogenous throughout the tumor. This implies that inner vessels are subjected to higher mechanical stress, and therefore their functionality is much lower and slightly different to that in exposed cancerous cells. Such heterogeneity of lymphatic function in the tumor, the opsonin protein corona formation during blood circulation and solid tumor cells compaction are key factors that affect the efficacy and efficiency of cancer nanomedicines in preclinical and clinical trials (Figure 15).
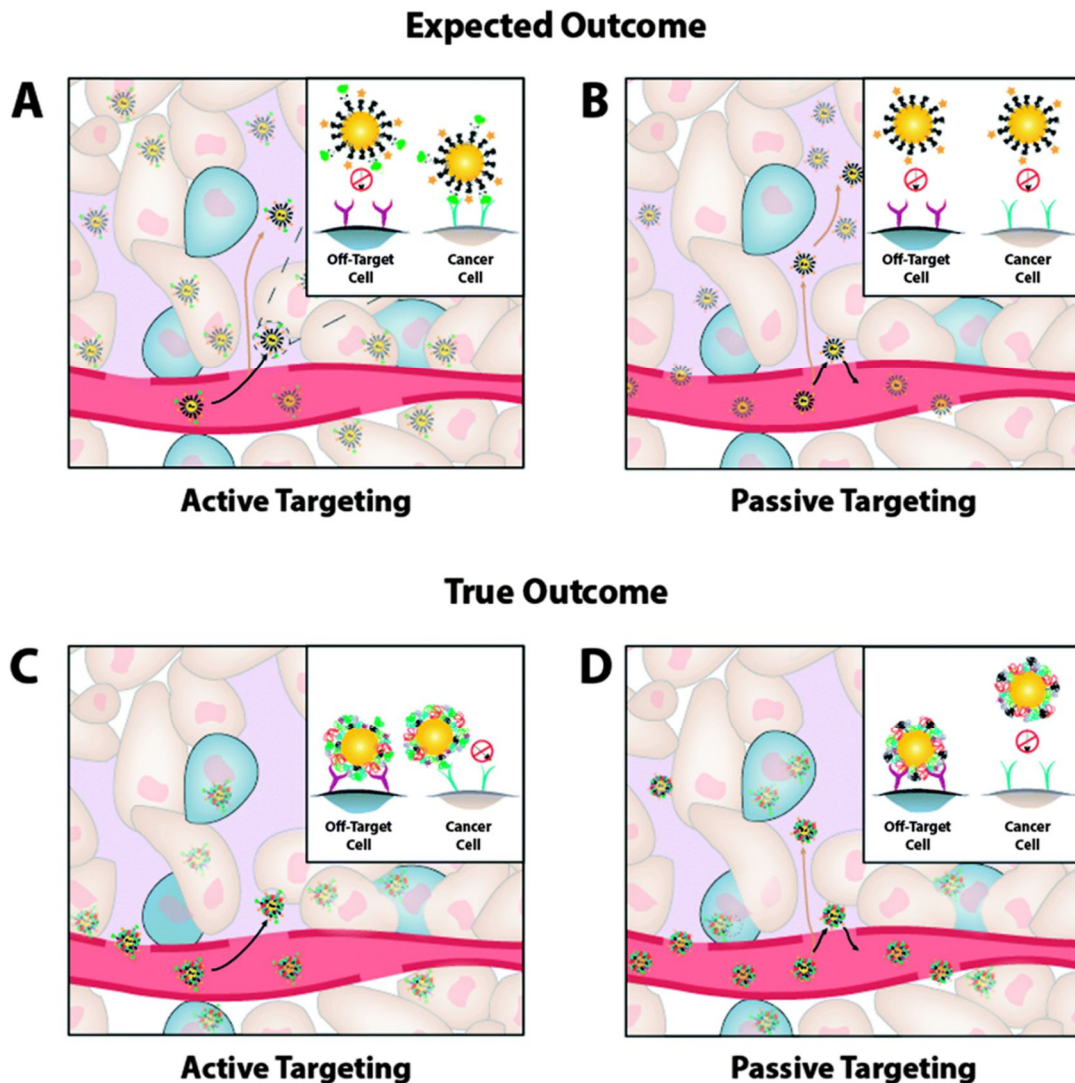
Figure 15. Ideal versus reality in nanoparticle-tumour targeting strategies. In tumours, the unique fenestrated vasculature facilitates nanoparticle extravasation from the blood and into the interstitium. The poor lymphatic drainage and high intratumoural pressure help retain the nanoparticles within the mass (EPR effect). In an ideal situation (*e.g. in vitro*) without nanoparticle–blood interactions: (a) nanoparticles are surface-functionalized with ligands, bind to cell surface receptors and undergo receptor mediated endocytosis for selective entry. b) Nanoparticles are coated with PEG to increase half-life, and provide greater opportunity to extravasate through leaky tumour endothelium and penetrate into the tumour. The true nanoparticle–blood interactions *in vivo* are very different. c) Protein corona formation sterically hinders and masks surface bound ligands, limits cancer cell receptor-mediated interactions and supports off-target cell binding (indicated by blue cells). d) Nanoparticles increase in size and limits their depth of penentration into the

tumour (i.e, the particles are more likely to stay near the vessel). Of note, the green and orange structures on nanoparticle surface in (A) and (B) represents a targeting ligand and cancer agent. Adapted from reference[40] with permission from the Royal Society of Chemistry.

6.2. Active targeting

Targeted nanomedicines are drug delivery nanosystems, usually NPs, loaded with therapeutic and/or imaging agents and exhibiting a targeting compound either physisorbed or chemically bound on their shell surface. To promote the specific interaction of NPs with cells overexpressing the receptor of interest, this targeting moiety can be a protein or antibody, a small molecule (e.g. peptide), carbohydrates (e.g. mannose) or a nucleic acid sequence. Usually, four requirements are fundamental to ensure effectively targeted nanomedicine:

- Eluding opsonisation and clearance by RES system, thereby allowing sufficiently long circulation in the organism
- Retention in target tissue
- Specific interaction between the targeting moiety and the tumor cell receptor
- Release of therapeutic and/or imaging agent at the targeted site

In addition, physicochemical properties like the ligand density, the size of the NPs and the choice of the targeting ligand might also affect the efficacy of the active targeting strategy *in vitro* and, more importantly *in vivo*.

The major difference with passively targeted nanomedicines is that passive ones make use of biological mechanisms to reach specific organs or disease sites such as phagocytosis by the cells of the reticuloendothelial system (RES) or the EPR effect observed for example in tumors with leaky vasculature REF.

7. Holistic considerations on therapy with polymer nanoparticles

There is commonly an erroneous tendency to believe that nanomedicines are able to, for example, kill any type of tumor or eradicate bacterial infections located in any body tissue. Sadly, this vision can lead to interpret nanotechnologies as a "one-for-all" remedy and even turn them into another bubble[114]. Like any other branch of science, the release of drugs in a controlled manner using polymer nanotechnology is a field involving multiple factors. This holistic view applied to nanomedicine aims to take into account the engineering of new high-throughput synthetic methodologies, the route of administration, the molecular composition of the nanosystem, the coordination with human temporal

cycles, and required adjustment of the safety measures and ethical regulations to reduce the hurdles in the translation of smart polymeric NPs from preclinical studies to clinical practice.

There is a great demand for the application of novel raw materials to produce polymeric nanomaterials in high purities, with minimal purification steps and using a green chemistry. The commercial availability of precursors and the straightforward scale-up of the final product are key aspects for the translation of lab nanosystems to day-by-day use of nanomedicines.

In many cases, it is also important to update whether the route of administration for a specific drug delivery system is selected on a rational basis. Active targeting by intravenous delivery is sometimes overestimated, and alternative administration routes for the same target may bring about better prospects for efficient delivery to the desired tissue. Moreover, instead of focusing attention on which bioactive targeting molecule is attached, it should be placed on how the physicochemical properties of the NP and the surrounding of the target tissue interact and modify either the drug delivery rate, the targeting efficiency, or the cytotoxicity. For example, pharmacokinetic studies performed for a specific controlled drug release nanosystem should be performed in accordance with the drug release profile observed under *in vivo*-like conditions. Whether the system releases the 100% of the drug in 6 hours or in 6 days will of course affect the pharmacokinetics, which should be designed adequately.

Specific and efficacious molecular targeting will be successful only when all the factors affecting it are thoroughly reviewed when engineering a nanosystem for *in vivo* delivery. Among the factors affecting targeting specificity, the most visible is perhaps the unintentional NP uptake observed in biodistribution experiments. In order to potentially solve such issues, NP morphology, such as size, shape, charge and cell-specific uptake, should be previously analyzed *in vitro* by modulating polymeric physicochemical properties such as crosslinking degree, HLB value, amphiphilic or amphoteric behavior, etc. and studying their contribution to uptake specificity in multicellular systems. The protein corona formation around the shell of a NP upon incubation in serum protein-rich environments has been demonstrated to cause undesired receptor-mediated uptake as well as an active distortion of the receptor-targeting molecule specific interaction. Several efforts have been therefore been channeled into coating NPs with stealth polymers to minimize physisorption of circulating proteins that promote sequestration by the RES[41]. Specific active targeting is also hampered by the non-tissue-unique overexpression of the molecular target. This is that the specific receptor turns out not to be so tissue-specific therefore leading to specific targeting but not only in diseased cells. A possible solution might be the local delivery of the nanosystem.

Long circulation is mandatory to achieve drug accumulation in the diseased tissue. Highly ligand-functionalized shells often cause increased immunogenicity and reduced circulation times, which should be appropriately addressed by modulating the amount of ligand to achieve minimal immuno-response and maximal cell specificity. Finally, the intracellular target on which the drug is intended to act needs to be reached. For example, if a NP is engineered to release its cargo upon interaction with cytosolic glutathione, the ability of the NP to escape the endosome-lysosome should be demonstrated accordingly by adequate methodologies (small enough NPs, changing amphiphilic surface, functionalization with a cell-penetrating peptide to enter the cytosol, etc.).

In the last fifteen years, chronopharmacological aspects of drug delivery systems have been addressed to increase patient compliance and drug efficacy. In the changing scenario of nanomedicines, drug delivery systems with sustained release became obsolete and modern smart self-controlled DDS emerged. Chronopharmaceutics serve to generate knowledge ranging from the biology of disease to the generation of models capable of designing and evaluating DDSs that meet biological circadian requirements. In this regard, modeling approaches are available in the broad fields of cardiovascular diseases, cancer chemotherapy, rheumatoid arthritis, and diabetes, among others. For example, it has been proved that the plasmatic levels of certain proteins involved in the pain suffered by arthritic patients are subject to a circadian rhythm. In this regard, drugs currently used to treat this pain show statistically significant differences in toxicity and efficacy depending on the time of the day they are administered.

Finally, the huge impact of nanoscience on today's society must be accompanied by adjusted safety measures and ethical regulations. In order to maximize the social and therapeutic benefits of nanomedicine and reduce the potential health hazards for human beings, regulatory systems should join forces and evaluate whether appropriate scientific and media infrastructures are available to provide regulatory and ethical guidelines for the safe development of nanotechnologies. Moreover, a special focus should be placed on informing society about the potential applications of nanotechnology, as well as its pros and cons, as a true alternative to classical medicine and on maintaining public funding in order to advance in this field.

In summary, PU and polyurea NPs emerge as suitable platforms to be manufactured in a high-throughput fashion, at industrial level, and using eco-friendly synthetic methods. Moreover, they allow the delivery of a wide range of drugs and can be rapidly adaptable to many clinical requirements. Furthermore, the ease with which the degradation of PUUa NPs can be controlled ensures the control over temporal aspects of drug delivery compared to other nanosystems. This diversity of potential applications renders PUUa

NPs attractive therapeutic delivery vehicles. However, to prevent failure and false hope, this diversity must be correlated with adequate safety and ethical guidelines for each new NP formulation developed.

References

1. Kamaly, N.; Xiao, Z.; Valencia, P. M.; Radovic-Moreno, A. F.; Farokhzad, O. C. Targeted polymeric therapeutic nanoparticles: design, development and clinical translation. *Chem. Soc. Rev.* **2012**, *41*, 2971–3010.

2. Ding, M.; Zhou, L.; Fu, X.; Tan, H.; Li, J.; Fu, Q. Biodegradable gemini multiblock poly(ε-caprolactone urethane)s toward controllable micellization. *Soft Matter* **2010**, *6*, 2087.

3. Ding, M.; Li, J.; Fu, X.; Zhou, J.; Tan, H.; Gu, Q.; Fu, Q. Synthesis, degradation, and cytotoxicity of multiblock poly(epsilon-caprolactone urethane)s containing gemini quaternary ammonium cationic groups. *Biomacromolecules* **2009**, *10*, 2857–65.

4. Jiang, X.; Li, J.; Ding, M.; Tan, H.; Ling, Q.; Zhong, Y.; Fu, Q. Synthesis and degradation of nontoxic biodegradable waterborne polyurethanes elastomer with poly(ε-caprolactone) and poly(ethylene glycol) as soft segment. *Eur. Polym. J.* **2007**, *43*, 1838–1846.

5. Jiang, X.; Yu, F.; Wang, Z.; Li, J.; Tan, H.; Ding, M.; Fu, Q. Fabrication and characterization of waterborne biodegradable polyurethanes 3-dimensional porous scaffolds for vascular tissue engineering. *J. Biomater. Sci. Polym. Ed.* **2010**, *21*, 1637–52.

6. Yang, C.; Ni, X.; Li, J. New thermogelling copolymers composed of heptakis(2,6-di-O-methyl)-β-cyclodextrin, poly(propylene glycol), and poly(ethylene glycol). *J. Mater. Chem.* **2009**, *19*, 3755.

7. Zhang, J.; Wu, M.; Yang, J.; Wu, Q.; Jin, Z. Anionic poly (lactic acid)-polyurethane micelles as potential biodegradable drug delivery carriers. *Colloids Surfaces A Physicochem. Eng. Asp.* **2009**, *337*, 200–204.

8. Brooks, B.; Brooks, A.; Grainger, D. Antimicrobial Medical Devices in Preclinical Development and Clinical Use. In *Biomaterials Associated Infection SE - 13*; Moriarty, T. F.; Zaat, S. A. J.; Busscher, H. J., Eds.; Springer New York, 2013; pp. 307–354.

9. Budnik, L. T.; Nowak, D.; Merget, R.; Lemiere, C.; Baur, X. Elimination kinetics of diisocyanates after specific inhalative challenges in humans: mass spectrometry analysis, as a basis for biomonitoring strategies. *J. Occup. Med. Toxicol.* **2011**, *6*, 9.

10. Diisocyanates toxicology http://www.epa.gov/oppt/auto/profile/toxicology1a.pdf (accessed May 7, 2015).

11. Tatiya, P. D.; Hedaoo, R. K.; Mahulikar, P. P.; Gite, V. V. Novel Polyurea Microcapsules Using Dendritic Functional Monomer: Synthesis, Characterization, and Its Use in Self-healing and Anticorrosive Polyurethane Coatings. *Ind. Eng. Chem. Res.* **2013**, *52*, 1562–1570.

12. Griffiths, G.; Nyström, B.; Sable, S. B.; Khuller, G. K. Nanobead-based interventions for the treatment and prevention of tuberculosis. *Nat Rev Micro* **2010**, *8*, 827–834.

13. Landfester, K.; Musyanovych, A.; Mailänder, V. From polymeric particles to multifunctional nanocapsules for biomedical applications using the miniemulsion process. *J. Polym. Sci. Part A Polym. Chem.* **2010**, *48*, 493–515.

14. Landfester, K. Miniemulsion Polymerization and the Structure of Polymer and Hybrid Nanoparticles. *Angew. Chemie Int. Ed.* **2009**, *48*, 4488–4507.

15. Jain, R. A. The manufacturing techniques of various drug loaded biodegradable poly(lactide-co-glycolide) (PLGA) devices. *Biomaterials* **2000**, *21*, 2475–2490.

16. Wang, Y.; Wu, G.; Li, X.; Chen, J.; Wang, Y.; Ma, J. Temperature-triggered redox-degradable poly(ether urethane) nanoparticles for controlled drug delivery. *J. Mater. Chem.* **2012**, *22*, 25217.

17. Ou, C.-W.; Su, C.-H.; Jeng, U.-S.; Hsu, S. Characterization of biodegradable polyurethane nanoparticles and thermally induced self-assembly in water dispersion. *ACS Appl. Mater. Interfaces* **2014**, *6*, 5685–94.

18. Ding, M.; Zeng, X.; He, X.; Li, J.; Tan, H.; Fu, Q. Cell internalizable and intracellularly degradable cationic polyurethane micelles as a potential platform for efficient imaging and drug delivery. *Biomacromolecules* **2014**, *15*, 2896–906.

19. Zhou, L.; Yu, L.; Ding, M.; Li, J.; Tan, H.; Wang, Z.; Fu, Q. Synthesis and Characterization of pH-Sensitive Biodegradable Polyurethane for Potential Drug Delivery Applications. *Macromolecules* **2011**, *44*, 857–864.

20. Yu, S.; He, C.; Ding, J.; Cheng, Y.; Song, W.; Zhuang, X.; Chen, X. pH and reduction dual responsive polyurethane triblock copolymers for efficient intracellular drug delivery. *Soft Matter* **2013**, *9*, 2637.

21. Yu, S.; Ding, J.; He, C.; Cao, Y.; Xu, W.; Chen, X. Disulfide cross-linked polyurethane micelles as a reduction-triggered drug delivery system for cancer therapy. *Adv. Healthc. Mater.* **2014**, *3*, 752–60.

22. Ding, M.; Song, N.; He, X.; Li, J.; Zhou, L.; Tan, H.; Fu, Q.; Gu, Q. Toward the next-generation nanomedicines: design of multifunctional multiblock polyurethanes for effective cancer treatment. *ACS Nano* **2013**, *7*, 1918–28.

23. Morral-Ruíz, G.; Melgar-Lesmes, P.; García, M. L.; Solans, C.; García-Celma, M. J. Design of biocompatible surface-modified polyurethane and polyurea nanoparticles. *Polymer (Guildf).* **2012**, *53*, 6072–6080.

24. Cass, P.; Knower, W.; Hinton, T.; Shi, S.; Grusche, F.; Tizard, M.; Gunatillake, P. Synthesis and evaluation of degradable polyurea block copolymers as siRNA delivery agents. *Acta Biomater.* **2013**, *9*, 8299–307.

25. Polyisocyanate/polyamine mixtures and their use for the production of polyurea coatings 1996.

26. Giraud, S.; Bourbigot, S.; Rochery, M.; Vroman, I.; Tighzert, L.; Delobel, R.; Poutch, F. Flame retarded polyurea with microencapsulated ammonium phosphate for textile coating. *Polym. Degrad. Stab.* **2005**, *88*, 106–113.

27. Morral-Ruíz, G.; Melgar-Lesmes, P.; López-Vicente, A.; Solans, C.; García-Celma, M. J. Biotinylated polyurethane-urea nanoparticles for targeted theranostics in human hepatocellular carcinoma. *Nano Res.* **2015**.

28. Morral-Ruíz, G.; Solans, C.; García, M. L.; García-Celma, M. J. Formation of Pegylated polyurethane and Lysine-coated polyurea nanoparticles obtained from O/W nano-emulsions. *Langmuir* **2012**, *28*, 6256–64.

29. Locatelli, P.; Woutters, S.; Lindsay, C.; Schroeder, S. L. M.; Hobdell, J. H.; Saiani,

A. Synthesis of polyurea–polyether nanoparticles via spontaneous nanoprecipitation. *RSC Adv.* **2015**, *5*, 41668–41676.

30. Morral-Ruíz, G.; Melgar-Lesmes, P.; Solans, C.; García-Celma, M. J. Multifunctional polyurethane-urea nanoparticles to target and arrest inflamed vascular environment: a potential tool for cancer therapy and diagnosis. *J. Control. Release* **2013**, *171*, 163–71.

31. Bhunia, S.; Chatterjee, N.; Das, S.; Das Saha, K.; Bhaumik, A. Porous polyurea network showing aggregation induced white light emission, applications as biosensor and scaffold for drug delivery. *ACS Appl. Mater. Interfaces* **2014**, *6*, 22569–76.

32. Svenson, S. The dendrimer paradox – high medical expectations but poor clinical translation. *Chem. Soc. Rev.* **2015**, *44*, 4131–4144.

33. Veerapandian, S.; Nasar, A. S. Amine- and blocked isocyanate-terminated polyurethane dendrimers: integrated synthesis, photophysical properties and application in a heat curable system. *RSC Adv.* **2015**, *5*, 3799–3806.

34. Veerapandian, S.; Sultan Nasar, A. Successful synthesis of distinct dendritic unimolecular initiators suitable for topologically attractive star polymers. *RSC Adv.* **2015**, *5*, 23034–23038.

35. Feast, W. J.; Rannard, S. P.; Stoddart, A. Selective Convergent Synthesis of Aliphatic Polyurethane Dendrimers. *Macromolecules* **2003**, *36*, 9704–9706.

36. Kojima, C.; Kono, K.; Maruyama, K.; Takagishi, T. Synthesis of Polyamidoamine Dendrimers Having Poly(ethylene glycol) Grafts and Their Ability To Encapsulate Anticancer Drugs. *Bioconjug. Chem.* **2000**, *11*, 910–917.

37. Matsumoto, N. M.; González-Toro, D. C.; Chacko, R. T.; Maynard, H. D.; Thayumanavan, S. Synthesis of Nanogel-Protein Conjugates. *Polym. Chem.* **2013**, *4*, 2464–2469.

38. Li, X.; Wang, Y.; Chen, J.; Wang, Y.; Ma, J.; Wu, G. Controlled release of protein from biodegradable multi-sensitive injectable poly(ether-urethane) hydrogel. *ACS Appl. Mater. Interfaces* **2014**, *6*, 3640–7.

39. Hsieh, F.-Y.; Lin, H.-H.; Hsu, S.-H. 3D bioprinting of neural stem cell-laden thermoresponsive biodegradable polyurethane hydrogel and potential in central nervous system repair. *Biomaterials* **2015**, *71*, 48–57.

40. Lazarovits, J.; Chen, Y. Y.; Sykes, E. A.; Chan, W. C. W. Nanoparticle–blood interactions: the implications on solid tumour targeting. *Chem. Commun.* **2015**, *51*, 2756–2767.

41. Kang, B.; Okwieka, P.; Schöttler, S.; Winzen, S.; Langhanki, J.; Mohr, K.; Opatz, T.; Mailänder, V.; Landfester, K.; Wurm, F. R. Carbohydrate-Based Nanocarriers Exhibiting Specific Cell Targeting with Minimum Influence from the Protein Corona. *Angew. Chemie Int. Ed.* **2015**, n/a–n/a.

42. Siqueira, G.; Bras, J.; Dufresne, A. New process of chemical grafting of cellulose nanoparticles with a long chain isocyanate. *Langmuir* **2010**, *26*, 402–11.

43. Yan, X.; Delgado, M.; Fu, A.; Alcouffe, P.; Gouin, S. G.; Fleury, E.; Katz, J. L.; Ganachaud, F.; Bernard, J. Simple but precise engineering of functional nanocapsules through nanoprecipitation. *Angew. Chem. Int. Ed. Engl.* **2014**, *53*, 6910–3.

44. Hamilton, H. J. A THERMODYNAMIC THEORY OF THE ORIGIN AND HIERARCHICAL EVOLUTION OF LIVING SYSTEMS. *Zygon�* **1977**, *12*, 289–335.

45. Tanford, C. The hydrophobic effect and the organization of living matter. *Science*

(80-.). **1978**, *200*, 1012–1018.

46. Muller, N. Search for a realistic view of hydrophobic effects. *Acc. Chem. Res.* **1990**, *23*, 23–28.

47. Félix, O.; Zheng, Z.; Cousin, F.; Decher, G. Are sprayed LbL-films stratified? A first assessment of the nanostructure of spray-assembled multilayers by neutron reflectometry. *Comptes Rendus Chim.* **2009**, *12*, 225–234.

48. Chandler, D. Interfaces and the driving force of hydrophobic assembly. *Nature* **2005**, *437*, 640–647.

49. Urban, M. W. Stimuli-responsive colloids: From stratified to self-repairing Polymeric Films and Beyond. *Curr. Opin. Colloid Interface Sci.* **2014**, *19*, 66–75.

50. Urban, M. W. Stratification, stimuli-responsiveness, self-healing, and signaling in polymer networks. *Prog. Polym. Sci.* **2009**, *34*, 679–687.

51. Maibaum, L.; Dinner, A. R.; Chandler, D. Micelle Formation and the Hydrophobic Effect †. *J. Phys. Chem. B* **2004**, *108*, 6778–6781.

52. Owen, S. C.; Chan, D. P. Y.; Shoichet, M. S. Polymeric micelle stability. *Nano Today* **2012**, *7*, 53–65.

53. Garbuzenko, O.; Barenholz, Y.; Priev, A. Effect of grafted PEG on liposome size and on compressibility and packing of lipid bilayer. *Chem. Phys. Lipids* **2005**, *135*, 117–29.

54. Chen, H.; Kim, S.; Li, L.; Wang, S.; Park, K.; Cheng, J.-X. Release of hydrophobic molecules from polymer micelles into cell membranes revealed by Förster resonance energy transfer imaging. *Proc. Natl. Acad. Sci.* **2008**, *105* , 6596–6601.

55. Zou, P.; Chen, H.; Paholak, H. J.; Sun, D. Noninvasive fluorescence resonance energy transfer imaging of in vivo premature drug release from polymeric nanoparticles. *Mol. Pharm.* **2013**, *10*, 4185–94.

56. Rocas Alonso, P.; Rocas Sorolla, J. Method for producing a microencapsulate and corresponding reactive amphiphilic compound, microencapsulate and composition. 2014, Ecopol Tech, S.L.

57. Rocas, P.; Fernández, Y.; Schwartz, S.; Abasolo, I.; Rocas, J.; Albericio, F. Multifunctionalized polyurethane–polyurea nanoparticles: hydrophobically driven self-stratification at the o/w interface modulates encapsulation stability. *J. Mater. Chem. B* **2015**, *3*, 7604–7613.

58. De Koker, S.; Hoogenboom, R.; De Geest, B. G. Polymeric multilayer capsules for drug delivery. *Chem. Soc. Rev.* **2012**, *41*, 2867–84.

59. Richardson, J. J.; Bjornmalm, M.; Caruso, F. Technology-driven layer-by-layer assembly of nanofilms. *Science (80-.).* **2015**, *348*, aaa2491–aaa2491.

60. Hosta-Rigau, L.; Städler, B.; Yan, Y.; Nice, E. C.; Heath, J. K.; Albericio, F.; Caruso, F. Capsosomes with Multilayered Subcompartments: Assembly and Loading with Hydrophobic Cargo. *Adv. Funct. Mater.* **2010**, *20*, 59–66.

61. Yan, Y.; Björnmalm, M.; Caruso, F. Assembly of Layer-by-Layer Particles and Their Interactions with Biological Systems. *Chem. Mater.* **2014**, *26*, 452–460.

62. Innominato, P. F.; Roche, V. P.; Palesh, O. G.; Ulusakarya, A.; Spiegel, D.; Lévi, F. A. The circadian timing system in clinical oncology. *Ann. Med.* **2014**, *46*, 191–207.

63. Cheng, R.; Feng, F.; Meng, F.; Deng, C.; Feijen, J.; Zhong, Z. Glutathione-responsive nano-vehicles as a promising platform for targeted intracellular drug and

gene delivery. *J. Control. Release* **2011**, *152*, 2–12.

64. Ali, H. Budesonide Loaded pH-sensitive PLGA Nanoparticles for the Treatment of Inflammatory Bowel Disease DISSERTATION zur Erlangung des Grades. **2013**.

65. Baier, G.; Cavallaro, A.; Vasilev, K.; Mailänder, V.; Musyanovych, A.; Landfester, K. Enzyme responsive hyaluronic Acid nanocapsules containing polyhexanide and their exposure to bacteria to prevent infection. *Biomacromolecules* **2013**, *14*, 1103–12.

66. Rosenbauer, E.-M.; Wagner, M.; Musyanovych, A.; Landfester, K. Controlled Release from Polyurethane Nanocapsules via pH-, UV-Light- or Temperature-Induced Stimuli. *Macromolecules* **2010**, *43*, 5083–5093.

67. Fleige, E.; Quadir, M. A.; Haag, R. Stimuli-responsive polymeric nanocarriers for the controlled transport of active compounds: concepts and applications. *Adv. Drug Deliv. Rev.* **2012**, *64*, 866–84.

68. Schmitt, S.; Silvestre, M.; Tsotsalas, M.; Winkler, A.; Shahnas, A.; Grosjean, S.; Laye, F.; Gliemann, H.; Lahann, J.; Bräse, S.; Franzreb, M.; Wöll, C. Hierarchically Functionalized Magnetic Core / Multi- Shell Particles and their Post-Synthetic Conversion to Polymer Capsules. **2015**.

69. Lai, J.; Shah, B. P.; Garfunkel, E.; Lee, K.-B. Versatile fluorescence resonance energy transfer-based mesoporous silica nanoparticles for real-time monitoring of drug release. *ACS Nano* **2013**, *7*, 2741–50.

70. Østergaard, H.; Tachibana, C.; Winther, J. R. Monitoring disulfide bond formation in the eukaryotic cytosol. *J. Cell Biol.* **2004**, *166*, 337–45.

71. Ma, N.; Li, Y.; Xu, H.; Wang, Z.; Zhang, X. Dual redox responsive assemblies formed from diselenide block copolymers. *J. Am. Chem. Soc.* **2010**, *132*, 442–3.

72. Ding, C.; Xu, S.; Wang, J.; Liu, Y.; Hu, X.; Chen, P.; Feng, S. Controlled loading and release of methylene blue from LbL polyurethane/poly(acrylic acid) film. *Polym. Adv. Technol.* **2012**, *23*, 1283–1286.

73. Pardini, F.; Faccia, P.; Amalvy, J. Evaluation of pH-sensitive polyurethane/2-diethylaminoethyl methacrylate hybrids potentially useful for drug delivery developments. *J. Drug Deliv. Sci. Technol.* **2015**.

74. Huang, F.; Cheng, R.; Meng, F.; Deng, C.; Zhong, Z. Micelles Based on Acid Degradable Poly(acetal urethane): Preparation, pH-Sensitivity, and Triggered Intracellular Drug Release. *Biomacromolecules* **2015**, *16*, 2228–36.

75. Hood, M. A.; Paiphansiri, U.; Schaeffel, D.; Koynov, K.; Kappl, M.; Landfester, K.; Muñoz-Espí, R. Hybrid Poly(urethane–urea)/Silica Nanocapsules with pH-Sensitive Gateways. *Chem. Mater.* **2015**, *27*, 4311–4318.

76. Naeem, M.; Kim, W.; Cao, J.; Jung, Y.; Yoo, J.-W. Enzyme/pH dual sensitive polymeric nanoparticles for targeted drug delivery to the inflamed colon. *Colloids Surf. B. Biointerfaces* **2014**, *123*, 271–8.

77. Cohn, D.; Sosnik, A.; Levy, A. Improved reverse thermo-responsive polymeric systems. *Biomaterials* **2003**, *24*, 3707–3714.

78. Cohn, D.; Lando, G.; Sosnik, A.; Garty, S.; Levi, A. PEO-PPO-PEO-based poly(ether ester urethane)s as degradable reverse thermo-responsive multiblock copolymers. *Biomaterials* **2006**, *27*, 1718–27.

79. Lv, C.; Wang, Z.; Wang, P.; Tang, X. Photodegradable Polyurethane Self-Assembled Nanoparticles for Photocontrollable Release. *Langmuir* **2012**, *28*, 9387–9394.

80. Mahkam, M.; Sharifi-Sanjani, N. Preparation of new biodegradable polyurethanes as a therapeutic agent. *Polym. Degrad. Stab.* **2003**, *80*, 199–202.

81. Gonzalo, T.; Lollo, G.; Garcia-Fuentes, M.; Torres, D.; Correa, J.; Riguera, R.; Fernandez-Megia, E.; Calvo, P.; Avilés, P.; Guillén, M. J.; Alonso, M. J. A new potential nano-oncological therapy based on polyamino acid nanocapsules. *J. Control. Release* **2013**, *169*, 10–16.

82. Oliveira, H.; Thevenot, J.; Garanger, E.; Ibarboure, E.; Calvo, P.; Aviles, P.; Guillen, M. J.; Lecommandoux, S. Nano-encapsulation of plitidepsin: in vivo pharmacokinetics, biodistribution, and efficacy in a renal xenograft tumor model. *Pharm. Res.* **2014**, *31*, 983–91.

83. Goñi-de-Cerio, F.; Thevenot, J.; Oliveira, H.; Pérez-Andrés, E.; Berra, E.; Masa, M.; Suárez–merino, B.; Lecommandoux, S.; Heredia, P. Cellular Uptake and Cytotoxic Effect of Epidermal Growth Factor Receptor Targeted and Plitidepsin Loaded Co-Polymeric Polymersomes on Colorectal Cancer Cell Lines. *J. Biomed. Nanotechnol.* **2015**, *11*, 2034–2049.

84. Baier, G.; Musyanovych, A.; Dass, M.; Theisinger, S.; Landfester, K. Cross-linked starch capsules containing dsDNA prepared in inverse miniemulsion as "nanoreactors" for polymerase chain reaction. *Biomacromolecules* **2010**, *11*, 960–8.

85. Paiphansiri, U.; Dausend, J.; Musyanovych, A.; Mailänder, V.; Landfester, K. Fluorescent polyurethane nanocapsules prepared via inverse miniemulsion: surface functionalization for use as biocarriers. *Macromol. Biosci.* **2009**, *9*, 575–84.

86. Baier, G.; Friedemann, K.; Leuschner, E.-M.; Musyanovych, A.; Landfester, K. pH Stability of Poly(urethane/urea) Capsules Synthesized from Different Hydrophilic Monomers via Interfacial Polyaddition in the Inverse Miniemulsion Process. *Macromol. Symp.* **2013**, *331-332*, 71–80.

87. Crespy, D.; Stark, M.; Hoffmann-Richter, C.; Ziener, U.; Landfester, K. Polymeric Nanoreactors for Hydrophilic Reagents Synthesized by Interfacial Polycondensation on Miniemulsion Droplets. *Macromolecules* **2007**, *40*, 3122–3135.

88. Landfester, K.; Mailänder, V. Nanocapsules with specific targeting and release properties using miniemulsion polymerization. *Expert Opin. Drug Deliv.* **2013**, *10*, 593–609.

89. Landfester, K. Miniemulsion Polymerization and the Structure of Polymer and Hybrid Nanoparticles. *Angew. Chemie Int. Ed.* **2009**, *48*, 4488–4507.

90. Sun, T.; Zhang, Y. S.; Pang, B.; Hyun, D. C.; Yang, M.; Xia, Y. Engineered Nanoparticles for Drug Delivery in Cancer Therapy Angewandte. **2014**, 12320–12364.

91. Cherng, J. Y.; Hung, W. C.; Kao, H. C. Blending of polyethylenimine with a cationic polyurethane greatly enhances both DNA delivery efficacy and reduces the overall cytotoxicity. *Curr. Pharm. Biotechnol.* **2011**, *12*, 839–46.

92. Liu, X.-Y.; Ho, W.-Y.; Hung, W. J.; Shau, M.-D. The characteristics and transfection efficiency of cationic poly (ester-co-urethane) - short chain PEI conjugates self-assembled with DNA. *Biomaterials* **2009**, *30*, 6665–73.

93. Tseng, S.; Tang, S.; Shau, M.; Zeng, Y.; Cherng, J.; Shih, M. Structural characterization and buffering capacity in relation to the transfection efficiency of biodegradable polyurethane. *Bioconjug. Chem. 16*, 1375–81.

94. Yang, T.; Chin, W.; Cherng, J.; Shau, M. Synthesis of novel biodegradable cationic polymer: N,N-diethylethylenediamine polyurethane as a gene carrier. *Biomacromolecules 5*, 1926–32.

95. Shau, M.-D.; Tseng, S.-J.; Yang, T.-F.; Cherng, J.-Y.; Chin, W.-K. Effect of molecular weight on the transfection efficiency of novel polyurethane as a biodegradable gene vector. *J. Biomed. Mater. Res. A* **2006**, *77*, 736–46.

96. Baier, G.; Musyanovych, A.; Dass, M.; Theisinger, S.; Landfester, K. Cross-Linked Starch Capsules Containing dsDNA Prepared in Inverse Miniemulsion as " Nanoreactors " for Polymerase Chain Reaction. **2010**, 960–968.

97. Nel, A. E.; Mädler, L.; Velegol, D.; Xia, T.; Hoek, E. M. V; Somasundaran, P.; Klaessig, F.; Castranova, V.; Thompson, M. Understanding biophysicochemical interactions at the nano-bio interface. *Nat. Mater.* **2009**, *8*, 543–57.

98. Bishop, C. J.; Kozielski, K. L.; Green, J. J. Exploring the role of polymer structure on intracellular nucleic acid delivery via polymeric nanoparticles. *J. Control. Release* **2015**, *219*, 488–499.

99. Lee, J. Y.; Choi, D.-Y.; Cho, M. Y.; Park, K. E.; Lee, S.-H.; Hun Cho, S.; Hong, K. S.; Lim, Y. T. Targeted theranostic nanoparticles: receptor-mediated entry into cells, pH-induced signal generation and cytosolic delivery. *Small* **2014**, *10*, 901–6.

100. Rejman, J.; Oberle, V.; Zuhorn, I. S.; Hoekstra, D. Size-dependent internalization of particles via the pathways of clathrin- and caveolae-mediated endocytosis. *Biochem. J.* **2004**, *377*, 159–69.

101. Canton, I.; Battaglia, G. Endocytosis at the nanoscale. *Chem. Soc. Rev.* **2012**, *41*, 2718–39.

102. Cohen, O.; Granek, R. Nucleus-targeted drug delivery: theoretical optimization of nanoparticles decoration for enhanced intracellular active transport. *Nano Lett.* **2014**, *14*, 2515–21.

103. Zaki, N. M.; Tirelli, N. Gateways for the intracellular access of nanocarriers: a review of receptor-mediated endocytosis mechanisms and of strategies in receptor targeting. *Expert Opin. Drug Deliv.* **2010**, *7*, 895–913.

104. Flórez-grau, G.; Rocas, P.; Cabezón, R.; España, C.; Panés, J.; Rocas, J.; Albericio, F.; Benítez-Ribas, D. Nanoencapsulated Budesonide Efficiently Induces the Generation of Human Tolerogenic Dendritic Cells.

105. Biswas, S.; Torchilin, V. P. Nanopreparations for organelle-specific delivery in cancer. *Adv. Drug Deliv. Rev.* **2014**, *66*, 26–41.

106. Bachelder, E. M.; Beaudette, T. T.; Broaders, K. E.; Paramonov, S. E.; Dashe, J.; Fréchet, J. M. J. Acid-Degradable Polyurethane Particles for Protein-Based Vaccines: Biological Evaluation and in Vitro Analysis of Particle Degradation Products. *Mol. Pharm.* **2008**, *5*, 876–884.

107. Paramonov, S. E.; Bachelder, E. M.; Beaudette, T. T.; Standley, S. M.; Lee, C. C.; Dashe, J.; Fréchet, J. M. J. Fully acid-degradable biocompatible polyacetal microparticles for drug delivery. *Bioconjug. Chem.* **2008**, *19*, 911–9.

108. Oh, N.; Park, J.-H. Endocytosis and exocytosis of nanoparticles in mammalian cells. *Int. J. Nanomedicine* **2014**, *9 Suppl 1*, 51–63.

109. Bertrand, N.; Wu, J.; Xu, X.; Kamaly, N.; Farokhzad, O. C. Cancer nanotechnology : The impact of passive and active targeting in the era of modern cancer biology ☆. *Adv. Drug Deliv. Rev.* **2014**, *66*, 2–25.

110. Xu, X.; Ho, W.; Zhang, X.; Bertrand, N.; Farokhzad, O. Cancer nanomedicine: from targeted delivery to combination therapy. *Trends Mol. Med.* **2015**, *21*, 223–232.

111. Matsumura, Y.; Maeda, H. A new concept for macromolecular therapeutics in

cancer chemotherapy: mechanism of tumoritropic accumulation of proteins and the antitumor agent smancs. *Cancer Res.* **1986**, *46*, 6387–92.

112. Maeda, H.; Wu, J.; Sawa, T.; Matsumura, Y.; Hori, K. Tumor vascular permeability and the EPR effect in macromolecular therapeutics: a review. *J. Control. Release* **2000**, *65*, 271–84.

113. Nakamura, H.; Jun, F.; Maeda, H. Development of next-generation macromolecular drugs based on the EPR effect: challenges and pitfalls. *Expert Opin. Drug Deliv.* 2014.

114. Möhwald, H.; Weiss, P. S. Is Nano a Bubble? *ACS Nano* **2015**, *9*, 9427–9428.

Chapter I.

Polymer Nanotechnology

for Cancer Treatment

Chapter I.

Chapter I. Introduction

Polyurethane-polyurea Nanoparticles for Cancer

Therapy and Imaging

Introduction I. Polyurethane-polyurea Nanoparticles for Cancer Therapy and Imaging

Nanoparticle biomedical systems

Nanoparticle biomedical systems (NBS) are widely used in nanomedicine research and in clinical stages to improve the efficacy of drugs i.e. antitumor, antibiotic, immunosuppressive, antiviral and anti-inflammatory[1–3]. Among the wide variety of nanosystems: liposomes; polymeric nanoparticles; polymeric micelles; silica, gold, silver and other metal nanoparticles; carbon nanotubes; solid lipid nanoparticles; and dendrimers[4–11] are the most currently used. The use of NBS aims to solve common drawbacks associated with some traditional drugs, such as poor aqueous solubility, low bioavailability and nonspecific distribution which in turn increases side effects in the body[12].

First generation NBS were developed to address single challenges, like the need to enhance drug stability *in vivo,* the half-life in the bloodstream, to improve delivery across a specific membrane, to keep elevated concentration of a drug in a specific organ through controlled constant delivery, or the desire to target a drug to the specific site of interest[13]. Today, research has evolved developing NBS that can perform more than just one function at the same time e.g. trespass impeded physiological barriers, improve the delivery rate and bring their loads (one or various) to the required target sites (such as organs, tissues, cells) or specific pathologies in the body[14]. The installation of multifunctionality in the NBS nanostructure includes the capability to carry enough cargo of a drug or DNA/RNA-related material[15], to have increased circulation times (through the use of hydrophilic polymers)[16] and to target the expected site of action both non-specifically (by the enhanced permeability and retention (EPR) effect)[17] and specifically (via the binding of site-specific targeting ligands)[18]. In addition, together to targeted, multifunctional NBS can react to certain stimuli that are specific of the target, via the inclusion of components that respond to changes in pH[19], temperature[20] and redox conditions[21], and in some cases to the upregulated concentration of specific biological molecules[22]. Multifunctional NBS can also respond to external stimuli, such as magnetic[11] or ultrasound fields[23] and UV radiation[24], and can be upgraded by the contribution of an imaging contrast moiety to allow their *in vivo* monitoring[25].

Although there is not any official classification of the abovementioned systems, they could be split up into three categories. The first group consists of drug-loaded NBS

conveying at least two functions, such as long circulation, site-targeted, stimuli-sensitivity or cell penetration[26]. The second group, besides the previously exemplified properties, are loaded with more than one drug and/or genetic therapy-related molecule[27], such as small interfering RNA (siRNA). The third group consists of the all-in-one theranostic NBS, which bear a diagnostic label (like a fluorescent label or contrast agent) for use with current clinical imaging modalities (such as near infrared spectroscopy, nuclear medicine, computer-assisted tomography, etc.) (Figure 1)[28].
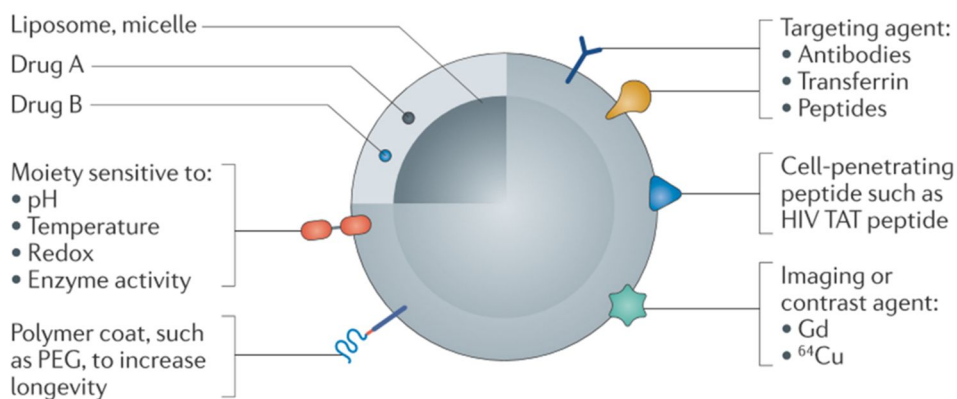
Figure 1. Polymer nanoparticle typical multifunctionalites for nanomedicine theranostics.

There are many polymeric nanosystems available for cancer nanotherapy based on PLA, PLGA, PGA, etc. They exhibit excellent biocompatibility and biodegradation, good encapsulation ability and acceptable tunability[29]. However, for *in vivo* purposes those aspects are not totally enough, as then come into play other issues such as early biodegradation[30,31], poor encapsulation stability[32] and limited tunability[33].

Therefore, innovation is needed to create novel systems able to overcome these drawbacks. To enhance the **encapsulation ability and stability**, typical top-used liposome-like polymeric structures formed by self-assembling of amphiphilic polymers do not fulfil all the requirements for in vitro and in vivo delivery as they might have a too diffuse and labile structure. This can be explained as a result of the lack of nanostructure control of the formed shell during the emulsification process that creates leaky walls due to random aggregation and irregular structuration. That kind of amphiphilic structures facilitate the superficial entrapment of hydrophobic cargos instead of deep encapsulations in the core and thus boost the interaction of the cargo with naturally present molecules such as, phospholipids, cholesterol, lipophilic proteins, etc[32,6,25]. We believe that to avoid such undesired effects, polymers should be tailor designed in order to create an impermeable multiwalled shell that prevents an

undesired release until reaching the desired target. Another issue that should be tackled in common DDS is the use of external surfactants. When surfactants are used to decrease the size of the nanodispersion, they also affect the interface where the polymerization takes place creating some diffusion channels and decreasing the global robustness and boosting Ostwald ripening effects, which need to be compensated with other external additives. This excess of free surfactants has also been proved as a primordial cause of later toxicities[16,34], e.g. by the immune system and therefore nanosystem failure.

Biodegradation is also crucial in cancer therapy as it is a must to achieve a non-toxic elimination of the polymeric residues after an efficient drug delivery. However, early degradation is a sometimes ignored issue that may trigger a non-effective drug delivery. This happens because of the non-fixed (non-crosslinked) shell structure which provokes polymeric shell de-structuration upon physical and chemical interaction with external biomolecules. In example, most used polyaminoacid polymers like polymeric PLGA self-assembled structures are too easily hydrolysed by esterase enzymes, which turns into a rapid loss of their protecting properties and a content release before being on-target[31,35].

The capacity of a polymer to convey multiple functions, **tunability**, is directly related to its intrinsic reactivity. Ideally, a polymer should exhibit high reactivity in intermediate stages to allow its bioactivation before final end-capping/crosslinking. In example, fluorescent tags, cell targeting compounds, biodegradation spots should be easily linked to the polymer backbone via covalent bonds to enhance its multifunctionality. Although, a polymer should be easily modulated in terms of structure to create not only linear or crosslinked structures but also tailored morphologies like dendrimers. To achieve such a broad range of structural morphologies is key to use a well-established chemistry in the industry and so have multiple chances to select one or another monomer depending on the desired final morphology[36,37].

For the build-up of polymeric nanoparticles with an ordered, controlled and functionalized structure, and with the capacity to contain actives (like cosmetics or drugs) in a high yield, it is missing a well-defined step by step building block synthetic process. The current existing polymeric systems to create nanoparticles are not always able to be functionalized in a specific and straightforward manner. They are mostly random-based and the monomers or oligomers used as starting materials are not designed in a way to participate in the self-structuration of the nanoparticle. The functionalization is normally carried out in a later step by laborious and costly multilayers one after the other. Different steps and intermediate purifications are necessary and the industrial scale up becomes difficult and expensive[34]. Therefore,

these systems are not suitable enough for the synthesis of multifunctional and sub-nano-structured nanoparticles.

The idea of creating architecturally controlled species arises from the desire to get materials with tailored structures at the nano-level. In example, other researchers have undertaken the challenge of nanostructuration taking profit of electrostatic interactions between contrary charged species to create multilayered and multifunctional nanomaterials by layer-by-layer techniques[38–40].

Self-stratified polyurethane-polyurea nanoparticles

In this chapter we propose an alternative, scalable methodology based on meticulously designed polyurethane-polyurea nanoparticles displaying a multiwalled and multifunctional structure to improve the encapsulation ability of lipophilic compounds and truly control their site-specific release. So, reactive prepolymers of different hydrophobicity with terminal isocyanate groups and long pendant side hydrophobic and hydrophilic chains have been synthesized according to our previously introduced patent[41]. In the outer part of the shell, the amphiphilic polymer (Amphil) is constituted by hydrophilic and hydrophobic dangling chains and disulfide bonds. The hydrophilic chain is a polyethoxylated difunctional diol (YMER™ N120) with the two hydroxyl groups very close to each other, and a long polyethoxylated side chain that is linked to the isophorone diisocyanate (IPDI) by urethane bonds forming the main chain. The hydrophilic polyethoxylated chain is sideways the urethane main chain (Figure 2).
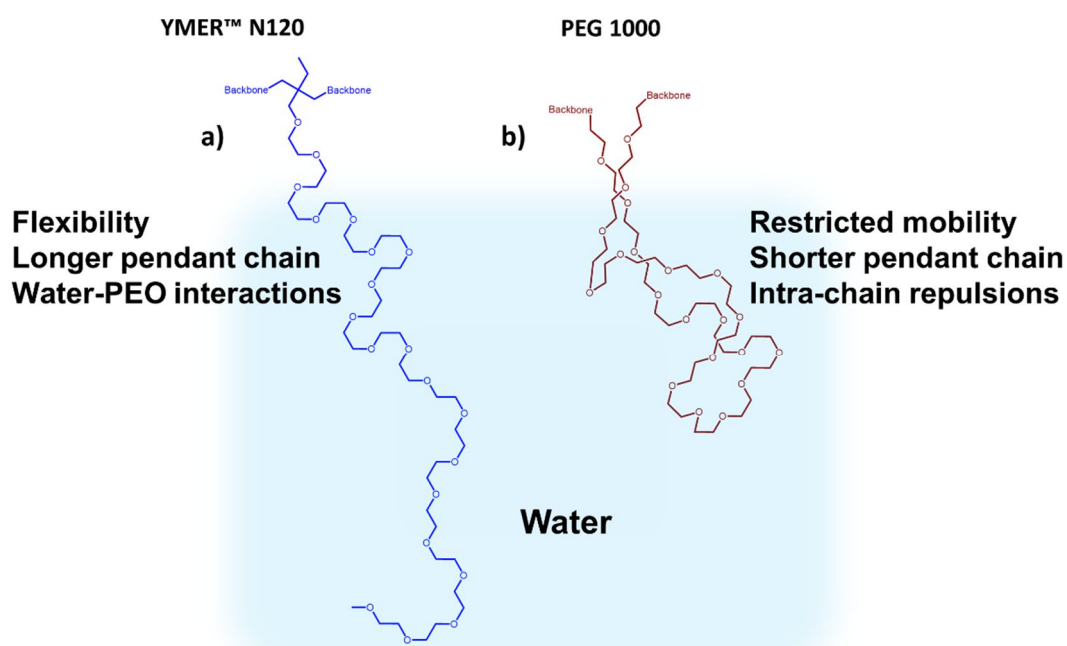
Figure 2. Representation of morphological characteristics of YMER™ N120 and PEG upon polymerized and emulsified in aqueous media.

It is also important to note the short distance between urethane bonds which promotes a compaction of the polymeric structure for a further better encapsulation ability to form more aggregated and robust shells, compared to similar hydrophilic diols like PEG, PAS, etc. where urethane groups are spatially far from each other.

Following the same rational, the hydrophobic chain is a long alkyl side chain diamine linked to the diisocyanate prepolymer by urea bonds. As before, the urea groups are closely located for the abovementioned reasons and the aliphatic long alkyl chain (either C12 or C18) is sideways them to readily interact hydrophobic species (Figure 3).
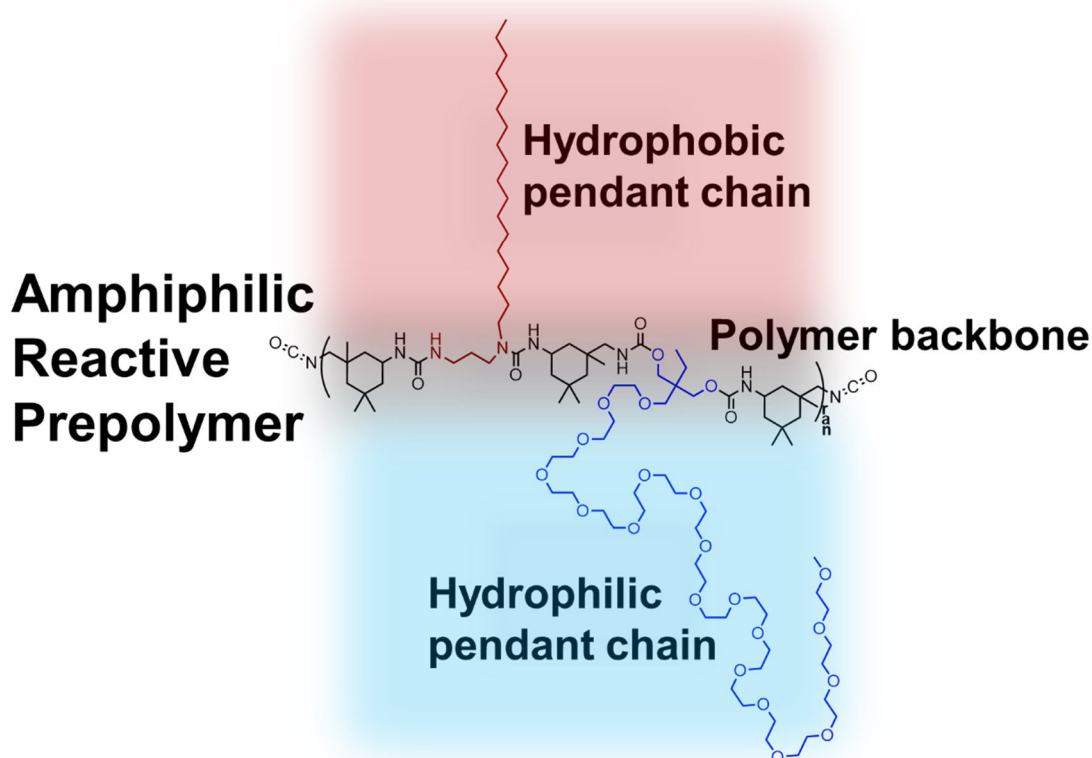
Figure 3. Ideal structure of an isocyanate-reactive amphiphilic prepolymer containing hydrophilic and hydrophobic pendant chains in an oil-in-water emulsion. Pendant hydrophobic chains will self-orient toward the oily phase and pendant hydrophilic chains toward the aqueous phase.

Disulfide bonds, namely 2-hydroxyethyl disulfide (DEDS), are incorporated via urethane chemistry through the reaction with IPDI with the purpose of displaying redox degradation by reductive enzymes or peptides (Glutathione) of the polymeric nanoparticle upon intracellular accumulation (Figure 4). In order to keep final isocyanate reactivity to this amphiphilic prepolymer, the diol and diamine monomers are added in defect respect to the diisocyanates[42].

In addition, a second hydrophobic compound (either a hydrophobic monomer or a hydrophobic prepolymer, Hyfob) with isocyanate reactivity is added to the pre-emulsification process mixture. The aim of adding a hydrophobic compound with isocyanate reactivity is to promote a first self-stratification of the polymeric shell by hydrophobic interactions and second, allow a further fixing-crosslinking step by via urea bonds of the whole multipolymeric shell[42] (Figure 4).
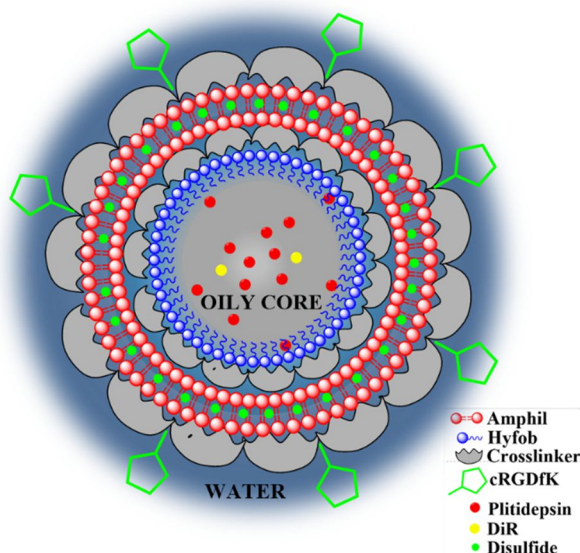
Figure 4. Ideal self-stratified structure of a multifunctional PUUa NP for drug delivery. The double red dots represent the hydrophobic and hydrophilic pendant chains of Amphil. Blue moieties represent the hydrophobic prepolymer. Grey functions represent the crosslinking amine that fixes the isocyanate reactive prepolymers. Green pentagons represent the cRGDfK conjugates with isocyanate reactivity. Green dots represent the disulfide moieties for PUUa NP biodegradation. Red dots represent an encapsulated hydrophobic model drug and yellow dots mean any encapsulated fluorophore for monitoring purposes.

The selection of isocyanate as terminal reactive group in the prepolymers is due to its high reactivity and quantitative reactions with amines and polyamines for functionalization or crosslinking in aqueous media[22,43]. Diisocyanates and polyisocyanates of different molecular size, structure and functionality allow the reaction of a wide range of diols, polyols, diamine and polyamines making possible the creation of tailored prepolymers conveying the right self-organizing properties[36].

Moreover, to bioactivate our nanoparticles to specifically interact with overexpressed αvβ3 integrins in the tumor cells surface, the nucleophilic amino group of the L-Lysine residue of cRGDfK peptide was coupled with a polyisocyanate linker. The resultant isocyanate reactive functional conjugate allowed the incorporation of bioactive cRGDfK moieties on the prepolymeric nanoemulsion with the rest of hydrophobic and amphiphilic reactive components. They self-organize together with the oily-drug core to

self-stratify in a hydrophobic/hydrophilic driven way, to finally be fixed via urea covalent bonding by crosslinking with the appropriate polyamines. Due to the relatively hydrophilic characteristics of the cRGDfK conjugate it is fixed by final crosslinking on the surface of the sub-nanostructured nanoparticle. More generally speaking, this patented technology allows the self-deposition of a functional moiety along the shell depending on its intrinsic hydrophilic-lipophilic balance. In fact, it could be located automatically in the core, the interface or surface of the nanoparticle by hydrophobic attraction or repulsion forces (Figure 4). Finally, the right selection of all the prepolymers with the adjusted reactivity, size, charge, hydrophilic-lipophilic balance, targeting rests, and the right extending and/or crosslinking polyamines would translate into control over stability, morphology, surface charge, biological activity or affinity and specific controlled delivery.

This technology enables new avenues of therapeutic, diagnostic and imaging tools for fighting against several diseases in a more selective way, in special for cancer treatment, where secondary effects of antitumoral drugs in healthy cells are very destructive. This new nanotechnological platform can be also very useful for many other industrial applications, not only in the pharmaceutical field, due to the fact that it uses available commercial intermediates, the reactions are controlled and quantitative avoiding purification steps, and definitively, it is a scalable and a versatile system.

In addition, in the following chapter, apart from the explanation of the synthetic and methodological process, the biological testing of PUUa NPs *in vitro* and *in vivo* is assessed and discussed.

1. Gharagozloo, M.; Majewski, S.; Foldvari, M. Therapeutic applications of nanomedicine in autoimmune diseases: From immunosuppression to tolerance induction. *Nanomedicine* **2015**, *11*, 1003–1018.

2. Mahkam, M.; Sharifi-Sanjani, N. Preparation of new biodegradable polyurethanes as a therapeutic agent. *Polym. Degrad. Stab.* **2003**, *80*, 199–202.

3. Griffiths, G.; Nyström, B.; Sable, S. B.; Khuller, G. K. Nanobead-based interventions for the treatment and prevention of tuberculosis. *Nat. Rev. Microbiol.* **2010**, *8*, 827–34.

4. Kirpotin, D. B.; Drummond, D. C.; Shao, Y.; Shalaby, M. R.; Hong, K.; Nielsen, U. B.; Marks, J. D.; Benz, C. C.; Park, J. W. Antibody targeting of long-circulating lipidic nanoparticles does not increase tumor localization but does increase internalization in animal models. *Cancer Res.* **2006**, *66*, 6732–40.

5. Graf, N.; Bielenberg, D. R.; Kolishetti, N.; Muus, C.; Banyard, J.; Farokhzad, O. C.; Lippard, S. J. A5β3 Integrin-Targeted PLGA-PEG Nanoparticles for Enhanced Anti-tumor Efficacy of a Pt (IV) Prodrug. *ACS Nano* **2012**, *6*, 4530–4539.

6. Chen, H.; Kim, S.; Li, L.; Wang, S.; Park, K.; Cheng, J.-X. Release of hydrophobic

molecules from polymer micelles into cell membranes revealed by Förster resonance energy transfer imaging. *Proc. Natl. Acad. Sci.* **2008**, *105* , 6596–6601.

7. Botella, P.; Abasolo, I.; Fernández, Y.; Muniesa, C.; Miranda, S.; Quesada, M.; Ruiz, J.; Schwartz, S.; Corma, A. Surface-modified silica nanoparticles for tumor-targeted delivery of camptothecin and its biological evaluation. *J. Control. Release* **2011**, *156*, 246–57.

8. Chen, D.; Luo, Z.; Li, N.; Lee, J. Y.; Xie, J.; Lu, J. Amphiphilic Polymeric Nanocarriers with Luminescent Gold Nanoclusters for Concurrent Bioimaging and Controlled Drug Release. *Adv. Funct. Mater.* **2013**, n/a–n/a.

9. Svenson, S. The dendrimer paradox – high medical expectations but poor clinical translation. *Chem. Soc. Rev.* **2015**, *44*, 4131–4144.

10. Urban, M. W. Stimuli-responsive colloids: From stratified to self-repairing Polymeric Films and Beyond. *Curr. Opin. Colloid Interface Sci.* **2014**, *19*, 66–75.

11. Cho, N.-H.; Cheong, T.-C.; Min, J. H.; Wu, J. H.; Lee, S. J.; Kim, D.; Yang, J.-S.; Kim, S.; Kim, Y. K.; Seong, S.-Y. A multifunctional core-shell nanoparticle for dendritic cell-based cancer immunotherapy. *Nat. Nanotechnol.* **2011**, *6*, 675–82.

12. Etheridge, M. L.; Campbell, S. A.; Erdman, A. G.; Haynes, C. L.; Wolf, S. M.; McCullough, J. The big picture on nanomedicine: the state of investigational and approved nanomedicine products. *Nanomedicine* **2013**, *9*, 1–14.

13. Matsumura, Y.; Maeda, H. A new concept for macromolecular therapeutics in cancer chemotherapy: mechanism of tumoritropic accumulation of proteins and the antitumor agent smancs. *Cancer Res.* **1986**, *46*, 6387–92.

14. Biswas, S.; Torchilin, V. P. Nanopreparations for organelle-specific delivery in cancer. *Adv. Drug Deliv. Rev.* **2014**, *66*, 26–41.

15. Roques, C.; Bouchemal, K.; Ponchel, G.; Fromes, Y.; Fattal, E. Parameters affecting organization and transfection efficiency of amphiphilic copolymers/DNA carriers. *J. Control. Release* **2009**, *138*, 71–7.

16. Knop, K.; Hoogenboom, R.; Fischer, D.; Schubert, U. S. Poly(ethylene glycol) in drug delivery: pros and cons as well as potential alternatives. *Angew. Chem. Int. Ed. Engl.* **2010**, *49*, 6288–308.

17. Maeda, H.; Wu, J.; Sawa, T.; Matsumura, Y.; Hori, K. Tumor vascular permeability and the EPR effect in macromolecular therapeutics: a review. *J. Control. Release* **2000**, *65*, 271–84.

18. Bertrand, N.; Wu, J.; Xu, X.; Kamaly, N.; Farokhzad, O. C. Cancer nanotechnology : The impact of passive and active targeting in the era of modern cancer biology ☆. *Adv. Drug Deliv. Rev.* **2014**, *66*, 2–25.

19. Pardini, F.; Faccia, P.; Amalvy, J. Evaluation of pH-sensitive polyurethane/2-diethylaminoethyl methacrylate hybrids potentially useful for drug delivery developments. *J. Drug Deliv. Sci. Technol.* **2015**.

20. Wang, Y.; Wu, G.; Li, X.; Chen, J.; Wang, Y. Temperature-triggered redox-degradable poly (ether urethane) nanoparticles for controlled drug delivery. *J. Mater. Chem.* **2012**, *300071*, 3–6.

21. Cheng, R.; Feng, F.; Meng, F.; Deng, C.; Feijen, J.; Zhong, Z. Glutathione-responsive nano-vehicles as a promising platform for targeted intracellular drug and gene delivery. *J. Control. Release* **2011**, *152*, 2–12.

22. Andrieu, J.; Kotman, N.; Maier, M.; Mailänder, V.; Strauss, W. S. L.; Weiss, C. K.; Landfester, K. Live monitoring of cargo release from peptide-based hybrid nanocapsules induced by enzyme cleavage. *Macromol. Rapid Commun.* **2012**, *33*, 248–53.

23. Fleige, E.; Quadir, M. A.; Haag, R. Stimuli-responsive polymeric nanocarriers for the controlled transport of active compounds: concepts and applications. *Adv. Drug Deliv. Rev.* **2012**, *64*, 866–84.

24. Rosenbauer, E.-M.; Wagner, M.; Musyanovych, A.; Landfester, K. Controlled Release from Polyurethane Nanocapsules via pH-, UV-Light- or Temperature-Induced Stimuli. *Macromolecules* **2010**, *43*, 5083–5093.

25. Zou, P.; Chen, H.; Paholak, H. J.; Sun, D. Noninvasive fluorescence resonance energy transfer imaging of in vivo premature drug release from polymeric nanoparticles. *Mol. Pharm.* **2013**, *10*, 4185–94.

26. Ding, M.; Song, N.; He, X.; Li, J.; Zhou, L.; Tan, H.; Fu, Q.; Gu, Q. Toward the next-generation nanomedicines: design of multifunctional multiblock polyurethanes for effective cancer treatment. *ACS Nano* **2013**, *7*, 1918–28.

27. Hu, S.-H.; Chen, S.-Y.; Gao, X. Multifunctional nanocapsules for simultaneous encapsulation of hydrophilic and hydrophobic compounds and on-demand release. *ACS Nano* **2012**, *6*, 2558–65.

28. Lee, J. Y.; Choi, D.-Y.; Cho, M. Y.; Park, K. E.; Lee, S.-H.; Hun Cho, S.; Hong, K. S.; Lim, Y. T. Targeted theranostic nanoparticles: receptor-mediated entry into cells, pH-induced signal generation and cytosolic delivery. *Small* **2014**, *10*, 901–6.

29. Jain, R. A. The manufacturing techniques of various drug loaded biodegradable poly(lactide-co-glycolide) (PLGA) devices. *Biomaterials* **2000**, *21*, 2475–2490.

30. Kumar, G.; Shafiq, N.; Malhotra, S. Drug-Loaded PLGA Nanoparticles for Oral Administration: Fundamental Issues and Challenges Ahead. *Crit. Rev. Ther. Drug Carr. Syst.* **2012**, *29*, 149–182.

31. Crotts, G.; Park, T. G. Protein delivery from poly(lactic-co-glycolic acid) biodegradable microspheres: Release kinetics and stability issues. *J. Microencapsul.* **2008**.

32. Xu, P.; Gullotti, E.; Tong, L.; Highley, C. B.; Errabelli, D. R.; Hasan, T.; Cheng, J.-X.; Kohane, D. S.; Yeo, Y. Intracellular drug delivery by poly(lactic-co-glycolic acid) nanoparticles, revisited. *Mol. Pharm.* **2009**, *6*, 190–201.

33. Bala, I.; Hariharan, S.; Kumar, M. R. PLGA Nanoparticles in Drug Delivery: The

State of the Art; *Crit. Rev. Ther. Drug Carrier Syst.* **2004**, *21*, 387–422.

34. Asua, J. M. Challenges for industrialization of miniemulsion polymerization. *Prog. Polym. Sci.* **2014**, *39*, 1797–1826.

35. Jalil, R.; Nixon, J. R. Biodegradable poly(lactic acid) and poly(lactide-co-glycolide) microcapsules: problems associated with preparative techniques and release properties. *J. Microencapsul.* **2008**.

36. Engels, H.-W.; Pirkl, H.-G.; Albers, R.; Albach, R. W.; Krause, J.; Hoffmann, A.; Casselmann, H.; Dormish, J. Polyurethanes: versatile materials and sustainable problem solvers for today's challenges. *Angew. Chem. Int. Ed. Engl.* **2013**, *52*, 9422–41.

37. Chattopadhyay, D. K.; Raju, K. V. S. N. Structural engineering of polyurethane coatings for high performance applications. *Prog. Polym. Sci.* **2007**, *32*, 352–418.

38. Richardson, J. J.; Bjornmalm, M.; Caruso, F. Technology-driven layer-by-layer assembly of nanofilms. *Science (80-.).* **2015**, *348*, aaa2491–aaa2491.

39. Ariga, K.; Ji, Q.; Hill, J. P.; Bando, Y.; Aono, M. Forming nanomaterials as layered functional structures toward materials nanoarchitectonics. *NPG Asia Mater.* **2012**, *4*, e17.

40. De Koker, S.; Hoogenboom, R.; De Geest, B. G. Polymeric multilayer capsules for drug delivery. *Chem. Soc. Rev.* **2012**, *41*, 2867–84.

41. Rocas Alonso, P.; Rocas Sorolla, J. Method for producing a microencapsulate and corresponding reactive amphiphilic compound, microencapsulate and composition. 2014, Ecopol Tech, S.L.

42. Rocas, P.; Fernández, Y.; Schwartz, S.; Abasolo, I.; Rocas, J.; Albericio, F. Multifunctionalized polyurethane–polyurea nanoparticles: hydrophobically driven self-stratification at the o/w interface modulates encapsulation stability. *J. Mater. Chem. B* **2015**, *3*, 7604–7613.

43. Breucker, L.; Schöttler, S.; Landfester, K.; Taden, A. Polyurethane Dispersions with Peptide Corona: Facile Synthesis of Stimuli-Responsive Dispersions and Films. *Biomacromolecules* **2015**, *16*, 2418–26.

5

10

15

20

25

Chapter I. Publication 1

PUUa Nanoparticles Methodological Patent

30

5

10

15

20

25

METHOD FOR PRODUCING A MICROENCAPSULATE AND CORRESPONDING
REACTIVE AMPHIPHILIC COMPOUND, MICROENCAPSULATE AND
COMPOSITION

5 **ABSTRACT**

Method for producing a polymeric, amphiphilic, highly functionalisable and versatile
microencapsulate/nanoencapsulate, which comprises 2 stages: dispersing a first liquid
10 phase in a second liquid phase forming an emulsion, in this way said first phase
remains dispersed in said second phase, and polymerising a polymer that forms the
wall of the microencapsulate. Between both phases an interphase is formed with a a
reactive amphiphilic compound, which is a prepolymer of the polymer. The amphiphilic
compound has two more main functional groups that react in the subsequent
15 polymerisation to produce the polymer. These two main functional groups are
separated from each other by between 4 to 12 links. The amphiphilic compound has at
least one hydrophilic or hydrophobic functional group in one chain which is sideways
with respect to the chain that links both main functional groups.

20

25

30

35

METHOD FOR PRODUCING A MICROENCAPSULATE AND CORRESPONDING REACTIVE AMPHIPHILIC COMPOUND, MICROENCAPSULATE AND COMPOSITION.

5   **DESCRIPTION**

Field of the invention

The invention relates to a method for producing a microencapsulate comprising the
10   following stages: [a] dispersing a first liquid phase in a second liquid phase forming an emulsion, so that the first phase is dispersed in the second phase, and [b] polymerising a polymer that forms the wall of the microencapsulate.

The invention also relates to a reactive amphiphilic compound with at least two
15   functional groups suitable for reacting in a subsequent polymerisation.

The invention also relates to a microencapsulate and a cosmetic or pharmaceutical composition comprising a microencapsulate.

20

State of the art

Various encapsulation methods are known. However most of them require high stirring, high concentrations of external emulsifying agents or solvent to obtain capsule sizes
25   smaller than one micron, etc.

It is known to use emulsifying agents which are, simultaneously, prepolymers of the polymer that will form part of the microencapsulate wall. Some examples can be found in documents US 6.262.152, US 7.199.185 and US 2007/0270508.

30

Generally, emulsifying agents can be of two main types: oil in water (normally indicated as O/W) or water in oil (normally indicated as W/O). Generally this invention is suitable in both cases, although the most usual are the O/W emulsions and therefore most of the examples will be of this type, but at no time must the invention be understood to
35   only refer to oil in water emulsions. In this specification and claims the term "first phase" has been used to indicate what will be the dispersed phase, and the term "second phase" to indicate what will be the continuous phase.

In this specification and claims the term microcapsules and/or microparticles is used broadly, so that it also includes capsules and/or particles which, due to their size, could have been classified instead as nanocapsules and/or nanoparticles.

5

Disclosure of the invention

The aim of the invention is a new method which allows obtaining small size
10 microcapsulates, and in relatively high concentrations. This purpose is obtained by means of a method according to the invention of the type indicated at the beginning characterised in that between the first phase and the second phase an interphase is formed that comprises a reactive amphiphilic compound, where the amphiphilic compound is a prepolymer of the polymer that will form the wall of the
15 microencapsulate, and the amphiphilic compound has at least two main functional groups that react in the subsequent polymerisation to form the polymer that will form the wall of the microencapsulate, where the amphiphilic compound has at least one hydrophilic or hydrophobic functional group in a chain that is sideways with respect to the chain that joins both main functional groups.

20

In fact the method according to the invention uses amphiphilic compounds that behave as dispersants and which self-emulsify the emulsion but which, at the same time, are reactive, which means that later they can be used to encapsulate, forming the wall of the microencapsulate. These amphiphilic compounds comprise a main chain, which
25 preferably is "short", and they have at least one of the hydrophilic and hydrophobic functions in side chains. In fact this is a very interesting concept because it means amphiphilic compounds that are particularly suitable for the invention can be obtained. It must be taken into account that in this specification and claims the term "main chain" has been used to designate the one that has at the ends thereof the two functional
30 groups (called main functional groups) which subsequently polymerise to form the polymer in the wall of the microencapsulate. This way, the amphiphilic compound is placed in the interphase between the two phases and is orientated so that it has the hydrophobic functions aimed towards the organic phase and the hydrophilic functions aimed towards the aqueous phase. This allows for a series of advantages. Between
35 the two main functional groups there is little separation, this favours polymerisation, improves the barrier effect to prevent the diffusion of the encapsulated material towards

the outside of the capsule, and makes encapsulation stable. For their part, the side chains are relatively flexible and adaptable.

Preferably, main "short" chain must be understood to mean that the two main functional groups of the amphiphilic compound are separated from each other by between 4 to 12 links, preferably between 5 to 10 links. Generally, the links will be of the –CH2- type, but they could be of another type (for example, substituents like O, N, S etc.). In fact, if there are more CH2 groups between the main functional groups, then the actual chain would already have a significant hydrophobic effect, which would counter the "side amphiphilic" concept and, also, it would have a negative effect on the rigidity (reducing it), as a greater number of CH2 groups in the main chain reduces the partial glass transition temperature (Tg). Therefore it is interesting to have a main short chain (with high rigidity and barrier effect) and to have longer side chains with the hydrophilic and hydrophobic functions.

So, for example in the case of O/W emulsions, the corresponding microcapsule will have an organic phase inside. The amphiphilic compound will have arranged itself so that its hydrophobic side chains are towards the hydrophobic inside of the capsules, and its hydrophilic side chains are towards the outside of the microcapsule and, during polymerising, this structure "froze" like this. This makes it possible later to obtain very stable microencapsulate dispersions, which do not aggregate, not even in the presence of saline or biological liquids that affect or promote their aggregation.

The prepolymer must have at least two main functional groups that react in the subsequent polymerisation for forming the polymer that will form the wall of the microencapsulate, however it can have more than two functional groups, with which better cross-linking will be achieved. Also it can have a mixture of amphiphilic compounds with a different number of main functional groups, so that the mixture makes it possible to obtain the degree of cross-linking required. In the event that the prepolymer has more than two main functional groups, it will be considered as the shortest main chain out of the possible chains that can be defined between the main functional groups.

Preferably the polymer (which forms the wall of the microencapsulate) is insoluble in the two phases, which is particularly important for obtaining a good barrier effect. In this respect, a particularly advantageous solution is that the polymer has urea and/or urethane type groups, and that these groups are near to one another.

As it can be seen, the basic concept of the invention consists in generating a dispersion from a first phase and a second phase, where the interphase is formed thanks to an amphiphilic compound. The amphiphilic compound is a reactive compound. By virtue of this, after forming the dispersion, the amphiphilic compound reacts forming a polymer that forms the wall of the microcapsules. Therefore, the amphiphilic compound is really a prepolymer of the polymer that forms the wall of the microcapsules. This method allows very small (even nanometric size) microencapsulates to be formed and in relatively high concentrations. It must be taken into account that, generally, when microcapsules are prepared, if they are not well stabilised and diluted, they tend to agglomerate, and when they dry they tend to join together and the wall of the capsules tends to break because of the force of the actual agglomeration and their thin walls. The microcapsules according to the invention can be air-dried where they agglomerate relatively little at relatively high concentrations. Also, the dispersions are formed with moderate stirring, which means that active ingredients "sensitive" to stirring can be encapsulated and, at the same time, large-scale industrial manufacturing is possible with less energy and less expensive stirring equipment.

In the known microencapsulating methods, in the first phase a prepolymer is added which subsequently will form the polymer that shapes the wall of the microcapsules. For example, it is known to use polyisocyanates to produce microcapsules from an O/W solution. However, these prepolymers (like the polyisocyanates used normally) are not amphiphilic or self-emulsifying. For example, one polyisocyanate used is isophorone diisocyanate (IPDI). IPDI cannot be considered to be amphiphilic because it does not have one part soluble in water and one part soluble in oil. Also, IPDI does not migrate to the interphase, because it is soluble in oil and its solubility in water is not significant. Therefore, it is necessary to add, usually in the continuous phase (which is normally the aqueous phase) some dispersing and/or emulsifying agents external to the prepolymer. These dispersing and/or emulsifying agents, for their part, can be amphiphilic, but they are not reactive, and therefore they are not part of the polymer that shapes the wall of the capsules. However, these agents can hinder the wall formation process. Generally, in the known methods, there are more spaces between the polymer cross-links, it is harder to arrange themselves in the interphase and there are interferences between the reagents and the remaining agents in the interphase. In this invention the same amphiphilic compound that is the emulsifying agent and forms the emulsion is also the one that is reactive and is therefore, a prepolymer of the

polymer that will form the wall of the microcapsules. This way, a wall with an improved barrier effect is obtained.

Based on this basic concept, the method according to the invention contemplates
5   different variants. In fact:

- The amphiphilic compound can be added already-formed in the first phase, before forming the emulsion.
- The amphiphilic compound is formed in the first phase by reacting some of the
10   precursors in the first phase, before forming the emulsion.
- The amphiphilic compound is formed "in situ" in the interphase of the emulsion, from precursors that are in the first phase and in the second phase, and that meet each other and react in the interphase.
- The polymer is made by polymerising the amphiphilic compound with itself,
15   either directly or by reacting with the solvent of the second phase (for example, in the case of the O/W solution where there are isocyanates in the disperse phase, thee isocyanates can react with the water (forming an amine) and later they can react with another isocyanate forming an urea).
- The polymer is formed by polymerising the amphiphilic compound with a
20   second compound, added in the second phase, or added in the already-formed dispersion.

Also, there may be methods wherein several of the above alternatives converge.

25   If the amphiphilic compound is formed before making the emulsion, the amphiphilic compound is such that, being amphiphilic, it is less soluble in the first phase than in the second phase. This way, the amphiphilic compound tends to go to the interphase due to its affinity with the second phase. This way the amphiphilic compound acts as the emulsifying agent (self-emulsifying) and, also, it positions itself appropriately for the
30   subsequent polymerisation reaction.

Preferably the amphiphilic compound, which is the prepolymer that will subsequently form the polymer that shapes the wall of the microencapsulate, is the main emulsifying agent in the emulsion and, very preferably, it is the only emulsifying agent. This aspect
35   is particularly important because it avoids external emulsifying agents, which often can precipitate when they come into contact with the microcapsules in saline media or

biological liquids (like blood or lymphatic liquid), and aggregate, which could cause damage to the biological organisms due to blocked arteries or veins, etc.

Advantageously the amphiphilic compound and/or the product derived from its polymerisation is the main stabilising agent, preferably it is the only stabilising agent in the emulsion.

Preferably no emulsifying and/or additional stabilising agent is added. In particular, the aqueous phase (particularly, when it is the second phase, i.e. the continuous phase) is free of emulsifying agents in the group made up alkyl carboxylates, alkyl sulphonates, alkyl ethoxylates (like the products sold under the names Tween ® and Span ®) and non-reactive amphiphilic polymers with the hydrophilic and hydrophobic chains in the main chain (like polypropylene glycol and polyethylene glycol, sold under the name Pluronic ®).

As already mentioned above, an alternative is that the first phase be the organic phase and the second phase be the aqueous phase. In this case it is advantageous that the amphiphilic compound has an HLB value (Hydrophilic lipophilic balance) higher than 10, preferably greater than 15. On the other hand, in the event that the first phase is the aqueous phase and the second phase is the organic phase, then it is advantageous that the amphiphilic compound has an HLB value less than 10. Generally, changing the proportion of lipophilic to hydrophilic functional groups in the prepolymer can obtain water in oil or oil in water type emulsions. Depending on the type of active ingredients that are to be encapsulated, one method or the other will be used. In the case of the oil in water systems the hydrophilic functional groups exceed the lipophilic groups in the prepolymer that later will form the wall of the capsules when it reacts. And vice versa, in the case of the water in oil emulsions the lipophilic groups exceed the hydrophilic groups in the prepolymer that is used to emulsify and form the wall subsequently.

Preferably the main functional groups of the amphiphilic compound are isocyanate (NCO) functional groups, suitable for forming urethane and/or urea type links when they react with alcohol (OH) functional groups and amine (NH), respectively. However, the general concept of the invention could also be applied with other main functional groups. So, for example, another interesting alternative consists in having main functional groups that are silanes instead of isocyanates. These silanes can be obtained, for example, from the reaction of some terminal isocyanates with

aminopropyl tri alkylsilane or alkyl aminopropyl trialkyl silane groups (like AMEO, aminopropyl-trimethoxysilane for example, or with the compound Dynasylan ® 1189 sold by Evonik Industries, which is a N-(n-butyl)-3-aminopropyltrimethoxysilane). These functional groups included in structures called hybrid as they are inserted into a base

5   polyurethane-polyurea, form hybrid organic-inorganic prepolymers of polyurea and/or polyurethane (considered organic) with silanes (considered inorganic). These types of hybrid prepolymers react by catalysis (acid, base or organometallic or combined) via the silane functional groups to yield cross-linked glass structures (as in one part of the molecule a glass type structure Si_xO_y is formed). In other words, the cross-linking in this

10   case would be between the silane itself and would not require polyamines. These are very stable to hydrolysis and can be interesting in some applications. In fact, the amphiphilic compound could be, in general, mixed, in the sense that its main functional groups can be different from one another. So, for example, in this particular case, the substitution of the NCO groups by silanes could be partial, whereby a hybrid

15   microencapsulate wall would be obtained.

The amphiphilic compound that accumulates in the interphase can be a compound that is added to the first liquid phase, or it can be a compound that is formed in the first liquid phase from a first precursor and a second precursor that react together, i.e. the

20   amphiphilic compound can be added to the already-formed first liquid phase or it can be formed "in situ". In fact, there could be a third precursor (or even more precursors). The first precursor would be the one that shapes the "main chain" of the amphiphilic compound and the second and third precursor are the ones that provide the hydrophilic and hydrophobic side chains, respectively. In fact, the third precursor can be included

25   in the first phase or it can be included in the second phase (both before making the emulsion and after making it). In the event that the third precursor is in the second phase, it is advantageous that, even being soluble in the second phase, it has greater affinity with the first phase. This will help it migrate towards the interphase, where it will be able to react with the product of the reaction between the first precursor and the

30   second precursor, thereby forming the amphiphilic compound directly in the actual interphase.

In the event that the amphiphilic compound is made from precursors, the length of the main chain of the amphiphilic chain "grows" quickly and usually it is no longer possible

35   to have between 4 to 12 links between its main functional groups. However, each of the precursors taking part in the formation of the amphiphilic compound has, in turn, two main functional groups (which are those that will remain included in the main chain of

the amphiphilic compound) and a main chain, which is the one extending between the main functional groups of the corresponding precursor and will form, therefore, part of the main chain of the amphiphilic compound. In this respect, it is advantageous that the two main functional groups of the first, second and/or third precursor are separated

5   from each other by between 4 to 12 links, preferably between 5 to 10 links. This way it is also possible to obtain the advantages of a short main chain indicated above. Preferably each and every one of the precursors making up the amphiphilic compound fulfils this condition.

10   To form the polymer, the prepolymer can polymerise itself. So, for example, in the event that the main functional groups are isocyanate (NCO), the prepolymer could react with the water in the aqueous phase and it could polymerise with itself. However, in certain cases, it is advantageous that this is not the case, and it can be achieved, following the example that the main functional groups are isocyanate, maintaining the

15   emulsion at a temperature that is low enough to ensure that the isocyanate does not react with the water (or, at least, does not react significantly). In return, it is advantageous that the second phase comprises a second compound, where the second compound comprises at least two functional groups suitable for reacting with the main functional groups of the amphiphilic compound, to form the polymer that

20   shapes the microencapsulate wall. So, for example, in the event that the main functional groups are isocyanates, the second compound can be a diol or a diamine (or a polyol or a polyamine if greater cross-linking is desired). This way the polymer would be formed, which would be a polyurethane or a polyurea. An advantageous alternative is that the second compound is also amphiphilic, this way it also tends to migrate

25   towards the interphase, and so finds the amphiphilic compound. On the other hand, in the event that the amphiphilic compound is formed "in situ", i.e., in the actual interphase, it is advantageous that this second compound performs the functions of the second precursor indicated above. In this same respect, there could be a third compound which performed the functions of the third precursor and, also, there could

30   be an additional compound that was only responsible for polymerising with the amphiphilic compound formed (i.e. a compound that does not include a hydrophilic or hydrophobic function).

Preferably the first precursor is an isocyanate from the group made up of isophorone

35   diisocyanate (IPDI), hexamethylene 1,6-diisocyanate (HDI) and hydrogenated diphenylmethane 4,4'-diisocyanate (HMDI). In fact, the ideal isocyanate would be a very small diisocyanate such as an ethane or a propane with an NCO function at each

end thereof, although they are compounds that are not used on an industrial level. Some of the diisocyanates have the facility of combining to each other forming dimers or trimers, such as for example in the case of HDI. Generally, this invention can use any diisocyanate or triisocyanate out of the ones indicated above as well as any dimer,

5   trimer, tetramer, pentamer, etc. which is derived therefrom. Some examples of these can be dimers of HDI urethdione, trimers of HDI trimethylpropane, trimers of HDI or IPDI isocyanurate, trimmers of HDI or IPDI biuret, HDI allophanates, etc.

Very preferably the isocyanate is an aliphatic isocyanate, which is more stable. It is

10   particularly interesting that the isocyanate be IPDI, or the HDI dimers or trimers, because they are less reactive.

A different alternative, for having amphiphilic compounds with a more acute fattier character, with low HLB, for obtaining water in oil emulsions and capsules in this

15   medium, it would be a fatty isocyanate sold by Cognis as DDI1410 diisocyanate.

Advantageously the second precursor is a hydrophilic compound, and, preferably, the second precursor comprises at least two functional groups suitable for reacting with functional groups of the first precursor. The second precursor preferably has its

20   hydrophilic function in a chain that is sideways with respect to the chain that joins the two functional groups suitable for reacting with functional groups of said first precursor, because, this way, the "main chain" of the amphiphilic compound will be formed from the "main chain" of the first precursor and the "main chain" of the second precursor, and the hydrophilic function will remain in a side position. The second precursor can be

25   a non-ionomeric compound, in which case preferably it is a polyethoxylenate compound with a molecular weight more than 100, very preferable more than 500. In principle, so that a polyethoxylenate compound has water solubility and is equivalent to an ionomeric compound, it must have a relatively high molecular weight (preferably higher than 500). However, the amphiphilic compound can include more than one

30   hydrophilic precursor, in this way their hydrophilic effect is added. Advantageously the polyethoxylenate compound has a molecular weight lower than 5.000, because with greater molecular weights it is probably difficult to adjust with the hydrophobic monomer. If the first precursor is an isocyanate, then this second precursor can be advantageously a mono- or polyalcohol (for example the diol sold under the name of

35   YMER N120 ®) or a mono- or polyamine (for example the monoamine sold under the name JEFFAMINE M1000 ®). So, for example, preferably, the YMER N120 ® would be used when the polyisocyanate is a diisocyanate, to therefore create a linear,

difuncional prepolymer with two functional isocyanate end groups (for which the reaction must be made to take place always with excess diisocyanate with respect to the diol); whereas preferably Jeffamine M1000 ® would be used when the polyisocyanate has a functionality greater than 2. Alternatively, the second precursor

5   can be of the ionomeric type, preferably with a carboxylic or sulphonic functional group. In this case, it is advantageous that it has this functional group in a side chain. Advantageously it can be a diol (or diamine) alkyl carboxylic or sulphonic, such as for example dimethylolpropionic acid (DMPA). Other anionomer or cationomer compounds are also possible. The second precursor can also be a mixture of ionomer and non-

10   ionomer compounds.

Preferably the third precursor is a hydrophobic C8-C22 compound, and comprises at least two functional groups suitable for reacting with functional groups of the first precursor. So, if the first precursor is an isocyanate, the third precursor is preferably an

15   alcohol (or polyol) or an amine (or a polyamine). The third precursor preferably has its hydrophobic function in a chain that is sideways with respect to the chain that links the two functional groups suitable for reacting with functional groups of the first precursor. The hydrophobic function can also be obtained by means of fluoropolymers diols or polysiloxans dioles.

20

Advantageously the reaction of the first precursor with the second precursor and the third precursor is carried out in the presence of an excess of the first precursor, to prevent the prepolymer from growing excessively and to get the prepolymer to remain reactive with free reactive functional groups.

25

Preferably the third precursor is a compound from the group made up of fatty diols or diamines C_{10}-C_{22}, and very preferably it is a monoglyceride glycerol, like the monooleate or monostearate glyceryl, a dimerdiol, a cocopropylene diamine or a C_{16}-C_{18} aminopropyl amine. A tallow oil propylene diamine, or a dimer diamine (Priamine)

30   can also be advantageous. As we will see later, another possibility would be that it is a fatty monoamine or fatty monoalcohol if the initial isocyanate has more than functionality 2. What is left over from functionality 2 is what would be captured with fatty mono amines or mono alcohols and hydrophilic mono amines or mono alcohols, so that in the end we have a reactive prepolymer with an amphiphilic nature and functionality

35   controlled at 2, to prevent prior cross-linking and insolubility while the prepolymer is formed, because there could be sub-reactions when putting polyisocyanates in contact with triamines or with triols before forming the emulsion. In other words, it is not in the

method's interest that there is cross-linking before time because the prepolymers would become insoluble (they would precipitate) and would not be able to be emulsified. The tri-functionalisation and cross-linking must emerge after the amphiphilic reactive prepolymer self-emulsifies (in principle linear with functionality 2 or less than 2) and

5   soluble in its phase.

Advantageously following the prepolymer forming reaction an active ingredient is added to said first liquid phase. This "subsquent" addition makes it possible to protect the active ingredient from any "aggression" which it could suffer during the production

10   of the prepolymer. In the case of an organic, disperse phase, the active ingredient will be hydrophobic, and preferably it can be an active ingredient from the group made up of lipophilic vitamins (like retinol, or tocopherol), coenzyme Q10, essential oils, medicinal oils and fragrances. If the disperse phase is aqueous, the active ingredient is preferably a hydrophilic peptide, or a water soluble protein. In fact, generally, it can be

15   any active ingredient in the disperse phase that is soluble (either organic or water, or even it itself can be the disperse phase) and which does not interfere with the reaction forming the interphase of the wall of the microparticles.

Very preferably the active ingredient is an antitumoral drug like paclitaxel, or plitidepsin

20   (sold by Pharmamar). These antitumoral drugs (cytotoxics) are hydrophobics and are not very functionalised and do not interfere with the interphasic reaction.

Advantageously the second compound, i.e. the compound that is added in the second phase, is a polyamine, preferably a diamine, triamine, tetraamine or pentaamine and

25   very preferably it is a polyamine from the group made up of ethylene diamine (EDA), diethylenetriamine (DETA), triethylenetetraamine (TETA) and L-lysine. However, it could also be a guanidine, or a sulphonated or carboxylated diamine (or polyamine), which can confer a greater superficial hydrophilic nature apart from cross-linking and closing the active ingredient within the end polymer.

30

Preferably a fourth precursor is added which, advantageously, comprises an acid group (like sulphonate, carboxylate or phosphate), a disulphide or a labile ester in the main chain. Below these cases are analysed in greater detail:

35   - A first option is that this fourth precursor comprises an acid group (sulphonate or carboxylate or phosphate) which would be included, for example, in the form of diamine alkylsulphonate (type EPS ® by Raschig or PolyEPS520 ® by Raschig). This fourth

precursor would be introduced after introducing the second precursor and the third precursor. Alternatively, instead of introducing this fourth precursor for producing the prepolymer (the amphiphilic compound), this compound can be introduced in the continuous phase, or once the emulsion is made. It could be after or before the

5 prepolymer reacts with the second compound or even together. Generally, it is advantageous to include any compound with a functional group that accelerates the hydrolysis in aqueous means in the presence of esterase type enzymes. This alternative, which introduces ionomeric groups (in principle anionomer, although they could be cationomers also) has a double influence, it can improve the emulsion and

10 stability in water and inhibit the adhesion of the nano or microcapsules to one another, and also it can enhance or accelerate the wall hydrolysis depending on the time. The water attacks the wall more in the presence of ionomers. In fact, a greater hydrophilic part in comparison with the hydrophobic part would also accelerate the hydrolysis of the capsule wall. It would probably also help the walls of the microcapsule to be

15 hydrolysed, for example, by esterases or other hydrolytic enzymes, that are expressed in the proximity of an inflammation (either tumoral or another kind), which would allow selectively releasing the content of the active ingredient in a certain inflamed area of the body.

20 - A second option is that this fourth precursor comprises a disulphide, which can be made from diamine diakyl disulphides (included at the end) or diol dialky disulphides (included in the prepolymer together with the hydrophilic diol). The disulphide increases the degradation capacity of the capsule wall vis-à-vis the enzymes with thiols in their active centre or glutathione (which is a peptide overexpressed in tumours and

25 inflammations). In both cases, probably there is an overexpression of the same ones around the tumour in the cytoplasm of the affected cells (tumoral cells) due to the exasperated reduction activity by the large amount of organic material in the tumour .

- A third option is that this fourth precursor comprises a labile ester. In this case, it

30 refers to the presence of ester groups that are particularly sensitive to the hydrolysis in the prepolymer. The presence of esters, which are more hydrolysable functional groups than the urethane or urea, would modulate the hydrolysis of the wall depending on the amount thereof present, again helping the esterases or thiols or other nucleophiles present in the tumoral or inflammed area to hydrolyse the walls of the capsule and

35 release the drug or active ingredient.

- Also, generally, the presence of this type of functional groups would make the unit more biodegradable.

The microencapsulate wall must comply with diverse properties. On the one hand, it must be a "good wall", in the sense that it must be hermetic, but, on the other hand, it must allow the release of the contents when it is convenient. It must also be taken into account that the wall is really a three-dimensional surface and that it is usually made up of a plurality of polymer layers. So, the polymer that shapes the wall must have a certain balance between rigidity and flexibility which, also, must be adjusted for each particular case. However, generally, it can be said that great cross-linking is not advisable. In this respect, the amphiphilic compound (i.e., the prepolymer of the polymer that forms the wall) is mainly difuncional (in the direction of the main functional groups, which are the ones that take part in forming the polymer). There can be a certain degree of trifunctionality (or even greater functionality), but the amphiphilic compound will be "mainly difuncional". The same can be said with respect to the second compound (which is the one that is present in the other phase). An excess of trifunctionality (or, generally, polyfunctionality) when forming the polymer can lead to problems with esters and the formation of gaps or cavities that jeopardise the barrier effect that the microcapsule wall must have. Taking this into account, two preferable strategies can be considered for producing the amphiphilic compound:

- the amphiphilic compound can be obtained from precursors that are all mainly difunctional as well. This is the philosophy of the preferred alternatives indicated in the preceding paragraphs. This way, amphiphilic compounds can be obtained which, for example, can be of the following type:

diisocyanate-diol-diisocyanate-diamine-diisocyanate

the diisocyanate can be a "small" diisocyanate (like IPDI which, on its own, is not amphphilic), the diol can have a hydrophilic side chain (like YMER N120 ®) and the diamine can have a hydrophobic side chain (like Duomeen C ® by Akzo Nobel, which is a fatty C12 diamine). The IPDI with the YMER N120 is too hydrophilic, and so its amphiphilic behaviour improves with the addition of Duomeen C or dimer diol (both have their functional groups (the two amines or the two OH) fairly close, and so the chain is not excessively long). As already mentioned, there can be variants, including some precursor with a greater (for example, by being a mixture of difunctional and trifunctional compounds) or lesser functionality. In short, the interesting point is a

reactive amphiphilic prepolymer with linearity and some (albeit little) trifunctionality, so that it is self-emulsifying. Generally, it is advantageous that the space between the hydrophilic and hydrophobic part is not large. It is also interesting that the polymer that shapes the wall has groups resistant to the water, oil or organic solvent used, as is the
5   case of the ureas and urethanes.

- another different strategy for obtaining the amphiphilic compound is from a first precursor (which, preferably is an isocyanate) with a high functionality (greater than 3) and forming the amphiphilic compound by joining the remaining precursors directly to
10   the first precursor, and not forming a chain as in the case above. In this case, the remaining precursors have low functionality (smaller than 2) to prevent excessive cross-linking in the unit. Generally, a certain molecule has to have a degree of functionality that must necessarily be a whole number. However many compounds are really a mixture of similar, but not identical, molecules. These compounds can have
15   functionality values that are not whole numbers, because they are, in fact, the average value of the functionalities of each component. In this respect the functionalities indicated in this specification and claims must be understood. A preferred way of implementing this alternative is by using a polyisocyanate (like a tetramer, or hexamethylene diisocyanate trimer allophanate, such as for example the compound
20   Bayhydur VPLS2319 ® (which is a polyisocyanate based on hexamethylene diisocyanate, and is sold by Bayer), which has a functionality of 3.8 and is already hydrophilised) to which an amine or mono-functional fatty alcohol is added (preferably linear or branched C10-C22, and very preferably linear C12-C18) (to provide the hydrophobic function) and functional amine or alcohol (such as for example Jeffamine
25   M1000) (to provide the hydrophilic function), although other precursors are also possible, like glycolic, glycine, taurine, monomethyl ethers of polyethoxylated alcohols, etc. The resulting amphiphilic compound will still have (or between 2 or 3) free isocyanates with which it will be able to form the polymer that shapes the wall of the microcapsules.
30

Preferably a second prepolymer is added to the first phase, where the second prepolymer has at least two main functional groups that react in the subsequent polymerisation for producing the polymer, where the second prepolymer is more hydrophobic than the amphiphilic compound if said first phase is organic, or the second
35   prepolymer is more hydrophilic than the amphiphilic compound if said first phase is aqueous. In fact, this way, this second prepolymer will tend to arrange itself as a second internal layer in the wall of the microcapsules, given its greater affinity to the

first phase. This second prepolymer will react also with the second compound thereby forming a wall with two layers, which confers greater robustness in the case of any possible subsequent liophilising, redispersion processes, etc., and, also, greater encapsulating power is achieved for the active ingredients included inside it. The two layer structure also means better control over the amount of functionalisations and the degradability of the particle. This second prepolymer can be, in turn, a mixture of two or more components, for example, in the case of an O/W emulsion they are preferably a diisocyanate (like isophorone diisocyanate) and a polyisocyanate (like Bayhydur 3100 ®, which is a hydrophilic, aliphatic polyisocyanate based on hexamethylene diisocyanate sold by Bayer).

Advantageously, the polymer comprises a functionalising group, such as for example a tumour cell directionaliser. The functionalising group has preferably two main functional groups in this way the functionalising group remains integrated in the main chain of the polymer or amphiphilic compound. The functionalising group can be preferably a monoclonal antibody or include a monoclonal antibody. Advantageously the polymer comprises a peptide, which can be incorporated directly into the amphiphilic compound. The peptide is preferably in the main chain and, if the wall has two layers, it is preferably in the outer layer or between the two layers, because it has to be able to interact with the outside medium. In fact, a particularly interesting solution in the invention is when this peptide is able to interact with overexpressed proteins outside the tumour cells (the integrins alpha beta). In this respect, it is particularly advantageous that the peptide be c-(RGDfK). Another preferred interaction strategy between particles and cancerous cells is carried out by means of folic acid (FA) incorporated in the same way as c-(RGDfK). The FA interacts with folate receptor proteins that are overexpressed in numerous cancer cells.

Generally, it may occur that the functionalising element (the peptide, the monoclonal antibody, or the functionalising molecule in general) does not have two main functional groups. In this case, the functionalising element can be made to react with a linker (linking element), such as for example a di- or polyisocyanate. This way, the link between the functionalising element and the linker makes it possible to obtain the functionalising group indicated above. So, preferably, the peptide is made to react with a di- or polyisocyanate (such as for example Bayhydur 3100 ®) and the reaction product is added to the first phase, which is the organic phase. Usually the amount of water present in the aqueous solution of the peptide is not enough to cause the complete emulsion, including the phase inversion. In these cases, subsequently more

water is added until the phase inversion takes place and then an aqueous solution continues to be added to the second compound (which preferably is a diamine and very preferably is DETA).

5 Generally, it is advantageous to add the second compound once the emulsion has already formed, including the phase inversion. In fact, when starting to add the second compound the formation of the microcapsule wall starts to form. Therefore, it is of interest that the microcapsules are already fully formed when the second compound is added. This is particularly important when the reactivity of the second compound is
10 high, such as for example in the case of DETA with isocyanates.

An advantageous embodiment of the method according to the invention when the emulsion is an O/W emulsion, comprises a stage of adding a polar, volatile organic solvent to the first phase, before stage [a], and a solvent evaporation phase, after stage
15 [b]. This makes it possible to obtain very small size microencapsulates and in relatively high concentrations. Preferably the solvent is acetone, methyl ethyl ketone or tetrahydrofuran, and very preferably it is acetone or tetrahydrofuran. If it is acetone, advantageously the amount of acetone added is smaller than 20% by weight of the amount of water in the second phase, whereas in the case of the methyl ethyl ketone
20 advantageously the amount of methyl ethyl ketone added is less than 15% by weight of the amount of water in the second phase.

Preferably the polymer or the amphiphilic compound is amphoteric. Advantageously at least one of the precursors used to form the amphiphilic compound is ionic. So,
25 preferably the amphiphilic compound includes protonated tertiary amines or quaternary ammoniums (or, generally, a cationomer) combined with anionomers in the same main chain. Therefore it is advantageous that some of the precursors used to form the polymer have two main functional groups and, also, a cationomer and/or an anionomer so that, once the polymer or amphiphilic compound is formed, this is amphoteric.

30

The aim of the invention is also an amphiphilic compound that is reactive with at least two main functional groups suitable for reacting in a subsequent polymerisation, characterised in that it has an HLB value greater than 10 (preferably greater than 15), and it has at least one hydrophilic functional group and other hydrophobic functional
35 group each in a chain which is sideways with respect to the chain that links both main functional groups. Also the aim of the invention is a reactive amphiphilic compound like the one above, but which has an HLB value smaller than 10. In both cases, preferably

the main functional groups of the amphiphilic compound are NCO functional groups, suitable for forming urethane and/or urea type links.

The aim of the invention is also a microencapsulate characterised in that its wall
5   comprises a reactive amphiphilic compound according to the invention.

Another object of the invention is a microencapsulate characterised in that the polymer which shapes its wall comprises, in its main chain, an acid group, a disulphide or an ester, where said acid group is preferably a sulphonate, carboxylate or phosphate
10   and/or where said ester is preferably a labile ester, or characterised in that the polymer that shapes its wall comprises a peptide.

Preferably the microencapsulate comprises, inside, an antitumoral active ingredient which, advantageously, is paclitaxel or plitidepsin.
15

Another advantageous solution is obtained when the microencapsulate according to the invention comprises, inside, an antibacterial agent. The bacterial agent is preferably a hydrophobic antibacterial, and very preferably it is a hydrophobic antibacterial agent from the family of macrolides. Particularly, these agents can be roxithromycin or
20   clarithromycin.

The aim of the invention is also a cosmetic or pharmaceutical composition characterised in that it comprises a microencapsulate according to the invention.

25   Finally, the aim of the invention is also a new use of a microencapsulate according to the invention, specifically for superficially coating a biocompatible material, preferably a biocompatible metal and very preferably titanium or its alloys.

30   ***Brief description of the drawings***

Other advantages and characteristics of the invention are appreciated from the following description, wherein, some preferable embodiments of the invention are described in a non-limiting manner, with reference to the accompanying drawings, in
35   which:

Figs. 1 to 4, size distribution of the capsules in Examples 1, 2, 3 and 4, respectively.

Figs. 5 to 9, SEM images of the capsules in Example 4.

Figs. 10 and 11, SEM and TEM images, respectively, of the capsules in Example 13.

5

Figs. 12 and 13, SEM and TEM images, respectively, of the capsules in Example 14.

Figs. 14 and 15, TEM images of a degrading of the capsules in Example 19, filtered 0.22 μm.

10

Figs. 16 and 17, TEM images of a degrading of the capsules in Example 19, filtered 0.45 μm.

Figs. 18 and 19, TEM images of another degrading of the capsules in Example 19, filtered 0.22 μm.

15

Figs. 20 and 21, TEM images of a degrading of the capsules in Example 18, filtered 0.22 μm.

20 Fig. 22, TEM image of the capsules in Example 28.

Fig. 23, TEM image of the capsules in Example 31.

Fig. 24, TEM image of the capsules in Example 35.

25

Figs. 25 and 26, size distribution of the capsules in Examples 18 and 34, respectively.

Figs. 27a to 27d, cytotoxicity study of nanocapsules relative to Example 28.

30 Fig. 28, biodistribution study in athymic mice without a tumour in the nanocapsules in Example 28 loaded with DiR.

Fig. 29, reaction diagram and theoretical representation of the ideal structure of the nanocapsule in Example 28 loaded and functionalised following Examples 31-33.

35

Figs. 30 and 31, size distribution of the capsules in Example 36.

Figs. 32 and 33, TEM images of the capsules in Example 36.

Figs. 34 and 35, evolution of the fragrance intensity over time of the capsules in Example 36.

Fig. 36, TEM image of the capsules in Example 37.

Fig. 37, diagram of the linker between the cRGDfK peptide and a microcapsule in Example 38.

Fig. 38, diagram of the amphiphilic prepolymer (AMPHYL) in Example 38.

Fig. 39, diagram of the hydrophobic prepolymer (HYFOB) in Example 38.

Fig. 40, theoretical representation of the ideal structure of the nanocapsule in Example 38.

Figs. 41 to 43, evolution over time of the degrading of the microcapsules in Example 38 due to the action of glutathione.

Fig. 44, diagrammatic representation of the functionalising process in Example 39.

Fig. 45, SEM image of the functionalised titanium surface in Example 39.

Fig. 46, fluorescence spectrum of the mixture of DiL and DiO in Example 41 after 84 hours at 37 ºC and the corresponding fluorescence spectrum of the mixture of nanocapsules 2.5 hours after adding GSH.

Fig. 47, representation of the FRET ratio in Example 41, calculated as $I_a/(I_d + I_a)$, where I_a e I_d are the fluorescence intensity of the acceptor (DiI) and donor (DiO), respectively against time.

Examples

Products used.

- Isophorone diisocyanate (IPDI),

- Ymer N120 ® (difunctional linear polyethylene glycol monomethyl ether) by Perstorp,

- Pripol 2033 ® (Dimerdiol) by Uniqema,

- Crodamol GTCC® by CRODA (which is a caprylic/capric triglyceride),

5   - olive oil,

- Lavandín ® and Aromatic Meadow ® fragrances,

- Tea tree oil,

- Retinol 10S ® by Bayer (retinol at 10% in soya oil),

- Paclitaxel by Fujian South Pharmaceutical,

10   - Plitidepsin by Pharmamar,

- c-(RGDfK) by PCB,

- Folic Acid (FA) by Aldrich,

- Roxithromycin by Aldrich,

- Clarithromycin by Aldrich,

15   - Clear Blue DFSB-C0 by Risk Reactor,

- Ethylenediamine propyl sulphonate (EPS) by Raschig,

- NaOH by Panreac,

- BYK-028 ® by BYK,

- Ethylenediamine (EDA),

20   - Diethylenetriamine (DETA),

- Triethylenetetramine (TETA) by Huntsman,

- Hexamethylene diamine (HMDA) by Panreac,

- Duomeen C ® (dodecylamine propyl amine (coconut)) by Akzo Nobel,

- Duomeen T ® (C16-C18 amino propylamine) by Akzo Nobel,

25   - TAP 100D (N-octadecyl- 1,3 –propanediamine, by Clariant, it is equivalent to Duomeen T by Akzo Nobel),

- Desmodur N3600 –1,6-hexamethylene diisocyanate, polymeric form

- Jeffamine M1000,

- Triameen C (N-cocoalkyl dipropylene triamine),

30   - LAP 100D (dodecyl amino propylamine (coconut), by Clariant, equivalent to Duomeen C by Akzo Nobel),

- Triameen T (N-tallowalkyl dipropylene triamine),

- Priamine 1074 (dimer diamine from C36 dimer acid) by Croda,

- DDI1410 disocyanate by Cognis (fatty isocyanate derived from dimer acid),

35   - Bayhydur 3100 ® (aliphatic hydrophilic polyisocyanate based on hexamethylene diisocyanate) by Bayer,

- Triethylamine by Aldrich,

- 2,2-dithiodiethanol (DEDS) by Aldrich,

- cystamine dihydrochloride by Aldrich,

- L-lysine by Aldrich,

- dibutyltin dilaurate (DBTL),

5 - tetrahydrofuran (THF),

- CTP (cell targeting peptide), such as for example c-(RGDfK))

Example 1. *Encapsulation of olive oil.*

10

In a 700 ml reactor 10.53 g of IPDI (which performs the function of the first precursor), 6.38 g of Dimerdiol (which performs the function of the second precursor), 20.38 g of olive oil and 20.83 g of Ymer (which performs the function of the third precursor) were loaded. The reaction was carried out at 160 rpm, at 85ºC and with nitrogen.

15

After 2 hours reaction time, the reactor was cooled to below 25ºC and 3 drops of BYK-028 antifoaming agent were added, the emulsion was made at 400 rpm with 250.00 g of water, adding it slowly on top of the amphiphilic prepolymer.

20 Once the emulsion was complete, 3.28 g drops of EPS (which performs the function of the fourth precursor), 0.36 g of NaOH and 10.20 g of water were added. After 20 minutes 0.43 g of DETA (which performs the function of the second compound) were added. The EPS was added to combine with the prepolymer and make it more hydrophilic, but essentially it was done to include a sulphonate that was a weak point in 25 the chain. It also allowed reducing the particle size a little. As already mentioned above, generally disulphide or labile ester groups can be added expressly, so that they are a weak point for breaking (for example, at the estearases). In the proximity of the tumours there is much reducing material that breaks the disulphide bridge. (See also Example 19).

30

A good white bluish emulsion was obtained. Using an optical microscope capsules sized smaller than 4 µm were observed. Using Light Scattering (DLS, Dynamic Light Scattering), it was confirmed that the capsules were sized between 0.4 and 4 µm.

35

Example 2. *Encapsulation of an Aromatic Meadow C55593P fragrance by Lucta.*

In a 700 ml reactor 10.53 g of IPDI (first precursor), 6.40 g of Dimerdiol (second precursor), 20.36 g of Aromatic Meadow and 15.52 g of Ymer (third precursor) were loaded. The reaction was carried out at 160 rpm, at 85ºC and with nitrogen. After 2 hours reaction time, the reactor was cooled to below 25ºC and 3 drops of BYK-028

5   antifoaming agent were added, the emulsion was made at 400 rpm with 250.00 g of water.

. Once the emulsion was complete, 3.17 g of EPS (fourth precursor), 0.35 g of NaOH and 10.00 g of water were added. After 20 minutes 0.79 g of DETA (second

10 compound) were added.

A good white bluish emulsion was obtained. Using an optical microscope capsules sized smaller than 4 μm were observed. Using Light Scattering, it was observed that the capsules were sized between 0.2 and 3 μm. The population was distributed

15 between 0.2 and 0.4 μm and again between 1 and 3 μm.

Example 3. *Encapsulation of Retinol 10S.*

20 Example 1 was repeated replacing the 20.38 g of olive oil with 20.34 g of Retinol 10S.

In this case a good emulsion was also obtained, but with capsules sized smaller than 10 μm. Using Light Scattering, it was observed that the capsules were sized between 0.15 and 10 μm. Most of the population was between 1 and 3 μm.

25

Example 4. *Encapsulation of the Aromatic Meadow C55593P fragrance by Lucta.*

Example 2 was repeated with TETA instead of DETA. By using YMER and DIMERDIOL, together they form a very soft capsule wall. In this case, using TETA

5   allowed for more intensive cross-linking. In those cases where with TETA the cross-linking was excessive, DETA could be used.

In a 700 ml reactor 10.52 g of IPDI, 6.57 g of Dimerdiol, 20.29 g of Aromatic Meadow and 15.37 g of Ymer were loaded. The reaction was carried out at 160 rpm, at 85ºC

10   and with nitrogen. After 2 hours reaction time, the reactor was cooled to below 25ºC and 3 drops of BYK-028 antifoaming agent were added, the emulsion was made at 400 rpm with 200.00 g of water. Once the emulsion was complete, 3.50 g of EPS, 0.39 g of NaOH and 10.50 g of water were added. After 20 minutes 1.00 g of TETA was added.

15   A good emulsion was obtained with capsules sized less than 4 μm. Using Light Scattering, it was observed that the capsules were sized between 0.3 and 4 μm. Most of the population was between 0.3 and 1 μm.

20   ***Example 5.*** *Encapsulation of the Lavandín 80101 fragrance by Chemir.*

Example 4 was repeated replacing the 20.29 g of Aromatic Meadow with 20.66 g of Lavandín fragrance.

25   In this case too a good emulsion was obtained, with capsules sized smaller than 4μm.

Example 6. *Encapsulation of Tea Tree Oil.*

Example 4 was repeated replacing the 20.29 g of Aromatic Meadow with 20.45 g of Tea Tree Oil.

5

In this case too a good emulsion was obtained with capsules sized smaller than 4 µm.

Example 7. *Encapsulation of Tea Tree Oil.*

10

Example 6 was repeated but with half the polymer.

In a 700 ml reactor 5.28 g of IPDI, 3.26 g of Dimerdiol, 20.45 g of Tea Tree Oil and 7.77 g of Ymer were loaded. The reaction was carried out at 160 rpm, at 85ºC and with

15   nitrogen. After 2 hours reaction time, the reactor was cooled to under 25ºC and 3 drops of BYK-028 antifoaming agent were added, the emulsion was made at 400 rpm with 155.00 g of water. Once the emulsion was complete, 1.68 g of EPS, 0.19 g of NaOH and 5.00 g of water were added. After 20 minutes 0.49 g of TETA were added.

20   A good emulsion was obtained and the distribution of the capsule size was between 4 and 0.1 µm.

Example 8. *Encapsulation of Tea Tree Oil.*

25

Example 7 was repeated but increasing the cross-linker (from 0.49 g of TETA to 0.72 g of TETA).

In this case too a good emulsion was obtained but with capsules that were not so

30   spherical, and the capsule diameter between 5 and 0.1µm.

Example 9. *Encapsulation of Paclitaxel.*

35   In a 700 ml reactor 10.53 g of IPDI, 6.58 g of Dimerdiol, 20.00 g of Crodamol GTCC and 15.39 g of Ymer were loaded. The reactor was carried out at 160 rpm, at 85ºC and with nitrogen. After 2 hours reaction time, the reactor was cooled to under 25ºC and

0.64 g of Paclitaxel, 3 drops of BYK-028 antifoaming agent were added and the emulsion was made at 400 rpm with 200.00 g of water. Once the emulsion was complete, 3.10 g of EPS, 0.68 g of NaOH and 10.00 g of water were added. After 20 minutes 1.00 g of TETA was added.

5

A good emulsion was obtained with capsules between 2 and 0.1 μm.

Example 10. *Encapsulation of Crodamol GTCC.*

10

In a 700 ml reactor 10.54 g of IPDI, 6.57 g of Dimerdiol, 20.29 g of Crodamol GTCC and 19.95 g of Ymer were loaded. The reaction was carried out at 85ºC and with nitrogen. After 2 hours reaction time, the reactor was cooled to under 25ºC. The emulsion was made at 15,000 rpm by adding the prepolymer on to 200,00 g of water,

15   once the emulsion was complete, 2.64 g of EPS, 0.29 g of NaOH and 10.50 g of water were added at 5 000 rpm. After about 3 minutes, 0.75 g of TETA were added.

A good emulsion was obtained, in the optical microscope capsules were observed between 0.1 and 4 μm. It was observed also that there was a lesser amount of large

20   capsules than in other Examples.

Example 11. *Encapsulation of Crodamol GTCC.*

25   This product is the same at Example 10 but with EDA instead of EPS. The EDA is less hydrophilic than the EPS.

A total of 10.78 g of IPDI, 6.67 g of Dimerdiol, 21.13 g of Crodamol GTCC and 20.36 g of Ymer were loaded. The reaction was carried out at 85ºC and with nitrogen. After 2

30   hours reaction time, the reactor was cooled to 25ºC, 2 drops of BYK-028 antifoaming agent were added and the emulsion was made with 200.00 g of water in the Ultra-Turrax at 15.000 rpm. Once the emulsion was complete, 0.39 g of EDA were added to 10.00 g of water with mechanical stirring. After 30 minutes 0.52 g of TETA were added.

35   A good white bluish emulsion was obtained, in the optical microscope capsules were observed sized 0.9 μm but also some agglomerated capsules. Using Light Scattering, it

was observed that the capsules were sized smaller than 0.9 μm. Most of the population was 246 nm.

5 ***Example 12.*** *Encapsulation of Crodamol GTCC.*

This product is the same as Example 11 but with less polymer.

A total of 5.85 g of IPDI, 3.35 g of Dimerdiol, 21.20 g of Crodamol GTCC and 10.17 g
10 of Ymer were loaded. The reaction was carried out at 85ºC and with nitrogen. After 2 hours reaction time, the reactor was cooled to 25ºC, 2 drops of BYK-028 antifoaming agent were added and the emulsion was made with 200.00 g of water in the Ultra-Turrax at 15,000 rpm. Once the emulsion was complete, 0.39 g of EDA were added to 10.00 g of water with mechanical stirring. After 30 minutes 0.52 g of TETA were added.
15

A good white bluish emulsion was obtained, in the optical microscope capsules were observed that sized 0.9 μm but there were also some agglomerated capsules.

20

Example 13. *Encapsulation of Crodamol GTCC.*

This Example used the system of creating the amphiphilic polymer at the same time as making the emulsion.

5

The following were mixed in a beaker:

5.26 g of IPDI (first precursor)

11.45 g of Ymer (second precursor)

6.05 g Crodamol GTCC

10

The following were mixed in another beaker:

3.15 g of Duomeen C (third precursor)

210.00 g of water

15 The organic solution was added to the aqueous one and it was stirred at 15,000 rpm for 30 minutes.

A good white bluish emulsion was obtained, in the optical microscope capsules were observed smaller than 450 nm. The product was filtered with a syringe and 0.45 μm

20 filter, and 88.2% of the capsules were smaller than 450 nm.

Duomeen, in spite of being hydrophobic, has sufficient dispersibility in water to put it in the continuous aqueous phase. However, as it is more hydrophobic than hydrophilic, it ends up going to the disperse, oily phase and there it reacts and is incorporated into

25 the prepolymer. This allows carrying out the reaction to introduce the hydrophobic part after making the emulsion from the the hydrophilic prepolymer IPDI-YMER part, in order to form the amphiphilic prepolymer just in the interphase. Then the capsule is closed fully (crosslinked) with the polyamines that wear the NCO that remain from the amphiphilic prepolymer formed in the actual interphase. Generally, this Duomeen will

30 have to be introduced into the prepolymer as in the case of the dimer diol, but a solvent is required because if not it will not work well because of its insolubility in the oil medium that is used. Duomeen, as it is a diamine, forms a diurea. The dimer diol is a different case, forming two urethanes. In certain cases it is solid enough, has a sufficiently high Tg, creates a sufficient barrier effect and is stable enough to withstand

35 the capsule contents, which is harder to achieve with a prepolymer based on dimer diol polyurethanes- YMER IPDI. In this case DETA is not added, or any diamine or small, hydrophilic polyamine, and instead it is left to react with the water.

Alternatively the Duomeen could have been introduced in the prepolymer with a suitable solvent as in the case of the dimer diol. And also it is possible to use a small amount of DETA to close (crosslink) and ensure the system's strength. However, the

5   results seem to be more repeatable than with the interphasic system in this Example. In the case of the dimer diol-IPDI-YMER, the formed wall of the capsule is more sensitive because the prepolymer has greater hardness (lower Tg) and is more soluble in the phases, therefore it is good to add DETA or TETA type polyamines to confer hardness and a barrier effect, etc.

10

Example 14. *Encapsulation of Crodamol GTCC.*

This Example used the system of creating the amphiphilic polymer at the same time as

15   making the emulsion.

A total of 1.71 g of IPDI, 5.04 g of Ymer N120 and 2.64 g of Crodamol GTCC were loaded. The reaction was carried out at 85ºC and with nitrogen. When NCO=1.372% was reached, the reactor was cooled and 211.60 g of acetone were added. In another

20   reactor 0.31 g of Duomeen C were added in 422.98 g of water. The acetonic phase was added on top of the aqueous phase at 400 rpm. Finally, 0. 08 g of DETA were added to 5.00 g of water and the acetone evaporated.

A very good emulsion was obtained, in the optical microscope capsules were observed

25   with a diameter smaller than 0.5 µm. % solids=2.00%

The product was filtered with a syringe and 0.45 µm filter, and 81.5% of the capsules were smaller than 450 nm.

30   *Examples 1 to 14 – Analysis and results*

In all the Examples a Titromatic 2S tritrator by Crison was used to check the NCO percentage of the prepolymer. Also the end of the reaction was checked using IR, observing the characteristic signals of the polyureas (1650-1500 cm^{-1}) and the absence

35   of signal due to the NCO (2270cm^{-1}).

The morphology and size of the capsules obtained in the Examples were studied using an optical microscope and SEM.

The size distribution of the capsules was studied using Light Scattering.

5 In all the Examples emulsions stable over time were obtained with capsules sized smaller than 5 µm, except in Example 3 where capsules smaller than 10 µm were obtained, and in Examples 13 and 14 where capsules smaller than 0.45 µm were obtained.

10 The graphs in Figs. 1 to 4 show the size distribution of the capsules in Examples 1, 2, 3 and 4, respectively.

In these graphs it can be observed that most of the capsules are under the micron (except Example 3) because the % volume is much greater in this area. Using filtration, 15 the larger capsules can be separated and even more stable emulsions can be obtained and with a more uniform distribution.

SEM was used to study the morphology and size of the capsules obtained in Example 4 (see Figs. 5 to 7). The images of the capsules were obtained after diluting them with 20 Millipore 1/100 water and coating them with gold.

Using 0.45 µm filters the diluted capsules were filtered to obtain clearer images and to remove the capsules sized larger than 0.45 µm (see Figs. 8 and 9).

25 Figs. 10 and 11 show the capsule images obtained using SEM (Scanning Electron Microscope) and TEM (Transmission Electron Microscope) respectively in Example 13, and Figs. 12 and 13 show the capsule images obtained using SEM and TEM respectively in Example 14.

30

Examples 1 to 14 - Conclusions

With this amphiphilic system and with different types of processes, various compounds can be encapsulated obtaining capsules sized less than 5 µm if using the system 35 wherein the amphiphilic polymer is formed before forming the O/W emulsion. Generally, preferably the emulsion is created by phase inversion by adding water to the prepolymer (generally, the continuous phase to the disperse phase). With stability and

without using external emulsionants, and less than 450 nm if using the system wherein the amphiphilic polymer is formed during the emulsion.

5 In both cases the emulsions obtained are very stable over time, the capsules do not join together and they are stable with respect to biological fluids, etc.

The stability of the products obtained in Examples 11, 13 and 14 was checked in different media: saline, PBS (Phosphate Buffered Saline) and blood plasma. The results were as follows:

10

Nanocapsules	Stability after 1 week			Stability after 1 month		
	SS	PBS	Blood plasma	SS	PBS	Blood plasma
Example 11	stable	stable	stable	stable	stable	unstable
Example13	stable	stable	stable	stable	stable	stable
Example 14	stable	stable	stable	stable	stable	unstable

15 It must be taken into account that the products known in the state of the art, with normal emulsifying agents outside the wall, are not stable in these media and precipitate.

Example 15.

20 A total of 19.02 g of Crodamol GTCC + 7.56 g Desmodur N3600 + 10 g methyl ethyl ketone (MEK) were added to a beaker. Slowly, with 50% magnetic stirring, first 8.34 g Jeffamine M1000 + 5 g MEK were added, then 2.13 g DuomeenT + 5 g MEK with 75% stirring. On this basis four tests were conducted with this prepolymer:

25 15-1 → 15 g of the product were added on to 90 g of water with 75% stirring, dropwise. The water contained 0.16 g of EDA.
15-2 → Dropwise, 88 g of water were added on to 15 g of the product. When the phase inversion was carried out, 2 g of water + 0.16 g of EDA were added.
15-3 → 15-1 was repeated, but by injection, not by adding water dropwise.
30 15-4 → Imitation of the ketonic method, 0.6 g of prepolymer were put in 20 ml acetone, and they were injected into 80 ml of water + 0.22 g EDA.

Results:

15-1 → The capsules were dented. There seemed to be capsules inside capsules. Size 2-16 microns.

15-2 → The capsules had a much more regular shape. The emulsion was stable. Capsule size approx. 2-6 microns.

15-3 → It worked out the same as 15-1, and it seemed that the injection was not a vital aspect, providing that the addition was carried out slowly.

15-4 → A transparent emulsion was obtained, with bluish tones. No capsules were observed with the optical microscope. SEM images showed capsules with a wide size distribution, from 7 to 100 nm, with an average of 20 nm. *(Amphil HLB12)*

Example 16.

An experiment similar to the one above, but using polymeric MDI (polymeric diphenylmethane diisocyanate (or methylene diphenyl diisocyanate)).

5

On to 21 g Crodamol GTCC + 4.90 g polymeric MDI + 5 g MEK first of all a mixture of 9.73 g Jeffamine M1000 + 10 g MEK was added, and later, 2.13 g Duomeen T + 5 g MEK, all dropwise, with 50% mechanical stirring. Subsequently, 0.6 g of this product were added by injection into 20 ml acetone onto 40 g water + 1 drop of DETA, the

10 injection lasted 1'. The emulsion was white-bluish and very stable (it did not separate or foam). The capsules could not be seen with the optical microscope.

Example 17.

15

Encapsulation using aromatic /aliphatic diisocyanate with triamine.

A total of 16.67 g Crodamol GTCC + 4.89 g TMXDI ((tetra methyl xylylene diisocyanate) + 5 g MEK were weighed.

20 Dropwise, with 50% magnetic stirring, 2.19 g TriameenC + 5 g MEK were added.
Subsequently, 6.95 g Jeffamine M1000 + 8 g MEK were added.
A total of 3 tests were conducted with this prepolymer using the methodology in Example 14, by injection:
A → 2.2% of solids, 4 drops of DETA in H2O.

25 B → 2.2% of solids, 1 drop of DETA in H2O.
C → 10% solids, 0.5 g of DETA in H2O.

Results:
A → Capsules measuring 2 microns, very narrow size distribution. Regular capsule

30 shape.
B → The same as A, but the shape of the capsules was much more irregular.
C → They came out joined together, but the distribution and size was the same as A.

35 **Example 18.** *Encapsulation of Crodamol GTCC*

Similar to Example 14 but the method was carried out in two stages:

1) A total of 6.01 g of Crodamol GTCC, 11.79 g of Ymer N120 and 5.72 g of IPDI were loaded. The bath was set at 85ºC with N_2 current. It was left to react during two and a half hours. When the theoretical NCO level was reached, the reactor was cooled to 50ºC and its contents was dissolved with 12.67 g dry MEK.

2) A total of 1.66 g of Duomeen C were dissolved in 25.50 g of MEK and added to the reactor. When the second theoretical NCO was reached, the system was cooled with a bath of water and ice and the emulsion was made by adding cold water dropwise. Then 0.42 g DETA dissolved in 3.76 g of water was added. Finally the MEK evaporated.

Product appearance:

White liquid and very small capsules mainly with a size smaller than a micron. The product was filtered very easily using micro filters with pores sized 0.450 and 0.200 µm.

The TEM and SEM product was observed, and nanocapsules were observed up to 20 nm in size. Also various repetitions of this product were made and the results were approximately repeatable insofar as the particle size. A DLS analysis was conducted and a main average population of 100 nm in size was observed. Fig. 21 shows an image obtained with the SEM where agglomerates of nanocapsules could be observed sized smaller than 100 nm.

Example 19. *Encapsulation of Crodamol GTCC*

This Example incorporates a disulphide bridge in the capsular wall. The fact that there is a disulphide in the chain favours the wall degradation with the glutathione and other reducing agents inside and around the tumour cells.

A total of 5.562 g IPDI + 10.338 g Crodamol GTCC + 12.5256 g dry Ymer were added to the reactor at an internal reactor temperature of 63 ºC. When the theoretical NCO % was reached a 520 µl (0.655g) micropipette was used to add 2.2-dithiodiethanol. It was observed that the 2.2-dithiodiethanol was denser and the stirring had to be optimum so that different phases did not form during the reaction. When the theoretical NCO% was reached the temperature was lowered to 50 ºC and 1.4368 g LAP 100D solublised in 20 g of dry MEK were added. After 20 minutes the reactor was cooled to 10 ºC. A clear thickening of the mixture was observed. A total of 3 drops of BYK-028 antifoaming agent were added. Next the dropwise addition of 230 ml of water cooled to 15 ºC started. When the phase inversion took place 155 µl (0.1479 g) of DETA was added in the addition funnel continuing with the more frequent dropwise addition of the rest of the milliQ water + DETA.

An IR was done before the emulsification to check the NCO presence in reaction. It was left under stirring and cooling to 10 ºC for 2 more hours after the emulsification.

White-bluish, even appearance. Stable over time, it was stored in the fridge. It was filtered easily in the 450 nm filter and also in the 220 nm one.

Degradation tests of the polymer functionalised with a disulphide bridge against the reducing agent glutathione (GSH)

- A total of 100µL of GSH 10mM + 100µL of Example 19 filtered at 0.22 µm were incubated for 30 min at 37ºC. See Figs. 14 and 15. A partial degradation was observed. Areas with nanocapsules were still observed.

- A total of 100µL of GSH 10mM + 100µL of Example 19 filtered at 0.45 µm was incubated for 30 min at 37ºC. See Figs. 16 and 17. Partial or derisory degradation was observed.

- Two new incubations were carried out with glutathione. 100µL of GSH 10mM + 50µL of Example 19 (filtered at 0.22 µm) for 24h at 37ºC. It was repeated twice and in the two cases considerable sample degradation was observed. Aggregates sized larger than the filtration performed appeared due to the break in the capsular wall and the subsequent destabilising of its amphiphilic nature. See Figs. 18 and 19.

- A new incubation was carried out with glutathione. The test was conducted to conclude whether the capsules synthesised without disulphide in the wall also degraded in a reducer medium (glutathione). 100µL of GSH 10mM + 50µL of Example 18 (filtered at 0.22 µm) for 24h at 37ºC. Apparently no wall degradation due to glutathione was observed.

In all the degradation tests the characterisations were carried out by TEM.

Degradation tests - Conclusions

- The 30 min treatment in GSH in Example 19 was not sufficient to degrade the wall.

- It was concluded that in Example 19 the polymeric capsular wall was functionalised with disulphide and this was degradable in the presence of a reducing medium in a concentration similar to that which can be found in the intracellular medium in tumour cells following incubation during 24h at 37ºC.

- It was also concluded that the nanocapsular wall not functionalised with disulphide in Example 19 without peptide was not degraded after an identical treatment to the one carried out in Example 19.

Example 20.

This Example is the same as Example 18 but incorporating a peptide in the nanocapsule wall.

Stage 1: The prepolymer was prepared as in Example 18.

A total of 5.98 g of Crodamol GTCC, 11.87 g of Ymer, 5.43 g of IPDI were loaded and heated to 85ºC in a N_2 atmosphere. The reaction was carried out during two and a half hours. Once the reaction had finished (valuing the NCO%) the reactor was cooled to 50 ºC and the contents was dissolved with 13.08 g of MEK. Then 1.64 g of Duomeen C

5   dissolved in 25.05 g of MEK were added and it was left to react one more hour. The end of the reaction was checked by valuing the NCO level. The prepolymer was unloaded and kept in the fridge.

Stage 2. A tenth of the prepared prepolymer was taken and work continued with it.

10

In a suitable reactor, 6.25 g of prepolymer were loaded and using an addition funnel 25.64 g of water were added, dropwise. The process was carried out at room temperature with magnetic stirring. Once the emulsion was made, the peptide c-(RGDfK) previously dissolved in 5.31 g of water and neutralised with 100 µl of NaOH

15   1N was added. It was left to react about 10 minutes and 0.0618 g of DETA dissolved in 2.00 g of water were added. Finally the MEK evaporated.

A white, fluid liquid was obtained.

20   When it was left to rest the separation of the two phases was observed, leading to a solid, white layer and leaving the barely transparent liquid. When observing the product with the optical microscope imperfect capsules were seen with a great variety in size (1-15 µm). The capsules were filtered with 0.45 µm micro filters and using Light Scattering it was observed that the capsules were mainly sized 6 nm, and the most

25   abundant populations were concentrated between 4 and 12 nm.

Example 21.

30   It began with preparing the prepolymer exactly as in the previous Example.

Prepolymer:

A total of 5.99 g Crodamol GTCC, 11.68 g Ymer and 5.92 g IPDI were added, it was

35   subjected to an inert N_2 atmosphere and heated to 85ºC and left to react for 2h 30min. When all the Ymer had finished reacting (valuation of excess NCO), it was cooled to 50ºC and the contents dissolved with 12.53 g of MEK. Then 1.65 g of Duomeen C

dissolved in 27.29 g of dry MEK was added. A second NCO valuation was made to check the total NCO reaction.

Incorporating the peptide:

5

A part weighting 6.2668 g was taken from the prepared polymer and the peptide solution c-(RGDfK) prepared with 0.054 g of it dissolved in 7.4168 g of DMSO (dimethylsulphoxide) and neutralised with 0.0104 g of triethylamine was added to it. After about 15 minutes 70 g of water were added and the emulsion was made. Then

10 0.034 g of DETA dissolved in 4.73 g of water were added. Finally the MEK was evaporated and the product was filtered.

White, fairly liquid emulsion. The capsules observed with the optical microscope were larger than in the previous Example, sized between 1 and 5 microns. Perfect, stable

15 spheres were observed. No non-encapsulated oil or polymer remains were seen. The product was easily filtered with 0.450 µm micro filters.

The DLS results show that the emulsion is made up of two groups of capsules mainly (2 and 5 nm).

20

Example 22.

The same method was used as in Example 18 but replacing part of the MEK with acetone.

5

Prepolymer:

Under an inert N_2 atmosphere and at 85 ºC, 11.6267 g of Ymer, 5.92 g Crodamol GTCC and 5.29 g IPDI were loaded. It was left to react for 2 hours. Once the reaction
10   had finished (real NCO = 3.863% and theoretical NCO = 4.335%), the reactor was cooled to 50ºC and the contents dissolved with 15.32 g of MEK. Then 1.5950 g of Duomeen C dissolved in 16.70 g of MEK were added.

It was checked that all the Duomeen C had reacted, by conducting an NCO in excess
15   valuation (real NCO = 0.030%, theoretical NCO = 0.883%). Finally, 12.00 g of acetone at a temperature below 15ºC were added. The product was unloaded and kept well-sealed in the fridge.

Various parts were taken from the prepolymer prepared and the following tests were
20   conducted.

Target:
A part weighing 6.8090 g was taken and put in the reactor under an inert atmosphere and at room temperature.

25

Under magnetic stirring, 25.13 g of water were added to make the emulsion. The water was added dropwise and the reactor was cooled with a mixture of water-ice. Then 0.0430 g DETA dissolved in 5.03 g of water were added. Finally the solvents evaporated and the product was filtered. A white, fluid emulsion was obtained and a
30   separation of two phases was observed, one transparent liquid phase and a second solid phase floating on the surface.

With the microscope well defined capsules were observed sized smaller than a micron. Also capsule agglomerates were observed.

35

To one part weighing 6.8794 g of the prepolymer synthesised before, 0.054 g of the c-(RGDfK) peptide dissolved in 0.70 g of water and neutralised with 0.0280 g of

triethylamine were added. The peptide action took place at temperatures below 15ºC and with magnetic stirring, and it was left to react for about 15 minutes. Once this time had elapsed, the product was emulsified with 26.44 g of water which were added gradually increasing the magnetic stirring. Then 0.0507 g DETA dissolved in 5.66 g of

5 water at room temperature were added. Finally, the solvents evaporated and the product was filtered.

The product obtained was white and fluid, and unstable because it separated into two phases; one solid layer floating on the surface of the transparent liquid phase. This

10 product was filtered using a 0.45 micron micro filter and the filtered transparent part was observed using SEM. Perfect, well defined and stable capsules were obtained when observed dry using SEM. This proved their structural stability in spite of their small size.

15

Example 23.

Example 18 was copied but incorporating the antitumoral agent, plitidepsin.

20 Under an N_2 atmosphere 11.5949 g Ymer, 6.03 g Crodamol GTCC and 6.21 g IPDI were loaded and the reaction was carried out at 75ºC for 2 hours. The NCO was valued to check that all the Ymer had reacted ($NCO_{theoretical}$ =5.624%, NCO_{real} =5.624%). The temperature was lowered to 50ºC and the mixture was dissolved with 14.08 g of MEK. Then 1.6431 g of Duomeen C dissolved in 25.08 g of MEK were

25 added.

After an hour another NCO valuation was made to check the end of the reaction ($NCO_{theoretical}$ =1.304%, NCO_{real} =0.770%). The reaction was stopped, the prepolymer was unloaded and kept well-sealed in the fridge.

30

Encapsulation of Plitidepsin

A part weighing 6.9108 g was taken from the prepolymer prepared and placed in a suitable reactor avoiding, as much as possible, any air entering by passing a current of

35 nitrogen. Then, carefully, 0.0108 g of plitidepsin (drug) was added with magnetic stirring. Once the drug was dissolved the emulsion was made with 20.68 g of water

added slowly using an addition funnel. Finally 0.0303 g DETA dissolved in 5.02 g of water were added and left under stirring for approximately one hour.

5 A white emulsion was obtained that separated into two phases. Under the optical microscope well rounded, perfect capsules were observed sized between 0.5 and 2 microns.

After filtering the emulsion was transparent and stable, and it did not separate into different phases.

10

Using SEM, nanocapsules were observed with an average size of between 6 and 10 nm. Using DLS two size population distributions were detected, one average size population around 13 nm and another average size of 350 nm.

15

Example 24.

This was conducted in the same way as Example 13 reducing the amount of the reagents and diluting the solids to half.

20

A total of 0.5056 g Duomeen C were dissolved in 75.31 g of water. Another solution was prepared separately by mixing 1.7825 g of Ymer, 0.9470 g of Crodamol GTCC, 0.82 g of IPDI and to fluidify this mixture 2 g approximately of acetone were added.

25 At room temperature the second mixture was added to the first and stirred with the Ultra-Turrax at 15,000 rpm for 30 min.

The emulsion obtained was stable and consisted on a white, fluid liquid. The capsules observed with the optical microscope were well-defined and stable and sized between 30 0.5 and 1.5 microns.

After the filtration and drying process nanocapsules with a diameter of about 150 nm could be observed.

35

Example 25.

This product was synthesised as in Example 24 above replacing part of the Duomeen C with c-(RGDfK) peptide and Triameen C to compensate the functionality.

A total of 0.9340 g of Crodamol GTCC, 1.7699 g Ymer and 0.83 g IPDI were mixed. The mixture was diluted with 2 g of acetone and another mixture prepared by dissolving 0.4192 g Duomeen C, 0.0808 g peptide and 0.0330 g of Triameen C in 75.12 g of water was added. It was shaken at 15,000 rpm for 30 minutes at room temperature.

A white, stable emulsion was obtained. The capsules observed with the optical microscope were sized between 0.5 and 1 micron

Example 26.

It was synthesised the same way as the product in Example 23 replacing part of the oil, Crodamol GTCC, with the drug.

A total of 1.7696 g Ymer were mixed with 0.9043 g Crodamol GTCC and 0.0229 g of drug (plitidepsin). This mixture was fluidified with 2 g de acetone.

Separately 0.4871 g Duomeen C were dissolved in 75.65 g of water and the previously prepared mixture was added to it. It was left to react half an hour under the same temperature and stirring conditions.

The emulsion had the same appearance as the ones in the last two Examples above and the capsules were sized smaller than a micron.

Example 27.

In this Example the two previous Examples were combined, based on the same philosophy as in Example 23. In other words the same methodology as in Example 23 was followed, but replacing part of the oil and part of the Duomeen C with the corresponding components.

A total of 0.9085 g of Crodamol GTCC, 1.7744 g Ymer, 0.8109 g IPDI and 0.0250 g of drug (plitidepsin) were mixed. The mixture obtained was dissolved with 2.5 g of acetone. Separately 0.081 g of c-(RGDfK) peptide, 0.4186 g Duomeen C and 0.0491 g Triameen C were dissolved in 75.26 g of water. The organic mixture was added to the

5 aqueous mixture and it was left to react for 30 minutes with stirring at 15,000 rpm.

A good, stable white emulsion was obtained and capsules sized smaller than a micron were observed.

10

Example 28.

This Example introduces a second hydrophobic prepolymer for increasing the encapsulation power, and the strength of the particles.

15

A total of 6.7632 g of IPDI, 5 g of Crodamol GTCC and 520 µl (0.655 g) of 2,2-dithiodiethanol (DEDS), previously stirred in vortex, were added simultaneously to a reactor at 50ºC. The remains were entrained with diethyl ether. It was observed that the 2,2-dithiodiethanol was more dense and appropriate stirring was required to ensure

20 that no phases were formed during the reaction. When the reaction started, the reaction medium turned cloudy.

One hour later 7.5 g of dry YMER N-120 were added, and entrained with 1 ml of dry acetone. The dry acetone can be replaced preferably with diethyl ether, which always

25 has a smaller water content and evaporates more quickly in the reaction medium.

When the theoretical NCO was reached (approximately after 4 to 5 hours reaction time) the heating bath was removed and 3.75 g of LAP 100D solubilised in 8g of dry MEK were added.

30

After 45 min the reactor was cooled to about 5-10ºC and 1.9425 g of IPDI and 1.8075 g of Bayhydur 3100 in 16 ml of dry MEK were added. These two isocyanates are the second prepolymer, which will form the second, internal layer of the wall. A distinctive thickening of the sample was observed. Two drops of BYK-028 antifoaming agent (at

35 the most there can be 40g of MEK overall) were added.

Before emulsifying, the NCO presence in the reaction was checked using IR.

Then, dropwise 260 ml of milliQ water basified to a pH between 11 and 12 and cooled to a temperature between 5 and 10 ºC, were added.

5   When the phase inversion took place (fairly viscose) 1024 µl (1.1461 g) of DETA were added in the compensated pressure funnel while continuing to add, dropwise, the rest of the water with the DETA at greater speed.

The stirring and the cooling to 10ºC were maintained until the NCO signal disappeared
10   from the IR spectrum.

An even, white-bluish product was obtained. The MEK was removed in the rotary evaporator. The pH was adjusted to 7 with diluted HCl and it was diluted to 10% solids.

15   A stable emulsion was obtained that was stored in the fridge. It was diluted to 1% for observation under the transmission electronic microscope. It lyophilised easily, by freezing it with liquid nitrogen, and obtaining a white powder. It was redispered in deionised water or in PBS without any problem, stirring for 3 min. Sometimes it is advisable to leave it to rest for 24 hour so that the emulsion is fully reconstituted.
20

This Example is a particularly advantageous embodiment of the invention.

Fig. 22 shows the TEM image of the particles obtained.

25   Figs. 27a to 27d show a cytotoxicity study on nanocapsules concerning Example 28 by MTT in cells with an overexpression of lucipherase (HCT-116.Fluc2.C9, HT-29.Fluc.C4, U87-MG.Fluc2.C9 and MDA-MB.231.Fluc2.C18), after 72 hours incubation with nanocapsules in antibiotic-free culture media (RPMI).

30   The maximum concentration tested was 10 µM of plitidepsin equivalent for the empty nanocapsules, and 1 µM of plitidepsin for the loaded nanocapsules, with 8 serial quarter log dilutions. For each concentration, in each assay, 6 replicas were tested. The assays were repeated at least 3 times.

35   The empty nanocapsules were not toxic at the concentration for therapeutic use.

Fig. 28 shows a biodistribution study on athymic mice without a tumour in the nanocapsules in Example 28 loaded with DiR.

The emulsions administered have been given maximum solubility and they were as
5　follows:

● NC-DiR_0.5 mg DiR/mL (20% solids)_2.5 mg DiR/kg_n (number of mice used)=4
● NC-DiR_0.25 mg DiR/mL (20% solids)_1.25 mg DiR/kg_n=3
● NC-DiR_0.13 mg DiR/mL (20% solids)_0.65 mg DiR/kg_n=4

10

All the mice survived the injections showing a prolonged photoluminescence.

Example 29.

15

This Example is the same as Example 28 above, but instead of using LAP 100D, Priamine 1074 was used.

A total of 4.5506 g of IPDI, 5 g of Crodamol GTCC and 0.6039 g of 2,2-dithiodiethanol
20　(DEDS), previously stirred in vortex agitator, were added simultaneously to a reactor at 50ºC. The remains were entrained with diethyl ether. It was observed that the 2,2-dithiodiethanol was more dense and appropriate stirring was required to ensure phases did not form during the reaction. When the reaction started, the medium turned cloudy.

25　An hour later 6.91 g of dry YMER N-120 were added, and entrained with 1ml of dry acetone.

When the theoretical NCO was reached (approximately after 4 hours reaction time) the heating bath was removed and 1.5625 g of Priamine 1074 solubilised in 8 g of dry MEK
30　were added and it was activated with 2 drops of triethylamine.

After 45 min the reactor was cooled to about 5-10ºC and 1.77 g of IPDI and 1.25 g of Bayhydur 3100 in 16 ml of dry MEK were added. These two isocyanates were the second prepolymer, which will form the second, internal layer of the wall. A distinctive
35　thickening of the sample was observed. Two drops of BYK-028 antifoaming agent (at the most there can be 40 g of MEK in total) were added.

Before emulsifying the NCO presence in the reaction was checked using IR.

Then, dropwise 260 ml of milliQ water basified to a pH between 11 and 12 and cooled to a temperature between 5 and 10 ºC, were added.

5   When the phase inversion took place (fairly viscose) 1237 µl (1.1778 g) of DETA were added in the compensated pressure funnel while continuing to add, dropwise, the rest of the water with the DETA at greater speed.

The stirring and the cooling to 10ºC were maintained until the NCO signal disappeared
10   from the IR spectrum.

An even, white-bluish product was obtained. The MEK was removed in the rotary evaporator. The pH was adjusted to 7 with diluted HCl and it was diluted to 10% solids.

15   A stable emulsion was obtained that was stored in the fridge. It was diluted to 1% for observation under the transmission electronic microscope. It lyophilised easily, by freezing it with liquid nitrogen, and obtaining a white powder. It was redispered in deionised water or in PBS without any problem, stirring for 3 min. Sometimes it is advisable to leave it to rest for 24 hour so that the emulsion is fully reconstituted.
20

This Example is a particularly advantageous embodiment of the invention.

Example 30.

25

This Example is a variation of Example 29 above, in that it is cross-linked with cystamine hydrochloride instead of with DETA.

A total of 4.5506 g of IPDI, 5 g of Crodamol GTCC and 0.6039 g of 2,2-dithiodiethanol
30   (DEDS), previously stirred in vortex agitator, were added simultaneously to a reactor at 50ºC. The remains were entrained with diethyl ether. It was observed that the 2,2-dithiodiethanol was more dense and appropriate stirring was required to ensure phases did not form during the reaction. When the reaction started, the medium turned cloudy.

35   An hour later 6.91 g of dry YMER N-120 were added, and entrained with 1ml of dry acetone.

When the theoretical NCO was reached (approximately after 4 hours reaction time) the heating bath was removed and 1.5625 g of Priamine 1074 solubilised in 8 g of dry MEK were added and it was activated with 2 drops of triethylamine.

5   After 45 min the reactor was cooled to about 5-10ºC and 1.77 g of IPDI and 1.25 g of Bayhydur 3100 in 16 ml of dry MEK were added. These two isocyanates were the second prepolymer, which will form the second, internal layer of the wall. A distinctive thickening of the sample was observed. Two drops of BYK-028 antifoaming agent (at the most there can be 40 g of MEK in total) were added.

10

Before emulsifying the NCO presence in the reaction was checked using IR.

Then, dropwise 260 ml of milliQ water basified to a pH between 11 and 12 and cooled to a temperature between 5 and 10 ºC, were added.

15

When the phase inversion took place (fairly viscose) 3,825 g of cystamine hydrochloride previously dissolved in as little an amount as possible of milliQ water basified to pH 11 were added, while continuing to add, dropwise, the rest of the water with the cystamine hydrochloride at greater speed.

20

The stirring and the cooling to 10ºC were maintained until the NCO signal disappeared from the IR spectrum.

An even, white-bluish product was obtained. The MEK was removed in the rotary 25   evaporator. The pH was adjusted to 7 with diluted HCl and it was diluted to 10% solids.

A stable emulsion was obtained that was stored in the fridge. It was diluted to 1% for observation under the transmission electronic microscope. It lyophilised easily, by freezing it with liquid nitrogen, and obtaining a white powder. It was redispered in 30   deionised water or in PBS without any problem, stirring for 3 min. Sometimes it is advisable to leave it to rest for 24 hour so that the emulsion is fully reconstituted.

Adding the cystamine hydrochloride in a base medium produces a certain degradation of the cystamine hydrochloride, therefore it loses part of its effectiveness. Therefore, 35   one alternative is to add the cystamine hydrochloride in an acid medium, in which case a longer waiting period is required (a few days) until the NCO signal disappears from the IR spectrum. This is also applicable in Example 35 below.

Example 31. *Method of Encapsulating plitidepsin*

5 Using a prepolymer formed at 50ºC with IPDI, DEDS, Crodamol GTCC and YMER N-120 (see, for example, Examples 28, 29 and 30) the bath heating was switched off and the necessary amount of LAP 100D in 10 g of MEK was added. It was left to react for 45 min and the formation of polyurea was controlled using IR.

10 Next the reactor was cooled to 10ºC and the rest of the MEK and the excess isocyanate was added. The reaction medium was homogenised and the proportional part of the prepolymer + MEK was taken. This proportional part of prepolymer was added to the amount of plitidepsin needed to be at 1% with respect to the prepolymer + the cross-linking amine (DETA) (the amount of MEK is not taken into consideration for 15 this calculation). This way, when it is emulsified so that it is at 10% solids, it will have 0.01% of plitidepsin.

Fig. 23 shows the TEM image of the particles obtained.

20

Example 32. *Method of derivatization of a peptide that promotes the nanocapsule wall.*

A total of 122 mg of Bayhydur 3100 were mixed with 36.3 mg of c-(RGDfK) dissolved in 0.9 ml of milliQ water at 5ºC and basified to a pH 11.5. It was left to react for 90 25 minutes, stirring in a vortex agitator every 10-15 minutes. The reaction was controlled by HPLC, after 90 min the peptide derivatization performance was 95%.

A prepolymer was emulsified (see, for example, the prepolymer in Example 28) + MEK + plitidepsin adding, dropwise, the already reacted aqueous mixture of Bayhydur 3100 30 with the c-(RGDfK). Before starting the emulsion, it was checked using IR, that there were still a large amount of free isocyanates. If the inversion phase had not taken place, more water would have been added until the inversion phase occurred. Once the inversion phase had taken place the rest of the cold, basified water was added together with the second compound (the cross-linking amine).

35

The MEK was removed in a rotary evaporator, leaving the product free of organic solvents and suitable for being lyophilised and then redispersed in PBS.

Example 33. *Method of encapsulating hydrophobic fluorophore.*

5   In a previously weighed (tarred) 100 ml round bottomed flask the prepolymer + MEK and plitidepsin, were added, where appropriate. A total of 5 mg of DIR (1,1′-dioctadecyl-3,3,3′,3′-tetramethylindotricarbocyanine iodide) dissolved in the minimum amount of dry acetone were added. The mixture was stirred and was ready for being emulsified following, for example, the method in Example 28.

10

Fig. 29 shows a reaction diagram and a theoretical representation of the ideal structure of the nanocapsule in Example 28 loaded and functionalised following Examples 31-33.

15   ***Example 34***.

This Example synthesises a variant of Example 28 replacing DEDS with 1,6-hexanediol. This way a similar product is obtained without disulphide in the membrane.

20   A total of 6.7124 g of IPDI, 6.6363 g of Crodamol GTCC and 0.4765 g of 1,6-hexanediol were added, simultaneously to a reactor at 55-60ºC under an inert gas current and it was left to react with stirring at 265 rpm for one hour. After one hour 10.2568 g of dry YMER N-120 were added.

25   When the theoretical NCO is reached (approximately after 4 hours reaction time) the heating batch was removed 3.0670 g of LAP 100D solubilised in 16,7756 g of dry MEK were added.

One hour later the reactor was cooled to about 5-10ºC and 2,0836 g of IPDI and
30   1.8408 g of Bayhydur 3100 in 23 ml of dry MEK were added. These two isocyanates are the second prepolymer, which will reinforce the wall forming a second, internal layer.

Before emulsifying the NCO presence in the reaction was checked using IR.
35

Then, dropwise 250 ml de milliQ water basified to a pH between 11 and 12 and cooled to a temperature between 5 and 10 ºC, were added. It was stirred up to 400 rpm.

When the phase inversion took place 1100 µl (1,1589 g) of DETA was added in the compressed pressure funnel while continuing to add, dropwise, the rest of the water with DETA.

5

The stirring and the cooling to 10ºC were maintained until the NCO signal disappeared from the IR spectrum.

An even, white, bluish product was obtained. The MEK evaporated. The pH was
10 adjusted to 7 with dilute HCl and it was diluted to 10% solids.

A stable emulsion was obtained which was stored in the fridge. Using electronic microscopy (SEM) agglomerated capsules were observed with diameters smaller than 200 nm.

15

Example 35.

A variant of Example 28 where a second very hydrophobic prepolymer was introduced,
20 which will form an internal wall with greater encapsulation power for very hydrophobic molecules. However it was cross-linked with cystamine hydrochloride instead of DETA so that the wall was highly degradable in a medium rich in Glutathione (GSH).

A total of 6.7632 g of IPDI, 5 g of Crodamol GTCC, 520 µl (0.655g) of 2,2-
25 dithiodiethanol (DEDS) and 8 g of YMER N-120, previously stirred in a cortex agitator, were added simultaneously to a reactor at 50ºC. The remains were entrained with diethyl ether. The stirring had to be vigorous so that phases did not form during the reaction. When the reaction started, the reaction medium turned cloudy.

30 Once the theoretical NCO was reached (approximately after 4 hours reaction time) the heating bath was removed and 3.6265 g of LAP 100D solubilised in 8 g of dry MEK were added.

At the same time, in a 100 mL round-bottom flask, 1.9425 g of IPDI and 1.8075 g of
35 Bayhydur 3100 dissolved in 20 ml of dry MEK were added. Next, in an inert atmosphere, dropwise, 3.34 g of Priamine dissolved in 8 mL of MEK/acetone were added. The reaction was followed using FT-IR.

After 45 min the reactor was cooled to 5-10ºC and the hydrophobic prepolymer of IPDI-PRIAMINE-B3100 dissolved in MEK/ACETONE were added. These two isocyanates and the Priamine were the second prepolymer, which will reinforce the wall forming a very hydrophobic second, internal layer. Two drops of BYK-028 antifoaming agent were added.

Before emulsifying the NCO presence in the reaction was checked using FT-IR.

Then, dropwise, 270 ml de milliQ water basified to a pH between 11 and 12 and cooled to a temperature between 5 and 10 ºC.

When the phase inversion took place 2,343 g of cystamine hydrochloride basified with triethylamine were added in the compressed pressure funnel while continuing to add, dropwise, the rest of the water with cystamine hydrochloride at greater speed.

The stirring and the cooling to 10ºC were maintained until the NCO signal disappeared from the IR spectrum.

An even, white, bluish product was obtained. Solvents were evaporated in the rotary evaporator. The pH was adjusted to 7 with dilute HCl and it was diluted to 10% solids.

A stable emulsion was obtained that was stored in the fridge. It was diluted to 1% for observation under the transmission electronic microscope. It lyophilised easily, by freezing it with liquid nitrogen, and obtaining a white powder. It was redispered in an 80:20 mixture of water/acetone stirring for 3 min. Sometimes it is advisable to leave it to rest for 24 hour so that the emulsion is fully reconstituted.

Fig. 24 shows the TEM image of the particles obtained.

Example 36. *NA-834 Prepolymer - Encapsulation of the Miami Vice® Fragrance*

Method for synthesising the NA-834 prepolymer

In a N_2 current, 49.2402 g of YMER N-120 and 30.0951 g IPDI (NCO:8/OH:2.5) were added. The reaction was carried out at 55-60ºC with mechanical stirring at 260 rpm.

After 3-3.5 hours, the total YMER N-120 reaction was checked by valuing the NCO level ($NCO_{theoretical}$= 8.949, NCO_{real}= 8.945). Then the Duomeen T dissolved in MEK was loaded. The end of the reaction was checked using IR0 follow-up.

5 Fragrance encapsulating method

A total of 32.3615 g of the previously synthesised NA-834 prepolymer were taken, and placed in a reactor with a N_2 atmosphere. The mixture was fluidified by adding, approximately, 9 g of MEK and stirring mechanically. A total of 24.5280 g of the
10 fragrance were added and then 4.6980 g of polymeric MDI were added, which will lead to the formation of the interior wall. Once the mixture was homogenised, the emulsion was formed by adding, dropwise, 70.0383 g of cold water (from the fridge, 4ºC). The emulsion was carried out by cooling the reactor with a water-ice mixture bath (0-5ºC). Finally, to the water remaining in the addition funnel (approximately 10 g), 1490 µl of
15 diethylenetriamine (DETA) were added, the amine stechiometric equivalents for finishing the reaction with the isocyanate still in excess. The reactions were controlled using IRs before and after adding each reagent.

Characterisation
20

Figs. 30 and 31 show a graphical representation of the particle size distribution by DLS (in Fig. 30 the ordinate axis indicates the % of units, and in Fig. 31 it indicates the % volume). Using TEM a defined main population of nanoparticles was observed, with a diameter of 10-30 nm (Figs. 32 and 33: images by transmission electron microscopy
25 (TEM) of fragrance nanocapsules at 20%.

To study the so-called long-lasting effect of the fragrance nanoparticles, three different product solutions were prepared:

30 A) control solution, made up of free fragrance (3%) in a mixture of water (22%) and ethanol (75%).
B) fragrance nanocapsules (3%), in aqueous medium (water+polymer (97%).
C) fragrance nanocapsules (3%), in water (water+ polymer 22%) and ethanol (75%).

35 The three prepared solutions were applied to two types of material; glass and cotton. On this basis, the evolution of the odour intensity over time was studied. Figs. 34 and

35 show the results, which were assessed aromatically, and independently, by 5 individuals.

This Example is a particularly advantageous embodiment of the invention.

5

Example 37. *Poly 620*

This Example cross-links with L-lysine, i.e.: the second compound is L-lysine. The size
10 of the nanocapsules was reduced considerably, obtaining nanocapsules with a size of
50 nm. As the L-lysine contains carboxylic groups, the nanocapsule's external
hydrophilic nature increases. Its formula is:
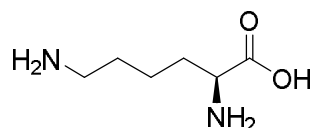
15

In a reactor duly equipped with mechanical stirring at 50ºC and with an inert
atmosphere 3.3814 g of IPDI, 0.75 g of Crodamol GTCC, 0.15 g of 2,2-dithiodiethanol
(DEDS), 5.5 g of YMER N-120 and 10 mg of DBTL were added. When the theoretical
NCO was reached (approximately after 4-5 reaction time) the heating bath was
20 removed and 1.375 g of TAP 100D solubilised in 8 g of dry THF were added. The
stirring was maintained and it was left to react for 30 min. The TAP 100D is more
hydrophobic than LAP 100D, so that with a smaller amount the same hydrophobic
nature was obtained. This way, the superficial hydrophilic nature could be increased by
adding YMER N120 and L-lysine if required to compensate the TAP 100D that was not
25 added. Its formula is
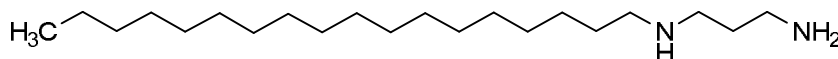
The reactor was cooled to about 5 to 10ºC and 0.485 g of IPDI and 0.904 g of
30 Bayhydur 3100 in 16 ml of dry MEK were added on top of the amphiphilic prepolymer
(AMPHIL). As already mentioned, the Bayhydur 3100 can behave as a linker (linking
element) between the cRGDfK peptide (in the event it is desirable to include a peptide
to convey it to the tumour cells) and the nanocapsule. The free IPDI will be the internal
hydrophobic prepolymer which will increase the barrier effect.

131

Then, dropwise, 140 mL of milliQ water basified to a pH between 11 and 12 cooled to a temperature between 5 and 10 ºC, was added.

5   After the phase inversion 1,110 g of L-lysine were added in the compensated pressure funnel while continuing to add, dropwise, the rest of the water with the L-lysine solution at greater speed.

After 20 min, using IR the formation of urea functional groups was observed. The
10   stirring was maintained and the cooling to 5 to 10ºC until the NCO signal disappeared from the IR spectrum.

Fig. 36 shows a TEM image of the nanoparticles obtained.

15   This Example is a particularly advantageous embodiment of the invention.

Example 38. *Poly 636 (AMPHIL-HYFOB)*

20   This Example introduced a second, hydrophobic prepolymer which, unlike previous Examples, also contained hydrophobic side chains and disulphide bridges in its main chain to increase the encapsulating power, but without losing degradability in the face of glutathione.

25   In a reactor duly equipped with mechanical stirring at 50ºC and with an inert atmosphere 3.3814 g of IPDI, 0.75 g of Crodamol GTCC, 0.15 g of 2,2-dithiodiethanol (DEDS), 5.5 g of YMER N-120 and 10 mg of DBTL were added. When the theoretical NCO was reached (approximately after 4 to 5 hours reaction time) the heating bath was removed and 1.45 g of TAP 100D solubilised in 8 g of dry THF were added. The
30   stirring was maintained and it was left to react for 30 min. This amphiphilic prepolymer is called AMPHIL in Figs. 38 and 40.

At the same time, in a 25 mL Schlenk at 50ºC purged with nitrogen, 0.486 g of IPDI, 0.15 g of DEDS and 10 mg of DBTL in 2 mL of dry THF were added. After 1 hour
35   reaction time, 0.15 g of TAP 100D in 4 mL of dry THF was added and the heating was switched off. The stirring was maintained and it was left to react for 30 min. This hydrophobic prepolymer is called HYFOB in Figs. 39 and 40.

The reactor was cooled to about 5 to 10ºC and the hydrophobic prepolymer (HYFOB) and 0.904 g of Bayhydur 3100 in 16 ml of dry MEK was added on to the amphiphilic compound (AMPHIL). Bayhydur 3100 behaved as a linker (linking element) between the cRGDfK peptide and the nanocapsule (see Fig. 37). HYFOB was the hydrophobic prepolymer with disulphide bridges in the wall to make it degradable in the face of glutathione.

Then, dropwise, 140 mL de milliQ water basified to a pH between 11 and 12 cooled to a temperature between 5 and 10 ºC, was added.

After the inversion phase, 0.500 g of L-lysine were added in the compensated pressure funnel while continuing to add, dropwise, the rest of the water with the L-lysine solution at greater speed.

After 20 min, using IR the formation of urea functional groups was observed.

Next 0.236 g of DETA were added. The stirring and the cooling to 5 to 10ºC were maintained until the NCO signal disappeared from the IR spectrum.

Fig. 40 shows a theoretical representation of the structure of the microcapsule in this Example.

Result: A sample of 0.2 mL 10 mg/mL previously filtered with a 220 nm filter, was mixed with 0.4 mL of GSH 10 mM at 37 ºC. Stirring continued at 37ºC and the degradation of 100 nm nanocapsules continued and consequently the formation of aggregates larger than 1 micron.

It was proved that adding disulphide groups to the HYFOB accelerated the degradation of the nanocapsules in a reducing medium similar to the one found in the cytosol of cancerous cells.

Figs. 41 to 43 represent the evolution of the degradation of microcapsules in this Example due to the reducing action of glutathione (GSH) according to the time period. Fig. 41 shows the initial state, Fig. 42 is after 12 hours, and Fig. 43 is after 48 hours

This Example is a particularly advantageous embodiment of the invention.

Example 39. *Coating biocompatible metals- Polytitanium*

5 This Example describes a new application of the microcapsules according to the invention. It consists of the surface coating of a biocompatible material, preferably a biocompatible metal and very preferably titanium or its alloys, with microcapsules according to the invention.

10 In this Example the cross-linking is done with EDA. Microcapsules are functionalised on top of a titanium alloy (Ti_6Al_4V), which is a suitable biocompatible alloy, for example, for producing dental implants.

In a reactor duly equipped with mechanical stirring at 50ºC and with an inert
15 atmosphere 3.3814 g of IPDI, 0.75 g of Crodamol GTCC, 0.15 g of 2,2-dithiodiethanol (DEDS), 5.5 g of YMER N-120 and 10 mg of DBTL were added. When the theoretical NCO was reached (approximately after 4 to 5 hours reaction time) the heating bath was removed and 1.375 g of TAP 100D solubilised in 8 g of dry THF were added. The stirring was maintained and it was left to react for 30 min.

20 The reactor was cooled to about 5 to 10ºC and 0.485 g of IPDI and 0.904 g of Bayhydur 3100 in 16 ml of dry MEK were added on to the amphiphilic prepolymer (AMPHIL). The hydrophobic prepolymer (HYFOB) and 0.904 g of Bayhydur 3100 in 16 ml of dry MEK were added on to the amphiphilic compound (AMPHIL).

25 Then, dropwise, 140 mL de milliQ water basified to a pH between 11 and 12 cooled to a temperature between 5 and 10 ºC, was added.

After the inversion phase, 50 % mass of the total EDA (ethylenediamine) to be added, was added. After 15 min, using IR a reduction in the isocyanate group signal was
30 observed.

Next, titanium discs (particularly, from the (Ti_6Al_4V) alloy, like the ones shown in Fig. 44), were immersed in the emulsion containing the partially cross-linked nanocapsules for 1 hour at 5 to 10ºC. The discs of titanium underwent a superficial activation process
35 thanks to which they had covalently linked amines on their surface. The microcapsules are reactive with the superficial amines on the titanium, in this way they react covalently with them and remain chemically attached to the surface of the metal.

After 1 hour the remaining 50 % of EDA was added. The stirring was maintained and the cooling to 5 to 10ºC until the NCO signal disappeared from the IR spectrum.

5 The surface of the titanium was observed using SEM and a fluorescence microscope in the case of nanocapsules containing fluorophore (See Fig. 45).

Cell adhesion and immunohistochemical tests were carried out to quantify the quality of the cell adhesion with satisfactory results.

10

This Example is a particularly advantageous embodiment of the invention.

Antibacterial agents used

15 Roxithromycin, clarithromycin (hydrophobic antibacterial agents from the macrolide family). Via the functionalisation of titanium with nanocapsules that encapsulate this type of antibacterial agents, its biocompatibility increased for use in dental implants and for preventing bacterial adhesion to metal. These antibacterial agents can be encapsulated, for example, by means of the same encapsulating method as shown in 20 Example 33.

Fluorophore used

Clear blue DFSB-C0 (highly fluorescent hydrophobic molecule). It was encapsulated in 25 microcapsules according to the invention and it was used to quantify in the fluorescence microscope the quality of the adhesion of nanocapsules to the titanium. The fluorophore can be encapsulated, for example, by means of the same Encapsulation Method as in Example 33.

30 Adhesion promoting peptide used

The nanocapsules were covered with cRGDfK peptide following Example 32.

35 ***Example 40.*** *(AMPHIL-HYFOB) without cross-linking agent*

This Example is the same as Example 38 but without adding a second compound, i.e.: without adding a cross-linker (L-lysine and DETA). Since no cross-linking agents are added, the nanocapsule is less stable in solution and degrades more easily when treated with GSH

5

In a reactor duly equipped with mechanical stirring at 50ºC and with an inert atmosphere 3.3814 g of IPDI, 0.75 g of Crodamol GTCC, 0.15 g of 2,2-dithiodiethanol (DEDS), 5.5 g of YMER N-120 and 10 mg of DBTL were added. When the theoretical NCO was reached (approximately after 4 to 5 hours reaction time) the heating bath was removed and 1.45 g of TAP 100D solubilised in 8 g of dry THF were added. The stirring was maintained and it was left to react for 30 min. This amphiphilic prepolymer is called AMPHIL in Figs. 38 and 40.

10

At the same time, in a 25 mL Schlenk at 50ºC purged with nitrogen, 0.486 g of IPDI, 0.15 g of DEDS and 10 mg of DBTL in 2 mL of dry THF were added. After 1 hour reaction time, 0.15 g of TAP 100D in 4 mL of dry THF was added and the heating was switched off. The stirring was maintained and it was left to react for 30 min. This hydrophobic prepolymer is called HYFOB in Figs. 39 and 40.

15

The reactor was cooled to about 5 to 10ºC and the hydrophobic prepolymer (HYFOB) and 0.904 g of Bayhydur 3100 in 16 ml of dry MEK was added on to the amphiphilic compound (AMPHIL). Bayhydur 3100 behaved as a linker (linking element) between the cRGDfK peptide and the nanocapsule (see Fig. 37). HYFOB was the hydrophobic prepolymer with disulphide bridges in the wall to make it degradable in the face of glutathione.

20

25

Then, dropwise, 140 mL de milliQ water basified to a pH between 11 and 12 cooled to a temperature between 5 and 10 ºC, was added.

30

After the inversion phase, 5 mL of triethylamine were added and left at room temperature for 72 hours until the NCO signal disappeared from the IR spectrum.

Example 41

35

A experiment was conducted to know the release kinetics of the inside of the nanocapsules of a FRET pair (Förster resonance energy transfer) of hydrophobic fluorophores in an aqueous medium.

Example 38 was repeated and, on the one hand, a product was synthesised in which DiI (1,1′-dioctadecyl-3,3,3′,3′-tetramethylindocarbocyanine perchlorate) was encapsulated and another product that encapsulates DiO (3,3′-dioctadecyloxacarbocyanine perchlorate). In both cases, for their encapsulation, Example 33 was followed. These two fluorophores represent a FRET pair, the DiO performing the function of donor and the DiI the acceptor. Once both products were synthesised, they were diluted to the desired concentration, mixed and the fluorescence analysis was carried out energising the donor to 450 nm.

A mixture's fluorescence was followed-up for 84 hours at 37ºC without GSH. As can be seen in Figures 46 and 47, it was concluded that there was no exchange of fluorophores from inside the nanocapsules. This data proves that the nanocapsules were hermetic in an aqueous medium.

When a GSH solution was added to the mixture of nanocapsules, a progressive FRET increase was observed, since the wall of the nanocapsule degraded, allowing a flow of fluorophores from its inside to the outside, making them mix together and lead to a clear FRET increase. Figure 47 show the FRET ratio expressed as $I_a/(I_d + I_a)$, where I_a and I_d are the fluorescence intensity of the acceptor (DiI) and donor (DiO), respectively.

This way, it is concluded that the nanocapsules are hermetic in an aqueous medium, but with GSH, they release hydrophobic fluorophores due to the degradation of the capsular wall as shown by FRET.

CLAIMS

1 - Method for producing a microencapsulate comprising the following stages: [a] dispersing a first liquid phase in a second liquid phase forming an emulsion, so that said first phase remains dispersed in said second phase, and [b] forming a polymer which forms the wall of said microencapsulate, characterised in that between said first phase and said second phase an interphase is formed which comprises a reactive amphiphilic compound, where said amphiphilic compound is a prepolymer of said polymer, and said amphiphilic compound has at least two main functional groups that react in the subsequent polymerisation for forming said polymer, where said amphiphilic compound has at least one hydrophilic or hydrophobic functional group in a chain which is sideways with respect to the chain that links both main functional groups,

where said main functional groups of said amphiphilic compound are NCO functional groups, able to form urethane and/or urea type links,

where said second phase comprises a second compound, where said second compound comprises at least two functional groups that react with said main functional groups of said amphiphilic compound, to form said polymer.

where said second compound is a polyamine,

where a second prepolymer is added to said first phase, where said second prepolymer has at least two main functional groups that react in the subsequent polymerisation for forming said polymer, where said second prepolymer is more hydrophobic than said amphiphilic compound if said first phase is organic, or said second prepolymer is more hydrophilic than said amphiphilic compound if said first phase is aqueous.

2 – Method according to claim 1, characterised in that said first phase is an organic phase and said second phase is an aqueous phase and in that said amphiphilic compound has an HLB value greater than 10.

3 - Method according to claim 1, characterised in that said first phase is an aqueous phase and said second phase is an organic phase and in that said amphiphilic compound has an HLB value smaller than 10.

4 – Method according to claim 1, characterised in that said two main functional groups of said amphiphilic compound are separated from each other by 4 to 12 links.

5   5 – Method according to claim 1, characterised in that said amphiphilic compound is added to said first liquid phase.

6 – Method according to claim 1, characterised in that a first precursor and a second precursor of said amphiphilic compound are added to said first liquid phase, and said

10   first and second precursors are made to react with each other,

where said first precursor is an isocyanate from the group made up of IPDI, HDI and HMDI,

15   where said second precursor is a hydrophilic compound, where said second precursor comprises at least two functional groups suitable for reacting with functional groups of said first precursor, said second precursor having its hydrophilic function in a chain which is sideways with respect to the chain that links the two functional groups that are suitable for reacting with functional groups of said first precursor.

20

7 – Method according to claim 6, characterised in that a third precursor of said amphiphilic compound is added to said first liquid phase or to said second liquid phase, and it is made to react with the product of the reaction between said first and/or second precursors,

25

where said third precursor is a hydrophobic C8-C22 compound, where said third precursor comprises at least two functional groups suitable for reacting with functional groups of said first precursor, said third precursor having its hydrophobic function in a chain which is sideways with respect to the chain that links the two functional groups

30   suitable for reacting with functional groups of said first precursor.

8 – Method according to of claims 6 or 7, characterised in that the two main functional groups of said first, second and/or third precursor are separated from one another by 4 to 12 links, preferably by 5 to 10 links.

35

9 – Method according to claims 6, characterised in that said second precursor is a hydrophilic compound from the group made up of polyethoxylenated compounds with a molecular weight over 100.

5   10 – Method according to claim 6, characterised in that said second precursor is a diol or a diamine with a carboxylic function or sulphonic function in a chain which is sideways with respect to the chain that links the two alcoholic functional groups or amines.

10   11 – Method according to claim 6, characterised in that the reaction of said first precursor with said second precursor, or with said second and third precursor, is carried out in the presence of an excess of said first precursor.

12 – Method according to claim 7, characterised in that said third precursor is a
15   compound from the group made up of fatty diols or diamines C_{10}-C_{22}.

13 – Method according to claim 6, characterised in that said first precursor has a degree of functionality higher than 3, and in that said second precursor and/or third precursor have a degree of functionality smaller than 2.

20

14 – Method according to claim 6, characterised in that after the reaction for forming said prepolymer an active ingredient is added to said first liquid phase, where said active ingredient is, in the case of an organic, disperse phase, from the group made up of lipophilic vitamins, coenzyme Q10, essential oils, medicinal oils and fragrances and,
25   if the disperse phase is aqueous, the active ingredient is a hydrophilic peptide or a water soluble protein.

15 – Method according to claims 6, characterised in that a fourth precursor is added, where said fourth precursor comprises an acid group, a disulphide or an ester.
30

16 – Method according to claim 1, characterised in that said polymer comprises, in its main chain, an acid group, a disulphide or an ester.

17 – Method according to claim 1, characterised in that said amphiphilic compound
35   comprises, in the chain that links both main functional groups, an acid group, a disulphide or an ester.

140

18 – Method according to claim 1, characterised in that said polymer or said amphiphilic compound comprises a functionalising group.

19 – Method according to claim 18, characterised in that said functionalising group is obtained from the reaction of a functionalising element with a linker, where said linker comprises two main functional groups.

20 – Method according to claim 18, characterised in that said polymer comprises a peptide.

21 – Method according to claim 18, characterised in that said amphiphilic compound comprises a peptide.

22 – Method according to claim 1, where said emulsion is an O/W emulsion, characterised in that it comprises a stage of adding at least one volatile, polar organic solvent to said first phase, before said stage [a], and a stage of evaporating said solvent, after said stage [b].

23 – Method according to claim 1, characterised in that said second prepolymer has a disulphide bridge in its main chain.

24 – Method according to claim 1, characterised in that said polymer or said amphiphilic compound is amphoteric.

25 – Amphiphilic compound obtainable according to claim 1.

26 – Microencapsulate characterised in that its wall comprises a reactive amphiphilic compound according to claim 25.

27 – Microencapsulate according to claim 26, characterised in that it comprises, inside, an antitumoral active ingredient.

28 – Microencapsulate according to claim 27, characterised in that said antitumoral ingredient is paclitaxel or plitidepsin.

29 – Microencapsulate according to claim 26, characterised in that it comprises, inside, a photosensitive hydrophobic fluorophore.

30 – Microencapsulate according to claim 26, characterised in that it comprises, inside, an antibacterial agent.

31 – Microencapsulate according to claim 30, characterised in that said antibacterial agent is roxithromycin or clarithromycin.

32 – Cosmetic or pharmaceutical composition characterised in that it comprises a microencapsulate according to claim 26.

33 – Use of a microencapsulate according to claims 26, for the superficial coating of a biocompatible material.
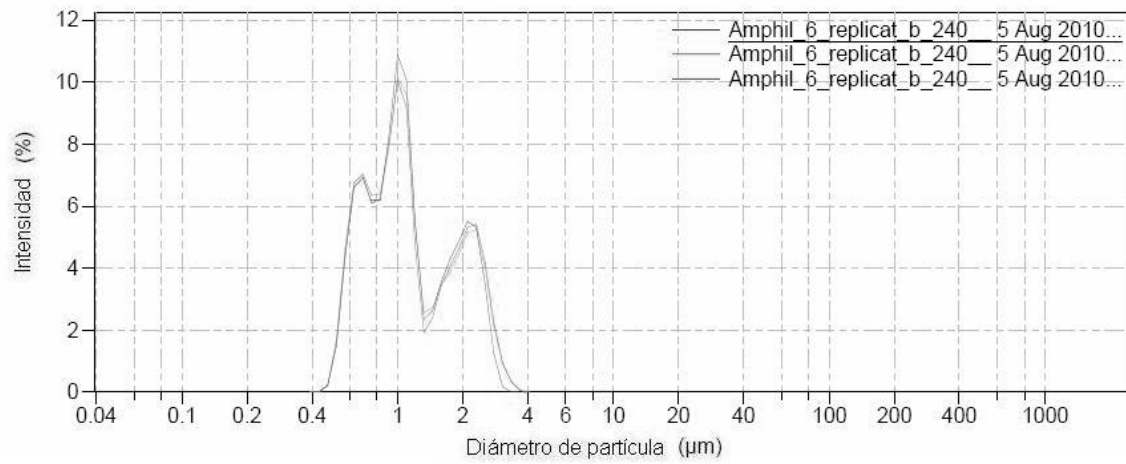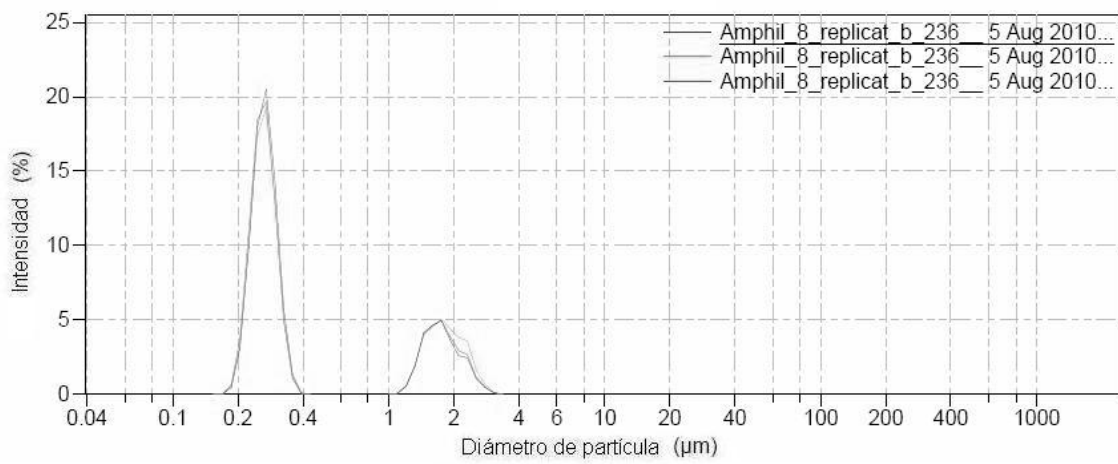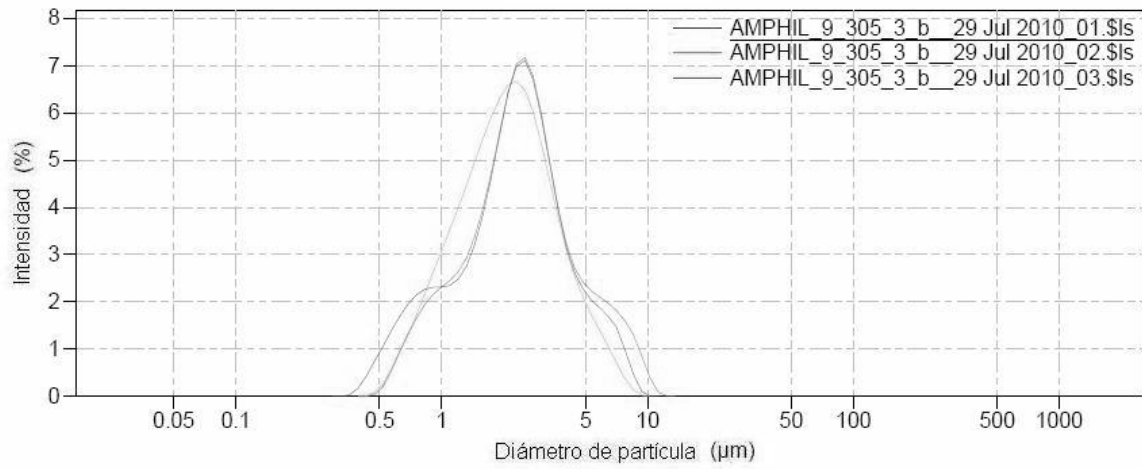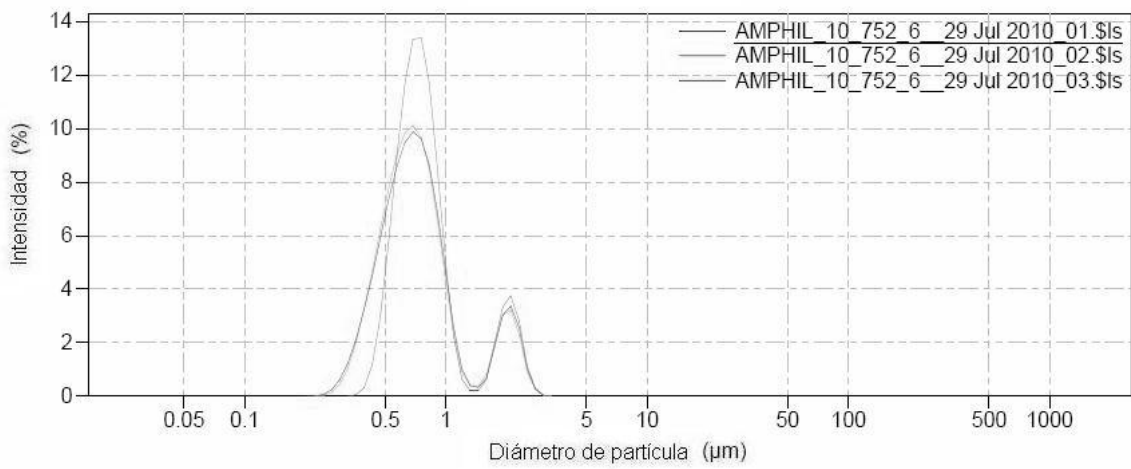
Fig. 1

Fig. 2

Fig. 3

Fig. 4
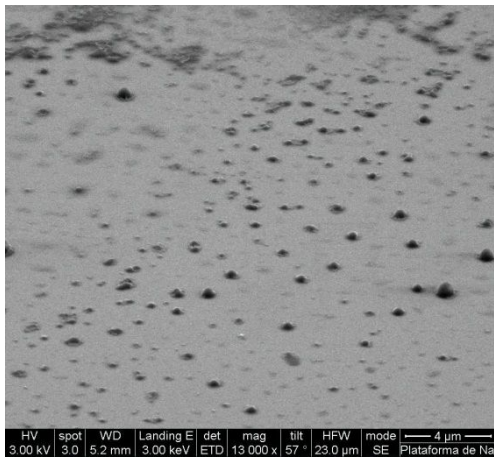
Fig. 5
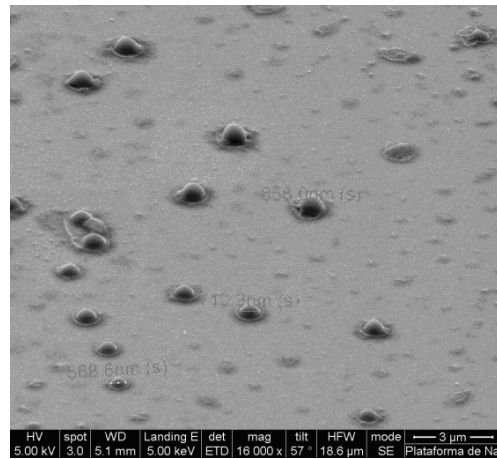
Fig. 6
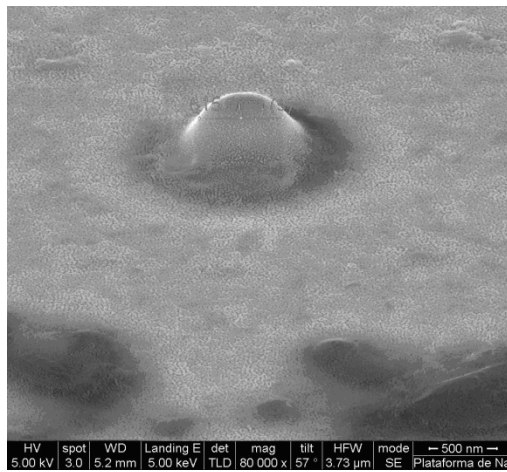
Fig. 7
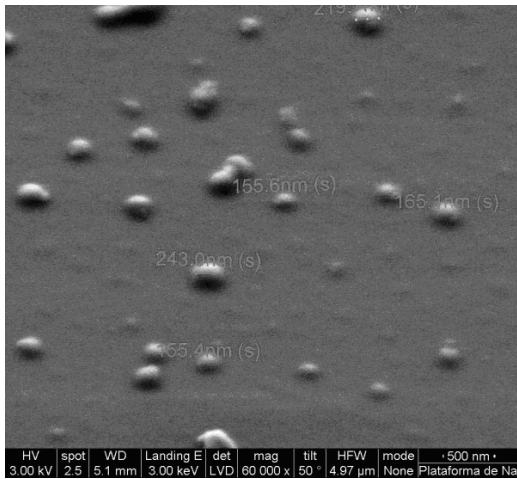
Fig. 8
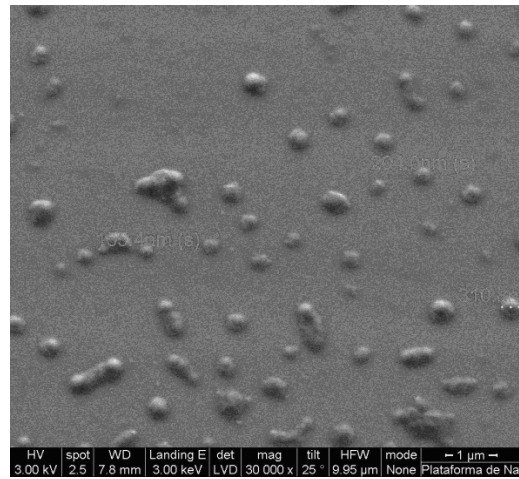
Fig. 9
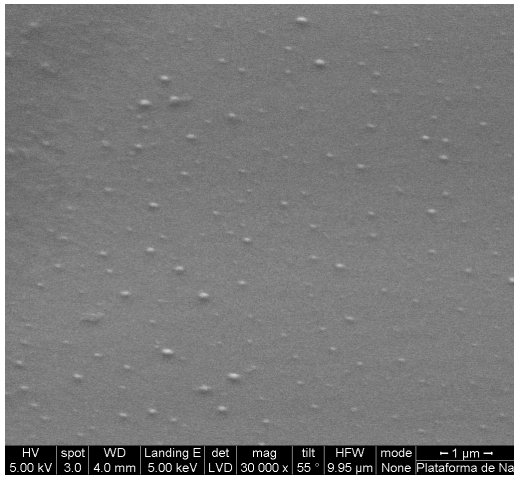
Fig. 10
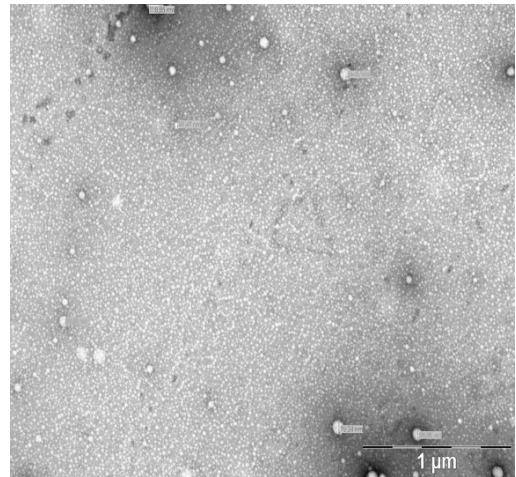
Fig. 11
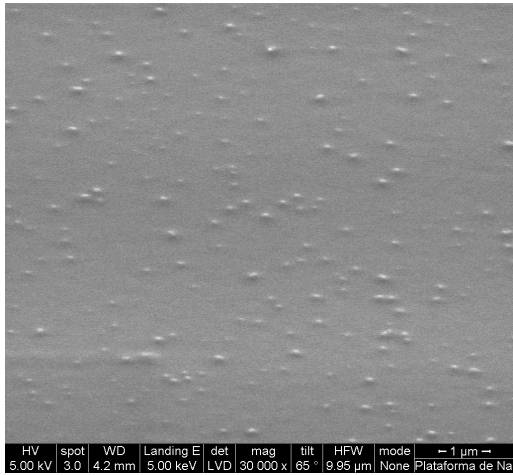
Fig. 12
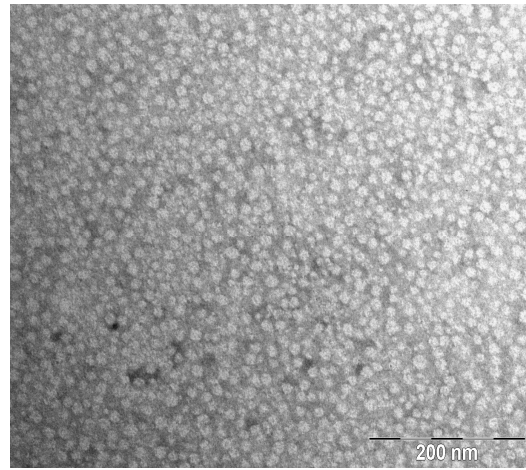
Fig. 13
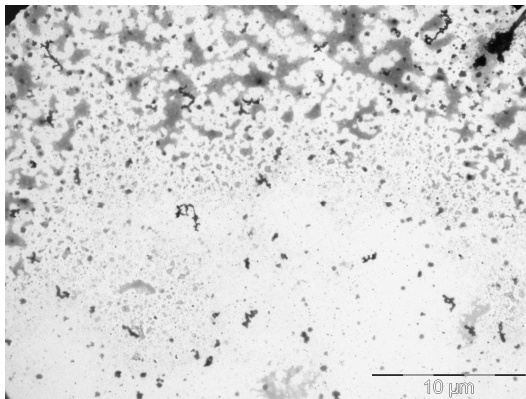
Fig. 14
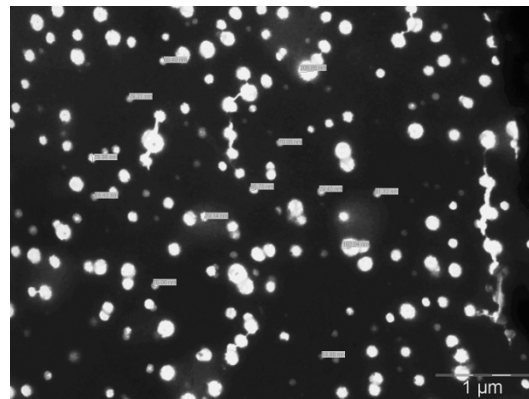
Fig. 15
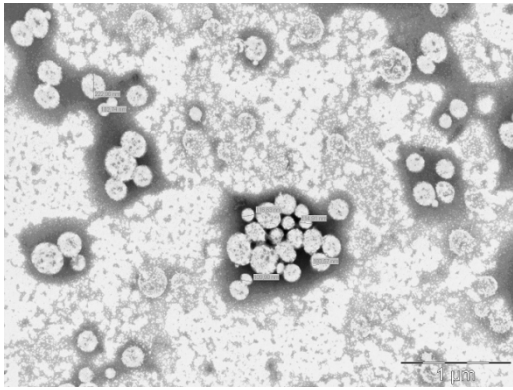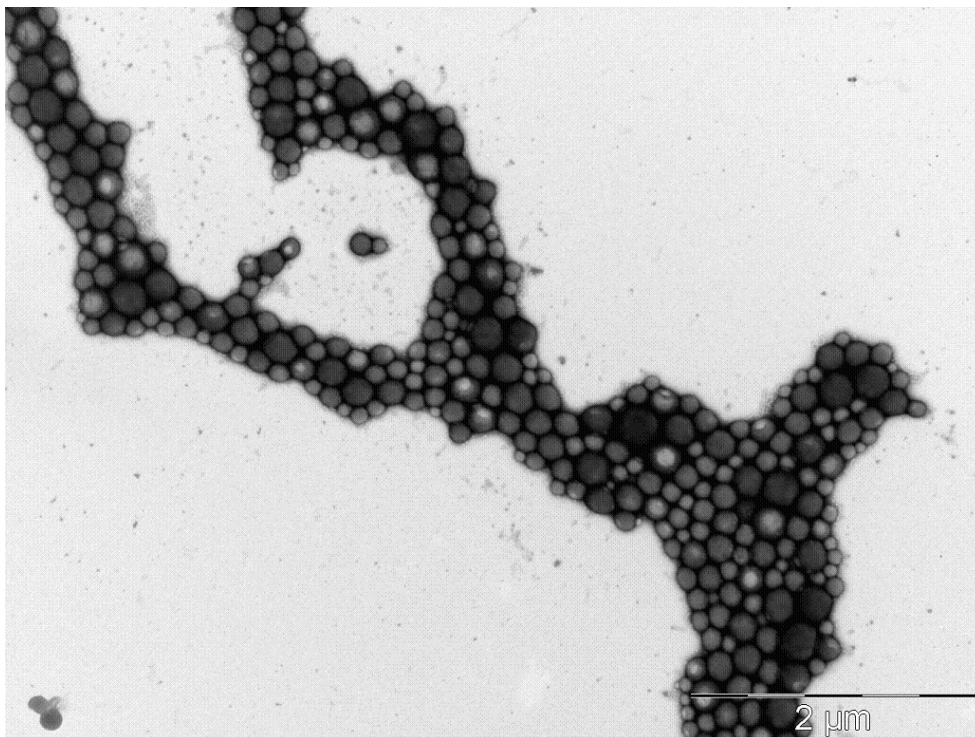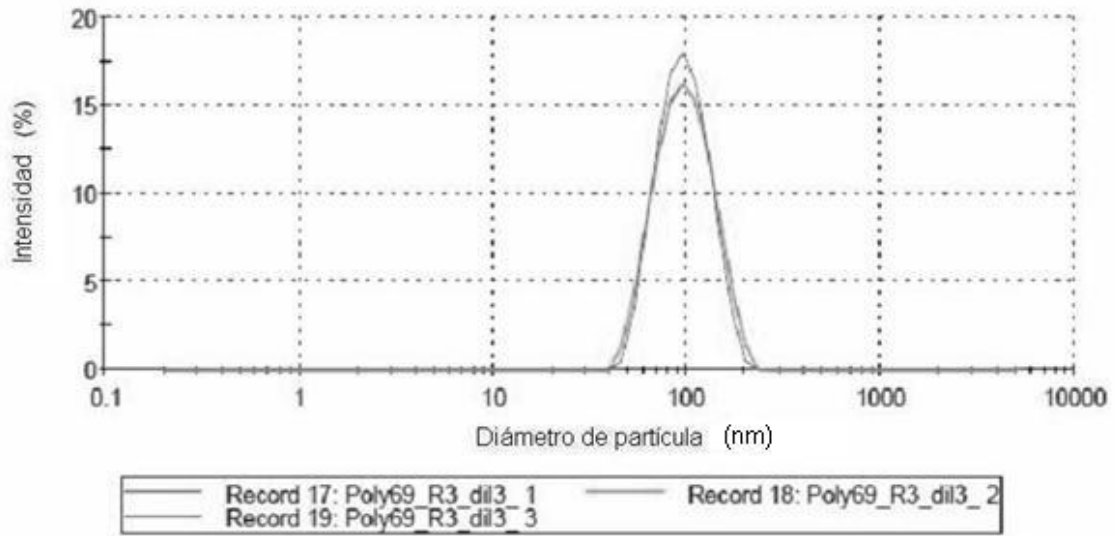
Fig. 16
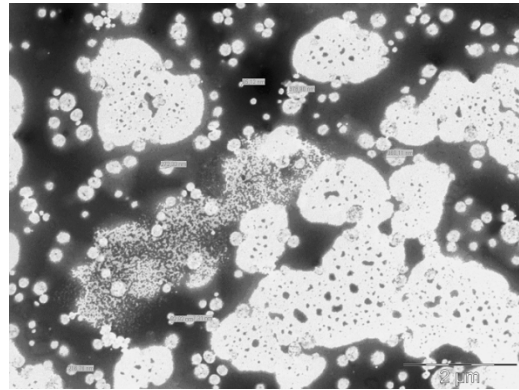
Fig. 17
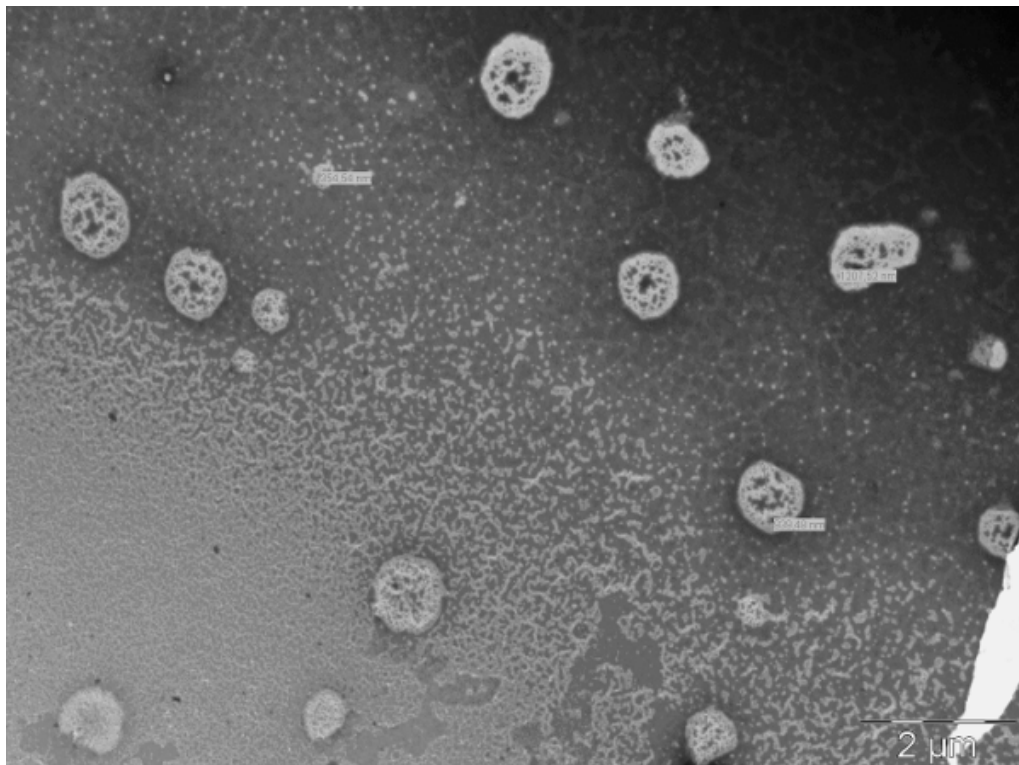
Fig. 18
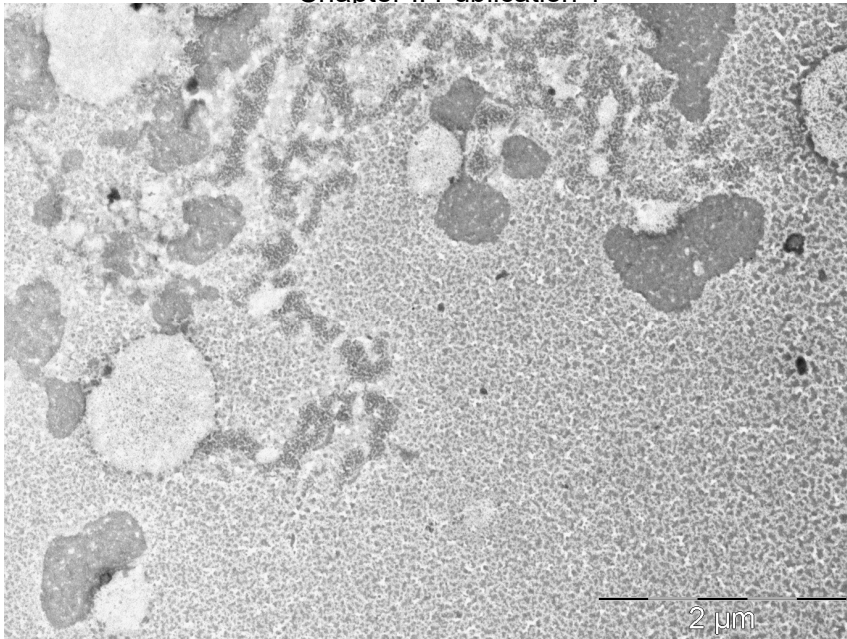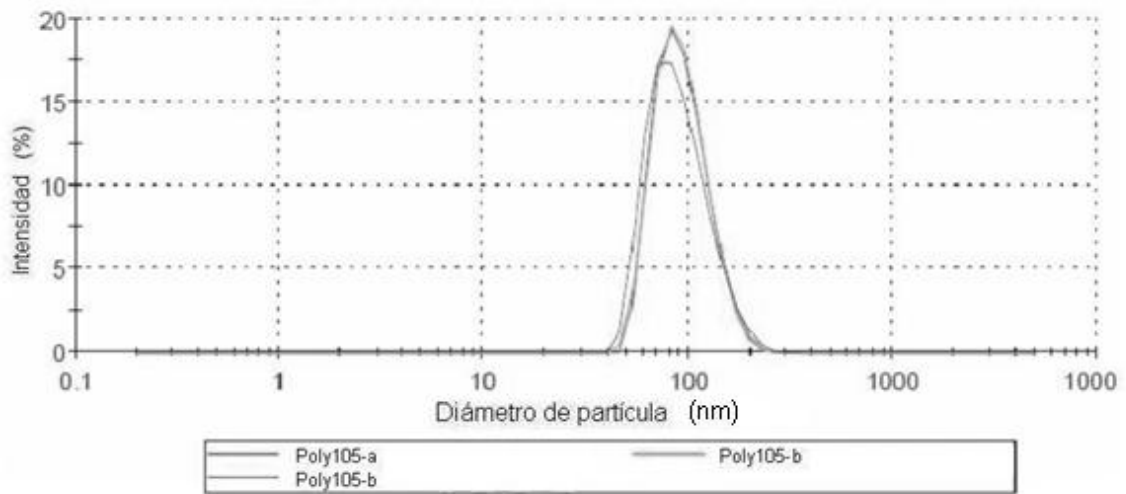
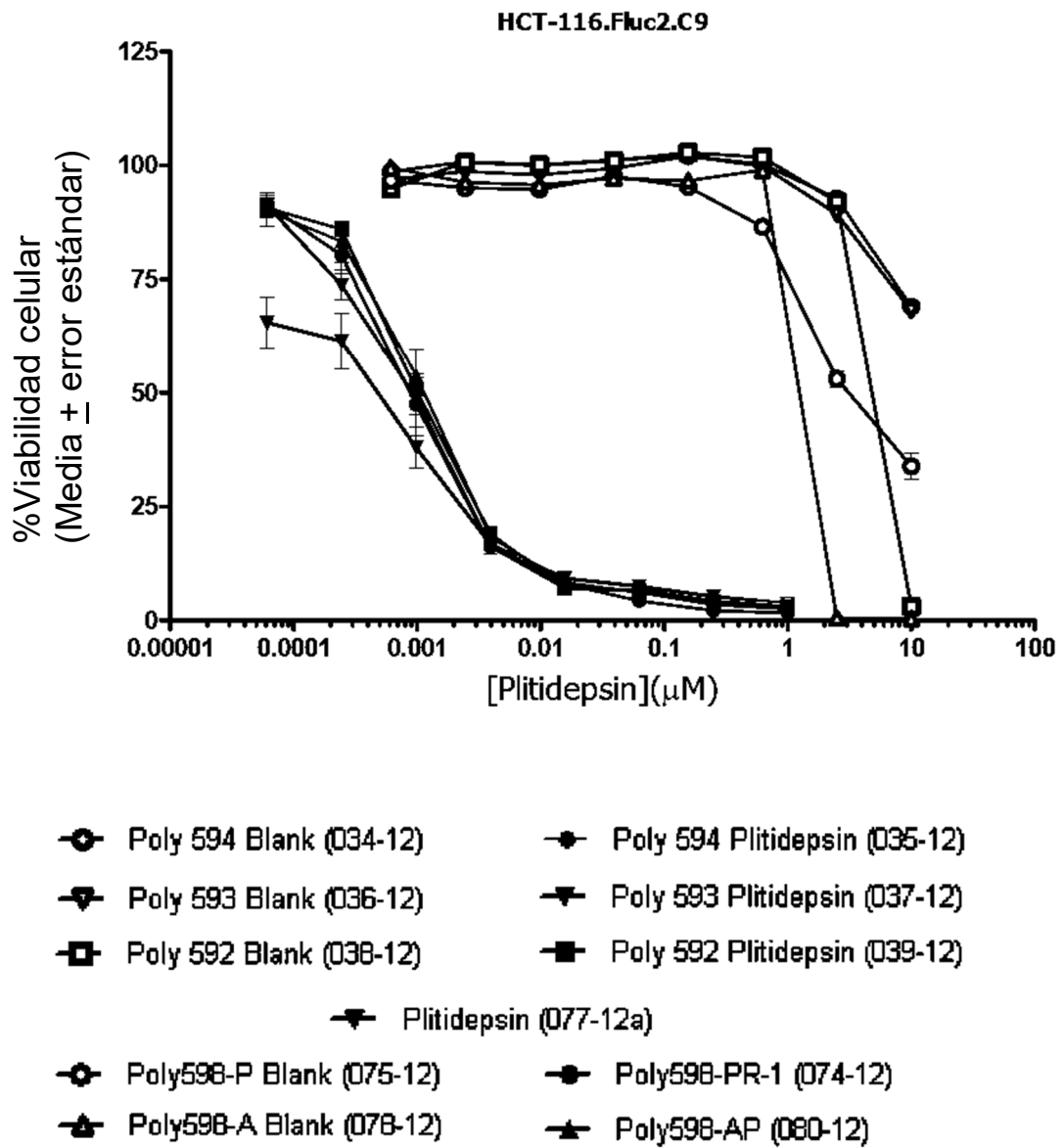Fig. 19
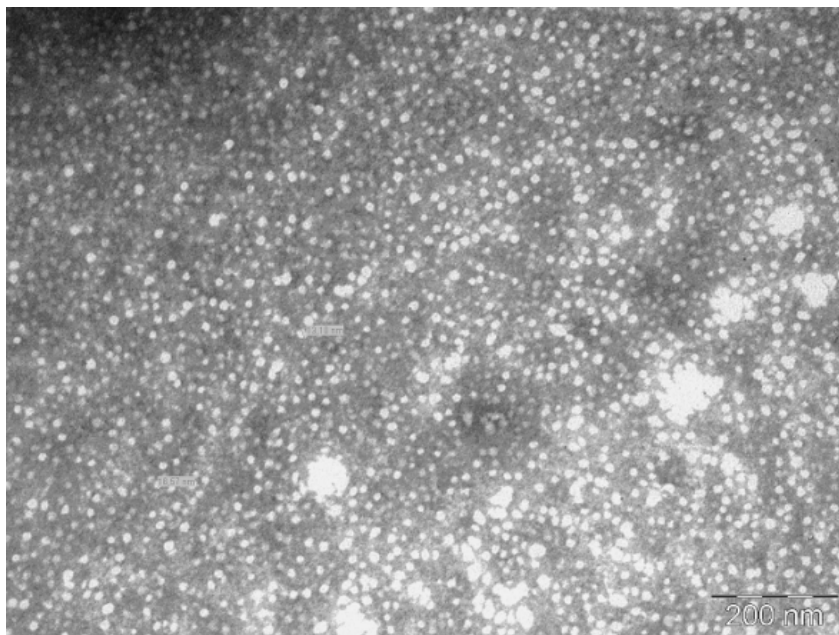
Fig. 20
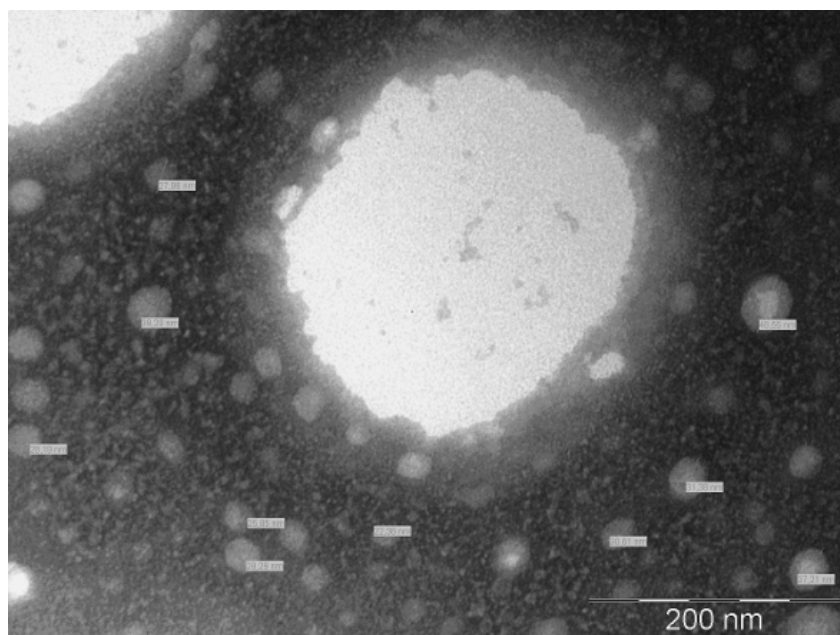
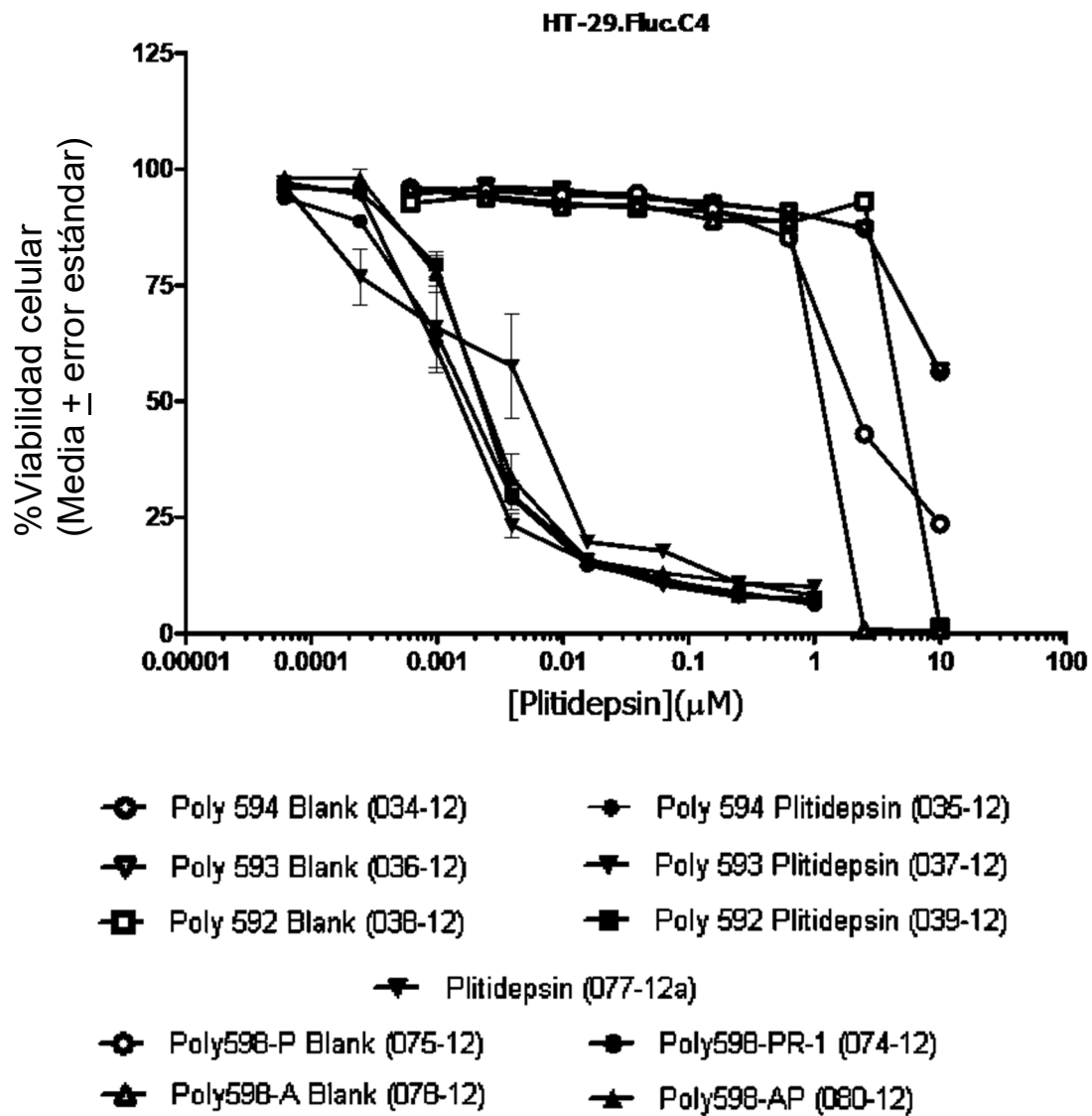Fig. 21
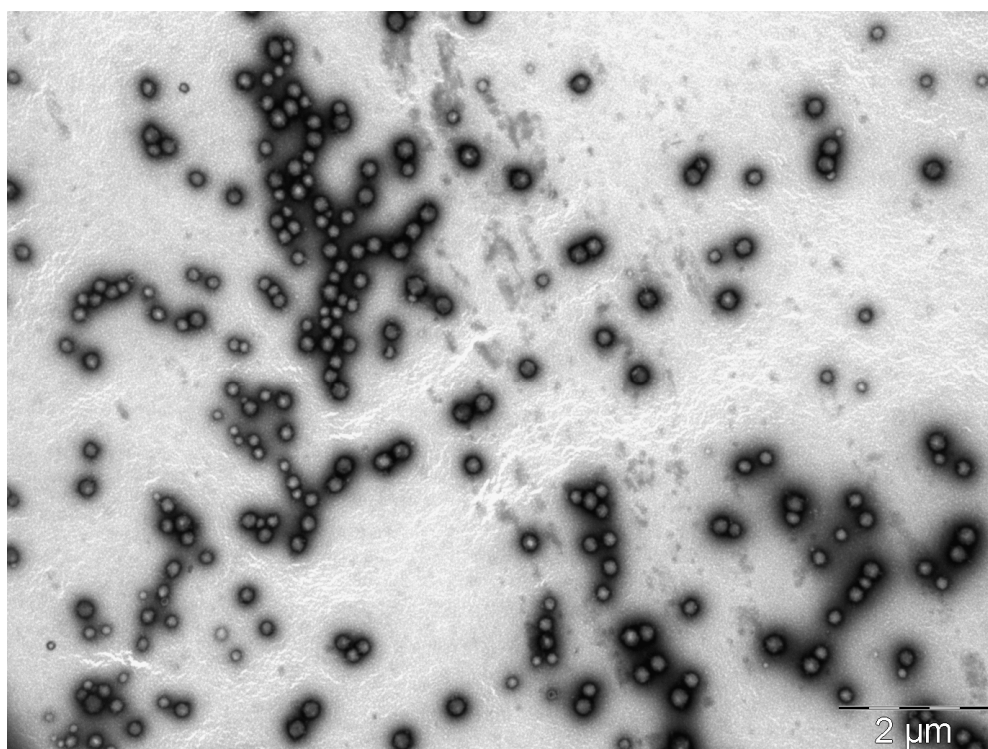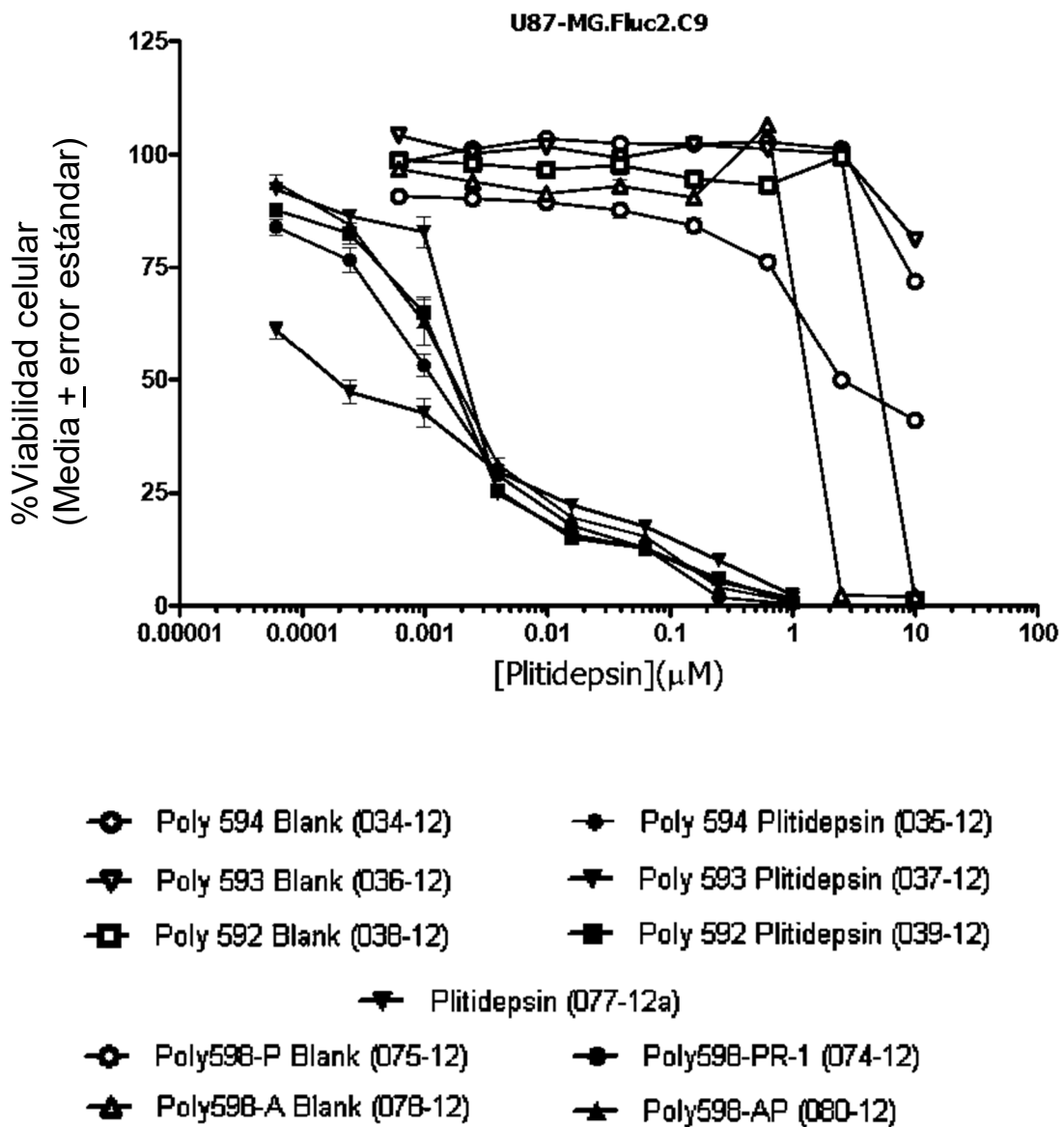

Fig. 22
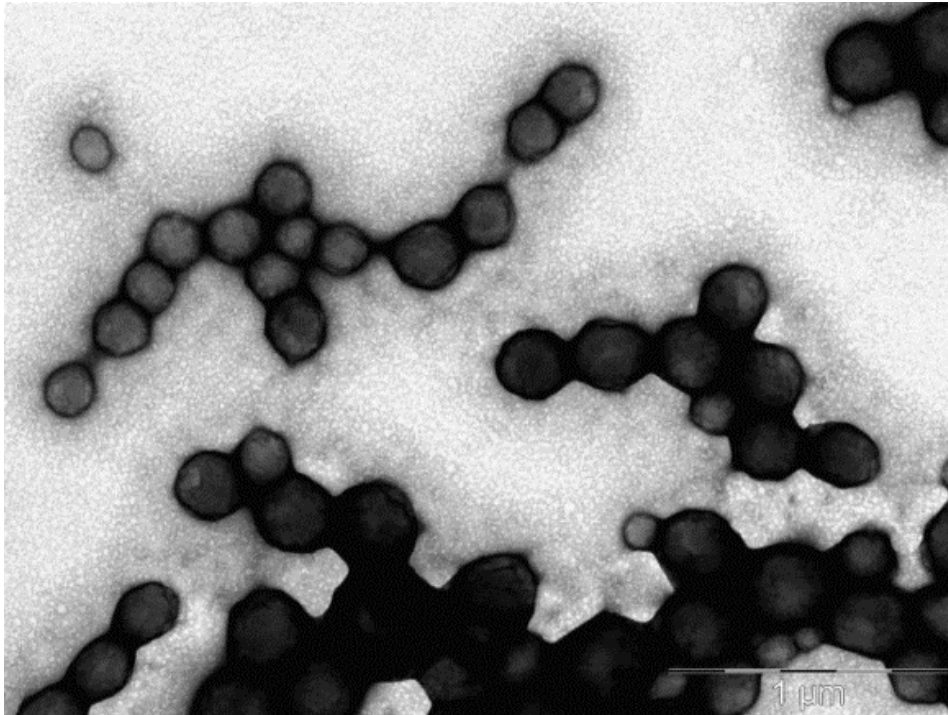
Fig. 23

Fig. 24

Fig. 25

Fig. 26

Fig. 27a

Fig. 27b

Fig. 27c

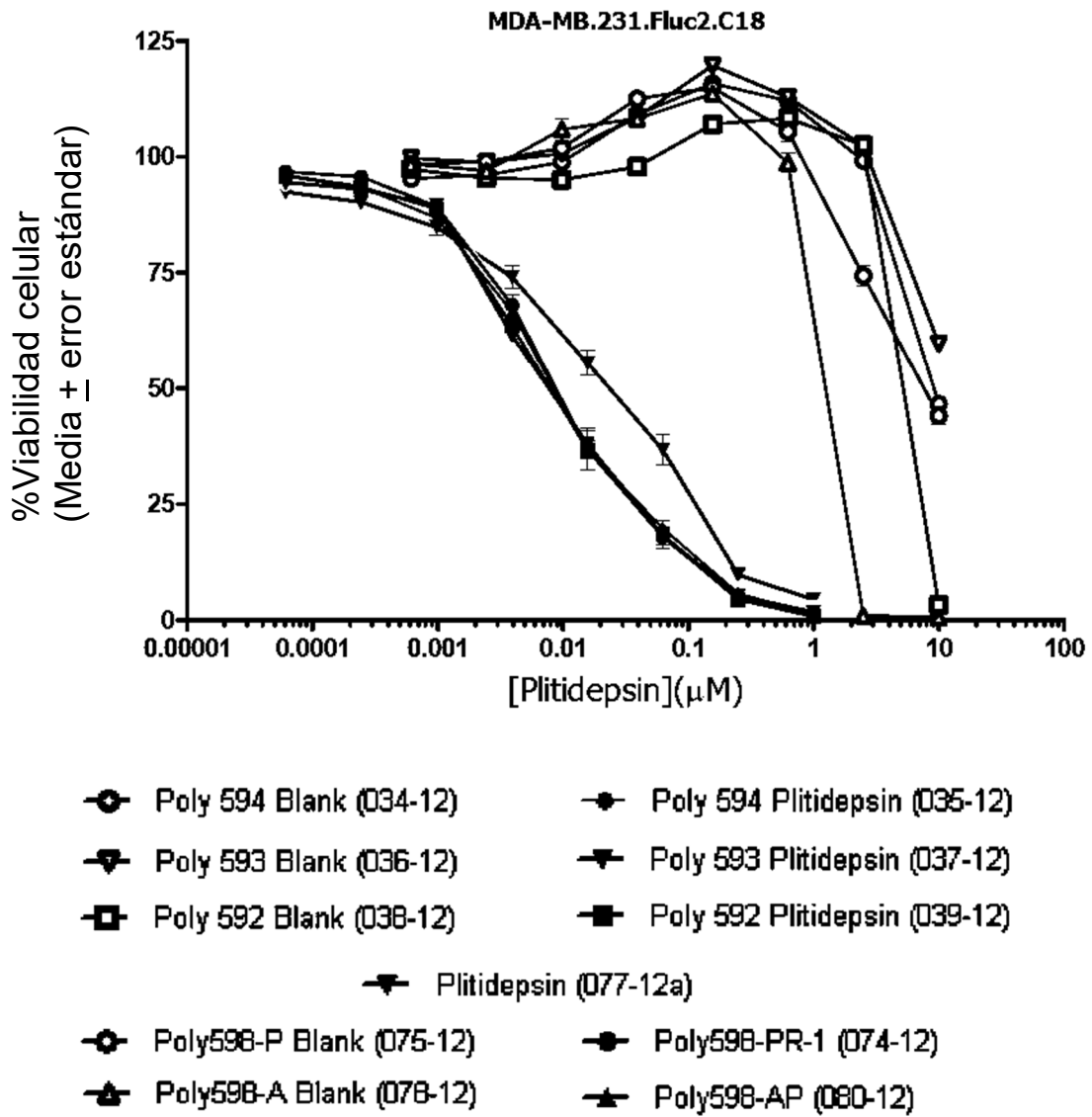Fig. 27d
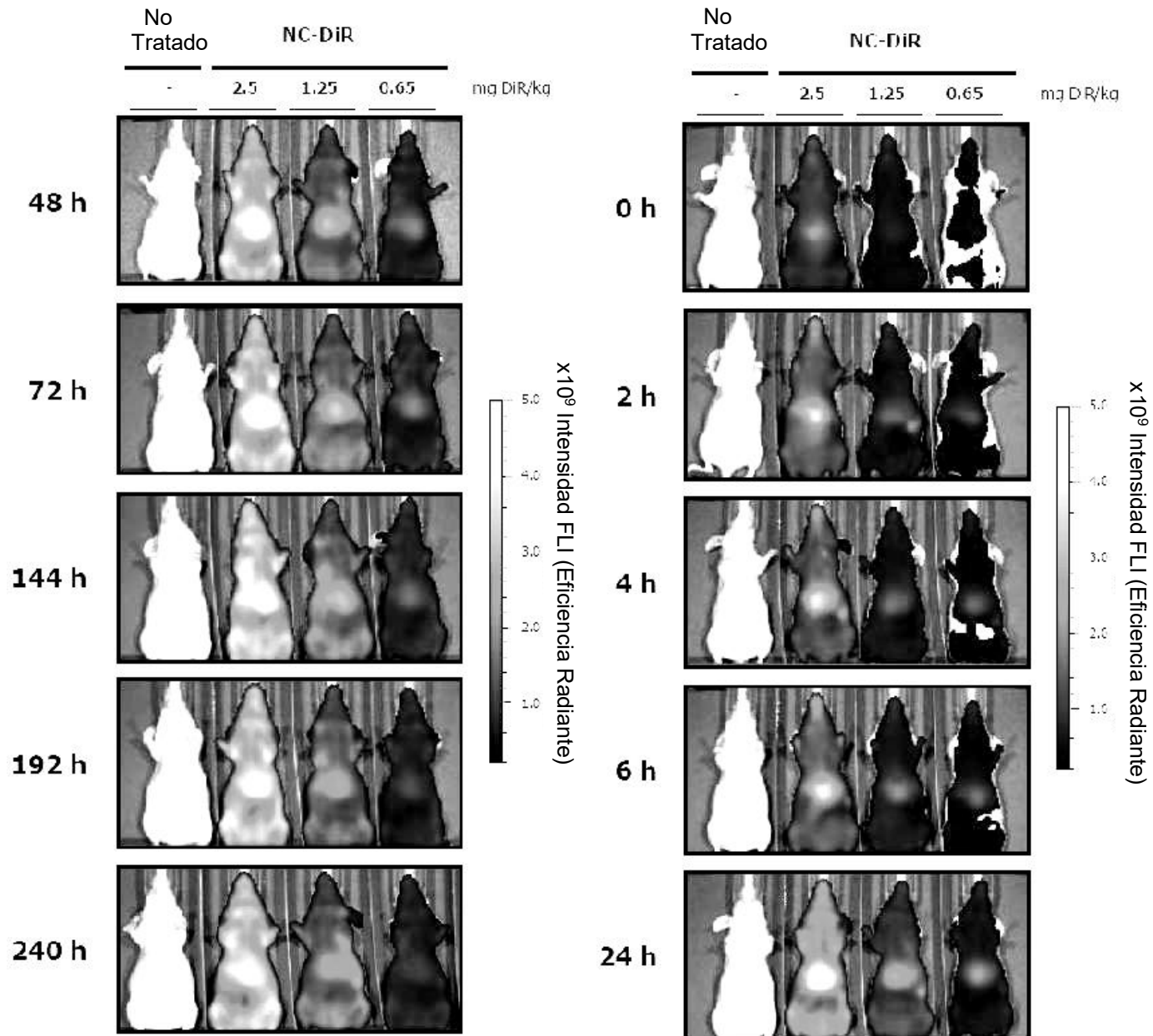
Fig. 28

POLY⁻598 ESQUEMA DE REACCIÓN

PARED ANFIFÍLICA
83% p/p

PARED HIDROFÓBICA
17% p/p

AGENTE RETICULANTE
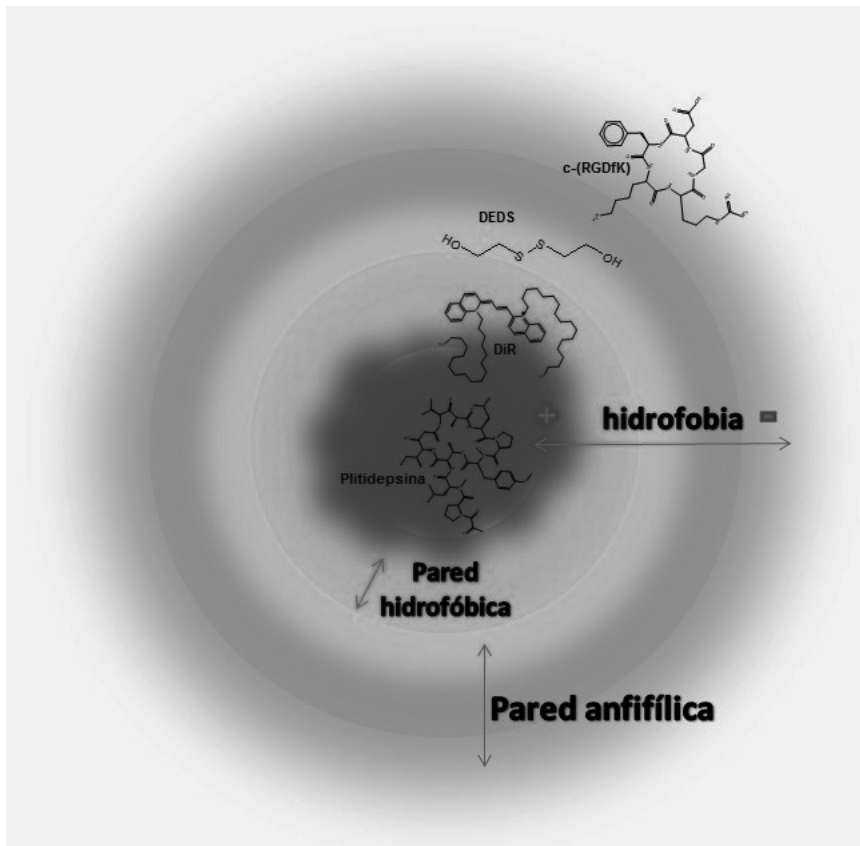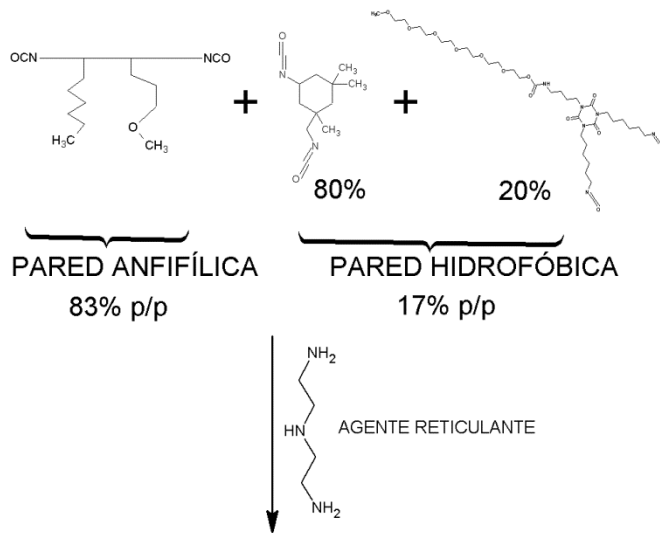
Fig. 29

Distribución de tamaño por nº
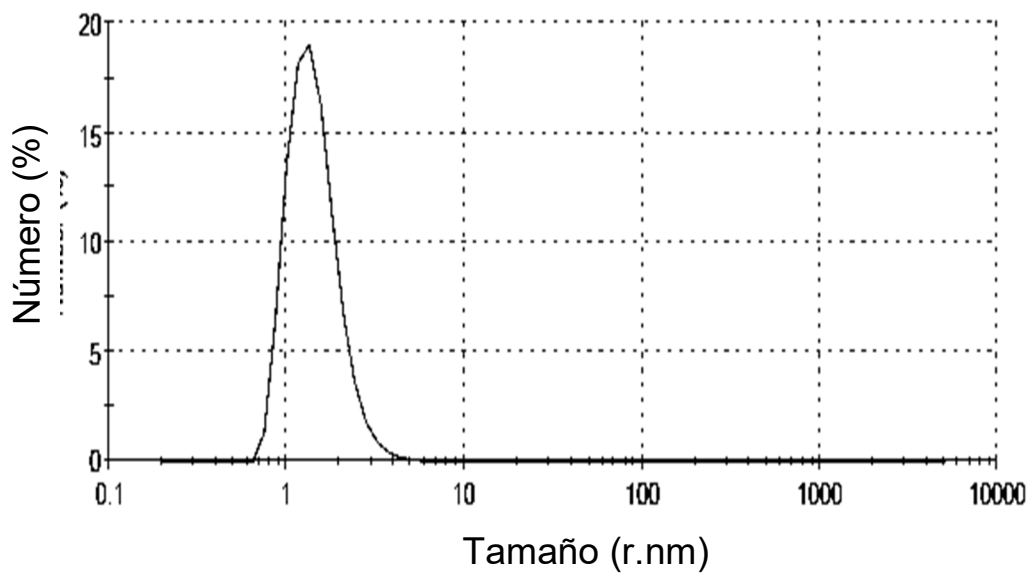
Fig. 30

Distribución de tamaño por volumen
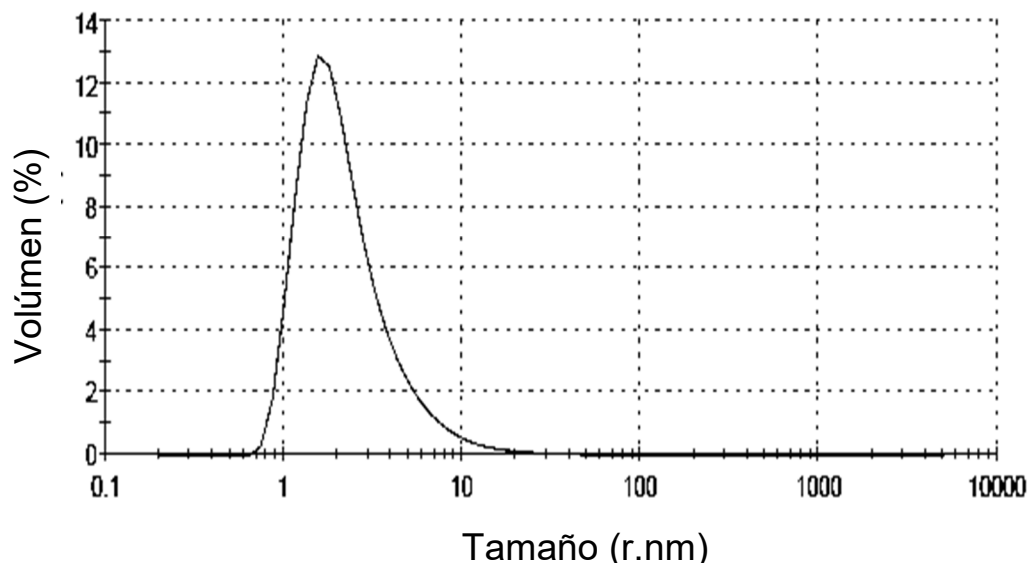
Fig. 31
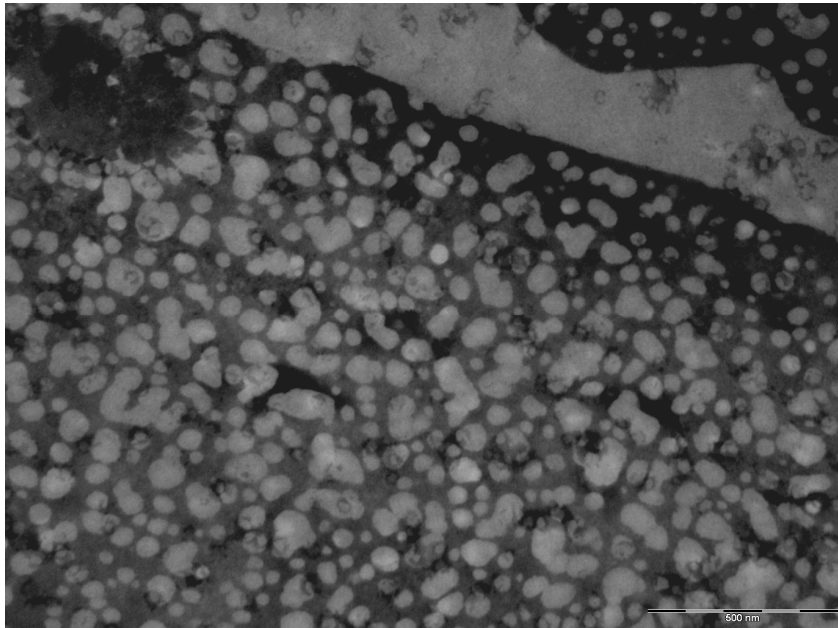
Fig. 32
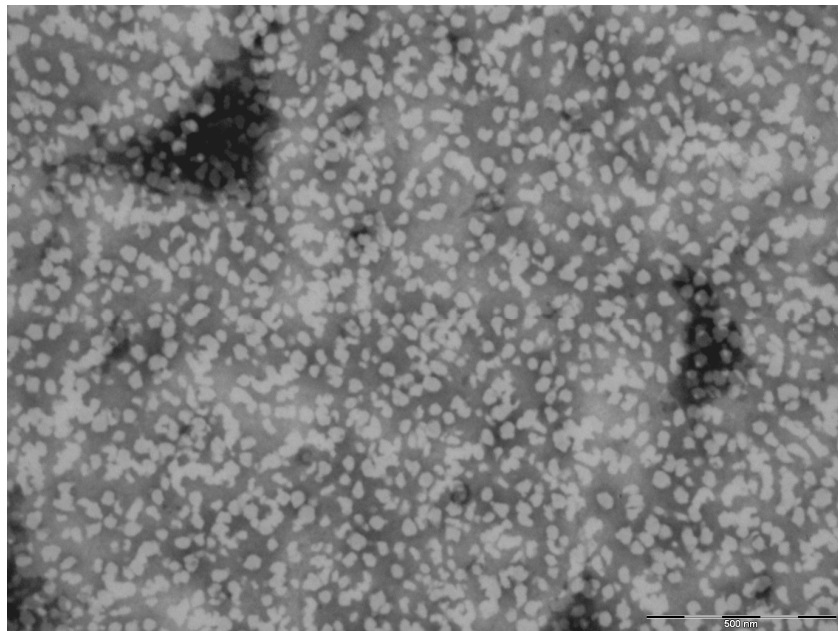
Fig. 33
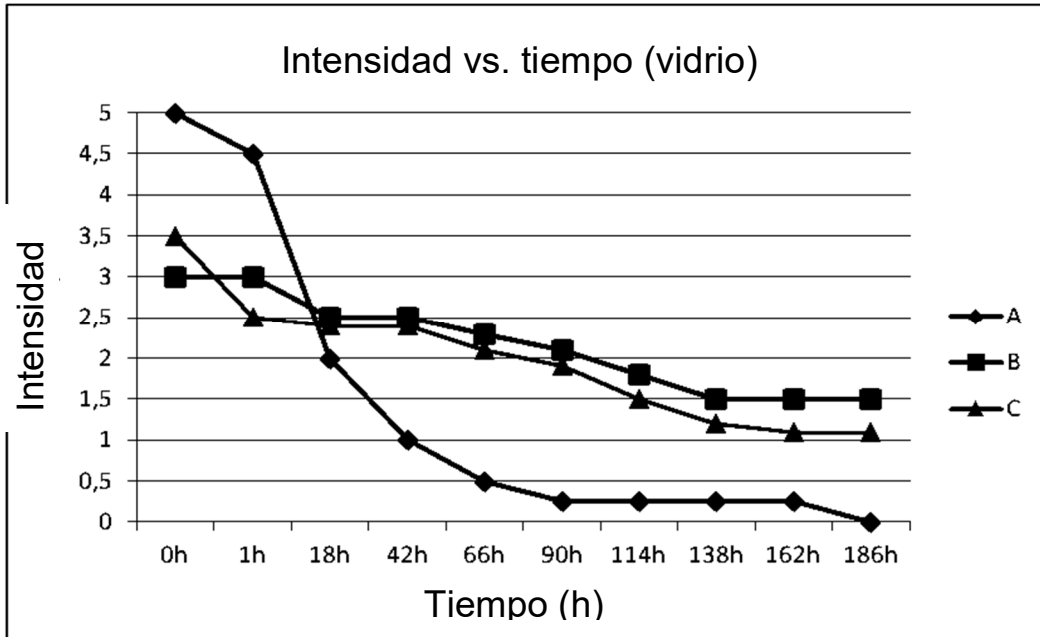
Fig. 34
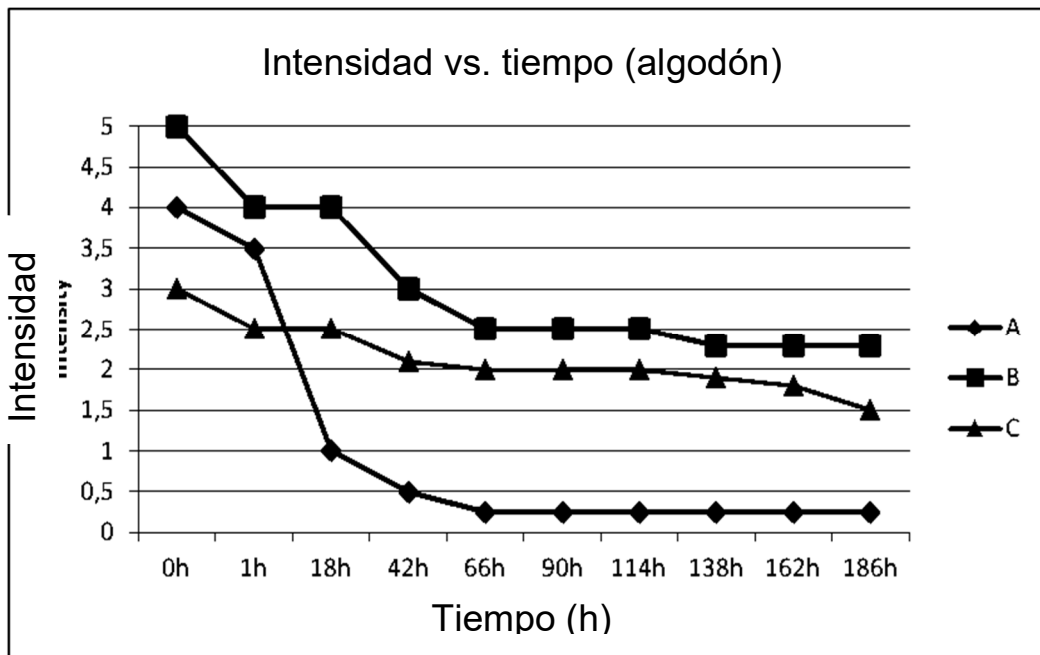
Fig. 35
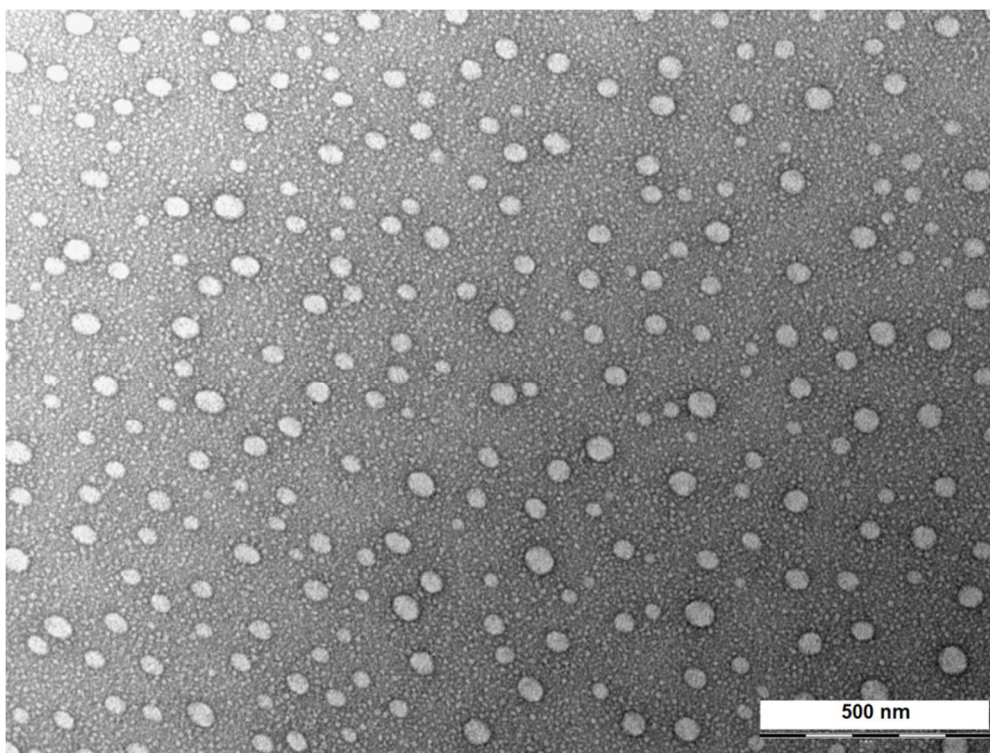
Fig. 36
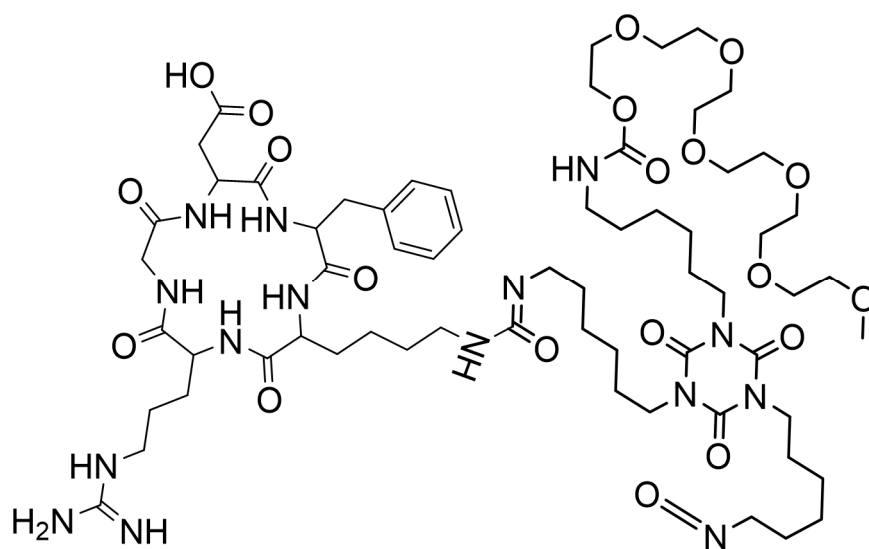
Fig. 37
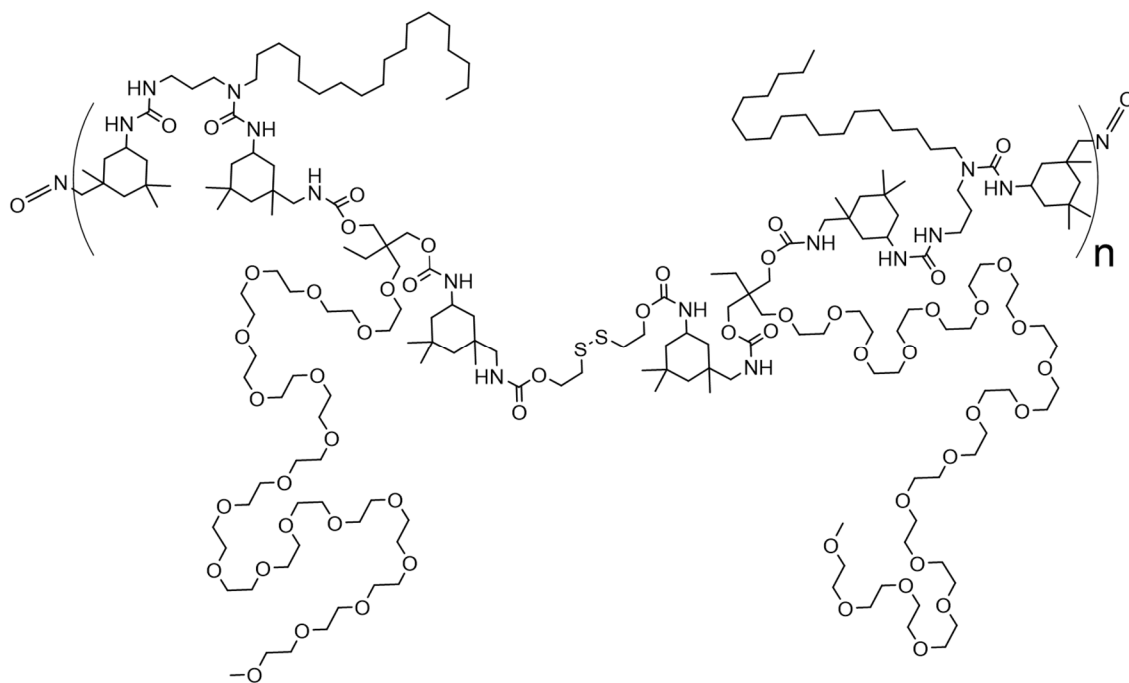
Fig. 38
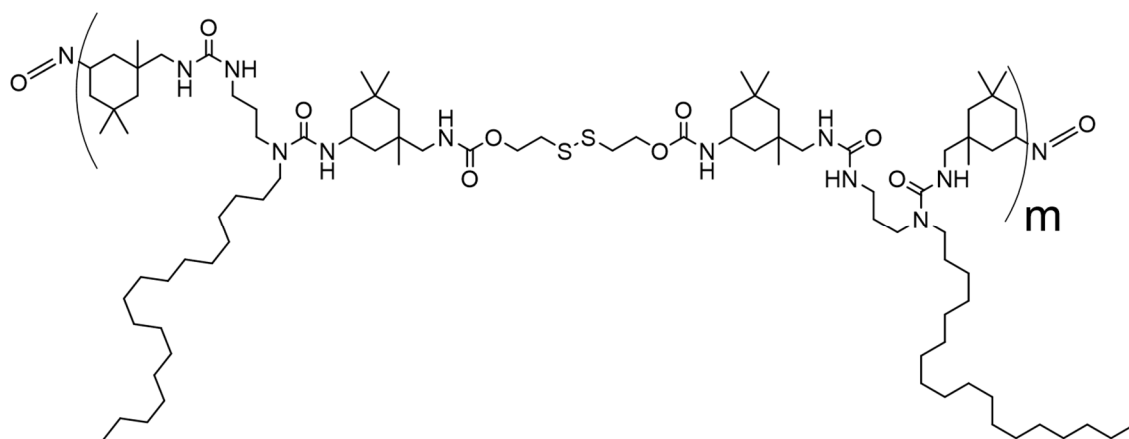
Fig. 39
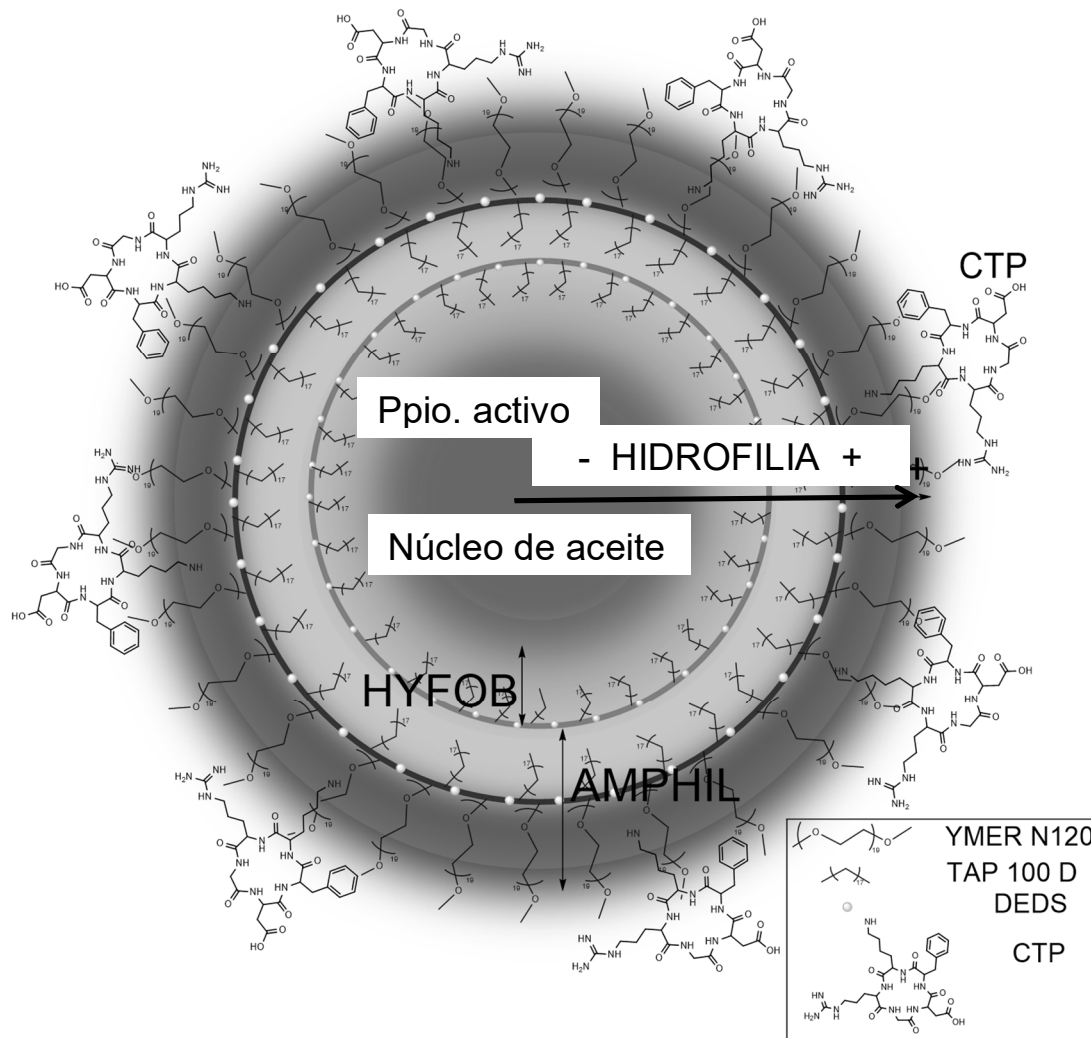
Fig. 40

Distribución de tamaño por intensidad
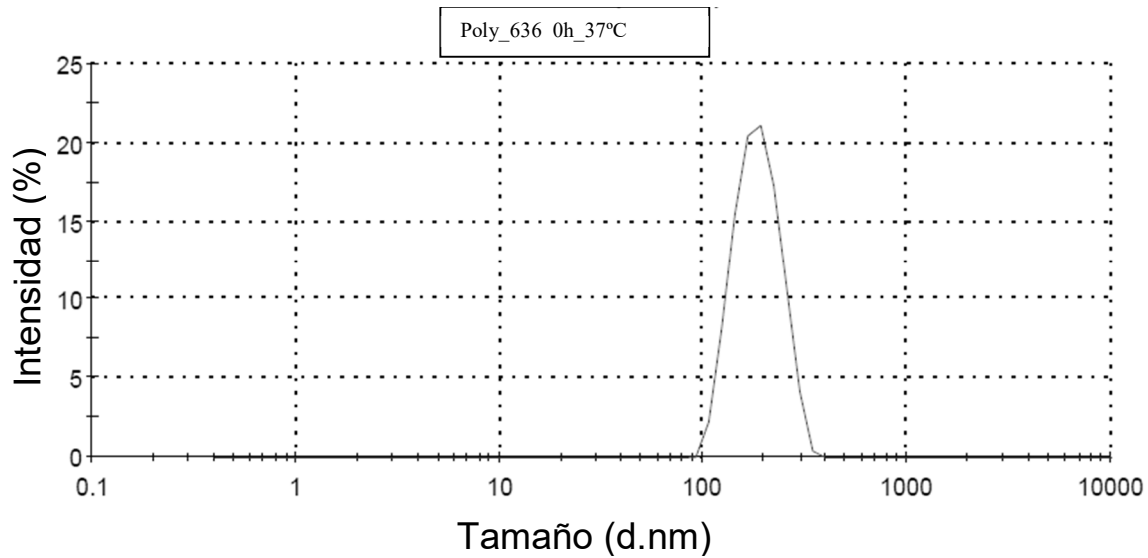
Fig. 41

Distribución de tamaño por intensidad

Fig. 42

Distribución de tamaño por intensidad

Fig. 43

= cRGDfK

NCO = Grupos Isocianato reactivos

NH_2 NH_2 NH_2 NH_2 NH_2

—Si—O—Si—O—Si—O—Si—O—Si—

TiO_2

Ti

$R-N=C=O$ + $R-NH_2$ ⟶ $-R-N-C-N-R-$

Nanocápsula reactiva   Superficie de titanio

Fig. 44

Fig. 45

Fig. 46

Fig. 47

Chapter I. Publication 2

PUUa Nanoparticles for Cancer treatment.

In vitro experiments

Multifunctionalized Polyurethane-Polyurea Nanoparticles: Hydrophobically Driven Self-Stratification at the o/w Interface Modulates Encapsulation Stability

Pau Rocas[a]*, Yolanda Fernández[b], Simó Schwartz Jr[b], Ibane Abasolo[b], Josep Rocas[c]*, Fernando Albericio[adef]*

Polyurethane-Polyurea (PUUa) reactive prepolymers with adjusted hydrophobic and hydrophilic dangling chains to achieve multiwalled sub-30 nm nanoparticles are presented. The combination of an amphiphilic and a hydrophobic prepolymer in the oil-in-water interface creates a stratified shell by hydrophobic interactions. These novel nanostructures enhance the encapsulation stability of lipophilic compounds compared to monowalled nanostructures and facilitate the selective and ordered functionalization along the multiwalled shell with bioactive motifs. As proof of concept, PUUa nanoparticles have been engineered with disulfide bonds and an αvβ3 integrin-selective cyclic RGD peptide (cRGDfK) providing our system with glutathione (GSH) triggered controlled release and cell targeting specificity to U87 tumor cells, respectively.

1. Introduction

Merging cross-functional fields as chemistry, engineering, medicine, and biology to achieve multifunctional stimuli responsive drug delivery systems (DDS) is one of the major challenges in modern medicine[1,2]. Therefore, large efforts are being undertaken to unravel the unknowns which provoke that even today an *in vivo* reliable and efficient smart nano-system has not been completely achieved. Obviously, in the past decade, great progress has been made in the creation of advanced DDS, although, these are usually formed through the emulsification of a hydrophobic drug in water using external surfactants[3,4]. Unwillingly, this kind of DDS commonly lack chemical tailorability, encapsulation efficiency, targeting selectivity, biocompatibility and controlled degradability, among others. One recurrent issue in top used multiblock polymeric systems like PLA, PLGA, PMMA, etc. is the lack of reactive sites that enable multifunctionality. So, smarter nano-systems with complex
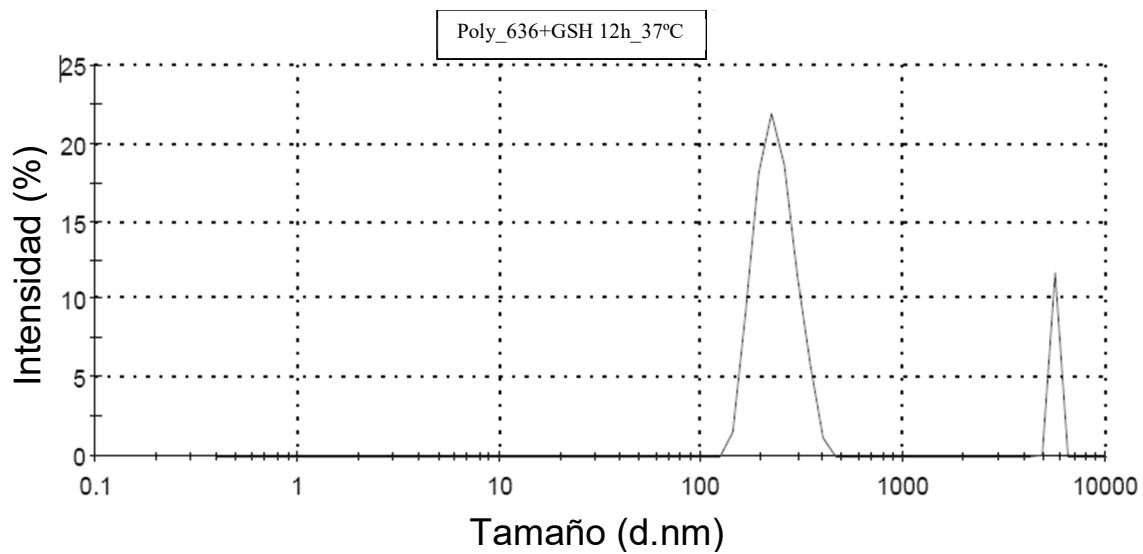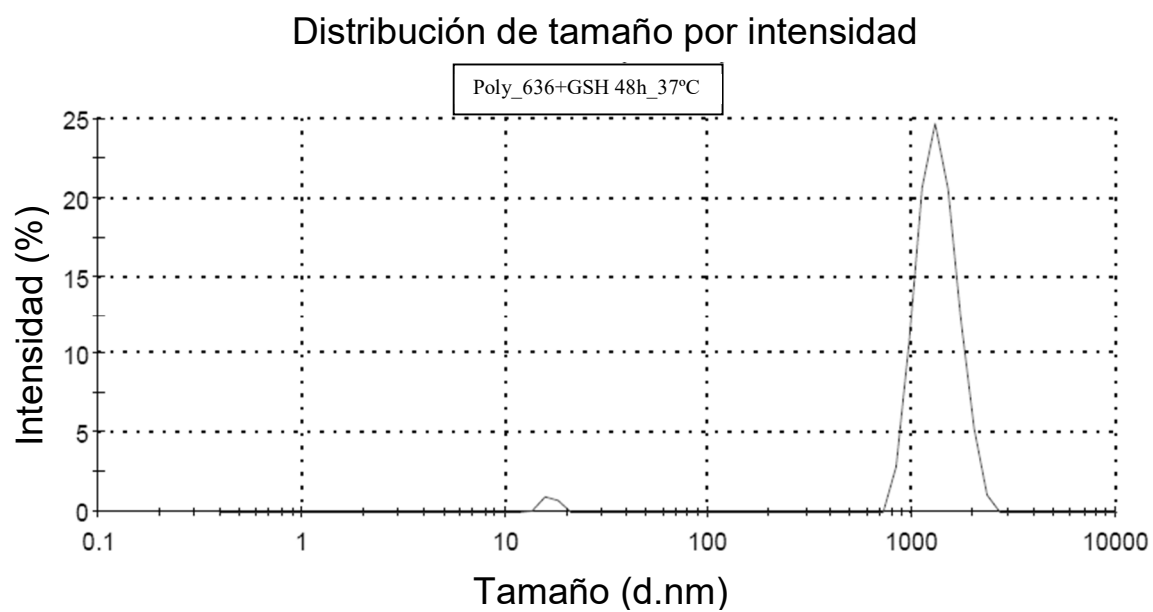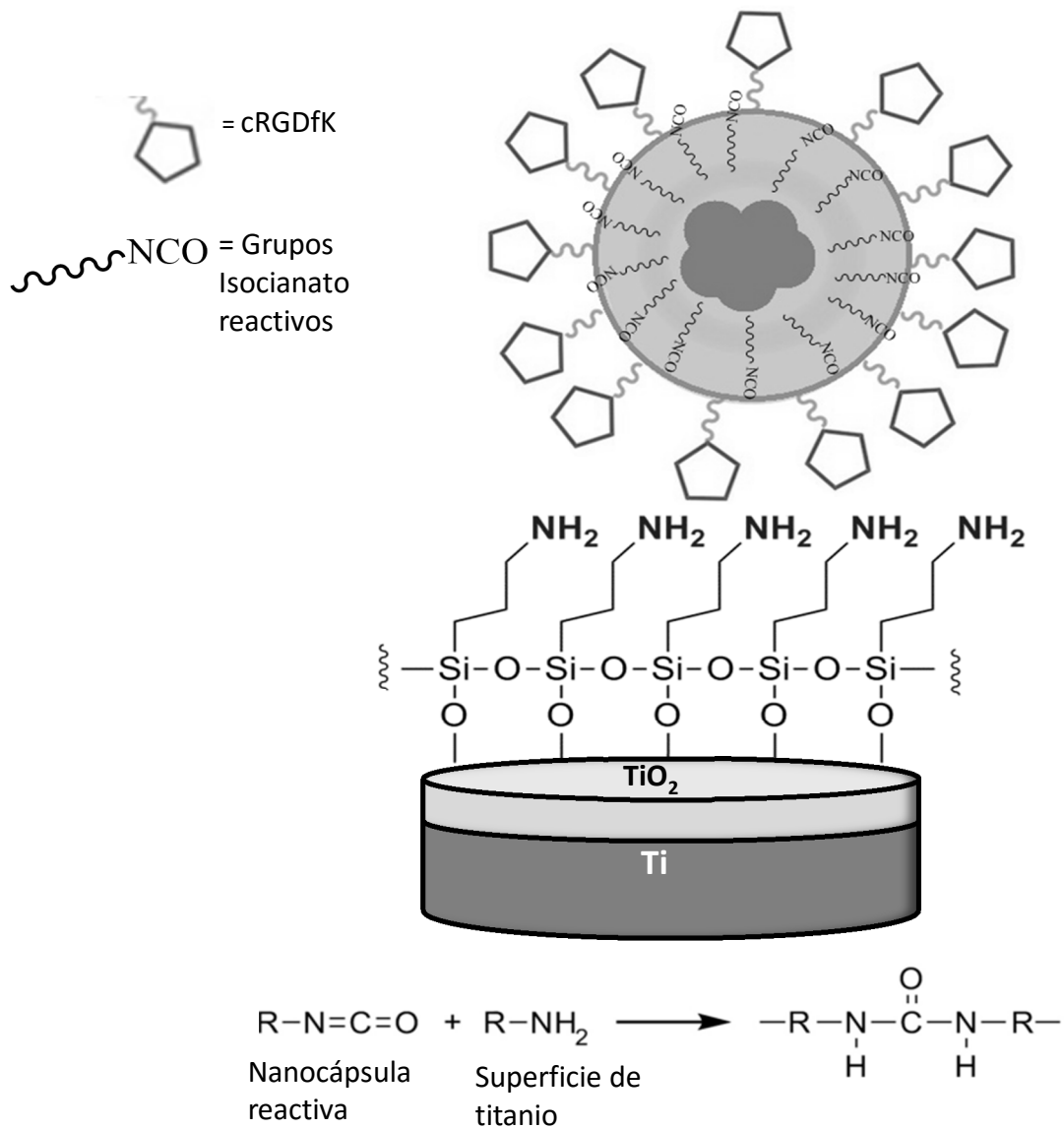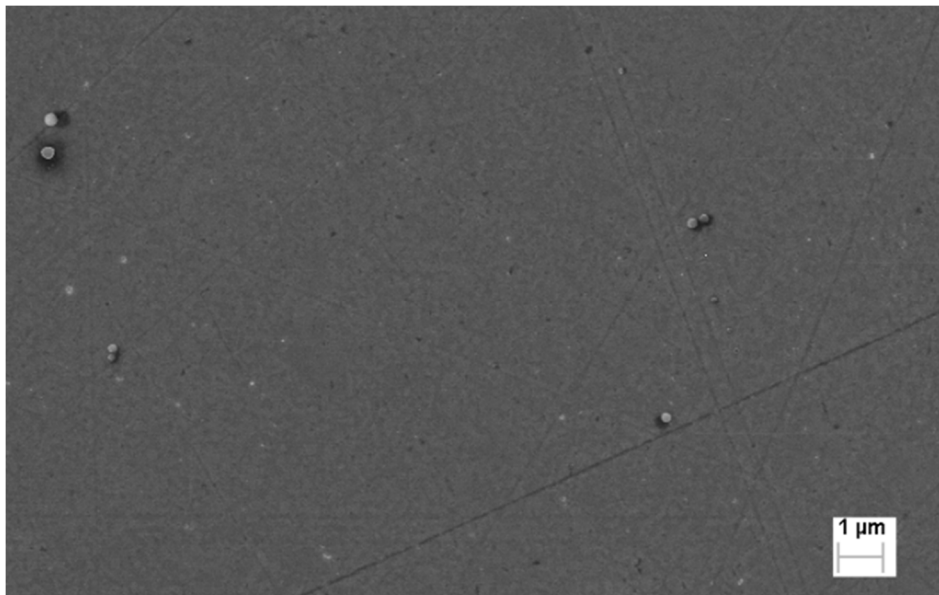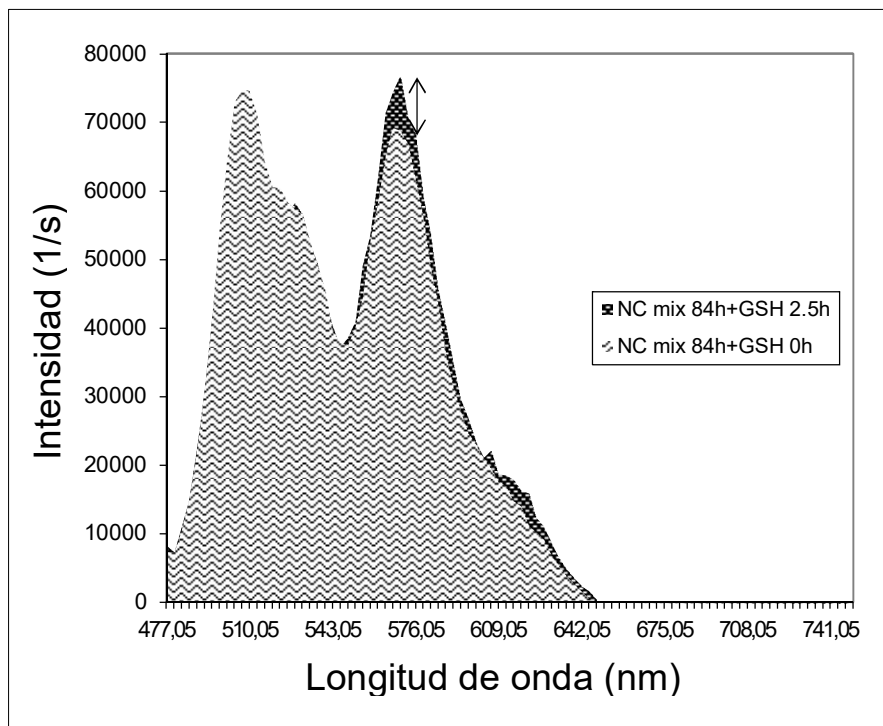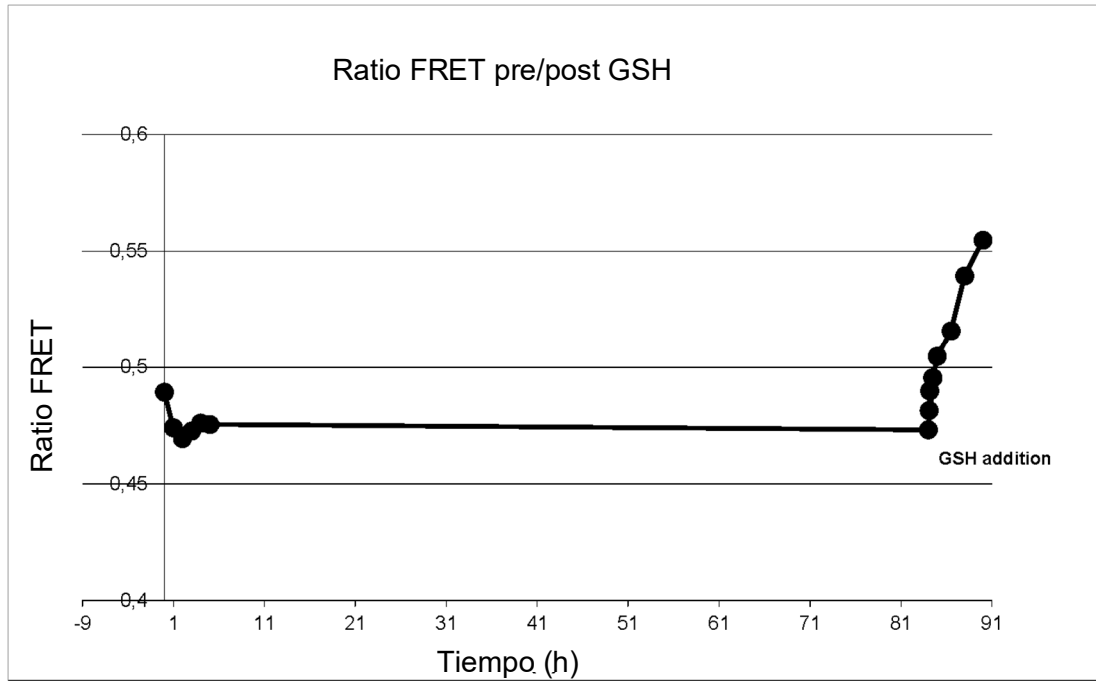
[a,d] Institute for Research in Biomedicine (IRB Barcelona), Baldiri Reixac 10, 08028 Barcelona Spain

[c] Nanobiotechnological Polymers Division, Ecopol Tech S.L., Indústria 7, 43720 L'Arboç, Tarragona, Spain

[d] Department of Organic Chemistry, University of Barcelona, Martí Franquès 1- 11, 08028 Barcelona, Spain

School of Chemistry & Physics, University of Kwazulu-Natal, 4041 Durban, South Africa

[b] CIBBIM-Nanomedicine, VHIR Vall d'Hebron Institut de Recerca, 08035 Barcelona, Spain

[b,d] CIBER-BBN, Networking Centre on Bioengineering Biomaterials and Nanomedicine, 08028 Barcelona, Spain

structures such as dendrimers or multibranched polymers arose. Sadly, sometimes the difficult syntheses, sometimes the costly purification steps limited their industrial and commercial translation. Accordingly, nanoparticles (NPs) fulfilling these structural, delivery and biological requirements are needed in the demanding field of nanomedicine. The scientific community is nowadays highly concerned with the possibility to achieve not only multifunctionality but also self-assembled nanostructured architectures for multiple purposes[5,6]. Concretely, the capacity of polymers to be self-

structured forming the shell of a nano-system is directly related to the ease with which their molecular structure can be modified. So, the tailored design of a polymer is only viable when it is not only chemically tunable but also cost-efficient[7,8]. Thus, to get structural control at the nano-level, a different kind of prepolymers with adjustable physico-chemical and bioactive characteristics is needed. Therefore, polyurethanes and polyureas constitute a potential choice to fulfill such needs. In this aspect, very few publications have reported on the application of reactive polymeric surfactants containing free isocyanate groups[9–11]. The high reactivity of isocyanates with hydroxyl and/or amine containing precursors allow a fast structure stabilization by crosslinking and an efficient functionalization of micro and nanoparticles via polyurethane and/or polyurea bonds. Specifically, PUUa diisocyanate prepolymers can create stable shells by anchoring a wide range of nucleophile-containing (amines, thiols, alcohols, etc.) bioactives[12]. In example, polyisocyanates with high functionality (f>2) allow multiple bonding of bioactive molecules that confer targeting properties and at the same time modulation of their intrinsic hydrophilic-lipophilic balance[13,14]. Of note, to ensure a good biocompatibility and reduce toxicity of biodegraded products aliphatic isocyanates need to be selected instead of aromatic ones[15–17]. Since the late sixties their biocompatibility for biomedical use has been well proven as it is one of the materials of choice in clinical use for development of catheters, stents, valves, etc. The quantitative synthetic procedures, facile scalable processes and broad chemistry of PUUa opens an infinite range of potential incorporation of functionalities. Multiple chemical complexities, biodegradation, targeting and biocompatibility are some of the clear advantages that PUUa polymers can bring to the table as future smart and nanostructured DDS.

Herein we depict the combination of two PUUa prepolymers (one amphiphilic and the other hydrophobic) in aqueous media to create hydrophobically ordered shells. That novel prepolymers contain dangling chains of sharply different polarity to promote a controlled stratification in the oil-water interface to achieve multiwalled nanostructures and bear terminal isocyanate groups for a final crosslinking step to "freeze" the preformed architecture. These nanostructures are designed to improve the encapsulation stability of hydrophobic cargos providing a deeper encapsulation in the NP core compared to monowalled nanostructures where cargos are

closer to the shell surface and burstly-released under *in vivo* conditions[18].

2. Materials and methods

2.1. Chemicals

Cyclo(-Arg-Gly-Asp-D-Phe-Lys) (cRGDfK) was synthesized in house according to previously reported protocols[19]. YMER N-120 was kindly provided by Perstorp (Perstorp, Sweden) and N-Coco-1,3-propylenediamine (Genamin TAP 100D) by Clariant (Barcelona, Spain). Capric/caprylic triglyceride mixture (Crodamol GTCC) was obtained from Croda (Barcelona, Spain) and Bayhydur 3100 was purchased from Bayer (Leverkusen, Germany). If not indicated otherwise, all other reagents were purchased from Sigma-Aldrich (St Louis, MO, USA). Extra dry acetone was used during all the synthetic process.

2.2. Cell lines and cell culture

Human glioblastoma cell line (U87-MG) and human colorectal cancer cell line (HT-29) used in cell internalization assays and human cervix carcinoma cell line (HeLa) used in cytotoxicity assays were obtained from the American Type Culture Collection. All cell lines were maintained as recommended. Briefly, U87-MG cells were maintained in DMEM medium and HT-29 and HeLa cells in RPMI 1640 medium, both from Life Technologies. All media were supplemented with 10% heat-inactivated fetal bovine serum (FBS) (56 °C, 30 min), penicillin (100 U/mL), streptomycin (100 µg/mL) and Fungizone (250 ng/mL) (Life Technologies, Madrid, Spain). Cells were maintained in a humid atmosphere at 37 °C with 5% CO_2.

2.3. Experimental methods

2.3.1. Synthesis of reactive prepolymers for Multiwalled PUUa NPs preparation

2.3.1.1. Preparation of the reactive amphiphilic prepolymer (Amphil).

To synthesize the amphiphilic prepolymer, a 500 mL four-necked reaction vessel was pre-heated at 50 ºC and purged with nitrogen. Then, YMER N-120 (5.50 g, 5.5 mmol), 2-Hydroxyethyl disulfide (DEDS) (0.15 g, 1 mmol), Crodamol GTCC (0.75 g) and IPDI (3.38 g, 15 mmol) were added to the reaction vessel under mechanical stirring with dibutyltin dilaurate (DBTL) as catalyst (3 mg, 4.65 µmol). The polyaddition reaction was maintained in these conditions until DEDS and YMER reacted quantitatively with IPDI as ensured by FT-IR (Fig. S5) and automatic titration[20] (Fig. S2). At this point, the vessel was cooled to 40 ºC and Genamin TAP 100D (1.45 g, 4.44 mmol) dissolved in 10 g of acetone was added under constant stirring and left to react for 30 min (Fig. S1). The formation of polyurethane and polyurethane-polyurea prepolymers was followed by automatic titration (Fig. S2) and FT-IR (Fig. S5) and characterized by NMR[21] (Fig. S7).

2.3.1.2. Preparation of the reactive hydrophobic prepolymer (Hyfob).

To synthesize the hydrophobic prepolymer, a schlenk flask of 20 mL was pre-heated at 50ºC and purged with nitrogen. Then, DEDS (0.15 g, 1 mmol) and IPDI (0.485 g, 2.18 mmol) in acetone (7 g) were added with DBTL as catalyst (0.24 mg, 0.37 µmol) and left to react during 1 h with magnetic stirring. At this point, the Schlenk flask was cooled to 40 ºC and Genamin TAP 100D (0.15 g, 0.5 mmol) in 3 g acetone was added under constant stirring and left to react for 30 min (Fig.

S1). The formation of polyurethane and polyurethane-polyurea prepolymers was followed by FT-IR (Fig. S4) and and characterized by NMR[21] (Fig. S7).

2.3.1.3. Preparation of Bayhydur 3100-cRGDfK conjugate (B3100-cRGDfK).

The peptide cRGDfK (36 mg, 0.0596 mmol) was dissolved in phosphate buffered saline (PBS) (1 mL, 5ºC) and 10 µL of pure triethylamine were added to the mixture (pH 10). Then, the previous solution was mixed with Bayhydur 3100 linker (B3100) (125 mg, 0.167 mmol) and allowed to react during 2 h at 5ºC under constant stirring (Fig. S1). The bonding of one cRGDfK molecule per B3100 linker, the reaction kinetics between cRGDfK and B3100, and the total concentration of linked cRGDfK in PUUa NP-RGD was ensured by MALDI-TOF MS (Fig. S9) and HPLC (Fig. S10 and Table S1), respectively.

2.3.2. Synthesis of Multiwalled polyurethane-polyurea nanoparticles.

2.3.2.1. PUUa NPs synthesis.

A previously homogenized aliquote of Amphil+Hyfob (1.69 g, mass ratio Amphil 13.35:1 Hyfob) (see section 2.3.1.) was added in a round-bottom flask containing B3100 (125 mg, 0.167 mmol) under nitrogen atmosphere. This organic mixture was then emulsified in PBS (16 mL, pH 7.4, 5ºC) in a magnetic stirrer under an ice bath to prevent isocyanate reaction with water. Once emulsified, L-lysine was added (68.56 mg, 0.47 mmol) and the interfacial polyaddition reaction was controlled by FT-IR. After 30 min, DETA (32.18 mg, 0.31 mmol) was added and the crosslinked nanoparticles were formed by a second interfacial polyaddition as proved by FT-IR. Acetone was mildly removed in the rotavapor. PUUa NPs were dialysed (100000 MWCO, Spectrum Laboratories, California, USA) against pure water during 72 h for Zeta potential experiments. For in vitro experiments PUUa NPs were dialysed against PBS during 72 hours.

2.3.2.2. PUUa DiI loaded NPs synthesis (PUUa NP-DiI).

These NPs were synthesized as previously described (see section 2.3.2.1.) adding Amphil+Hyfob in a round bottom flask containing DiI (2.5 mg, 2.67 µmol) as fluorophore. The organic mixture was homogenized and subsequently, section 2.3.2.1 followed without modifications.

2.3.2.3. PUUa DiO loaded NPs synthesis (PUUa NP-DiO).

These NPs were synthesized as previously described (see section 2.3.2.2.) using DiO (2.5 mg, 2.83 µmol) as fluorophore instead of DiI.

2.3.2.4. All-in-one PUUa NPs formation (PUUa NP-DiI-RGD).

These PUUa NPs were synthesized as previously described (see section 2.3.2.1.) using B3100-cRGDfK as targeting conjugate. Amphil+Hyfob organic mixture was mixed with the previously described B3100-cRGDfK conjugate solution (see section 2.3.1.3.) (16 % w/w) followed by emulsification in PBS (16 mL, pH 7.4, 5ºC) in a magnetic stirrer under an ice bath to prevent isocyanate reaction with water. At this point, section 2.2.1. was followed without modifications.

2.3.2.5. PUUa NPs DETA crosslinked

Section 2.3.2.1. was followed but crosslinked by interfacial polyaddition only with DETA (64.36 mg, 0.62 mmol).

2.3.2.6. PUUa NPs Lys crosslinked

Section 2.3.2.1. was followed but crosslinked by interfacial polyaddition only with L-lysine (137.12 mg, 0.94 mmol).

2.3.3 Synthesis of reactive prepolymer for Monowalled PUUa NPs preparation

2.3.3.1. Preparation of the reactive amphiphilic prepolymer (Amphil).

To allow a logical comparison between nanoparticles, monowalled ones contained the same total amount of monomers than multiwalled ones but just in one Amphil prepolymer. To synthesize the amphiphilic prepolymer, a 500 mL four-necked reaction vessel was pre-heated at 50 ºC and purged with nitrogen. Then, YMER N-120 (5.50 g, 5.5 mmol), 2-Hydroxyethyl disulfide (DEDS) (0.30 g, 2 mmol), Crodamol GTCC (0.75 g) and IPDI (3.866 g, 17 mmol) were added to the reaction vessel under mechanical stirring with dibutyltin dilaurate (DBTL) as catalyst (3.24 mg, 5.02 µmol). The polyaddition reaction was maintained in these conditions until DEDS and YMER reacted quantitatively with IPDI as ensured by FT-IR and automatic titration[20]. At this point, the vessel was cooled to 40 ºC and Genamin TAP 100D (1.6 g, 4.94 mmol) dissolved in 10 g of acetone was added under constant stirring and left to react for 30 min. The formation of polyurethane and polyurethane-polyurea prepolymers was followed by FT-IR.

2.3.4. Synthesis of Monowalled polyurethane-polyurea nanoparticles

2.3.4.1. PUUa DiI loaded NPs synthesis (PUUa NP-DiI).

A previously homogenized aliquote of Amphil (1.69 g) (see section 2.3) was added in a round-bottom flask containing DiI (2.5 mg, 2.67 µmol) as fluorophore and B3100 (125 mg, 0.167 mmol) under nitrogen atmosphere. This organic mixture was then emulsified in PBS (16 mL, pH 7.4, 5ºC) in a magnetic stirrer under an ice bath to prevent isocyanate reaction with water. Once emulsified, L-lysine was added (68.56 mg, 0.47 mmol) and the interfacial polyaddition reaction was controlled by FT-IR. After 30 min, DETA (32.18 mg, 0.31 mmol) was added and the crosslinked nanoparticles were formed by a second interfacial polyaddition as proved by FT-IR. Acetone was mildly removed in the rotavapor. PUUa NPs were dialysed (100000 MWCO, Spectrum Laboratories, California, USA) against pure water during 72 h for FRET experiments.

2.3.4.2. PUUa DiO loaded NPs synthesis (PUUa NP-DiO).

These NPs were synthesized as previously described (see section 2.3.4.1.) using DiO (2.5 mg, 2.83 µmol) as fluorophore instead of DiI.

2.4. Analytical techniques

2.4.1. Transmission electron microscopy. The nanoparticles morphology was studied in a Jeol JEM 1010 (Peabody, MA, USA). A 200 mesh copper grid 0,75% FORMVAR coated was deposited on a drop of 10 mg/mL of nanoparticles in water during 1 min. Nanoparticles excess was removed by fresh milliQ water contact for 1 min. Then, the grid was deposited on a drop of Uranyl acetate 2 % w/w in water for 30 sec. The Uranyl acetate excess was blotted off and air-dried before measurement. For the degradation experiment, 10 µL of filtered (0,22 µm) PUUa NPs (100mg/mL) were added into 1 mL solution of GSH (10 mM) and incubated at 37 ºC during 24 h under constant stirring. For statistical analysis, 5 different zones of the copper grid were randomly counted with ImageJ software (NIH, Bethesda, MD, USA).

2.4.2. B3100-cRGDfK reaction control. The reaction solution containing B3100 and cRGDfK (see section 2.1.3.) was analysed at 0 and 2 hours of reaction. Analytical HPLC runs of B3100-cRGDfK were performed in a WATERS 2998 HPLC (Milford, MA, USA) using a X-Bridge BEH130, C18, 3.5 µm, 4.6 X 100 mm reverse phase column with the following gradient: 5-15% B in 9 min at a flow rate of 1 mL/min; eluent A: H_2O with 0.045% TFA (v/v); eluent B: CH_3CN with 0.036% TFA.

2.4.3. PUUa NP-RGD conjugation yield quantification. A calibration curve was performed by preparing 5 standard solutions of cRGDfK peptide containing L-phenylalanine amide as internal standard for quantitative HPLC analysis. Analytical HPLC runs of the PUUa NP-RGD were performed in a WATERS 2998 HPLC (Milford, MA, USA) using a X-Bridge BEH130, C18, 3.5 µm, 4.6 X 100 mm reverse phase column with the following gradient: 5-30% B in 9 min at a flow rate of 1 mL/min; eluent A: H_2O with 0.045% TFA (v/v); eluent B: CH_3CN with 0.036% TFA.

2.4.4. Size distribution by DLS. PUUa NP and PUUa NP-RGD were analysed on a Malvern Zetasizer Nano-ZS90 (Malvern, UK) at 1 mg/mL in pure water at 37 ºC.

2.4.5. Zeta Potential measurements. PUUa NP and PUUa NP-RGD were analysed on a Malvern Zetasizer Nano-ZS90 (Malvern, UK) at 20 mg/mL in pure water at 37 ºC.

2.4.6. Infrared spectra. IR spectra were performed in a FT-IR Nexus Termo Nicolet 760 (Waltham, MA, USA) by depositing a drop of previously dissolved prepolymer at 1 % in acetone on a NaCl or BaF_2 (for aqueous samples) disk.

2.4.7. Automatic titration. Prepolymer sample after dissolved in dry toluene reacted with excessive di-n-Butylamine standard, and residual di-n-Butylamine was back-titrated with 1M hydrochloric acid up to the endpoint. The content of Isocyanate was calculated from titration volume.

2.4.8. FRET experiments.

Control experiment. To evaluate the kinetics of hydrophobic molecules leakage, 10 µL of 100 mg/mL PUUa NP containing DiI (0.15 mg/mL) and 10 µL of 100 mg/mL PUUa NP containing DiO (0.15 mg /mL) were diluted to 1 mL pure fresh water. Experiments in spectrofluorimeter Varian Cary Eclipse (Palo Alto, CA, USA) were carried out by excitation of the donor at 470 nm and measuring the emission from 480 to 650 nm with constant magnetic stirring at 37 ºC during 24 h.

GSH experiment. The same experiment was repeated adding the needed mg of GSH in the cell to be at 10 mM after 3 h of experiment.

PC-Chol liposomes experiment. The same experiment was repeated adding 10 µL of 100 mg/mL PUUa NP containing DiI (0.15 mg /mL) and 10 µL of 100 mg/mL PUUa NP containing DiO (0.15 mg /mL) to a 1 mL, 10 mM solution of PC-Chol liposomes previously filtered under 0.45 µm.

2.4.9. MALDI-TOF MS. B3100-cRGDfK conjugate formation was ensured by MALDI-TOF MS. The experiment was carried out on an Applied Biosystems Voyager-DETMRP mass spetrometer (Waltham, MA, USA), using α-cyano-4-hydroxycinnamic acid (ACH) as matrix. B3100 and B3100-cRGDfK at 1 mg/mL after 2 h reaction were analysed.

2.4.10. NMR. NMR spectra were recorded on a Varian Mercury (400 MHz) (Agilent) (Santa Clara, CA, USA). Reactive prepolymers Hyfil, Amphil and Hyfob were previously dissolved in $CDCl_3$ at 100 mg/mL.

2.4.11. Lyophilization and redispersion procedures. Previously dialysed samples (100 mg/mL) were lyophilized and directly redispersed at the desired concentration by overnight stirring at 1500 rpm. Lyophilized and redispersed samples were examined by TEM and DLS to ratify optimal size and morphology characteristics.

2.5. Biological studies

2.5.1. Integrin expression characterization. Expression of $\alpha_V\beta_3$ and $\alpha_V\beta_5$ was analyzed by flow cytometry using monoclonal antibodies against both heterodimers (MAB1976H and MAB1961F from Millipore). Precisely, cell suspensions deattached using PBS-EDTA (5mM) were incubated with 3 µg of $\alpha_V\beta_3$ antibody and 1 µg of $\alpha_V\beta5$ antibody during 20 min at 4ºC. IgG2 isotype controls from eBioscience (San Diego, CA, USA) were included. Cells were analyzed using FacScalibur Becton Dickinson (Franklin Lakes, NJ, USA) and FCS Express 4 software De Novo Software (Los Angeles, CA, USA).

2.5.2. Cell internalization by flow cytometry. Time dependent internalization of targeted and non-targeted PUUa NPs was studied by flow cytometry. Precisely, exponentially growing cultures were detached using PBS-EDTA (5 mM), resuspended in Ca^{2+} and Mg^{2+} free PBS and incubated at 37ºC with a final concentration of 38.5 µg/mL of NPs containing 10 µg/mL of DiI. After the incubation, cells were washed twice with PBS and stained with DAPI (50 µg/mL) to include only viable cells into the analysis. Cells were analyzed using LRS Fortessa Becton Dickinson (Franklin Lakes, NJ, USA) and FCS Express 4 software De Novo Software (Los Angeles, CA, USA).

2.5.3. Cell internalization and lysosomal colocalization by confocal microscopy. Cells were seeded in 24 well-plates containing coverslips (50,000 cells/well) and left overnight at 37 °C with 5% CO_2 to allow cell attachment. Cells were then washed carefully with PBS and 1 µg/mL of DiI containing PUUa NPs (with or without RGD targeting moieties) were added to the cultures diluted in complete cell growing media. After the incubation period, cells were washed twice with PBS and stained 15 min with 10 µM of Lysotracker Green (Life Technologies) and directly visualized using confocal microscope (FV1000, Olympus). Confocal images of the same Z plane were obtained for Lysotracker (green signal) and for DiI (red signal), using excitation peaks at 488/561 nm and emission at 522/585 nm for Lysotracker and DiI, respectively and merged afterwards to demonstrate that some of the nanoparticles are allocated inside acidic organelles labeled by Lysotracker. Images were acquired at 60x magnification. Quantification of the NP signal outside the lysosomes was performed using Fiji ImageJ[22] (NIH, Bethesda, MD, USA) in confocal images taken from at least three different fields. Red signal in every cell in each field (8-14) was quantified for each z-plane, and then compared statistically using the *t*-student test with GraphPad software (La Jolla, CA, USA).

Cytotoxicity studies. In vitro cytotoxicity of NPs was tested by 3-[4,5-dimethylthiazol-2-yl]-2,5-diphenyltetrazolium bromide (MTT) method after 72 h incubation[23]

can be obtained due to the versatile polyurethane chemistry. In fact, the novel kind of NPs based on reactive polyurethane and polyurea prepolymers introduced herein allowed controlled stratification at the nano-interface and tunable functionality in their multiwalled structure[24] (Fig. 1a and 1b). As proof of concept for cancer therapy, disulfide bonds were successfully included in the prepolymers to enable a tailored degradation and a controlled intracellular release of encapsulated hydrophobic molecules at intracellular GSH concentration. Moreover, a cyclic hydrophilic RGD peptide located on the outer shell of the NP was selected and innovatively conjugated to mediate specific targeting to cells overexpressing αvβ3 integrin (Fig. 1c). Finally, to strengthen this stratified structure a crosslinking step with polyamines was key to form an isocyanate-free, ordered and robust nanostructure[25–27].

Thus, we synthesized two new reactive prepolymers by successive quantitative polyaddition reactions of difunctional monomers with an aliphatic diisocyanate (Isophorone diisocyanate) (see monomers description in the ESI and Fig. S1 and Table S1) and characterized them by automatic titration (Fig. S2), FT-IR (Fig. S3 and Fig. S4) and NMR (Fig. S5 and Fig. S6 in the ESI). On one hand, the reactive amphiphilic prepolymer (Amphil) contained disulfide bonds (2-Hydroxyethyl disulfide) in the main chain, hydrophilic (polyethylene glycol monomethyl ether) and hydrophobic (N-Coco-1,3-propylenediamine) dangling side-chains and terminal isocyanate groups. The hydrophilic side-chains self-oriented toward the aqueous surrounding media and emulsifed in water the whole pre-formed PUUa NP. The hydrophobic chains stabilized and encapsulated the inner hydrophobic prepolymer (Hyfob, see below) and the oily core by hydrophobic interactions. Thus, Amphil worked as an all-in-one polymer ensuring oil and water miscibility, redox-degradability and isocyanate reactivity. On the other hand, the hydrophobic reactive prepolymer (Hyfob) bore disulfide bonds in the main chain, terminal isocyanate groups and just hydrophobic dangling side-chains. The idea to introduce a Hyfob in the shell was based on the wish to prevent premature leakage of the encapsulate without renouncing to redox-degradability. In this regard, to achieve this hydrophobically stratified structure, it was also crucial to use a 5% (w/w) of an ultrahydrophobe as core material, such as the biocompatible capric-caprylic triglyceride (Crodamol GTCC). Its solubilizing effect of hydrophobic therapeutically active molecules[28] and ability to decrease coacervation of oily core nanoparticles due to Ostwald Ripening effect[29] made it the product of choice. In addition, as introduced previously, to convert these hydrophobically driven self-stratified structures into covalently stable isocyanate-free PUUa NPs, the reactive polymeric shell was crosslinked with small polyamines (Fig. S7 in the ESI). Hence, as seen from figure 3 we

3. Results and discussion

As we have shown in our recent methodological patent many nanoparticles with multiple structural and biological functionalities
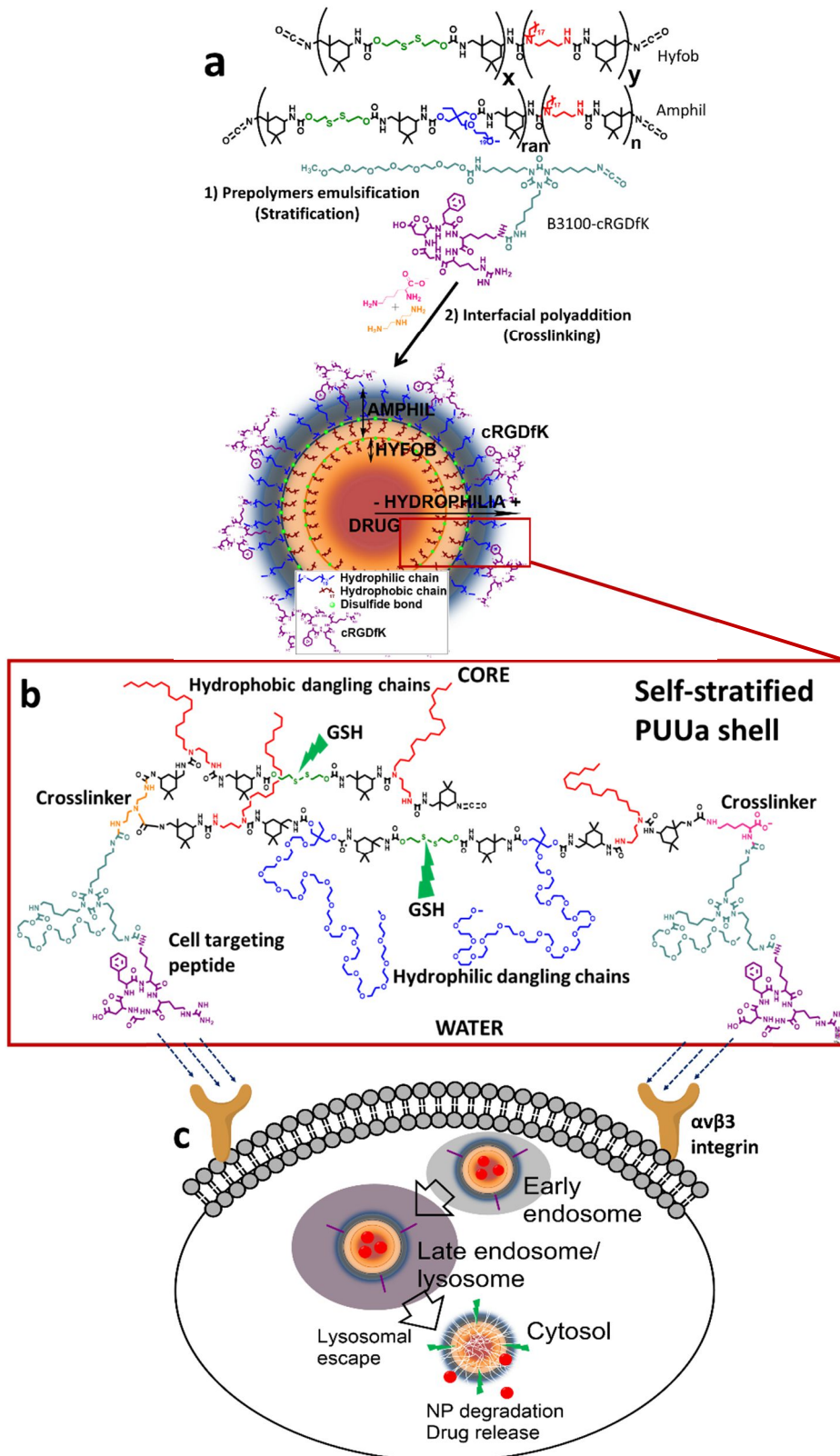
Figure 1. Schematic illustration of PUUa NPs synthesis, structure and application. After emulsification of prepolymers in water, the self-stratified shell is consolidated by a two-step interfacial crosslinking creating a robust multiwalled NP a). Dangling side-chains of functional prepolymers self-orient through the oil-water interface and drive the self-assembly by hydrophobic and hydrophilic interactions. The hydrophilic cRGDfK peptide is covalently linked via urea bonds to the more external part of the shell b). Scheme of PUUa NPs receptor mediated internalization and cytosolic delivery of hydrophobic cargo c).

observed that addition of L-Lysine (Lys), a diaminocarboxylate moiety, into the emulsified reactive prepolymers as pre-crosslinker and extender, reduced the NP size as a result of the enhanced internal emulsifying effect of carboxylate rest[30,31] compared to NPs carrying only polyethylene glycol monomethyl ether (YMER N-120) as hydrophilic precursor. Finally, in any of the formulations the shell was consolidated by a highly reactive small triamine, diethylenetriamine (DETA) (Fig. S8 in the ESI prove isocyanates disappearance by FT-IR after crosslinking reaction).

At this point, with the aim of conferring to our system cell targeting specificity, a novel method was developed to anchor the broadly used hydrophilic cRGDfK cyclic pentapeptide to our PUUa NPs via urea linkage without loss of bioactivity[32]. Concretely, Bayhydur 3100 hydrophilic polyisocyanate linker[33] (B3100) and the cRGDfK free primary amino group of Lys residue were effectively coupled in aqueous media (pH 10, 5 ºC) (Fig. S9 in the ESI). By optimizing the reaction stoichiometry we were able to maintain free NCO moieties in the conjugate for further PUUa NP functionalization with only one peptide per linker molecule, as ensured by MALDI-TOF MS experiments (Fig. S10 in the ESI). Furthermore, the PUUa NP functionalization with B3100-cRGDfK conjugate (PUUa NP-RGD) occurred in a high yield (98.5 %), as quantified by HPLC calibration
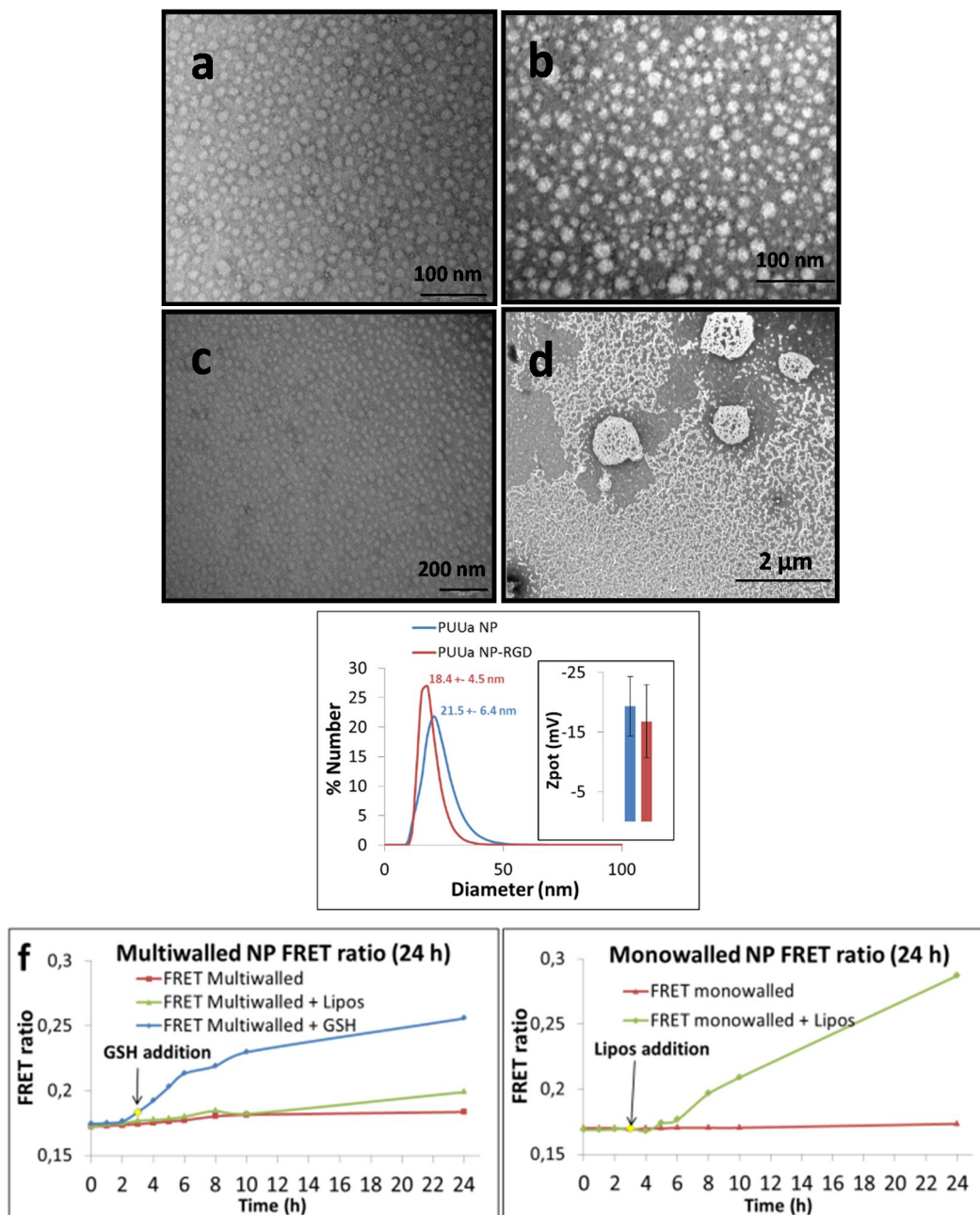
Figure 2. TEM images of multiwalled PUUa NP a) and PUUa NP-RGD b). TEM images of PUUa NPs before c) and after treatment with GSH 10 mM at 37 ºC during 24 h d). After treatment with GSH clear degradation of PUUa NPs is achieved and degraded polymers form aggregates up to 1 µm size. e) Hydrodynamic diameter by DLS and Zeta Potential of PUUa NP-RGD (blue) and PUUa NP (red). Release dynamics comparison between multiwalled and monowalled PUUa NPs f). Aqueous media (Red), *in vivo*-like media (green) and 10 mM reduced GSH (blue).

curve (Table S2 in the ESI). Then, B3100-cRGDfK isocyanate reactive conjugate was fixed in the prepolymeric shell via the previously explained crosslinking step yielding around 2 % cRGDfK per PUUa NP. Transmission Electron Microscopy (TEM) and Dynamic Light Scattering (DLS) revealed monomodal size distributions of about 20 nm for PUUa NP-DiI and PUUa NP-DiI-RGD (Fig. 2a and Fig. 2b). Zeta Potential (Zpot) measurements of dialysis-purified nanoparticles exhibited similar slightly negative surface charges due to the Lys carboxylate (Fig. 2e). This experimental result further corroborated that the hydrophilic character of Lys located him in the outer part of the shell thus proving the self-stratified nanostructure by hydrophobic interactions. In addition, the multiwalled nanoparticles robust structure and hydrophilic surface made them lyophilizable and redispersable in aqueous media without cryoprotectants‡.

Shell biodegradability and specific cargo release are fundamental features in drug delivery systems. To this end, the presence of disulfide bonds in the shell facilitated polymer degradation by reductive enzymes and peptides overexpressed in the cytosolic environment of tumor cells[34]. Concretely, reduced glutathione has an intracellular concentration of 2–10 mM in the cytosol while the extracellular concentration is about 2–20 µM. Taking profit of this intracellular concentration, PUUa NPs degradation and cargo release under reductive conditions were studied by transmission electron microscopy (TEM) and Förster resonance energy transfer (FRET) techniques, respectively. Thus, NPs degradation was determined by TEM before and after a 24 h treatment with 10 mM GSH. Significant differences in size were detected due to polymer aggregates formation after redox-triggered degradation (Fig. 2c and Fig. 2d). To confirm the differences on the release properties of multiwalled and
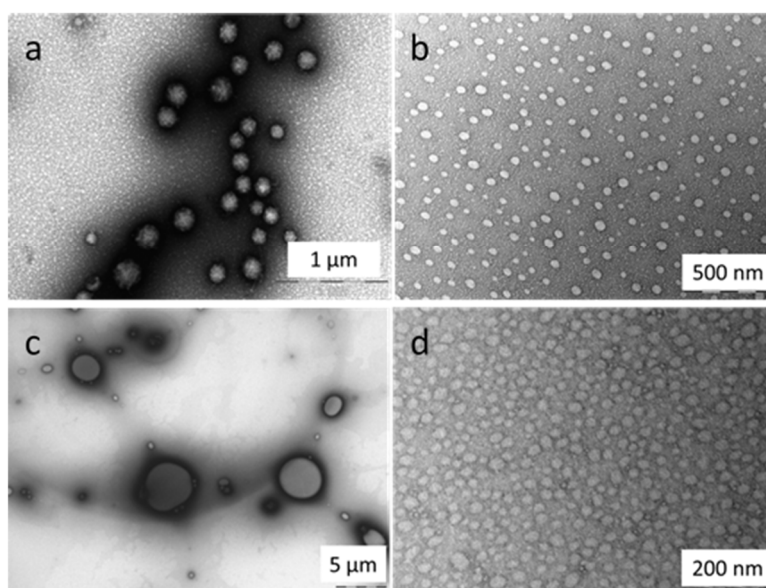
Multiwalled Samples	Diameter (nm)	SD (nm)	PDI
a) DETA-crosslinked PUUa NP	170.3	32.0	0.04
b) Lys-crosslinked PUUa NP	53.2	22.8	0.18
c) Non-crosslinked PUUa NP	207.7	590.8	5.91
d) Lys-DETA-crosslinked PUUa NP	29.0	5.0	0.03

Figure 3. TEM micrographs of multiwalled PUUa NPs showing the importance of the crosslinking process to get a monodisperse sample. After emulsification of reactive prepolymers in water PUUa NPs were crosslinked by successive additions of Lys and/or DETA, respectively a, b, d). Non-crosslinked PUUa NPs were kept under magnetic stirring during 3 days until isocyanate group disappeared from the IR spectra due to reaction with water. It can be observed that without crosslinker, NPs are not interfacially stabilized and a highly polydisperse sample is obtained c). Images were statistically analyzed by random recording of 5 different zones of the copper grid.

monowalled nanostructures, first, monowalled NPs were morphologically characterized by TEM (Fig. S11) and then, FRET experiments where performed in different media. Thus, we encapsulated two typical cell membrane staining agents[35] as fluorescent lipophilic cargos, namely DiI and DiO, in separate PUUa NPs. As already described by FRET mechanism, changes in fluorophores proximity allowed us to evaluate the release dynamics and potential leakiness of different PUUa NPs[36]. So, both fluorescent probes were encapsulated at a total concentration of 0.15 % w/w to avoid static quenching[37] (Encapsulation efficiency 100 %, Data not shown). PUUa NP-DiI and PUUa NP-DiO were then mixed (FRET PUUa NPs) and the FRET ratio was represented against time as $I_a/(I_d + I_a)$, where I_a was the maximum intensity of the acceptor and I_d the maximum intensity of the donor. The slope of the linear fit was defined as the release coefficient at 37 ºC for the first 10 h of the experiment (Fig. S13 in the ESI). For both multiwalled and monowalled NPs the release coefficient appeared to be almost negligible in water (0.001 h^{-1} and 0.0001 h^{-1} respectively), which corroborated their outstanding encapsulation stability. Further, as PUUa NPs are expected to stably encapsulate the lipophilic drug until reaching the cytosol of the tumor cell, we wanted to ratify that the cargo would not be released unspecifically during cell internalization. With this in mind, we sought to mimic a cellular microenvironment by mixing egg phosphatidylcholine-cholesterol previously reported liposomes (Lipos)[38] (2:1 w/w) to our FRET PUUa NPs (10 mM). Confirming our expectations, multiwalled NPs were stable during the first 10 h (0.001 h^{-1}), but monowalled NPs exhibited a pronounced increase of the FRET ratio upon mixing with Lipos (0.007 h^{-1}) due to unspecific release. Additionally, under treatment with 10 mM GSH, multiwalled PUUa NPs clearly showed a FRET increase (0.01 h^{-1}) caused by disulfide bonds cleavage and sudden release and mixing of the fluorophores (See Fig. 2f and Fig. S12 in the ESI).

In a final proof of principle study, we first tested that PUUa NPs were not cytotoxic to cells (Fig. S14 in the ESI) and then internalization assays were performed. To that end, PUUa NPs were incubated with HT-29 and U87-MG cancer cells, known to have very low and high expression of αvβ3 integrins, respectively (Table S2). Flow cytometry and confocal studies revealed that, due to the RGD outer localization in the multiwalled structure, PUUa NP-RGD encapsulating DiI fluorophore (PUUa NP-DiI-RGD) entered αvβ3 integrin expressing cells more efficiently (Fig. 4a) than non-functionalized ones. Moreover, internalization of PUUa NP-DiI-RGD in αvβ3-negative HT-29 cells was similar to non-targeted NP, indicating that the enhanced uptake of cRGDfK functionalized NPs observed in U87-MG cells was specific.

Confocal images also showed colocalization of NPs with lysosomal markers (Lysotracker Green), confirming that NPs entered cells through the endocytic pathway, and that the uptake and the lysosomal colocalization was clearly enhanced in the case of PUUa NP-DiI-RGD (Fig. 4b). In order to trace the final cytosolic release of the NPs cargo, U87-MG cells were incubated 1 h with PUUa NP-DiI-RGD washed thoroughly and observed immediately and 24 h later. The initially observed distinctive punctuated signal corresponding to the lysosomal localization changed to a more diffuse uniform fluorescent cell cytoplasm distribution, which, in line with abovementioned FRET experiments proved that our system was able to escape from the lysosome and spread their cargo through the cytosol (Fig. S15 in the ESI).
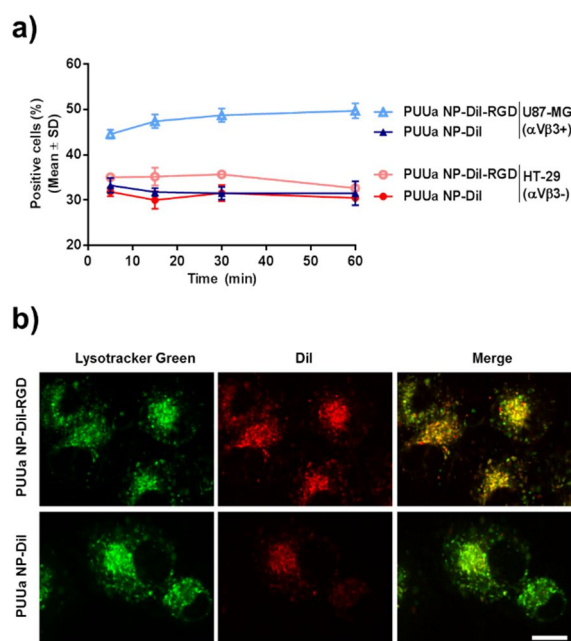
Figure 4. PUUa NP internalization. a) Flow cytometry studies were performed in U87-MG (αvβ3-positive) and HT-29 (αvβ3-negative) cancer cells at different time points with 10 μg/mL of DiI (38.5 μg/mL of NPs). b) Confocal images of U87-MG cells incubated 24 h with 1 μg/mL of DiI and stained with Lysotracker Green to show lysosomal localization of PUUa NPs. Magnification bar corresponds to 10 μm.

In conclusion, we have depicted a novel methodology to develop self-stratified PUUa NPs based on the amphiphilic properties of the different designed pre-polymers, and we have clearly evidenced the better encapsulation ability of multiwalled NPs compared to their monowalled counterparts. This multiwalled structure has been experimentally proved by FRET studies, Zpotential measurements and cell internalization experiments. The use of L-Lysine as extender or pre-crosslinker modulated the size of the micelles reaching very small entities that finally were stabilized by crosslinking with DETA. Cargo delivery and nanoparticle shell degradability were also controlled by incorporating DEDS, a redox moiety that responded to intracellular glutathione. The use of a specifically designed reactive conjugate containing a hydrophilic RGD peptide ensured the straightforward functionalization of the outer part of the nanoparticles shell. These systems convey a multiwalled nanostructure with on-demand release properties and cancer cell targeting behavior. This confirms our PUUa NPs as outstanding platforms for smart drug delivery and opens up a new era in nanostructured systems with multiple targeting and degradation possibilities that generate an enormous range of application opportunities. New characterization techniques are being explored to visually proof the sub-30 nm self-stratified structures. Biological studies with a variety of antitumor drugs are also underway.

Acknowledgements

Notes and references

‡ All data presented belongs to experiments performed with lyophilized and redispersed multiwalled PUUa NPs (For more details see section 3 in supporting information).

1   V. P. Torchilin, *Nat. Rev. Drug Discov.*, 2014, **13**, 813–827.

2   N. Kamaly, Z. Xiao, P. M. Valencia, A. F. Radovic-Moreno and O. C. Farokhzad, *Chem. Soc. Rev.*, 2012, **41**, 2971–3010.

3   K. Landfester, *Angew. Chemie Int. Ed.*, 2009, **48**, 4488–4507.

4   F. Tiarks, K. Landfester and M. Antonietti, *Langmuir*, 2001, **17**, 908–918.

5   L. Wu and J. Baghdachi, *Functional Polymer Coatings: Principles, Methods, and Applications*, WILEY-VCH Verlag GmbH, 2015.

6   Z. Zhang, R. L. Marson, Z. Ge, S. C. Glotzer and P. X. Ma, *Adv. Mater.*, 2015, **27**, 3947–52.

7   D. K. Chattopadhyay and K. V. S. N. Raju, *Prog. Polym. Sci.*, 2007, **32**, 352–418.

8   J. Y. Cherng, T. Y. Hou, M. F. Shih, H. Talsma and W. E. Hennink, *Int. J. Pharm.*, 2013, **450**, 145–162.

9   B. K. Kim and J. C. Lee, *Polymer (Guildf).*, 1996, **37**, 469–475.

10   S.-H. Son, H.-J. Lee and J.-H. Kim, *Colloids Surfaces A Physicochem. Eng. Asp.*, 1998, **133**, 295–301.

11   Heming, A. M.; Mulqueen, P. J.; Scher, H. B.; Shirley, I. M. Use of Reactive Polymeric Surfactants in the Formation of Emulsions, US7199185 B2, 2002, PCT/GB2002/002744, 2002.

12   J. Andrieu, N. Kotman, M. Maier, V. Mailänder, W. S. L. Strauss, C. K. Weiss and K. Landfester, *Macromol. Rapid Commun.*, 2012, **33**, 248–53.

13   M. Ding, N. Song, X. He, J. Li, L. Zhou, H. Tan, Q. Fu and Q. Gu, *ACS Nano*, 2013, **7**, 1918–28.

14   U. Paiphansiri, J. Dausend, A. Musyanovych, V. Mailänder and K. Landfester, *Macromol. Biosci.*, 2009, **9**, 575–84.

15   S. A. Guelcher, *Tissue Eng. Part B. Rev.*, 2008, **14**, 3–17.

16   L. T. Budnik, D. Nowak, R. Merget, C. Lemiere and X. Baur, *J. Occup. Med. Toxicol.*, 2011, **6**, 9.

17   S. A. Guelcher, K. M. Gallagher, J. E. Didier, D. B. Klinedinst, J. S. Doctor, A. S. Goldstein, G. L. Wilkes, E. J. Beckman and J. O. Hollinger, *Acta Biomater.*, 2005, **1**, 471–84.

18   P. Zou, H. Chen, H. J. Paholak and D. Sun, *Mol. Pharm.*, 2013, **10**, 4185–94.

19   X. Dai, Z. Su and J. O. Liu, *Tetrahedron Lett.*, 2000, **41**, 6295–6298.

20   I. R. Clemitson, *Castable Polyurethane Elastomers*, CRC Press, 2008.

21   A. Prabhakar, D. K. Chattopadhyay, B. Jagadeesh and K. V. S. N. Raju, *J. Polym. Sci. Part A Polym. Chem.*, 2005, **43**, 1196–1209.

22   J. Schindelin, I. Arganda-Carreras, E. Frise, V. Kaynig, M. Longair, T. Pietzsch, S. Preibisch, C. Rueden, S. Saalfeld, B. Schmid, J.-Y. Tinevez, D. J. White, V. Hartenstein, K. Eliceiri, P. Tomancak and A. Cardona, *Nat. Methods*, 2012, **9**, 676–82.

23   P. Botella, I. Abasolo, Y. Fernández, C. Muniesa, S. Miranda, M. Quesada, J. Ruiz, S. Schwartz and A. Corma, *J. Control. Release*, 2011, **156**, 246–57.

24   J .Rocas Sorolla; P. Rocas Alonso. Process for the Manufacture of a Microencapsulated and Reactive Amphiphilic Compound, and Corresponding Microencapsulated Composition, WO2014114838 A3, 2014.

25   X. Yan, M. Delgado, A. Fu, P. Alcouffe, S. G. Gouin, E. Fleury, J. L. Katz, F. Ganachaud and J. Bernard, *Angew. Chem. Int. Ed. Engl.*, 2014, 1–5.

26   J.-W. Yoo, N. Doshi and S. Mitragotri, *Adv. Drug Deliv. Rev.*, 2011, **63**, 1247–1256.

27   K. Landfester and V. Mailänder, *Expert Opin. Drug Deliv.*, 2013, **10**, 593–609.

28   R. G. Strickley, *Pharm. Res.*, 2004, **21**, 201–30.

29   K. Landfester, N. Bechthold, F. Tiarks and M. Antonietti, *Macromolecules*, 1999, **32**, 5222–5228.

30   Peihong Ni, Mingzu Zhang and Nianxi Yan, *J. Memb. Sci.*, 1995, **103**, 51–55.

31   G. Morral-Ruíz, C. Solans, M. L. García and M. J. García-Celma, *Langmuir*, 2012, **28**, 6256–64.

32   R. Haubner, R. Gratias, B. Diefenbach, S. L. Goodman, A. Jonczyk and H. Kessler, *J. Am. Chem. Soc.*, 1996, **118**, 7461–7472.

33   Heming, A. M.; Mulqueen, P. J.; Scher, H. B.; Shirley, I. M. Use of Reactive Polymeric Surfactants in the Formation of Emulsions, US7199185 B2, 2002.

34   R. Cheng, F. Feng, F. Meng, C. Deng, J. Feijen and Z. Zhong, *J. Control. Release*, 2011, **152**, 2–12.

35   R. W. Sabnis, *Handbook of Biological Dyes and Stains: Synthesis and Industrial Applications*, 2010.

36   S. Jiwpanich, J.-H. Ryu, S. Bickerton and S. Thayumanavan, *J. Am. Chem. Soc.*, 2010, **132**, 10683–5.

37   H. Chen, S. Kim, L. Li, S. Wang, K. Park and J.-X. Cheng, *Proc. Natl. Acad. Sci.* , 2008, **105** , 6596–6601.

38   T. M. Allen and A. Chonn, *FEBS Lett.*, 1987, **223**, 42–46.

SUPPORTING INFORMATION

Multifunctionalized Polyurethane-Polyurea Nanoparticles: Hydrophobically Driven Self-Stratification at the o/w Interface Modulates Encapsulation Stability

Pau Rocas*, Yolanda Fernández, Simó Schwartz Jr, Ibane Abasolo, Josep Rocas*, Fernando Albericio*

1. Monomers information

Ymer N120 is a polymeric non-ionic hydrophilic building block containing two primary hydroxyl groups and a long ethoxylated capped side chain. From a synthetic point of view, YMER N-120, was chosen because of its low melting point and viscosity, features that make it amenable for direct addition to the prepolymer acting as co-solubilizer in the formulation and eliminating the need of an extra co-solvent. We considered YMER N-120 an interesting intermediate to create a polymer backbone with longer side-chains sideways than equivalent PEG (polyethylene glycol, 1000 g/mol) which should fold up within itself upon contact with water.

Isophorone diisocyanate (IPDI) is an organic compound in the class known as aliphatic diisocyanates. Interestingly, aliphatic isocyanates are less pulmonary sensitizing and not carcinogenic compared to aromatic ones. Is particularly noteworthy that fully reacted isocyanate polymers to form its respective urethane or urea bonds do not contain toxicity referred to the isocyanate group[1]. In addition, degradation products of IPDI such IPDA (isophorone diamine) are rapidly eliminated via urinary excretion[2].

Genamin TAP 100D is a hydrophobic building block containing a C18 fatty chain and two reactive amines for polymerization. We focused on it attracted by its high hydrophobicity and low melting point which allowed us to perform a more green chemistry avoiding large amounts of solvents.

Bayhydur 3100 is a hydrophilic aliphatic polyisocyanate based on hexamethylene diisocyanate (HDI) and is solvent-free. It was interesting for our purposes due to its high hydrophilicity and high NCO functionality which allowed as to work in aqueous media and decorate it easily and fast with a cyclic RGD peptide via urea linkage. More interestingly was that adjusting the stoichiometry we got conjugates of just one peptide per B3100 molecule maintaining NCO reactivity for further shell functionalization. In addition it complies with FDA food contact regulations.

*Please refer to figure S1 in the supporting information to see their chemical structure in detail.

1)

Amphil

a) DBTL (cat), Crodamol GTCC, N$_2$, 50ºC, 4 h*. b) Acetone, N2, 40ºC, 30 min

2)

Hyfob

a) DBTL (cat), N$_2$, 50ºC, 4 h. b) Acetone, N2, 40ºC, 30 min

3)

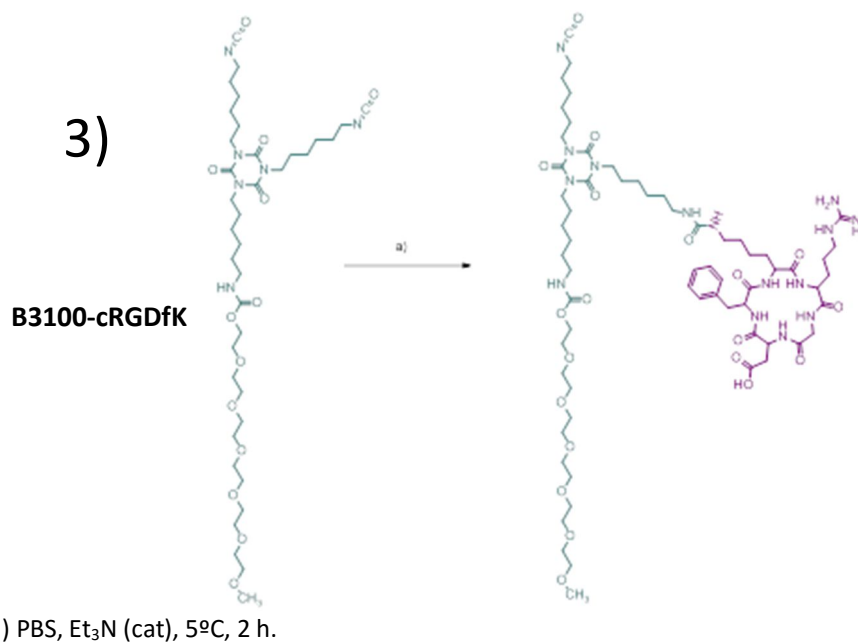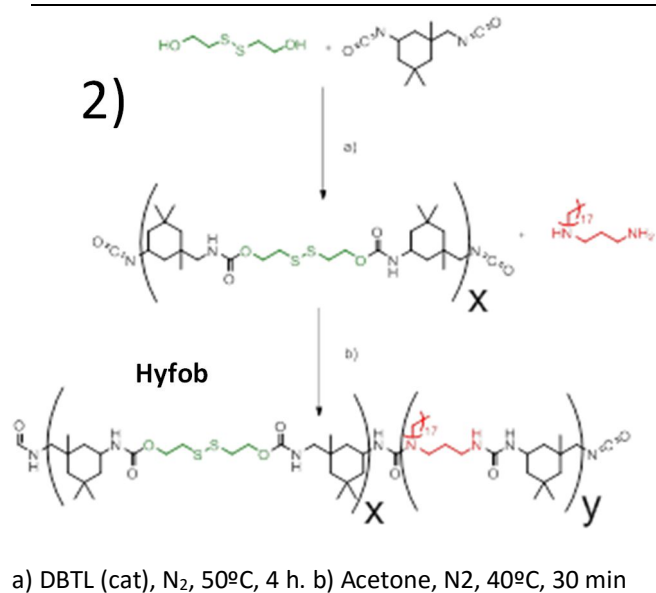**B3100-cRGDfK**

a) PBS, Et$_3$N (cat), 5ºC, 2 h.
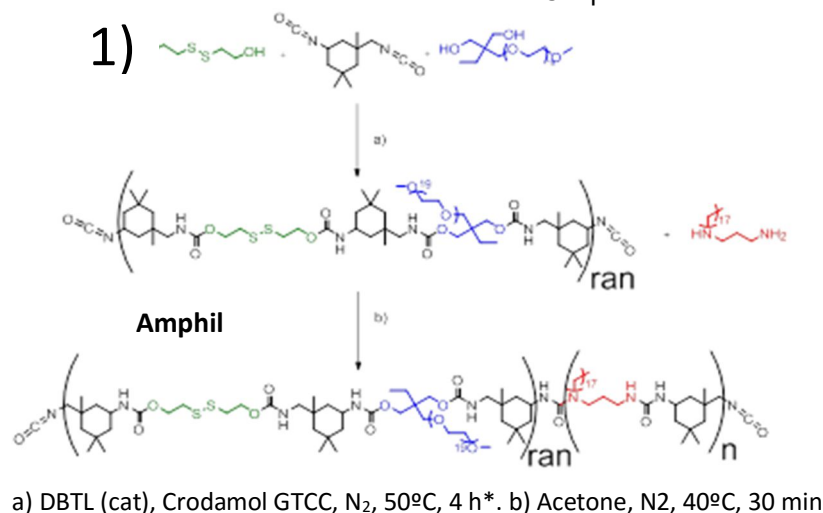
Figure S1. Synthetic process of the idealized structures of reactive prepolymers that form the PUUa NP. 1) Amphil polymerization process. *Hyfil was formed by random polymerization of DEDS and YMER N-120 with IPDI. 2) Hyfob polymerization process. 3) B3100-cRGDfK conjugation reaction.

	IPDI	DEDS	YMER N-120	GENAMIN TAP 100D	L-LYSINE	DETA	B3100	cRGDfK
w/w % Amphil[a]	24.29	1.08	39.50	10.41	-	-	-	-
w/w % Hyfob[a]	3.48	1.08	-	1.08	-	-	-	-
w/w % B3100-cRGDfK[a]	-	-	-	-	-	-	6.49	1.95
w/w % PUUa NP[b]	27.77	2.15	39.5	11.49	7.2	3.39	6.49	1.95
Equivalents fraction[c]	9.29	1.04	2.93	2.65	1.83	1.83	1	0.12

Table S1. The quantitative reaction of the monomers was ensured by automatic titration and HPLC (Fig. S2 and Fig. S9 respectively) and qualitatively by FT-IR (Fig. S3 and S4). a) Relative mass proportion of each monomer in the prepolymer regarding the multiwalled PUUa NP. b) Total mass proportion of each monomer in the multiwalled PUUa NP. c) Equivalents fraction of reactive species (either NCO, OH or NH2)
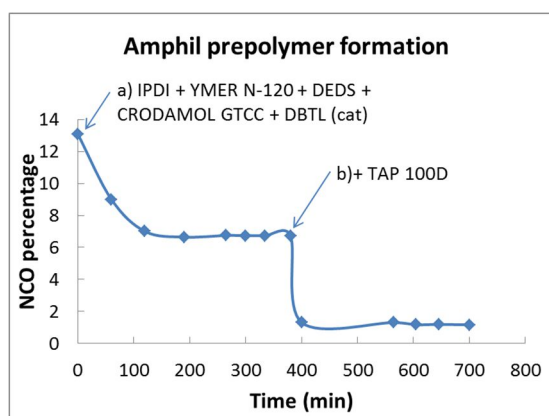
$$NCO\%\ Hyfil = 6.7\ \%\quad NCO\%\ Amphil = 1.2\ \%$$

Figure S2. Back titration of free isocyanate. Disappearance of NCO by a first random reaction with –OH groups to form urethane prepolymer (a), Hyfil) and a second stage with –NH2 groups to form urethane-urea prepolymer (b), Amphil). As expected, urethane bonds were formed progressively (almost 3h). Urea bonds were formed immediately after addition of Genamin TAP 100D hydrophobic diamine. When every monomer is totally reacted NCO percentage remains constant over time, which proves its scalability. As desired, remaining isocyanate functionality for further crosslinking is maintained after total consumption of Genamin TAP 100D free amino groups.
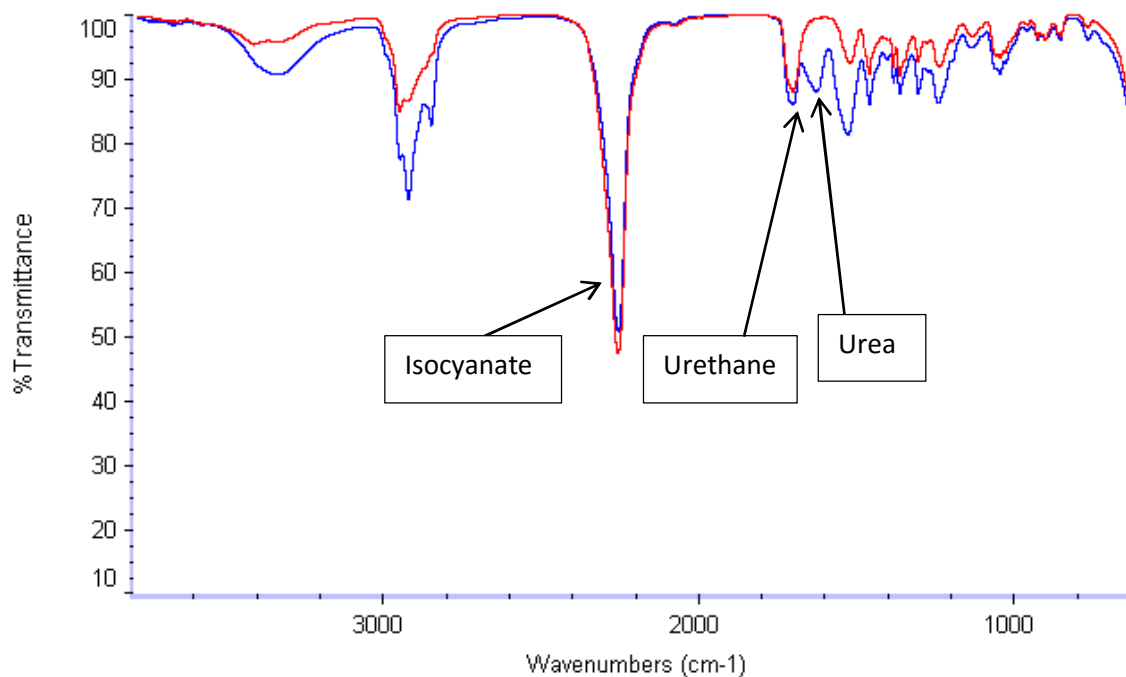
Figure S3. IR spectra corresponding to the synthetic process of Hyfob reactive prepolymer. It can be observed how isocyanate band of polyurethane prepolymer (red) decreases when Genamin TAP 100D is added and polyurea bonds (Hyfob) are formed (Blue)
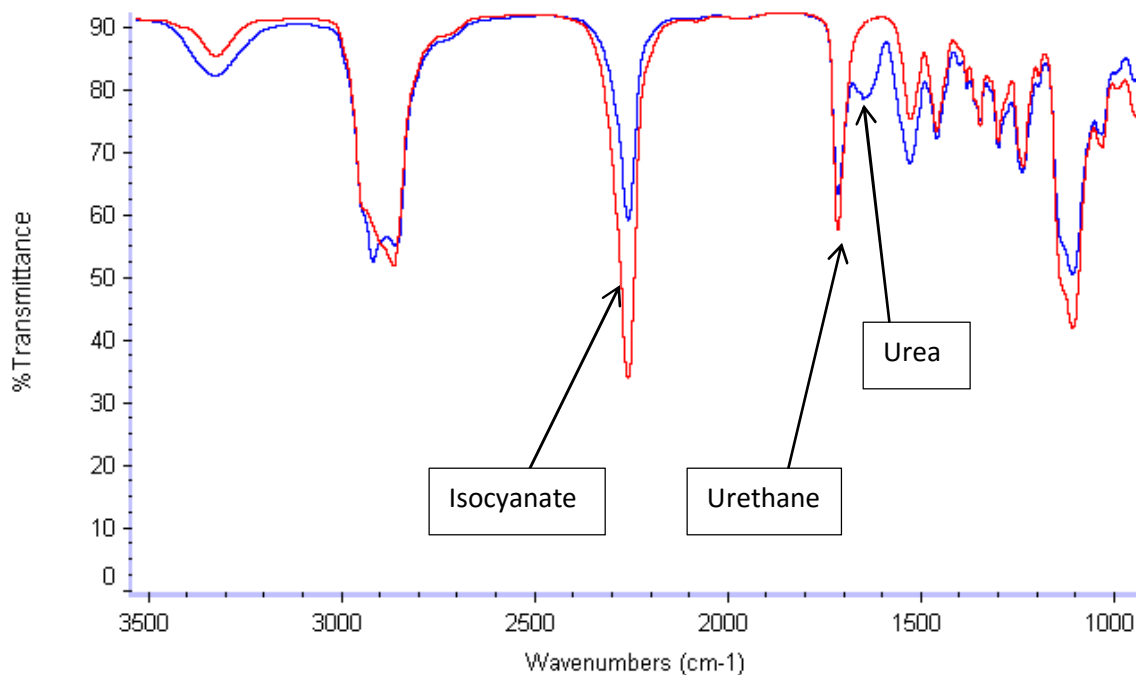
Figure S4. IR spectra corresponding to the synthetic process of Amphil reactive prepolymer. It can be observed how isocyanate band of polyurethane prepolymer (red) decreases when Genamin TAP 100D is added and polyurea bonds (Amphil) are formed (Blue).
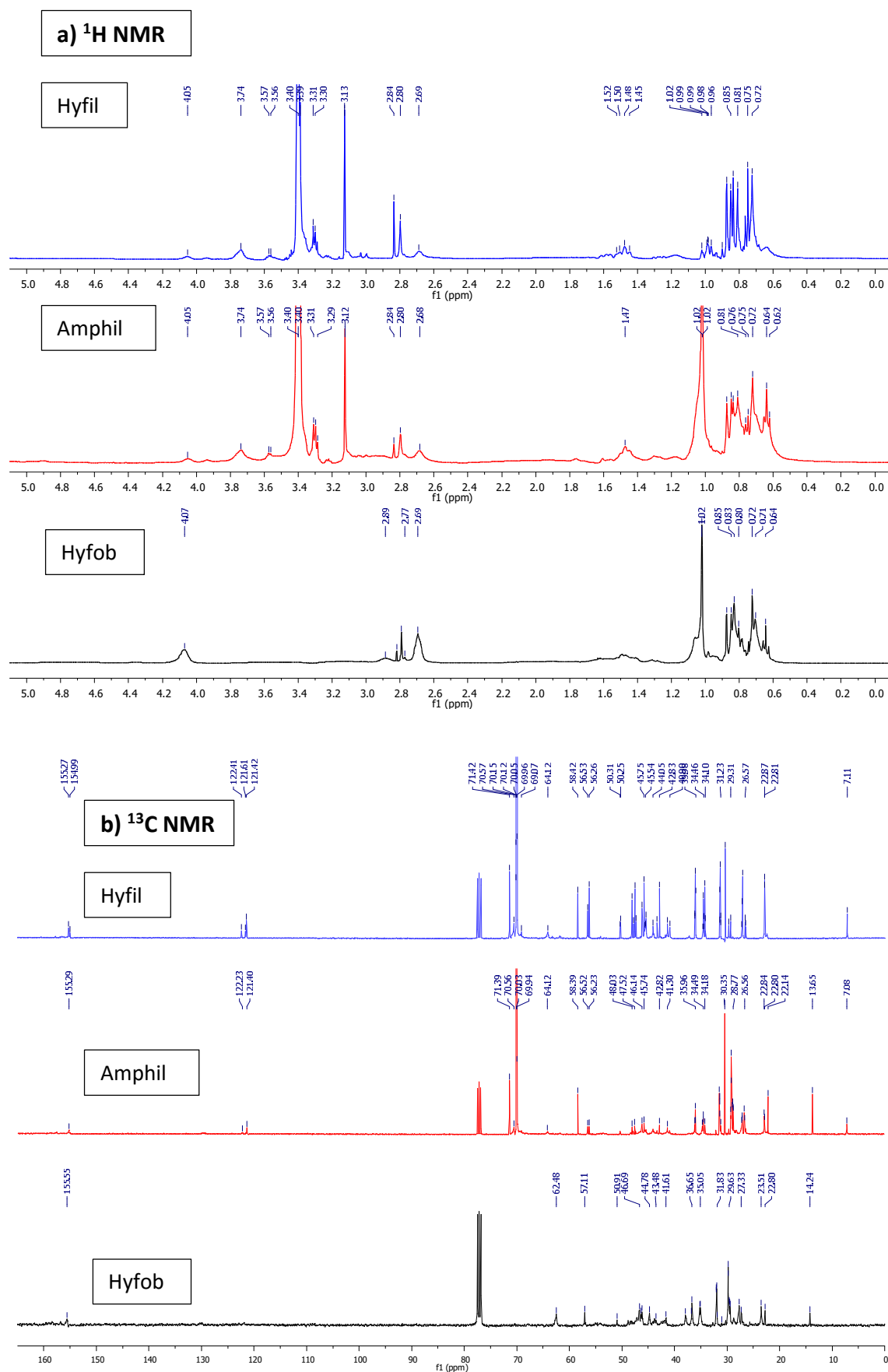
Figure S5. 400 MHz ^{1}H NMR spectra a) and 400 MHz ^{13}C NMR spectra b) of reactive prepolymers in CDCl$_3$. The blue and red spectra correspond to Hyfil and Amphil prepolymers respectively. All the peaks in the reactive prepolymers spectra have been assigned by a previous singular ^{13}C and ^{1}H NMR spectra of each monomer (spectra not shown) and previosuly reported

bibliography[3]. As seen from Amphil 1H NMR spectra, the peaks at 0.72, 0.85, 1.47, 1.61 and 2.80 ppm are assigned to IPDI methylene groups. The peak at 0.64, which can not be found in the Hyfil spectra, corresponds to the fatty diamine methyl group. The methylene groups of the fatty diamine appear at 1.02, 1.47 and 1.76. The chemical shifts at 0.72 and 3.30 are ascribed to YMER methyl groups and the peaks at 3.12 and 3.40 correspond to YMER methylene groups. The peak at 2.68 is ascribed to DEDS (CH_3-S-) and those at 3.74 and 4.07 to Amphil and Hyfob (CH_3-O-) respectively.

In the ^{13}C NMR spectra the peaks at 22.80, 42.81, 43.27, 45.40, 45.75, 47.53, 48.03, 56.24 and 56.52 are ascribed to methylene groups of IPDI stereoisomers mixture. The methyl groups of IPDI mixture correspond to the signals at 26.53, 27.08 and 29.21. The IPDI methine group was ascribed to the small signals at 36.05, 34.51 and 31.30. It can be observed some IPDI peaks appearing as doblets due to stereoisomers and rotamers. The peaks at 7.10, 58.39 and 22.84, 70.03, 70.56, 71.39 are assigned to YMER N-120 methyl and methylene groups respectively. The peak appearing only in the Amphil spectra at 13.65
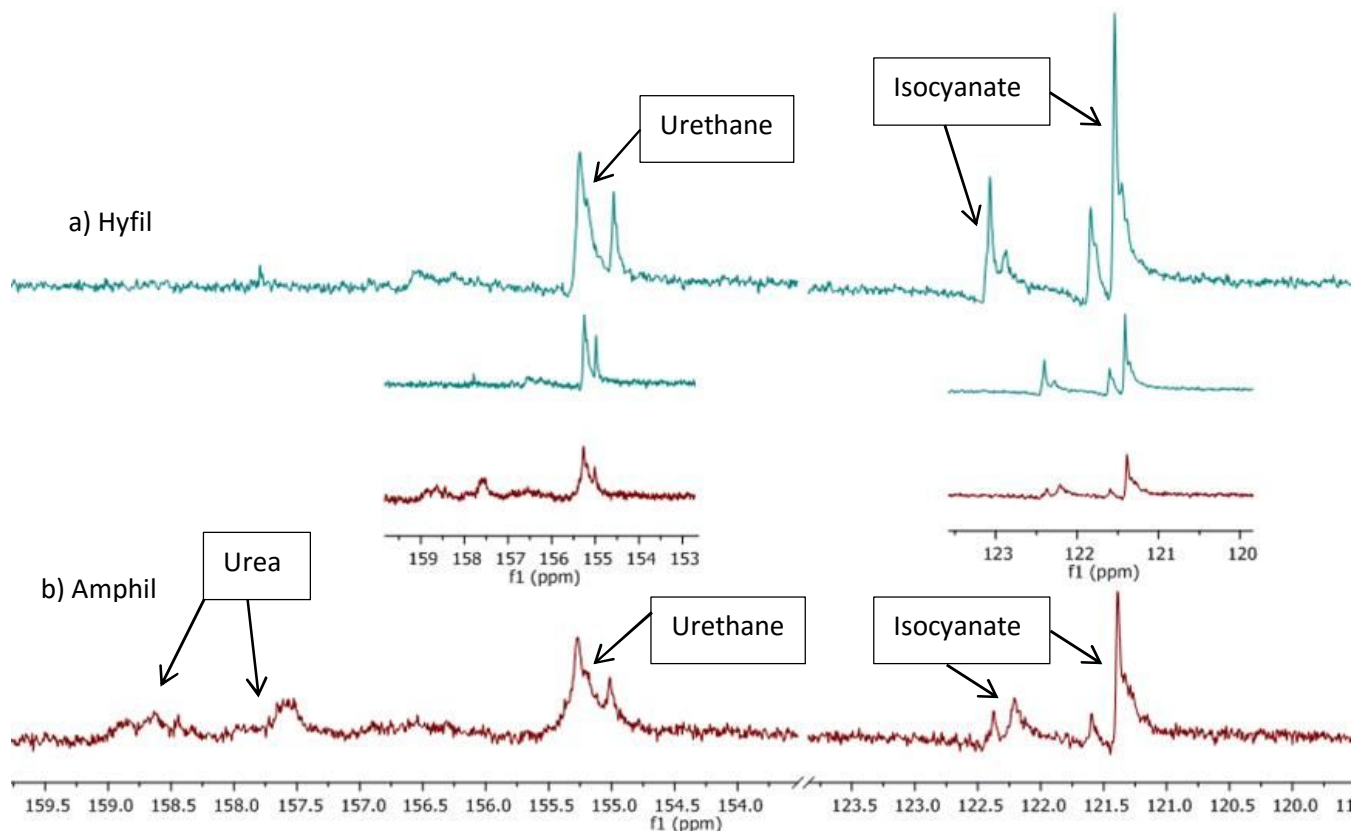
correspond to methyl groups of Genamin TAP 100D and its methylene groups are ascribed to the singlet at 22.14 and the fatty chain multiplet at 29 ppm. The DEDS methylene groups are ascribed to the broad signals at 40.86 (CH_3-S-) and 64.06 (CH_3-0-).

Figure S6. The cut-out is an amplification of 400 MHz ^{13}C NMR spectra to identify isocyanate, polyurethane and polyurea carbons during prepolymers formation. a) The signals between 121 and 123 ppm are ascribed to isocyanate carbons of the prepolymer. Polyurethane carbon signal is ascribed to the bands at 155 ppm. b) In the Amphil, when Genamin TAP 100D diamine is added multiple bands between 157 and 159 appear due to urea bonds formation.
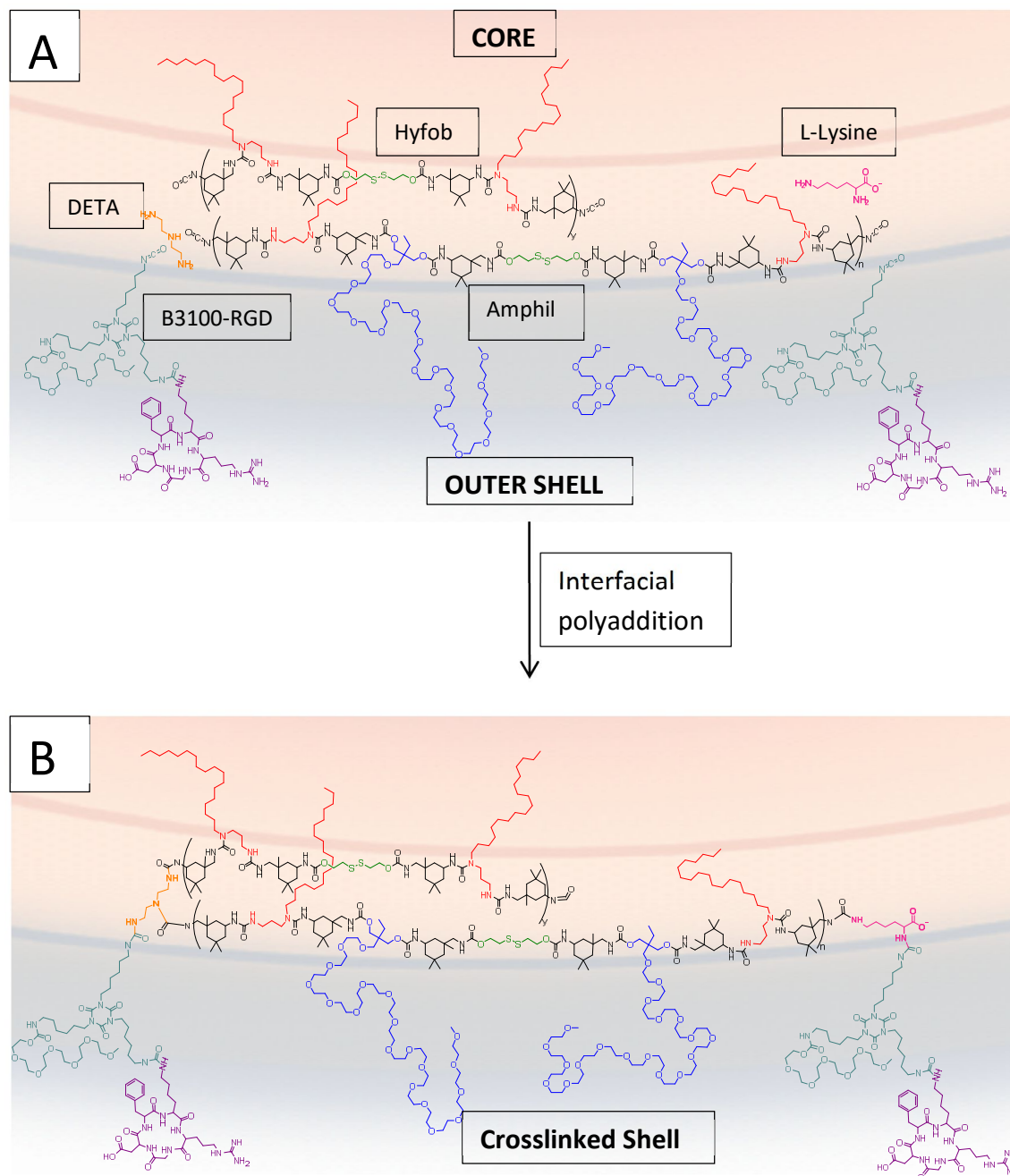
Figure S7. Crosslinking process of the nanoparticle. Amphil, Hyfob and B3100-cRGDfK self-stratify after emulsification with water A). After addition of crosslinkers, interfacial polyaddition with the reactive prepolymers occurs to form the crosslinked shell. Presumably, due to L-Lysine higher hydrophilia, it will join the most hydrophilic prepolymers (Amphil and B3100-cRGDfK). DETA, which is more reactive and less hydrophilic, will penetrate the inner shell and join Hyfob, Amphil and B3100-cRGDfK creating the PUUa NP B).
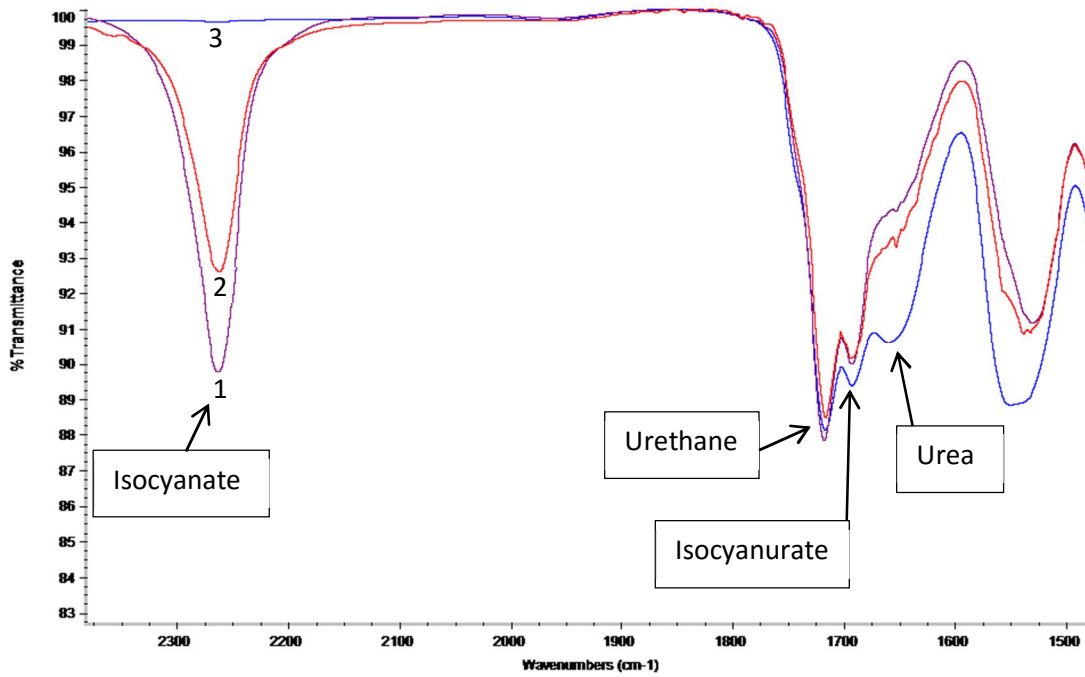
Figure S8. 1, 2, 3 spectra corresponding to the emulsified nanoparticles before Lys addition, 30 min after Lys addition and 10 min after DETA addition respectively. Isocyanate band decreases over time as amino crosslinkers are added and polyurea shell (PUUa NP) is formed. The IR bands at 2270 cm^{-1} correspond to the stretching of the –N=C=O functional group. The sharp band at 1715 cm^{-1} is ascribed to urethane C=O stretching. At 1690 cm^{-1} appears the isocyanurate C=O stretching band corresponding to the B3100 linker structure. The increasing band at 1653 cm^{-1} corresponds to the urea C=O stretching.
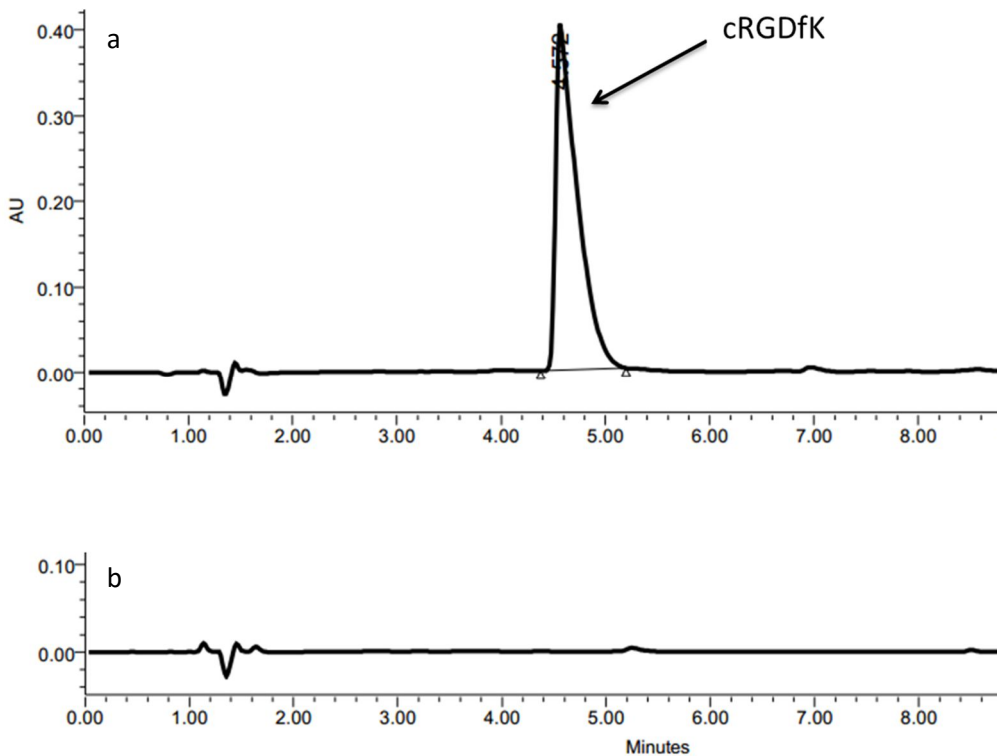
Figure S9. Conjugation reaction monitoring of cRGDfK peptide with B3100 linker by HPLC at 0 h a) and after 2 h reaction b).
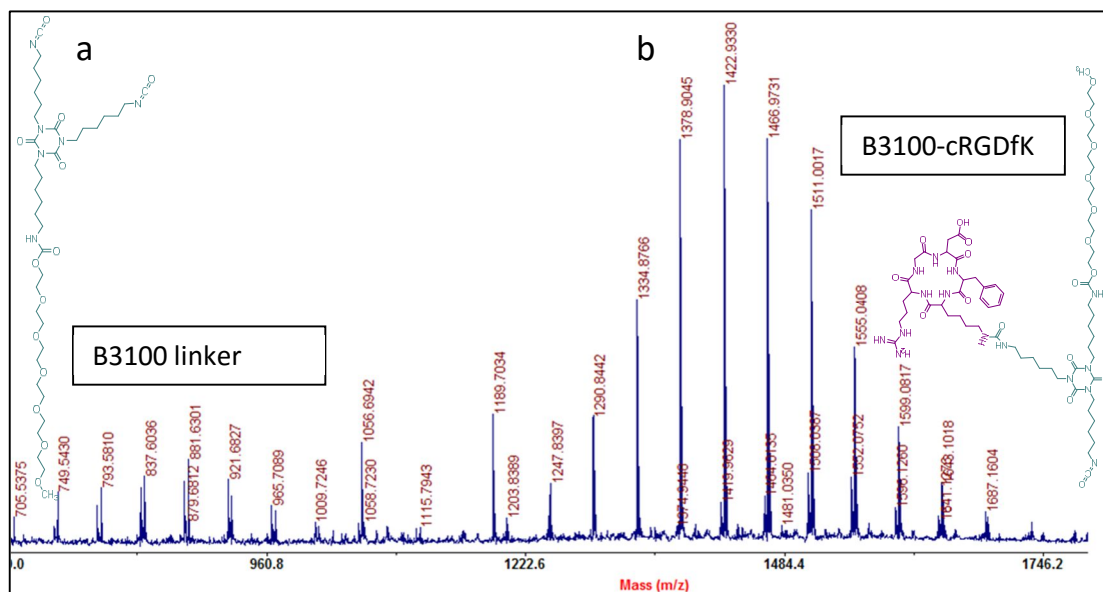
Figure S10. As seen from MALDI-TOF MS spectrum, the linker Bayhydur 3100 (B3100) has a gauss distribution of 700-900 g/mol (average 800 g/mol)) **a).** After 2h reaction a new gauss distribution of masses appears centred on 1400 (800 + 603.68 g/mol) which is consistent with the mass of the B3100-cRGDfK conjugate **b).**

FREE cRGDfK (mM)	FREE cRGDfK (mg/mL)	Conjugated cRGDfK (mg/mL)	Yield (%)
0.046	0.028	1.93	98.5

Table S2. Quantification of non-reacted cRGDfK peptide to PUUa NP-RGD. A calibration curve by HPLC analysis was performed with standard solutions of cRGDfK using L-Phenylalanine as internal standard.
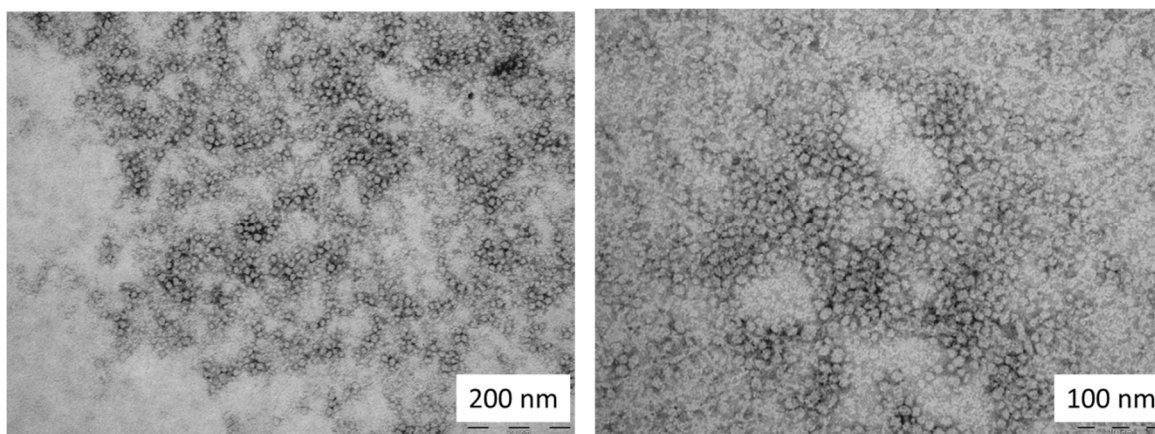
Sample	Diameter (nm)	SD (nm)	PDI
Monowalled PUUa NP	11.3	1.3	0.01

Figure S11. TEM micrographs of monowalled NPs. Monowalled NPs did not contain Hyfob prepolymer, just Amphil. Amphil prepolymer was then crosslinked with Lys and DETA. The absence of Hyfob lead to PUUa NPs with sizes around 10 nm. Monowalled NPs showed a much more diffuse and less defined shell compared to Multiwalled ones.
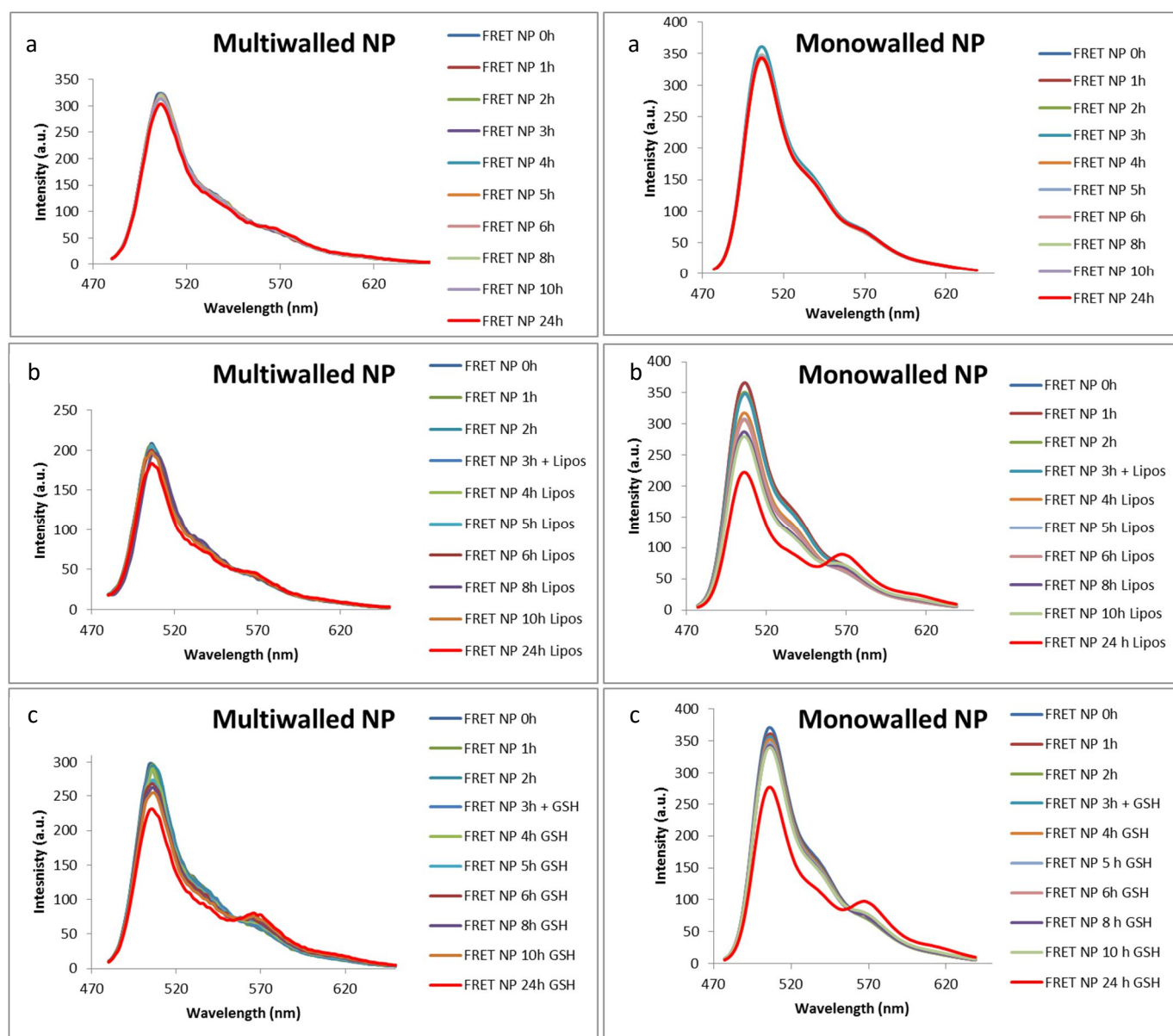
Figure S12. Comparison of fluorescence emission spectra over 24 h of multiwalled and monowalled NPs. Control FRET NPs a), FRET NPs mixed with Phosphatidyl choline-Cholesterol in PBS b), and FRET NPs with GSH c).
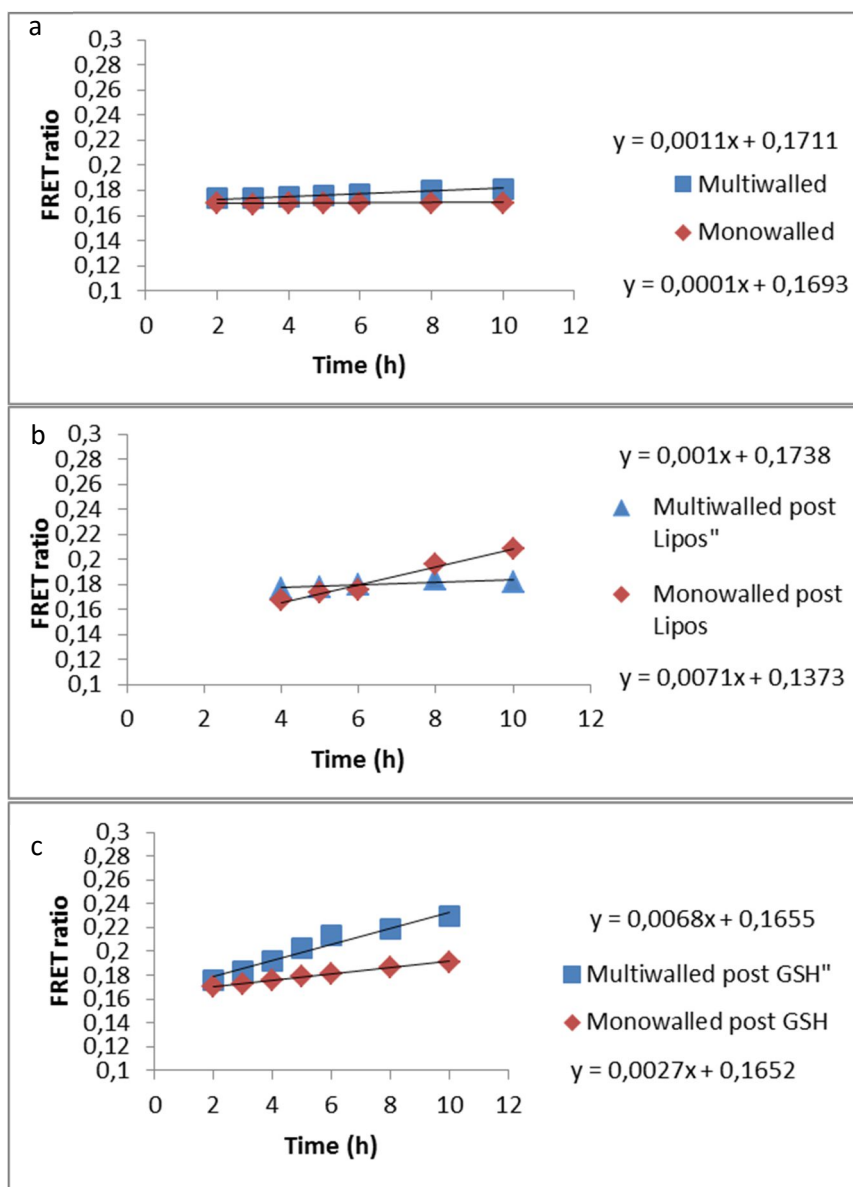
Figure S13. Comparison of measured FRET ratios between multiwalled and monowalled NPs during the first 10 h. FRET ratio of NPs in water a) FRET ratio of NPs mixed with Phosphatidyl choline-Cholesterol in PBS b) FRET ratio post GSH addition in PBS c).

Cell line	Integrin expression (% positive cells)	
	$\alpha_V\beta_3$	$\alpha_V\beta_5$
U87-MG	98.41	0.0
HT-29	3.63	60.30

Table S3: Expression of $\alpha_V\beta_3$ and $\alpha_V\beta_5$ in U87-MG and HT-29 human cancer cell lines (from glioma and colon cancer, respectively).
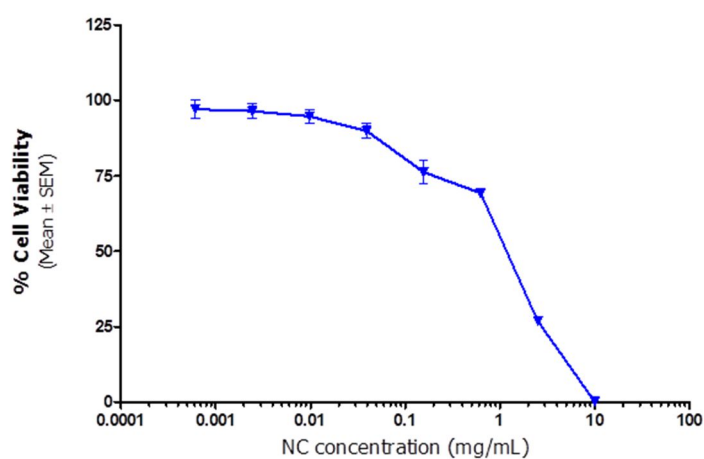
Figure S14. Cytoxicity of DiI loaded NP after 72 h incubation as measured by MTT cell viability assay. Concentrations below 0.1 mg/mL of NP are clearly non-toxic to HeLa cells.
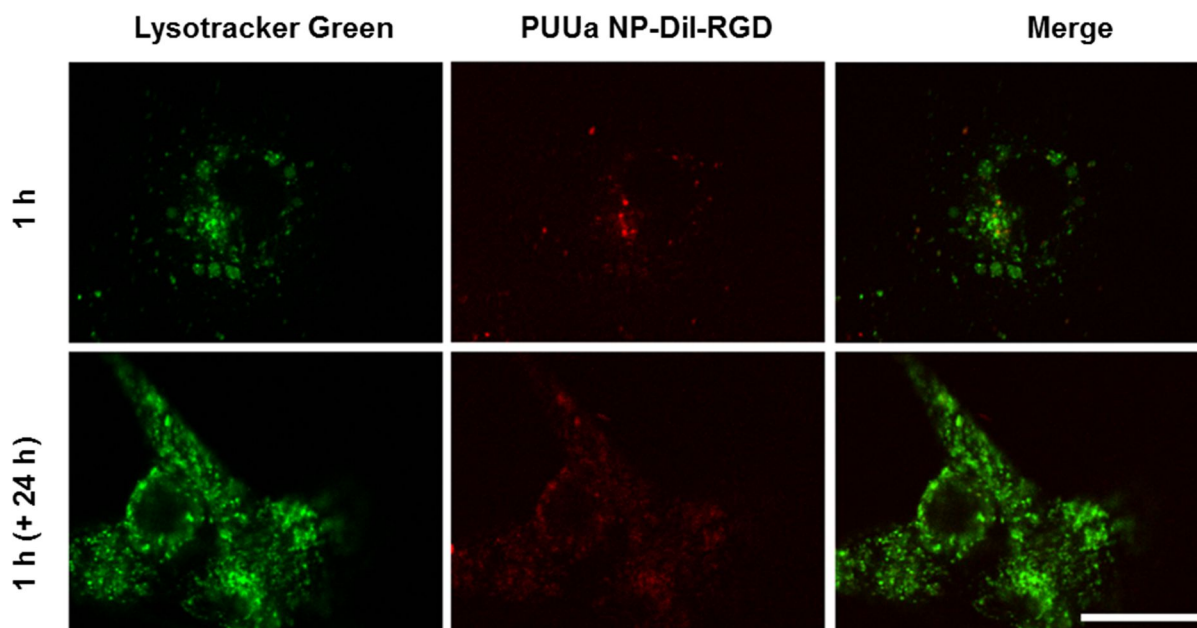
Figure S15. NP trafficking. Confocal images of U87-MG cells incubated 1 h with 1 µg/mL of DiI and stained with Lysotracker Green right after the incubation period (upper panel) or 24 h later (lower panel). Significant differences were observed in confocal images after quantification of the fluorescence signal (z-stacks) confirming that cells pulsed during 1 h and imaged 24 h later showed up to 20 % increase of DiI signal outside lysosomes compared to cells imaged after 1 h incubation (p < 0.001). Magnification bar corresponds to 20 µm. For more details see section 2.5.3. of Materials and Methods.

1   US Environmental Protection Agency_Diisocyanates Toxicology.
        http://www.epa.gov/oppt/auto/profile/toxicology1a.pdf (accessed May 7, 2015).

2   L. T. Budnik, D. Nowak, R. Merget, C. Lemiere and X. Baur, *J. Occup. Med. Toxicol.*, 2011, **6**, 9.

3   A. Prabhakar, D. K. Chattopadhyay, B. Jagadeesh and K. V. S. N. Raju, *J. Polym. Sci. Part A Polym. Chem.*, 2005, **43**, 1196–1209.

Chapter I. Publication 3

PUUa Nanoparticles for Cancer treatment.

In vivo experiments

Improved Pharmacokinetic Profile of Lipophilic Anti-Cancer Drugs Using αvβ3-targeted Polyurethane-Polyurea Nanoparticles

Pau Rocas [a,b,1], Yolanda Fernández [c,d,1], Natalia García-Aranda [c,d], Laia Foradada [c,d], Pilar Calvo [e], Pablo Avilés [e], María José Guillén [e], Simó Schwartz Jr. [c,d], Josep Rocas [b*], Fernando Albericio [a,d,f,g*], Ibane Abasolo [c,d*]

[a] Institute for Research in Biomedicine (IRB Barcelona), Baldiri Reixac 10, 08028 Barcelona, Spain

[b] Nanobiotechnological Polymers Division, Ecopol Tech S.L., Indústria 7, 43720 L'Arboç, Spain

[c] Functional Validation & Preclinical Research (FVPR), Drug Delivery and Targeting Group, CIBBIM-Nanomedicine, Vall d'Hebron Institut de Recerca (VHIR), Universitat Autònoma de Barcelona (UAB), 08035 Barcelona, Spain

[d] Networking Research Center on Bioengineering, Biomaterials and Nanomedicine (CIBER-BBN), Barcelona, Spain

[e] PharmaMar S.A., Avda de los Reyes, 1 Pol. Ind. La Mina, 28770 Colmenar Viejo, Madrid, Spain

[f] Department of Organic Chemistry, University of Barcelona, Martí Franquès 1-11, 08028 Barcelona, Spain

[f] School of Chemistry & Physics, University of Kwazulu-Natal, 4041 Durban, South Africa

[1] Both authors contributed equally to this work, PR performed the synthesis and physicochemical characterization of the nanoparticles while YF was in charge of *in vitro* and *in vivo* assays.

*Corresponding authors:

Functional Validation & Preclinical Research (FVPR), Passeig Vall d'Hebron 119-129. 08035 Barcelona, Spain
E-Mail: ibane.abasolo@vhir.org
Nanobiotechnological Polymers Division, Ecopol Tech S.L., Indústria 7, 43720 L'Arboç, Spain
E-mail: direccio@ecopoltech.com
Department of Organic Chemistry, University of Barcelona, Martí Franquès 1-11, 08028 Barcelona, Spain
E-mail: albericio@ub.edu

ABSTRACT

Meticulously designed nanosystems conveying multiple functionalities and complex multiwalled nanostructures will likely enhance pharmacokinetics and biodistribution of lipophilic chemotherapeutic agents. In the present study, polyurethane-polyurea nanoparticles (PUUa NP) with a disulfide-rich multiwalled structure have been synthesized, characterized and biologically tested. Specifically, glutathione degradable PUUa NP were synthesized with sizes around 100 nm, a neutral Zeta potential and tremendous encapsulation efficiency (above 90%) for a very lipophilic anticancer drug, called plitidepsin. Moreover, PUUa NP were functionalized with a cyclic RGD peptide binding αvβ3 integrins, for further improving their biodistribution and cell internalization.

In vitro cell toxicity assays revealed that PUUa NP release their cargo, rendering half maximal inhibitory concentration (IC50) values similar to those of the free plitidepsin. *In vivo* toxicity studies indicated that the maximum tolerated dose (MTD) of plitidpesin could be increased from 0.9 mg/kg to 3 mg/kg when the drug was delivered in PUUa NP. Moreover, pharmacokinetic parameters such as the maximum concentration (Cmax), area under curve (AUC) and plasma half-life times were higher for the plitidepsin loaded PUUa NP as compared to the free drug. *In vivo* biodistribution assays of fluorescently (DiR) labelled PUUa NP showed that RGD-decorated PUUa NP tended to accumulate less in the liver than the non-decorated version. *Ex vivo* analysis of fluorescent DiR and plitidpesin content confirmed that integrin-targeted nanoparticles had lower accumulation rates in liver and spleen, suggesting that targeted nanoparticles avoid sequestration by macrophages from the reticuloendothelial system.

Overall, our results indicate that the polyurethane-polyurea nanoparticles represent a very valuable nanoplatform for the delivery of lipophilic drugs, such plitidepsin. Without affecting its cytotoxic activity, encapsulation of plitidepsin improves the toxicological, pharmacokinetic and whole-body biodistribution profiles of the anticancer drug. In addition, the functionalization of the PUUa NP surface with targeting moieties seems to improve the stealth properties of the delivery system.

KEYWORDS

Drug delivery systems, nanomedicines, polyurethane-polyurea nanoparticles, RGD peptides, plitidepsin, cancer, *in vivo* fluorescent imaging

INTRODUCTION

Most of the treatment regimes for fighting cancer are based in the use of chemotherapeutic drugs. However, many chemotherapeutic agents are water insoluble, which greatly reduce their effectiveness, and even known anticancer drugs such etoposide, paclitaxel or camptothecin are lipophilic, polar and unstable in aqueous media. These characteristics do not only compromise the formulation of the active principle but also their final efficacy. Poorly soluble lipophilic drugs, have usually low bioavailability, do not distribute properly in the body and do not effectively accumulate in the tumors. Consequently, higher doses of drugs are needed and side-effects and mechanisms of drug resistance appear. Encapsulation of poorly water-soluble molecules in nanoparticles has been seen as a way to overcome these problems. Different types of nanomedicines incorporating chemotherapeutic drugs have already reached the market[1]. However, the necessity to develop alternative delivery vehicles with improved efficacy/toxicity profiles persists.

When dealing with chemotherapeutic drugs, encapsulation of the active principle is desirable over the covalent linkage of the drug to the carrier, because it facilitates the manufacturing process without altering drugs activity. In this type of systems, it is necessary to have a very efficient and stable encapsulation, meaning that the system will have a high loading capacity with little release of the drug outside the tumor. Although many nanosystems have shown stability in water or buffered media such PBS, upon contact with common molecules in the blood they show a non-specific release of the drug or even aggregation problems[2]. Thus, systems preventing drug leakage and nanoparticle aggregation are highly needed. In this regard, few investigators have put efforts to create multiwalled nano-microstructures in order to enhance encapsulation and stability of the drugs without the need of covalently linking the active principle to the carrier[3,4].

Overall, drugs with small plasma half-lives are usually encapsulated in systems that protect them from fast metabolization or excretion. These systems get decorated with polyethylene glycol (PEG) or other molecules than can reduce the opsonization and the phagocytosis from the reticuloendothelial system (RES). As the nanoparticles are not efficiently scavenged by macrophages, the resulting increase in blood circulation time and hence bioavailability is expected to extend the duration of the controlled drug delivery or to improve the prospects for nanoparticles to reach target sites by extravasation[5]. This is specially relevant for targeting to solid tumors, where extension in circulation time is combined with the phenomena known as enhanced permeability and retention (EPR)[6,7] that explains how the leaky vasculature of the tumors and their defective lymphatic drainage retain the macromolecular systems within the tumor. Most of the nanomedicines currently in the market are not targeted, and they relay in these passive mechanisms to accumulate in the tumors. However, the functionalization of nanoparticles to effectively target the cancer cells has demonstrated to be a good mechanism to increase the efficacy of the anti-cancer therapies. In some cases, the presence of the targeting moiety changes the biodistribution profile of the nanoparticle by increasing its presence in the

tumors[8]. But it might also happen that the targeting enhances the activity of the system without altering the tumor accumulation *versus* the non-targeted system, merely because the functionalized systems internalize better in cancer cells[9,10]. In this sense, nanosystems functionalized with specific arginine-glycine-aspartic acid (RGD)-containing peptides binding integrin αvβ3 overexpressed on activated endothelial cells of growing vessels and on tumor cells have shown not only to increase integrin affinity and clustering but also to induce an active integrin-mediated internalization[11,12].

The goal of this work has been to obtain multiwalled drug delivery systems based in polyurethane-polyurea nanoparticles (PUUa NP) to improve encapsulation stability of poorly water-soluble drugs, and thus enhance its pharmacokinetic parameters *in vivo*. Nanoparticles with a liquid oily core and a crosslinked shell combining a hydrophobic, an amphiphilic and a hydrophilic targeting conjugate were efficiently developed following procedures recently described by our group, including the functionalization with a cyclic RGD peptide binding αvβ3 integrin[13–15]. PUUa NP offer specific advantages as drug delivery systems for anti-cancer drugs: possibility of high range of chemical modulation of polymer shell thanks to the high reactivity of isocyanates with amino and hydroxil groups, very stable and efficient encapsulation of drugs and easy formulation (lyophilizable without cryoprotectants and fast redispersion in aqueous media).

As a drug model, we used plitidepsin (Pli), a marine origin drug originally marketed by Pharmamar S.A. (Aplidin®), currently in Phase III of clinical stage for myeloma[16,17]. Although originally isolated from the Mediterranean tunicate *Aplidium albicans*, Pli is currently produced by chemical synthesis. Pli is highly hydrophobic drug, and although it has shown strong anticancer activity against a large variety of cultured human cancer cells[18], its poor biodistribution and bioavailability renders a pretty narrow therapeutic window for the drug. With the aim of improving the efficacy/toxicity balance of Pli, we first synthesized and characterized Pli-loaded PUUa NP superficially functionalized with cyclic RGD peptides. Following extensive *in vitro* characterization of PUUa NP, we assessed the *in vivo* proof-of-principle for their capacity to improve the maximum tolerated dose (MTD), the pharmacokinetic parameters and the whole-body biodistribution of the nanoencapsulated Pli compared to the reference formulation (Cremophor® EL Pli solution).

MATERIAL AND METHODS

1. Chemicals

Pli was kindly provided by PharmaMar S.A. (Madrid, Spain). Cyclo(-Arg-Gly-Asp-D-Phe-Lys) (cRGDfK) was synthesized in house according to previously reported protocols (23151901). YMER™ N-120 was obtained as a free sample from Perstorp (Perstorp, Sweden), the same as N-dodecyl-1,3-propylenediamine (LAP 100D) by Clariant (Barcelona, Spain). Capric/caprylic

triglyceride mixture (Crodamol GTCC) was obtained from Croda (Barcelona, Spain) and Bayhydur 3100 was purchased from Bayer (Leverkusen, Germany). If not indicated otherwise, all other reagents were purchased from Sigma-Aldrich (St Louis, MO, USA). Extra dry acetone was used during all the synthetic process.

2. Synthesis of reactive prepolymers

Preparation of the reactive amphiphilic prepolymer (Amphil) and the Bayhydur 3100-cRGDfK conjugate (B3100-cRGDfK) followed previously described methods with slight changes[13].

To synthesize the amphiphilic prepolymer, a 500 mL four-necked reaction vessel was pre-heated at 50ºC and purged with nitrogen. Then, YMER™ N-120 (3.77 g, 15 mmol), DEDS (0.30 g, 1.95 mmol), Crodamol GTCC (2.5 g) and IPDI (3.38 g, 15 mmol) were added to the reaction vessel under mechanical stirring with dibutyltin dilaurate (DBTL) as catalyst (3 mg, 4.65 µmol). The polyaddition reaction was maintained in these conditions until DEDS and YMER reacted quantitatively with IPDI as ensured by FT-IR and automatic titration[13,19]. At this point, the vessel was cooled to 40ºC and LAP 100D (1.87 g, 7.50 mmol) dissolved in 20 g of acetone was added under constant stirring and left to react for 30 min. The formation of polyurethane and polyurethane-polyurea prepolymers was followed by FT-IR and characterized by NMR[13,15,20].

To obtain the Bayhydur 3100-cRGDfK conjugate (B3100-cRGDfK), cRGDfK (36 mg, 0.0596 mmol) was dissolved in phosphate buffered saline (PBS) (1 mL, 5ºC) and 10 µL of pure triethylamine were added to the mixture (pH 10). Then, the previous solution was mixed with Bayhydur 3100 linker (B3100) (121 mg, 0.167 mmol) and allowed to react during 2 h at 5ºC under constant stirring. The binding of one cRGDfK molecule per linker and the total concentration of reacted cRGDfK in these conditions was ensured by MALDI-TOF MS and HPLC, respectively[13,15].

3. Synthesis of polyurethane-polyurea nanoparticles (PUUa NP)

A previously homogenized aliquote of Amphil+IPDI (1.73 g, mass ratio Amphil 10.6:1 IPDI) was added in a round-bottom flask containing B3100 (125 mg, 0.167 mmol) or B3100-cRGDfK (16% w/w) and DiR (1,1'-dioctadecyl-3,3,3',3'-tetramethylindotricarbocyanine iodide) fluorochrome (5 mg, 5 µmol) and/or Pli under nitrogen atmosphere. This organic mixture was then emulsified in PBS (16 mL, pH 7.4, 5ºC) in a magnetic stirrer under an ice bath to prevent isocyanate reaction with water. Once emulsified, diethylenetriamine (DETA) (76 mg, 0.73 mmol) was added and crosslinked nanoparticles were formed by interfacial polyaddition as proved by FT-IR. Acetone was mildly removed in the rotavapor. PUUa NP were dialyzed (100000 MWCO, Spectrum Laboratories, California, USA) against pure water during 72 h for Zeta-potential experiments. For *in vitro* and *in vivo* experiments PUUa NP were dialyzed against PBS during 72 h.

4. Physicochemical characterization techniques

Physicochemical characterization of PUUa NP included transmission electronic microscopy (TEM) for studying the size and morphology of nanoparticles, size distribution and Z-potential measurements by Dynamic Light Scattering (DLS) and quantification by HPLC of the RGD conjugation. All these methods have been extensively described in a previous publication by our group[13] and are explained in the supplementary data.

Every experiment shown in the main text was performed from lyophilized and redispersed PUUa NP either in pure milliQ grade water or in PBS. Previously dialyzed formulations at 10% solids (w/w) were lyophilized and directly redispersed at the desired concentration by overnight stirring at 1,500 rpm. They were then examined by TEM and DLS to ratify optimal size and morphology characteristics, confirming that the size and shape of the nanoparticles did not differ significantly after the lyophilization process (see Supplementary Information).

5. Pli and DiR encapsulation and release

To quantify the total amount of encapsulated Pli in PUUa NP, a calibration curve was performed by preparing standard solutions of Pli in $CH_3CN:H_2O$ (1:1 v/v) for HPLC analysis. Lyophilized PUUa NP loaded with Pli (5 mg) were emulsified in 2 mL $CH_3CN:DMSO$ (95:5 v/v) during one week at 37ºC to extract the drug and placed in a centrifugal 3 KDa filter unit (Microcon, Carrigtwohill, Ireland) and centrifuged at 14,000 g for 30 min. Analytical HPLC runs of the filtrate were appropriately diluted in $CH_3CN:H_2O$ (1:1 v/v) and analysed in triplicate in a Waters 2998 HPLC using a X-Bridge BEH130, C18, 3.5 µm, 4.6 X 100-mm reverse-phase column with the following gradient: 50 to 100% of B in 8 min at a flow rate of 1 mL/min; eluent A: H_2O with 0.045% TFA (v/v); eluent B: CH_3CN with 0.036% TFA (v/v) and UV detection at 225 nm.

In vitro drug release from the nanoparticles was evaluated either in a control buffer formed by PBS (0.01 M) with 4% (w/w) bovine serum albumin (BSA) and 1% (w/w) Tween 20 surfactant or in a nanoparticle degradation buffer formed by the same components plus 10 mM glutathione (GSH). The concentration of Pli in the medium was studied by ultrafiltration measuring the difference between the filtrated and the encapsulated Pli. The study was performed during 144 h due to the low release rates at short time periods probably because of the highly stable encapsulation method. The filtrate was appropriately diluted in $CH_3CN:H_2O$ 1:1 and analyzed at different time intervals. In order to correctly monitor PUUa NP *in vivo,* their stability was also ensured by measuring the release of DiR (1,1'-dioctadecyl-3,3,3',3'-tetramethylindotricarbocyanine iodide) fluorochrome. To that end, PUUa NP-DiR were incubated in PBS with 4% of BSA and 1% of Tween 20, ultrafiltrated in a centrifugal 3 KDa filter unit (Microcon, Carrigtwohill, Ireland) and centrifuged at 14,000 g for 30 min. The amount of free DiR over time was analyzed in a Waters 2695 HPLC using a Sunfire C18 column (100 x 4.6 mm x 5 mm, 100 Å, Waters) and software EmpowerPro 2 with the following gradient: 70 to 100% of B in 8 min at a flow rate of 1 mL/min; eluent A: H_2O with 0.045% TFA (v/v); eluent B: CH_3CN with 0.036% TFA (v/v) and fluorescence detection (excitation/emission wavelength, 748/780 nm).

6. *In vitro efficacy studies*

Based on the potential indications for Pli, cell lines derived from human glioblastoma (U87-MG) colorectal cancer (HT-29 and HCT 116) and breast cancer (MDA-MB-231) were used in cytotoxicity assays. All cells were obtained from the American Type Culture Collection and maintained as recommended. Briefly, U87-MG cells were cultured in DMEM medium and HT-29 and HCT 116 cells in RPMI 1640 and MDA-MB-231 in DMEM/F12 medium (Life Technologies, Madrid, Spain). All media were supplemented with 10% heat-inactivated fetal bovine serum (FBS) (56°C, 30 min), penicillin (100 U/mL), streptomycin (100 μg/mL) and Fungizone (250 ng/mL) (Life Technologies). Cells were maintained in a humid atmosphere at 37°C with 5% CO_2. Expression of αvβ3 and αvβ5 integrins in these cell lines was analyzed by flow cytometry using monoclonal antibodies against both heterodimers (MAB1976H and MAB1961F from Millipore) as previously described[13]. All cell lines express different levels of both integrins, ensuring the receptor mediated internalization of RGD-functionalized PUUa NP.

In vitro cytotoxicity of nanoparticles was tested by 3-[4,5-dimethylthiazol-2-yl]-2,5-diphenyltetrazolium bromide (MTT) method after 72 h incubation following procedures previously described[13,21,22]. Pli-loaded PUUa NP were tested starting at a maximum concentration of 1 μM of Pli. For non-loaded PUU NP, maximum concentration was set at 10 μM of Pli equivalents.

7. Toxicological evaluation

The acute toxicity studies of Pli formulated in PUUa NP and PUUa NP-RGD was performed in CD-1 female after single intravenous (i.v.) administration of different doses of Pli (0.5 – 1.2 mg/kg). Animals were randomly allocated to dose groups (n=5 per group), and received a single i.v. administration of the formulation to establish the Maximum Tolerated Dose (MTD). Body weight, clinical signs and mortality were recorded daily during the whole assay (14 days). Any mouse showing signs of extreme weakness, toxicity or in a moribund state was euthanized. The MTD was defined as the dose level resulting in less of 15% of weight loss and without any mortality record. All procedures for animal handling, care and treatment were carried out according the procedures approved by the regional Institutional Animal Care and Use Committees.

8. Pharmacokinetic parameters evaluation

The pharmacokinetic studies were performed in athymic female mice (n=54) upon a single i.v. administration of 2 different formulations (integrin targeted PUUa NP-DiR-Pli-RGD and non-targeted PUUa NP-DiR-Pli) at 0.20 mg/kg of Pli. Blood samples were collected in EDTA microtubes at the following times post administration: 0, 5, 15 and 30 min, and 1, 2, 4, 8 and 24 h. The samples were centrifuged at 4,000 g for 15 min at approximately 5ºC, and the resulting plasma was frozen at -20ºC analysis by HPLC-MS/MS. Pli concentrations were quantified by HPLC-MS/MS after solid-liquid extraction with a mixture of tert-butyl methyl ether

(TBME):hexane (1:1, v/v). The pharmacokinetic parameters of Pli were performed using a non-compartmental pharmacokinetic method a WinNonlin™ Professional Version 4.01 (Pharsight Corporation, Mountain View, CA, USA). The AUC values given are normalized to the dose given. Again, all procedures for animal handling, care and treatment were carried out according the procedures approved by the regional Institutional Animal Care and Use Committees.

9. *In vivo* biodistribution of PUUa NP-DiR

Biodistribution studies of near infrared fluorescence labeled nanoparticles were preformed in 6 week-old female athymic nude mice (Harlan Interfauna Iberica, Barcelona, Spain). Mice were treated intravenously with a single dose of integrin targeted PUUa NP-DiR-Pli-RGD and non-targeted PUUa NP-DiR-Pli at 1.7 mg/kg of Pli (0.4 mg/kg of DiR) or the empty integrin targeted PUUa NP-DiR-RGD and non-targeted PUUa NP-DiR (0.4 and 1.5 mg/kg of DiR) resuspended in saline. At 4, 6, 24, 48 and 72 h post administration, the mice were anesthetized and non-invasive DiR fluorescence images were acquired in order to track *in vivo* whole-body biodistribution of drug-loaded and empty PUUa NP. Mice were euthanized at 24 and 72 h post administration. Blood was collected from each animal by cardiac puncture and processed for plasma fractionation. The major organs such as liver, spleen, kidneys and lungs were dissected from mice, weighted and imaged by *ex vivo* fluorescence imaging (FLI). Plasma and tissues samples were harvested and stored at −80°C to quantify Pli levels by HPLC. The *in vivo* and *ex vivo* tissue biodistribution of the labeled-nanoparticles was monitored non-invasively by FLI using the IVIS Spectrum imaging system with the Living Image 4.3 software (PerkinElmer, MA, USA) (21756949). Animals were anesthetized using 1–3% isoflurane (Abbott Laboratories, Abbott Park, IL). Five mice were imaged at a time, and imaging settings were set depending on the fluorescence of the tissues. The light emitted from the fluorescent PUUa NP containing DiR was detected, digitalized and electronically displayed as a pseudocolor overlay onto a gray scale animal image. Regions of interest (ROI) from displayed images were drawn manually around the fluorescent signals and quantified as Radiant Efficiency. The mean FLI intensities, mean DiR tissue accumulations, and corresponding standard errors of the mean (SEM) were determined for each experiment. All the analyses and graphs were performed using Prism 5 software (GraphPad, San Diego).

Animal care was handled in accordance with the Guide for the Care and Use of Laboratory Animals of the Vall d'Hebron University Hospital Animal Facility, and following experimental procedures previously approved by VHIR's Animal Experimentation Ethical Committee (AEEC). All the *in vivo* biodistribution studies were performed by the ICTS "NANBIOSIS", more specifically by the CIBER-BBN's *In Vivo* Experimental Platform of the Functional Validation & Preclinical Research (FVPR) area (Barcelona, Spain).

RESULTS AND DISCUSSION

In this work, we describe the development and physicochemical characterization of PUUa NP as drug delivery systems, taking Pli and the near infrared lipophilic dye DiR as model

molecules. The encapsulation and delivery of both molecules and the ability of PUUa NP to modify the toxicity, pharmacokinetic and biodistribution profiles of Pli are herein discussed.

1. Preparation and characterization of PUUa NP

Novel PUUa NP were synthesized from a first step of polyaddition reaction followed by emulsification in water. Afterwards, crosslinking of preemulsified reactive monomers by interfacial polyaddition reaction was performed by adding a polyamine. The resulting PUUa NP (Fig. 1) encompassed disulfide bonds in their crosslinked shell, allowing a controlled intracellular release upon contact with cytosolic GSH and the interior core, while the oily core incorporated the drug (Pli) and/or the near infrared dye (DiR) for *in vivo* monitoring purposes. In addition, PUUa NP were superficially decorated with the cRGDfK targeting peptide.
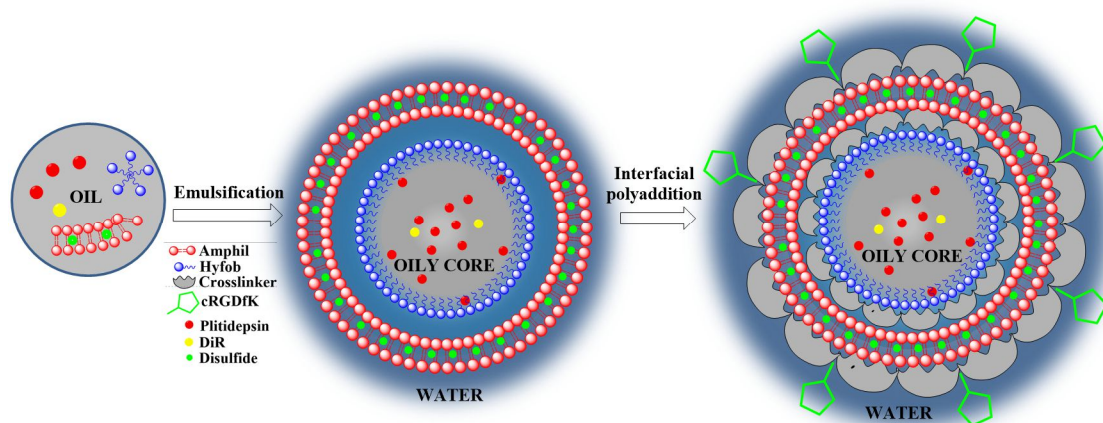
Fig. 1. PUUa NP synthetic process.

PUUa NP were based on emulsifying in water an isocyanate reactive amphiphilic prepolymer (Amphil) together with isophorone diisocyanate monomer (IPDI). Interestingly, Amphil beared hydrophobic and hydrophilic side chains that confer water dispersability and great encapsulation capacity respectively. In order to enhance the encapsulation stability, IPDI hydrophobic monomer (Hyfob) was added with Amphil to create a hydrophobic inner shell. Amphil prepolymer promoted self-stratification in the oil-water interface from the more hydrophobic internal core to the more hydrophilic external phase, sorted by their intrinsic hydrophilic-lipophilic balance (HLB). Interestingly, the pendant chains driving the self-stratification of the shell by hydrophobic assembly were located orthogonally to the main polymer backbone. Therefore, interaction of the hydrophobic dangling chains with the hydrophobic monomer (inner shell) and the oily core was geometrically favored. Very conveniently, as the stratification was controlled by hydrophobic interactions, we could control the localization of each polymer in the

interface by chemically tuning their HLB values. For example, the disulfide containing prepolymer (Amphil) was amphiphilic, meaning that would be primordially located in the middle of the shell; in change, the targeting peptide conjugate, which was hydrophilic, would be mainly located in the surface of the shell, ready to interact with cell integrin receptors. At last, Hyfob, which was completely insoluble in water would be stabilized in the inner shell of the nanoparticle. When the system was completely self-assembled in its multiwalled ordered form (Oil-Hyfob-Amphil-cRGDfK-Water), a step of crosslinking of the isocyanate prepolymers with DETA wss cornerstone to fix the tricomponent polymeric shell. This interfacial polyaddition reaction strengthened by polyurea linkages the previous hydrophobic and hydrophilic interactions in the shell.

Robust multiwalled nanoparticles were fully characterized in terms of morphology, size distribution and surface charge. These three aspects might determine the failure-success rate of nanoparticles including cellular uptake by RES, targeting to target cells, in vivo distribution, and corona formation with proteins in body fluids and matrix structures[23,24]. In this regard, PUUa NP showed a polymeric dense morphology with monodisperse sizes around 90-110 nm, which are between the optimal size range to achieve tumor accumulation *in vivo* by EPR and active targeting phenomena (Fig. 2 and Table 1)[25]. Neutral or slightly positive surface charges have been reported as the most adequate for cell internalization and PUUa NP indeed showed Z-potential values ranging from 0 to 1. Moreover, these values did not changed when PUUa NP were loaded with Pli or DiR or functionalized with cRGDfK, cyclic RGD peptide (Table 1). This moiety specifically binds $\alpha v \beta 3$ integrins allowing a faster and more efficient internalization in cancer cells overexpressing such integrins[13]. To effectively couple the RGD peptide to the nanoparticles surface we applied our recently described new method consisting on two steps. First, the cRGDfK reacted with a hydrophilic polyisocyanate (Bayhydur 3100) via urea bond formation with the amino group of cRGDfk quantitatively[13,15] (almost 100% conjugation yield) forming the isocyanate-reactive targeting conjugate. Afterwards, the free isocyanate reactive targeting conjugate was immediately fixed in the shell surface via urea bonds during the interfacial crosslinking with DETA, bearing 0.02 mg of cRGDfk per mg of PUUa NP.
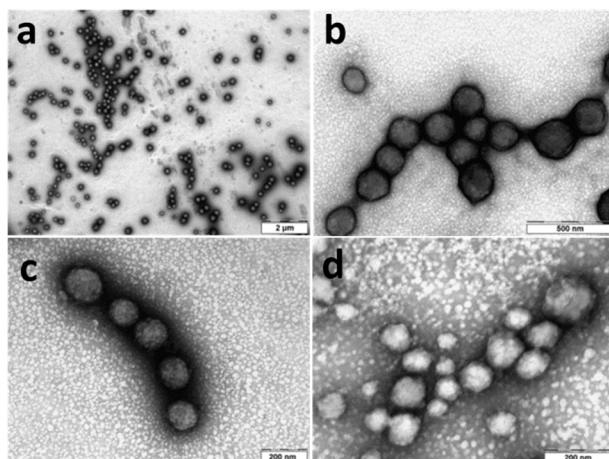
Fig. 2. TEM micrographs of PUUa NP. **a)** PUUa NP-DiR; **b)** PUUa NP-DiR-Pli; **c)** PUUa NP-DiR-RGD; and **d)** PUUa NP-DiR-PLli-RGD.

Table 1. Characterization of size, Z-potential and polidispersity indez (PDI) of different PUUa NP loaded with DiR (0.25 mg/mL) and Pli (0.9 mg/mL), respectively. Mean ± SD are indicated with an n=3 in all cases

Nanoparticle	**TEM (nm), PDI**	**DLS (nm), (PDI)**	**Z-Pot** (mV)
PUUa NP DiR	111 ± 26, (0,06)	105 ± 37, (0.13)	0.90 ± 0.15
PUUa NP DiR-RGD	105 ± 31, (0,09)	106 ± 38, (0.13)	0.45 ± 0.10
PUUa NP DiR-Pli	108 ± 30, (0,08)	96 ± 33, (0.11)	0.38 ± 0.20
PUUa NP DiR-Pli-RGD	89 ± 37, (0,17)	91 ± 33, (0.13)	0.66 ± 0.10

2. Drug encapsulation and release studies

Many types of cancer are associated with elevated intracellular concentrations of GSH. GSH is a tripeptide with reductive potential involved in proliferative responses and is essential for cell cycle progression. So, PUUa NP polymeric shell contained disulfide moieties to be biodegraded by intracellular levels of GSH. The degradation by GSH and the changes on nanoparticles morphology were studied during one week by TEM. As seen from TEM micrographs (Fig. 3), PUUa NP were gradually degraded and polymeric aggregates clearly appeared after one week of incubation in 10 mM GSH at 37 ºC.
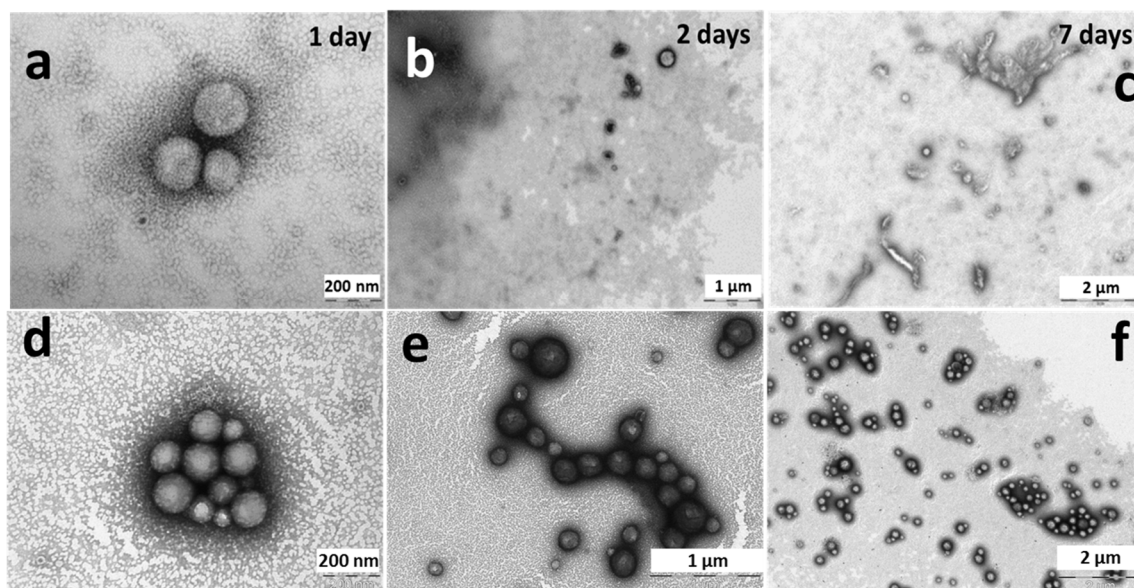
Fig. 3. TEM micrograph proving the nanoparticles degradation process over time in 10 mM GSH at 37ºC. **a)** During the first day, spherical shaped nanoparticles start to exhibit a diffuse shell. **b)** After 2 days of incubation, irregular aggregates larger than 0.22 μm appear. **c)** Seven days after incubating cells with GSH, degradation of polymers in the nanoparticles results in shell destabilization and aggregates larger than 2 μm are formed. **d)**, **e)**, **f)** Disulfide-free PUUa NP were incubated with the same conditions and no degradation was observed.

Pli was loaded into the polymer nanoparticles with high encapsulation efficiency (99%) at a final drug loading of 1% (w/w) (0.9 mg/mL of Pli). Such results were attributed to the high affinity of the drug for the oily core. The drug release experiment confirmed that PUUa NP were very stable and only released the drug in presence of GSH. When PUUa NP-Pli were incubated with PBS-BSA-TW20 (control buffer) minimal release was observed over 144 h (Fig. 4). However, when PUUa NP-Pli were incubated with PBS-BSA-TW20-GSH (degradation buffer) a quite rapid released was observed for the first 10 h (~30%) that followed with a slower release rate that was sustained at 144 h (70%). In addition, inexistent release of DiR dye after 24 h incubation of PUUa NP-DiR in PBS containing BSA (4% w/w) and Tween 20 (1% w/w) was observed, which made them particularly appropriated for the *in vivo* fluorescent monitoring.
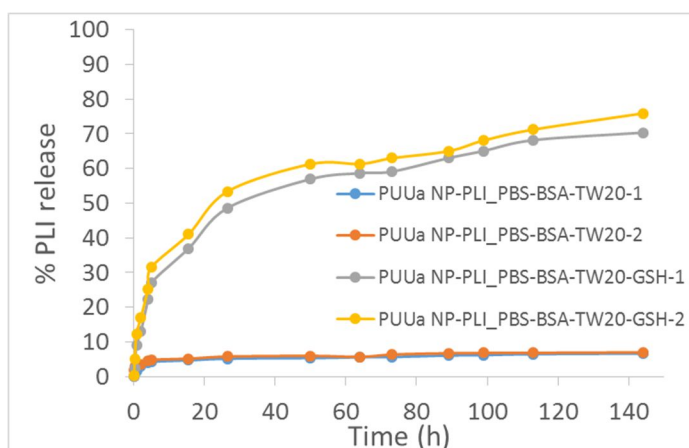
Fig 4. Pli drug release in control media (PBS-BSA-Tween20, red dots) and degradation media (PBS-BSA-Tween20 + 10 mM GSH, blue dots). Mean ± SD are indicated with an n=3 in all cases.

3. Freeze-drying studies of plitidepsin-loaded PUUa nanoparticles

Although polyurethanes and particularly polyureas are highly resistant to hydrolysis in aqueous media[26,27], PUUa NP were specifically designed to be lyophilizable and redispersable without the addition of any cryoprotectant or external surfactant and avoiding ultrasonication steps. Lyophylized PUUa NP were characterized by TEM and DLS after redispersion (Table 1S and Fig. 1S) results indicated that shape, size and surface charge of the nanoparticles did not change significantly after lyophilization. To the best of our knowledge, this is the first time that PUUa crosslinked NP have been lyophilized and redispersed without any external surfactants or cryoprotectants. Thus, this finding is expected to, on the one hand, facilitate the handling and storage of PUUa NP, and the other hand, avoid the use of cryoprotective agents that could cause side-effects *in vivo*.

4. *In vitro* efficacy

Cell cytotoxicity assays clearly showed that Pli loaded PUUa NP were as effective as the free drug (Fig. 5 and Table 2). Interestingly, in MDA-MB-231 cells, know to be resistant to many chemotherapeutic agents the efficacy of the drug was improved (IC50 value of drug loaded and targeted NP was 9.684 ± 2.688 µM) compared to the free drug (IC50 value of 22.100 ± 7.357 µM). These differences could be related with the intrinsic endocytic capacity of the cells or their relative levels of GSH.

In this case, no differences were observed between targeted (PUUa NP-Pli-RGD) and non-targeted (PUUa NP-Pli) systems, probably because the extended incubation time (72 h). Shorter incubation times would allow seeing differences in cell internalization and efficacy[13]. However, long incubation times were warranted to test the potential toxicity of empty nanocarriers[28].
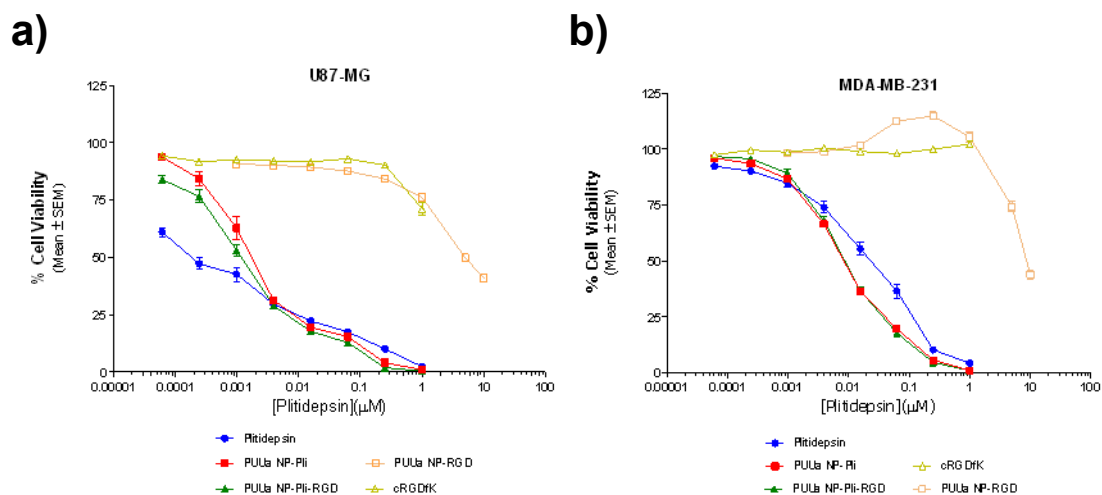
Fig. 5. *In vitro* efficacy of Pli loaded PUUa NP *versus* empty PUUa NP after 72 h incubation as read by MTT assay.**a)** U87-MG and **b)** MDA-MB-231 cells. Results of the Pli-loaded nanoparticles were compared to equivalent doses of non-loaded PUU NP or non-conjugated cRGDfK PUUa NP.

Table 2. IC50 values of Pli-loaded PUUa NP.. Values represent the mean ± SEM in Pli concentration (µM) of 3 independent experiments

Cell line	PUUa NP-Pli-RGD	PUUa NP-Pli	Pli
U87-MG	1.258 ±0.378	2.069 ±0.927	2.261 ± 1.265
MDA-MB-231	9.684 ± 2.688	8.980 ±1.217	22.10 ± 7.357
HCT-116	1.117 ± 0.639	1.216 ± 0.586	0.616 ± 0.473
HT-29	2.304 ± 1.206	3.288 ± 1.663	0.904 ± 0.289

5. Toxicological evaluation

The toxicity of Pli-loaded PUUa NP was evaluated by determining the MTD in CD-1 mice. Previous studies had already established that the MTD of the reference formulation of Pli (Cremophor® EL/ethanol/water 15/15/70 w/w/w) was 0.3 mg/kg[29]. In our case, the MTD of Pli-loaded PUUa NP in CD-1 mice was 0.9 mg/kg for both, targeted and non-targeted PUUa NP. Thus, encapsulation of Pli in PUUa NP reduces significantly the toxicity associated to the administration of Pli, widening the therapeutic window of the drug. Moreover, there are differences in the maximum toxicity of targeted and non-targeted PUUa NP, indicating that the addition of the RGD moiety does not alter significantly the toxicological profile of the PUUa NP. Interestingly, alternative drug delivery systems for Pli based in polyglutamic acid (PGA) – polyethylenglicol (PEG) has also a reported MTD of 0.9 mg/kg[29]. However, Gonzalo *et al*. only studied the plasmatic pharmacokinetic profile of non-targeted PGA systems. They did not study

tissue biodistribution of the PGA-based systems, nor did they offer alternatives to avoid RES sequestration other than PEGylating the nanoparticles.

Furthermore, no toxicity was observed upon administration of the unloaded nanoparticles up to 1 g/kg of solid weight. From these results it can be inferred that the maximum toxicity reduction was achieved for Pli-loaded RGD-targeted and non-targeted PUUa NP (MTD 3 times higher than that of the reference formulation, respectively).

6. Pli pharmacokinetic profile by PUUa NP

The objective of encapsulating Pli into PUUa NP was to improve the plasma residence time of the drug and to improve its biodistribution, as a way to enhance drug's antitumoral efficacy. In order to assess the plasma half-life of the drug encapsulated in PUUa NP, Pli reference formulation as well as RGD-targeted and non-targeted Pli-loaded PUUa NP were administered intravenously to healthy CD-1 mice. The plasmatic drug concentrations following i.v. administration of the different formulations are shown in Fig. 6.

It can be note that Pli plasmatic levels achieved after administration of drug-loaded targeted and non-targeted PUUa NP are much higher than those corresponding to the free Pli. Similar conclusions can be drawn from Table 3, which shows the pharmacokinetic parameters associated to all formulations. Non-targeted PUUa NP showed higher half-life times compared to RGD-targeted and free Pli. Both RGD-targeted and non-targeted PUUa NP showed lower clearance compared to the free Pli.
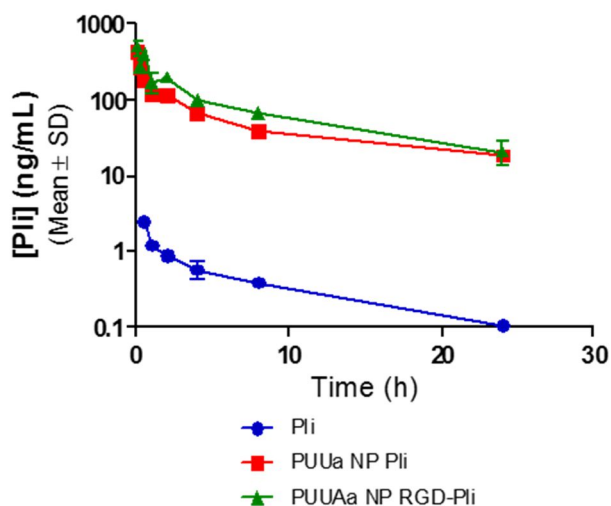
Figure 6. Pharmacokinetic profile of Pli after i.v. administration to mice of 2 mg/kg Pli PUUa NP. Each point represents the mean and SD of n = 3.

Table 3. Pharmacokinetic parameters of Pli-loaded PUUa NP after single i.v. administration to mice.

Nanoparticle	Cmax	AUC$_{0-24}$	t$_{1/2}$	CLp	Vdss
	(ng/mL)	(ng.h/mL)	(h)	(mL/h/kg)	(mL/kg)
PUUa NP-DiR-Pli	434.3	1212.8	11.7	0.0001	0.0018
PUUa NP-DiR-Pli-RGD	506.0	1871.9	8.9	0.0001	0.0009
Pli	2.6	11.4	8.5	15657.9	137035.5

7. *In vivo* biodistribution of RGD-targeted PUUa NP

A unique dose of PUUa NP-DiR RGD-targeted and non-targeted were well tolerated up to 72 h post administration. At 72 h post administration, the treated to control (T/C) body weight ratio were -6% and -1% for the PUUa NP-DiR-RGD and PUUa NP-DiR, respectively. The non-invasive *in vivo* FLI of targeted and non-targeted DiR-labelled PUUa NP demonstrated that *in vivo* monitoring of PUUa NP biodistribution was feasible using DiR at a concentration of 1.5 and 0.4 mg DiR/kg (see Supplementary Data). Non-invasive *in vivo* FLI showed that targeted RGD-decorated PUUa NP-DiR tended to accumulate less in liver that the non-targeted PUUa NP-DiR (see Fig. 7a). Liver accumulation ratio increased up to 48 h post administration, and then after, the fluorescent signal tended to diminish for up to 72 h post administration. To further confirm the results obtained by *in vivo* FLI at 24 and 72 h post administration, a subgroup of mice were euthanized and livers were collected. As expected, *ex vivo* results corroborated what observed *in vivo*; that was that targeted PUUa NP-DiR-RGD were less uptaken by the liver than the non-targeted PUUa NP-DiR (Fig. 7b). Moreover, the liver accumulation slightly decreased from 24 to 72 h.
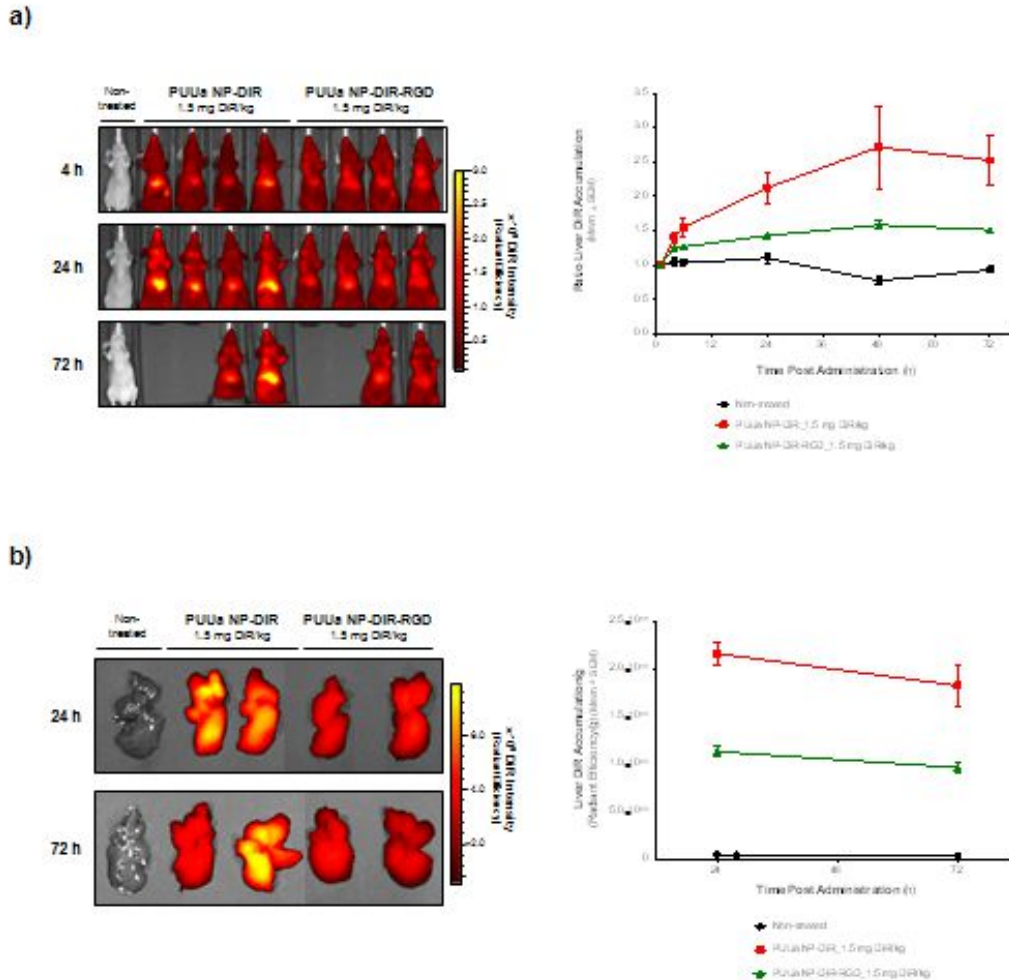
Figure 7. Liver accumulation of DiR labelled PUUa NP RGD-targeted and non-targeted in mice. **a)** Non-invasive *in vivo* FLI images of PUUa NP-DiR and PUUa NP-DiR-RGD tissue biodistribution over time (*left panel*), and the semiquantitative estimation of fluorescence DiR intensity ratio in the liver in respect to 1 h post administration (*right panel*). **b)** *Ex vivo* FLI liver images and the quantification of liver DiR fluorescence *per* weight of tissue at 24 and 72 h end time points. Pseudocolor scale bars were consistent for all images in order to show relative changes with time.

Moreover, the whole-body biodistribution of the PUUa NP-DiR RGD-targeted and non-targeted loaded with Pli as a therapeutic drug were evaluated after a unique i.v. dose of the PUUa NP loaded with 1.7 mg/kg of Pli and labeled with 0.4 mg/kg of DiR fluorophore. A unique dose of PUUa NP-DiR-Pli RGD-targeted and non-targeted induced body weight loss up to 72 h post administration. At 72 h post administration, the T/C body weight ratio were -13% and -21% for the PUUa NP-DiR-Pli-RGD and PUUa NP-Pli-DiR, respectively. Moreover, other side effects such as apathy and hypothermia were detected and associated to Pli toxicity. It is worth mentioning that MTD of Pli, as a free drug, is 0.3 mg/kg. The dose of 1.7 mg/kg, although toxic, is one order of magnitude higher the MTD described for Pli, and 5 times greater than that described for other drug delivery systems carrying Pli[29].

The semiquantitative estimation of fluorescence DiR intensity in plasma, liver, spleen, lung, kidney, heart, muscle and skin were analyzed by e*x vivo* FLI at 24 and 72 h post administration of the targeted and Pli-loaded PUUa NP-DiR-RGD-Pli and the non-targeted PUUa NP-DiR-Pli. Results showed that PUUa NP greatly biodistribute into liver, spleen and lungs (Figure 8). This is an expected biodistribution for nanoparticulated drug delivery systems administered intravenously. The accumulation of nanoparticles in liver and spleen responds to the fact that these two organs have fenestrated vessels that allow the extravasation of nanoparticles. In addition, both organs are home of macrophages of RES, known to be responsible of the fast clearance of nanoparticles from the bloodstream. However, our results show that along time RGD-decorated PUUa NP accumulate less in liver and spleen than non-targeted PUUa NP, indicating that the functionalization of the nanoparticles reduces the sequestration of nanoparticles by the RES. In the case of plasma, no significant differences were observed between RGD-targeted and non-targeted PUUa NP levels at 72 h post administration. As for the other tissues, similar tissue accumulation patters were also observed in kidneys, heart, muscle and skin.
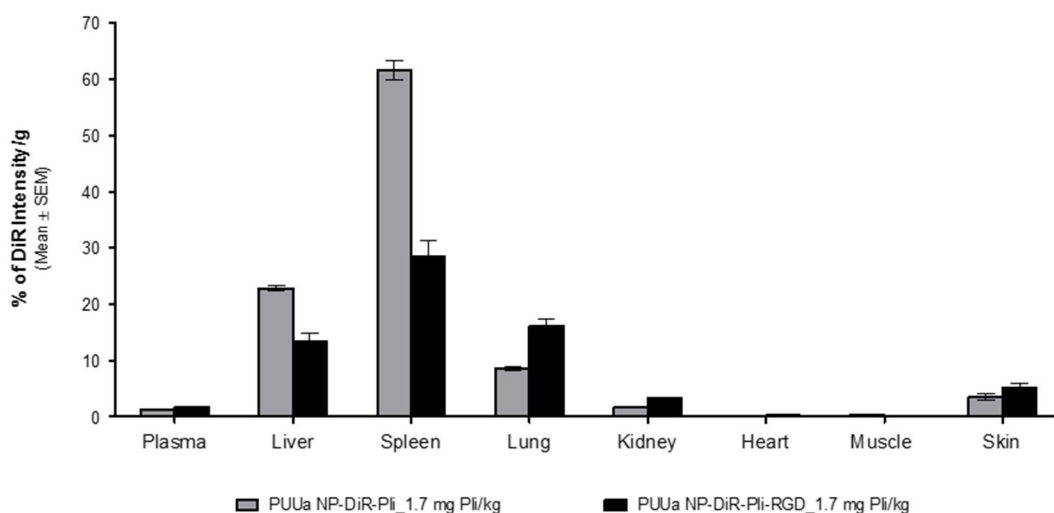
Figure 8. Tissue biodistribution of integrin targeted and non-targeted PUUa NP loaded with Pli in mice. *Ex vivo* plasma and tissue intensity *per* tissue weight at 72 h post administration of integrin targeted PUUa NP-DiR-Pli-RGD and non-targeted PUUa NP DiR-Pli at 1.7 mg Pli/kg and 0.4 mg DiR/kg by i.v. administration route is shown. Mean percentage values of each corresponding formulation tissue-accumulation per tissue weight in respect to the total maximal tissue fluorescence and corrected by DiR light emission in each compound are displayed.

DiR biodistribution results were further corroborated by the quantification of Pli levels in tissues collected 24 h post administration of a single dose of DiR labelled PUUa NP. Liver and spleen tissues accumulated higher levels of drug when Pli was delivered in non-targeted PUUa NP, whereas these tissues showed lover levels of drug when RGD-decorated PUUa NP were administered.

Table 4. Tissue accumulation of Pli (ng/mL) 24 h after a single administration of DiR labeled PUUa NP at 1.5 mg/kg Pli to athymic nude mice. Values indicate the mean +/- SD of two independent samples.

Nanoparticle	Liver	Spleen
PUUa NP-DiR-Pli	4315 ± 346	34100 ± 15698
PUUa NP-DiR-Pli-RGD	3680 ± 325	22100 ± 8061

Interestingly, in the case of the targeted nanoparticles, the linkage of the RGD through the amine residue leaves two charges per molecule, one positive and one negative, available in the surface of the nanoparticle, without altering the overall neutral surface charge. This zwitteronic characteristic of the RGD-decorated nanoparticles, could explain the observed differences between the targeted and non-targeted systems. Zwitteronic coatings reduce the opsonization and the adsorption of a protein corona, since they prevent electrostatic interactions between circulating proteins and charged polymer surface and cancel the subsequent release of counterions and water molecules from the nanoparticle surface[30]. As a consequence, nanoparticles with zwitteronic surfaces are known to escape the fagocitosis by the RES. Kuppfer cells in the hepatic sinusoids of the liver and marginal zone and red pulpe macrophages in the spleen are the principal contributors to the RES, and this explains the significantly lower accumulation of our targeted PUUa NP in these two organs. Moreover, this fact has been already demonstrated for smaller size nanoparticles such quantum dots[31]. Sun et al, showed that the extent of uptake by the liver and spleen was about 3–6-fold lower for the zwitterionic quantum dots[32] and furthermore, Choi et al. also shown that the RGD functionalization can be achieved in nanoparticles while maintaining their zwiteronic characteristics[33]. These optimized biodistribution of the targeted nanoparticles, could also help to widen the therapeutic window of nanoparticles by reducing potential toxicities due to a lower degree of off-target binding.

CONCLUSION

Herein, we report the use of PUUa NP for improving the toxicity, pharmacokinetic and biodistribution profile of a highly insoluble drug. The *in vitro* efficacy of Pli in different cancer cell lines was maintained when drug was non-covalently encapsulated in polyurethane-based nanosystems. *In vivo*, toxicity and pharmacokinetic profiles of the Pli in PUUa was greatly improved when compared to the standard formulation of Pli. Moreover, the functionalization of PUUa NP with cRGDfk moieties ameliorate the biodistribution of the nanosystem and the drug by avoiding their accumulation in tissues with high presence of macrophages such liver and tissue. Overall, this study highlights the promising potential of RGD-targeted and non-targeted PUUa NP as delivery carrier systems for anticancer drugs.

REFERENCES

[1]   M.L. Etheridge, S.A. Campbell, A.G. Erdman, C.L. Haynes, S.M. Wolf, J. McCullough, The big picture on nanomedicine: the state of investigational and approved nanomedicine products., Nanomedicine. 9 (2013) 1–14. doi:10.1016/j.nano.2012.05.013.

[2]   P. Zou, H. Chen, H.J. Paholak, D. Sun, Noninvasive fluorescence resonance energy transfer imaging of in vivo premature drug release from polymeric nanoparticles., Mol. Pharm. 10 (2013) 4185–94. doi:10.1021/mp4002393.

[3]   K. Ariga, Q. Ji, J.P. Hill, Y. Bando, M. Aono, Forming nanomaterials as layered functional structures toward materials nanoarchitectonics, NPG Asia Mater. 4 (2012) e17. doi:10.1038/am.2012.30.

[4]   J. RODRIGUEZHERNANDEZ, F. CHECOT, Y. GNANOU, S. LECOMMANDOUX, Toward "smart" nano-objects by self-assembly of block copolymers in solution, Prog. Polym. Sci. 30 (2005) 691–724. doi:10.1016/j.progpolymsci.2005.04.002.

[5]   S.M. Moghimi, A.C. Hunter, J.C. Murray, Long-circulating and target-specific nanoparticles: theory to practice., Pharmacol. Rev. 53 (2001) 283–318. http://www.ncbi.nlm.nih.gov/pubmed/11356986 (accessed October 13, 2015).

[6]   Y. Matsumura, H. Maeda, A new concept for macromolecular therapeutics in cancer chemotherapy: mechanism of tumoritropic accumulation of proteins and the antitumor agent smancs., Cancer Res. 46 (1986) 6387–92. http://www.ncbi.nlm.nih.gov/pubmed/2946403 (accessed October 17, 2015).

[7]   H. Maeda, J. Wu, T. Sawa, Y. Matsumura, K. Hori, Tumor vascular permeability and the EPR effect in macromolecular therapeutics: a review., J. Control. Release. 65 (2000) 271–84. http://www.ncbi.nlm.nih.gov/pubmed/10699287 (accessed November 6, 2015).

[8]   Y. Zhong, F. Meng, C. Deng, Z. Zhong, Ligand-directed active tumor-targeting polymeric nanoparticles for cancer chemotherapy., Biomacromolecules. 15 (2014) 1955–69. doi:10.1021/bm5003009.

[9]   D.W. Bartlett, H. Su, I.J. Hildebrandt, W.A. Weber, M.E. Davis, Impact of tumor-specific targeting on the biodistribution and efficacy of siRNA nanoparticles measured by multimodality in vivo imaging., Proc. Natl. Acad. Sci. U. S. A. 104 (2007) 15549–54. doi:10.1073/pnas.0707461104.

[10]   D.B. Kirpotin, D.C. Drummond, Y. Shao, M.R. Shalaby, K. Hong, U.B. Nielsen, et al., Antibody targeting of long-circulating lipidic nanoparticles does not increase tumor localization but does increase internalization in animal models., Cancer Res. 66 (2006) 6732–40. doi:10.1158/0008-5472.CAN-05-4199.

[11]   E. Garanger, D. Boturyn, P. Dumy, Tumor targeting with RGD peptide ligands-design of new molecular conjugates for imaging and therapy of cancers., Anticancer. Agents Med. Chem. 7 (2007) 552–8. http://www.ncbi.nlm.nih.gov/pubmed/17896915 (accessed December 2, 2015).

[12]   L. Auzzas, F. Zanardi, L. Battistini, P. Burreddu, P. Carta, G. Rassu, et al., Targeting alphavbeta3 integrin: design and applications of mono- and multifunctional RGD-based peptides and semipeptides., Curr. Med. Chem. 17 (2010) 1255–99. http://www.ncbi.nlm.nih.gov/pubmed/20166941 (accessed December 2, 2015).

[13]   P. Rocas, Y. Fernandez, S. Schwartz, I. Abasolo, J. Rocas, F. Albericio, Correction: Multifunctionalized polyurethane-polyurea nanoparticles: hydrophobically driven self-stratification at the o/w interface modulates encapsulation stability, J. Mater. Chem. B. 3 (2015) 8421. doi:10.1039/C5TB90134K.

[14]   P. Rocas Alonso, J. Rocas Sorolla, Method for producing a microencapsulate and corresponding reactive amphiphilic compound, microencapsulate and composition., WO2014114838A3, Ecopol Tech S.L., 2014.

[15]   P. Rocas, M. Hoyos-Nogués, J. Rocas, J.M. Manero, J. Gil, F. Albericio, et al., Installing Multifunctionality on Titanium with RGD-Decorated Polyurethane-Polyurea Roxithromycin Loaded Nanoparticles: Toward New Osseointegrative Therapies., Adv. Healthc. Mater. 4 (2015) 1956–60. doi:10.1002/adhm.201500245.

[16]   Study of Plitidepsin (Aplidin®) in Combination With Bortezomib and Dexamethasone in Patients With Multiple Myeloma - Full Text View - ClinicalTrials.gov, (n.d.). https://clinicaltrials.gov/show/NCT02100657 (accessed November 6, 2015).

[17]   R. Plummer, P. Lorigan, E. Brown, R. Zaucha, V. Moiseyenko, L. Demidov, et al., Phase I-II study of plitidepsin and dacarbazine as first-line therapy for advanced melanoma., Br. J. Cancer. 109 (2013) 1451–9. doi:10.1038/bjc.2013.477.

[18]   M.J. Muñoz-Alonso, L. González-Santiago, T. Martínez, A. Losada, C.M. Galmarini, A. Muñoz, The mechanism of action of plitidepsin., Curr. Opin. Investig. Drugs. 10 (2009) 536–42. http://www.ncbi.nlm.nih.gov/pubmed/19513942 (accessed November 6, 2015).

[19]   I.R. Clemitson, Castable Polyurethane Elastomers, CRC Press, 2008.

[20]   A. Prabhakar, D.K. Chattopadhyay, B. Jagadeesh, K.V.S.N. Raju, Structural investigations of polypropylene glycol (PPG) and isophorone diisocyanate (IPDI)-based polyurethane prepolymer by 1D and 2D NMR spectroscopy, J. Polym. Sci. Part A Polym. Chem. 43 (2005) 1196–1209. doi:10.1002/pola.20583.

[21]   L.L. Romero-Hernández, P. Merino-Montiel, S. Montiel-Smith, S. Meza-Reyes, J.L. Vega-Báez, I. Abasolo, et al., Diosgenin-based thio(seleno)ureas and triazolyl

glycoconjugates as hybrid drugs. Antioxidant and antiproliferative profile., Eur. J. Med. Chem. 99 (2015) 67–81. doi:10.1016/j.ejmech.2015.05.018.

[22]   P. Botella, I. Abasolo, Y. Fernández, C. Muniesa, S. Miranda, M. Quesada, et al., Surface-modified silica nanoparticles for tumor-targeted delivery of camptothecin and its biological evaluation., J. Control. Release. 156 (2011) 246–57. doi:10.1016/j.jconrel.2011.06.039.

[23]   D.F. Moyano, M. Ray, V.M. Rotello, Nanoparticle – protein interactions : Water is the key, 39 (2014) 1069–1073. doi:10.1557/mrs.2014.255.

[24]   A.E. Nel, L. Mädler, D. Velegol, T. Xia, E.M. V Hoek, P. Somasundaran, et al., Understanding biophysicochemical interactions at the nano-bio interface., Nat. Mater. 8 (2009) 543–57. doi:10.1038/nmat2442.

[25]   M. Howard, B.J. Zern, A.C. Anselmo, V. V. Shuvaev, S. Mitragotri, V. Muzykantov, Vascular Targeting of Nanocarriers: Perplexing Aspects of the Seemingly Straightforward Paradigm, ACS Nano. 8 (2014) 4100–4132. doi:10.1021/nn500136z.

[26]   A. Pegoretti, L. Fambri, A. Penati, J. Kolarik, Hydrolytic resistance of model poly(ether urethane ureas) and poly(ester urethane ureas), J. Appl. Polym. Sci. 70 (1998) 577–586. doi:10.1002/(SICI)1097-4628(19981017)70:3<577::AID-APP20>3.0.CO;2-X.

[27]   J. Kozakiewicz, G. Rokicki, J. Przybylski, K. Sylwestrzak, P.G. Parzuchowski, K.M. Tomczyk, Studies of the hydrolytic stability of poly(urethane–urea) elastomers synthesized from oligocarbonate diols, Polym. Degrad. Stab. 95 (2010) 2413–2420. doi:10.1016/j.polymdegradstab.2010.08.017.

[28]   R. Duncan, Y.-N. Sat-Klopsch, A.M. Burger, M.C. Bibby, H.H. Fiebig, E.A. Sausville, Validation of tumour models for use in anticancer nanomedicine evaluation: the EPR effect and cathepsin B-mediated drug release rate., Cancer Chemother. Pharmacol. 72 (2013) 417–27. doi:10.1007/s00280-013-2209-7.

[29]   T. Gonzalo, G. Lollo, M. Garcia-Fuentes, D. Torres, J. Correa, R. Riguera, et al., A new potential nano-oncological therapy based on polyamino acid nanocapsules., J. Control. Release. 169 (2013) 10–16. doi:10.1016/j.jconrel.2013.03.037.

[30]   Z.G. Estephan, P.S. Schlenoff, J.B. Schlenoff, Zwitteration as an alternative to PEGylation., Langmuir. 27 (2011) 6794–800. doi:10.1021/la200227b.

[31]   K. Pombo García, K. Zarschler, L. Barbaro, J.A. Barreto, W. O'Malley, L. Spiccia, et al., Zwitterionic-coated "stealth" nanoparticles for biomedical applications: recent advances in countering biomolecular corona formation and uptake by the mononuclear phagocyte system., Small. 10 (2014) 2516–29. doi:10.1002/smll.201303540.

[32]   M. Sun, D. Hoffman, G. Sundaresan, L. Yang, N. Lamichhane, J. Zweit, Synthesis and characterization of intrinsically radiolabeled quantum dots for bimodal detection., Am. J. Nucl. Med. Mol. Imaging. 2 (2012) 122–35. http://www.pubmedcentral.nih.gov/articlerender.fcgi?artid=3477726&tool=pmcentrez&rendertype=abstract (accessed November 10, 2015).

[33]   H.S. Choi, W. Liu, F. Liu, K. Nasr, P. Misra, M.G. Bawendi, et al., Design considerations for tumour-targeted nanoparticles., Nat. Nanotechnol. 5 (2010) 42–7. doi:10.1038/nnano.2009.314.

SUPPORTING INFORMATION

Improved Pharmacokinetic Profile of Lipophilic Anti-Cancer Drugs Using αvβ3-targeted Polyurethane-Polyurea Nanoparticles

Pau Rocas [a,b,1], Yolanda Fernández [c,d,1], Simó Schwartz Jr. [c,d], Natalia García-Aranda [c,d], Laia Foradada [c,d], Pilar Calvo [e], Pablo Avilés [e], Maria José Guillén [e], Josep Rocas [b]*, Fernando Albericio [a,d,f,g]*, Ibane Abasolo [c,d]*

[a] Institute for Research in Biomedicine (IRB Barcelona), Baldiri Reixac 10, 08028 Barcelona, Spain

[b] Nanobiotechnological Polymers Division, Ecopol Tech S.L., Indústria 7, 43720 L'Arboç, Spain

[c] Functional Validation & Preclinical Research (FVPR), Drug Delivery and Targeting Group, CIBBIM-Nanomedicine, Vall d'Hebron Institut de Recerca (VHIR), Universitat Autònoma de Barcelona (UAB), 08035 Barcelona, Spain

[d] Networking Research Center on Bioengineering, Biomaterials and Nanomedicine (CIBER-BBN), Barcelona, Spain

[e] PharmaMar S.A., Avda de los Reyes, 1 Pol. Ind. La Mina, 28770 Colmenar Viejo, Madrid, Spain

[f] Department of Organic Chemistry, University of Barcelona, Martí Franquès 1-11, 08028 Barcelona, Spain

[f] School of Chemistry & Physics, University of Kwazulu-Natal, 4041 Durban, South Africa

[1] Both authors contributed equally to this work, PR performed the synthesis and physic-chemical characterization of the nanoparticles while YF was in charge of in vitro and in vivo assays.

*Corresponding authors:

Functional Validation & Preclinical Research (FVPR), Passeig Vall d'Hebron 119-129. 08035 Barcelona, Spain

E-Mail: ibane.abasolo@vhir.org

Nanobiotechnological Polymers Division, Ecopol Tech S.L., Indústria 7, 43720 L'Arboç, Spain

E-mail: direccio@ecopoltech.com

Department of Organic Chemistry, University of Barcelona, Martí Franquès 1-11, 08028 Barcelona, Spain

E-mail: albericio@ub.edu

1. SUPPORTING METHODS

1.1. Analytical techniques

2.1.1. Physicochemical characterization techniques

Transmission electron microscopy. The nanoparticles morphology was studied in a Jeol JEM 1010 (Peabody, MA, USA). A 200 mesh copper grid 0,75% FORMVAR coated was deposited on a drop of 10 mg/mL of nanoparticles in water during 1 min. Nanoparticles excess was removed by fresh milliQ water contact for 1 min. Then, the grid was deposited on a drop of Uranyl acetate 2 % w/w in water for 30 sec. The Uranyl acetate excess was blotted off and air-dried before measurement. For the degradation experiment 10 µL of filtered (0,22 µm) PUUa NPs (100mg/mL) were added into 1 mL solution of GSH (10 mM) and incubated at 37 ºC during 1 week under constant stirring. Samples were withdrawn at the desired intervals and TEM analyzed following the explained above methodology. For statistical analysis, 5 different zones of the copper grid were randomly counted with ImageJ software (NIH, Bethesda, MD, USA).

Peptide conjugation yield quantification. A calibration curve was realised by preparing 5 standard solutions of cRGDfK peptide containing L-phenylalanine amide as internal standard for quantitative HPLC analysis. Analytical HPLC runs of the PUUa NP-RGD were performed in a WATERS 2998 HPLC (Milford, MA, USA) using a X-Bridge BEH130, C18, 3.5 µm, 4.6 X 100 mm reverse phase column with the following gradient: 5-30% B in 9 min at a flow rate of 1 mL/min; eluent A: H2O with 0.045% TFA (v/v); eluent B: CH3CN with 0.036% TFA.

Size distribution and zeta potential measurements. PUUa NPs were analysed on a Malvern Zetasizer Nano-ZS90 (Malvern, UK) at 1 mg/mL in pure water at 37 ºC.

Infrared spectra. IR spectra were performed in a FT-IR Nexus Termo Nicolet 760 (Waltham, MA, USA) by depositing a drop of previously dissolved prepolymer at 1 % in acetone on a NaCl or BaF2 (for aqueous samples) disk.

MALDI-TOF MS. Coupling reaction between B3100 and cRGDfK was ensured by MALDI-TOF MS. The experiment was carried out on an Applied Biosystems Voyager-DETMRP mass spetrometer (Waltham, MA, USA), using α-cyano-4-hydroxycinnamic acid (ACH) as matrix. B3100 and B3100-cRGDfK at 1 mg/mL after 2 h reaction were analysed.

NMR. NMR spectra were recorded on a Varian Mercury (400 MHz) (Agilent) (Santa Clara, CA, USA). Reactive prepolymers Hyfil, Amphil were previously dissolved in CDCl3 at 100 mg/mL.

1.2. Flow cytometry assays

Integrin expression characterization. The expression of αVβ3 and αVβ5 was analyzed by flow cytometry using monoclonal antibodies against both heterodimers (MAB1976H and MAB1961F

from Millipore). Specifically, the cell suspensions detached using PBS–EDTA (5 mM) were incubated with 3 mg of avb3 antibody. 1 mg of avb5 antibody for 20 min at 4 1C, and IgG2 isotype controls from eBioscience (San Diego, CA, USA) were included. Cells were analyzed using FacScalibur Becton Dickinson (Franklin Lakes, NJ, USA) and FCS Express 4 software De Novo Software (Los Angeles, CA, USA).

2. SUPPORTING RESULTS

2.1 Lyophilization of nanoparticles

Supplementary Table 1. Size and surface charges of empty PUUa NP before and after lyophilization process.

PUUa NP	Size TEM	Size DLS
Before	109 ± 28	101 ± 21
After	105 ± 31	103 ± 33

Supplementary Figure 1. TEM pictures of PUUa NP before a) and after b) lyophilization process.
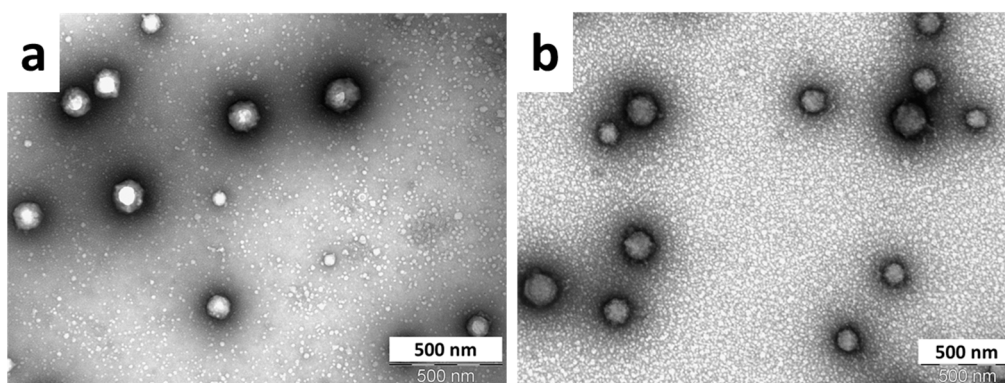
2.2 Expression of αVβ3 and αVβ5 integrins

Supplementary Table 2. Percentage of positive cells for αVβ3 and αVβ5 integrins as determined by flow cytometry. HMEC-1, human microvasculature endothelial cell, were used as positive controls.

Cell line	αVβ3	αVβ5
HMEC-1	97.49	17.10
U87-MG	98.41	0.95
MDA-MB-231	29.21	15.48
HCT-116	14.56	53.40
HT-29	3.63	60.30

Chapter II.

Nanobiomaterials for

Tissue Regeneration

Chapter II.

Chapter II. Introduction

Nanobiomaterials for Tissue Regeneration and Infection Prevention

Introduction 2. Nanobiomaterials for Tissue Regeneration and Infection Prevention

Nanoparticle-coated titanium implants

Globally, more than 1000 tons of titanium are implanted into patients in the form of biomedical devices every year[1]. Metallic prostheses, fixation and anchoring devices are used extensively for dental, orthopedic, and craniofacial rehabilitation and their effects on the body are generally perceived to be predictable after initial implantation[2]. Its biocompatibility, resistance to corrosion, and excellent mechanical properties converts titanium implants as the gold-standard for bone substitution[3]. Currently, the excellent biocompatibility of titanium is associated with a high degree of "bioinertness", which in some cases may be translated into poor rates of osseointegration[3]. Therefore, Ti implants functionalization is being studied to improve the surface bioactivity for effective adhesion between an implant surface and the host bone tissue to lower the risk of implant loosening over time and implant failure. Hence, an osteoinductive or "bioactive" surface capable of promoting the rapid adhesion of osteoblasts[4], as well as the osteogenic differentiation of mesenchymal stem cells at the site of injury, may ensure a faster osseointegration and improve the clinical outcome of implant materials[5].

Mimicking the natural environment that supports and mediates bone growth on the metallic surface represents a very powerful approach to install bioactivity on such materials. This approach, also known as biofunctionalization, focuses on grafting biomolecules derived from bone extracellular matrix (ECM) on the surface of the implant. These ECM-derived molecules are capable of interacting with cell-expressed receptors like integrins, which trigger essential biological processes of most cells. In particular, integrins $\alpha v\beta 3$ and $\alpha 5\beta 1$ (widely expressed by osteoblasts and osteoprogenitor cells) have been described to have crucial functions in the development of bone tissue[6,7].

In recent years, interest in treating Ti surfaces with bioactive agents, such as variable Arg-Gly-Asp (RGD) peptide sequence or osteoinductive growth factors, has grown because these agents can mediate cellular responses and promote osteogenic activity in osteoblastic cells[5,8]. Of these emergent biochemical approaches, incorporating RGD peptides onto Ti surfaces is recognized as one of the most promising methods to stimulate new bone formation and osseointegration[6,9,10]. However RGD peptides alone lack multifunctionality and novel macromolecular structures conveying multiple

functions are needed in the complex bone environment[11,12]. Multifunctionality, is the intrinsic characteristic of a material to perform different functions at the same time, which is obviously a plus in medicine. Regarding this matter, polymeric materials, and more concretely polyurethanes, bring light into this concern as they can be easily synthesized in one pot procedures by quantitative and solvent-free reactions and have been more than sufficiently proven to be biocompatible as implantable materials for clinical purposes[13–15]. Moreover, polyurethane materials allow a broad range of chemical properties (biodegradability, stiffness, hydrophilicity, etc.) from simple and commercial monomers[16,17]. Multiple chemical structures can be formed such as linear, star-like, dendrimeric, crosslinked polymers depending on the functionality (f) of the precursors used. In example, if a diisocyanate and a diol are mixed a linear polyurethane will be formed. In change, if a diisocyanate and a tetrafunctional glycol are reacted, a crosslinked polyurethane structure will be created in a couple of hours, quantitative yields and green chemistry[18]. More interestingly, nanoparticulate systems can be engineered by the meticulous combination of amphiphilic materials with hydrophobic and hydrophilic segments enclosing not only biomolecules in their polymeric shell surface but also in its hydrophobic core. Potentially, by coating implant surfaces with nanoparticles, nanomaterials would upgrade combining multiple functions such as drug delivery, diagnostics and imaging[4].

Titanium implants infection

The number of patients with a need for orthopedic implants has increased rapidly over the past few years with the optimization of orthopedic surgery techniques and the material performance of orthopedic implants[2]. Due to bacterial contamination and soft-tissue damage, particularly in invasive orthopedic surgery, patients show a higher susceptibility to infection. As a result, an undesired raise of the risk of infection related to implants has been observed during the first 6 hours post-implantation and even over long-time periods, being therefore cornerstone the long lasting effect of antibacterial implants[19]. Implant-related infections following invasive orthopedic surgery are a major clinical problem and are one of the main causes of implant failure[20,21]. Primary bacterial colonizers belong mainly to the Streptococci family (*Streptococcus Sanguis*)[22]. Current strategies for the management of implant-associated infections are the administration of perioperative systemic antibiotics. Although antibiotics can be administered systemically as part of routine clinical therapy, a high concentration of the drug is delivered unspecifically throughout the body losing important amounts far away of the desired site. Systemic antibiotic administration may result in various systemic

toxicities, side-effects and the development of antibiotic-resistant micro-organisms. Hence, a localized, controlled release antibiotic delivery strategy, where the antibiotic is targeted to the desired site and released at high concentrations over a prolonged period of time, is a potential promising alternative approach to systemic antibiotic administration.

Multifunctional Titanium surfaces

In this chapter, a novel approach will be followed to biofunctionalize the implant materials focusing on the use of a new class of multifunctional polyurethane-polyurea nanoparticles (PUUa NPs) to coat materials with high targeting specificity for αvβ3-expressing cells and drug-encapsulation capacity[4,23]. The biodegradable PUUa NPs are composed of a stratified multiwalled amphiphilic nanostructure and display the following features (Figure 1):

i) Shell functionalization with an αvβ3-selective cyclic RGD peptide to provide cell specificity.

ii) High capacity to encapsulate hydrophobic drugs in the NP oily core.

iii) Tunable drug-release by diffusion or degradation mechanisms based on the polymers functionality.

iv) Tunable isocyanate-reactive shell for implant high-throughput functionalization of biomaterials.
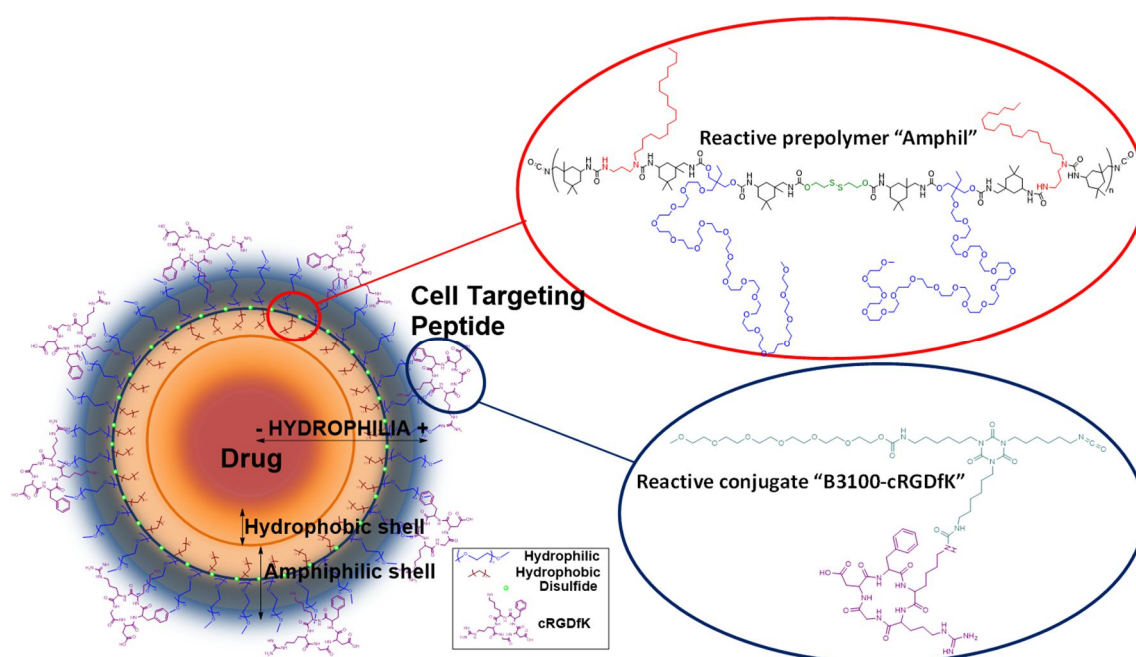
Figure 1. Schematic representation of multifunctional PUUa NPs structure.

Concretely, we developed a new methodology named Interfacial Functionalization to coat amine-containing titanium surfaces with isocyanate-containing PUUa NPs. The urea bonds formation reaction took place at the interface of material-nanoparticle in water during one hour, obtaining homogeneously coated surfaces (Figure 2).
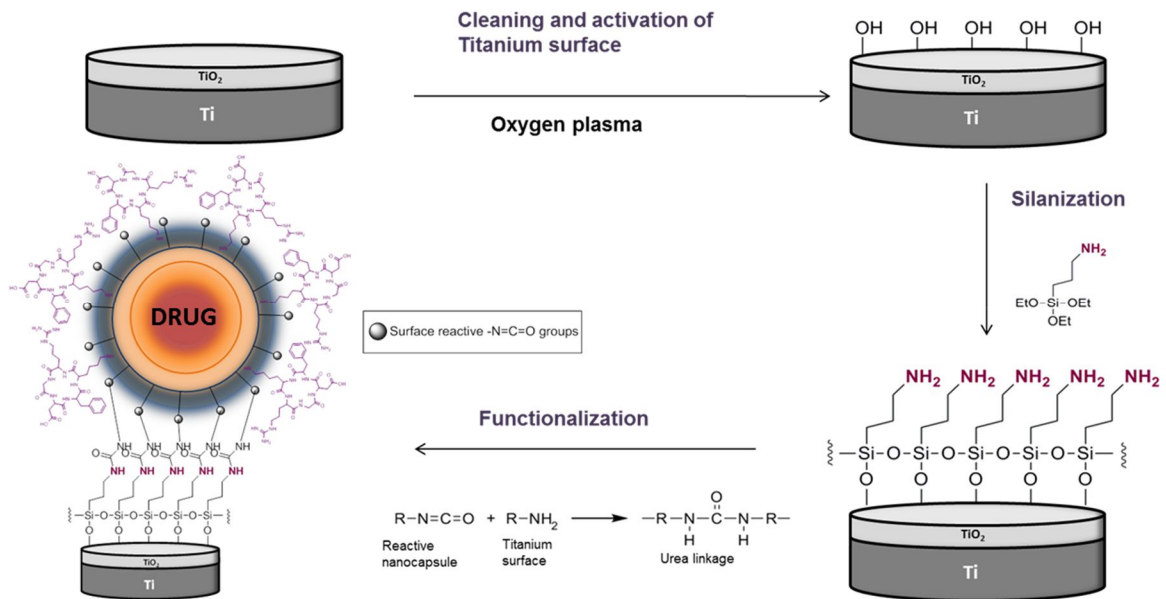
Figure 2. Interfacial Functionalization of titanium implants with isocyanate-reactive multifunctional PUUa NPs.

Thus, functionalization of porous titanium with RGD-decorated PUUa NPs loaded with roxithromycin antibiotic drug will enhance implants osseointegration via a dual effect: enhancing the adhesion of osteoblasts, and reducing the occurrence of bacterial adhesion and/or unwanted inflammatory syndromes (Figure 3).
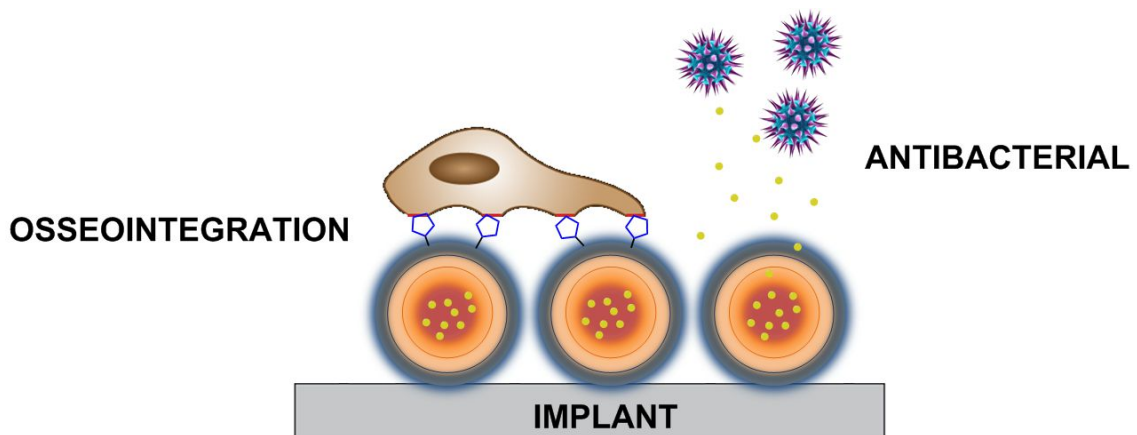
Figure 3. Dual-effect approach to bioactivate titanium impants.

The following chapter proposes a highly multidisciplinary approach exploiting the synergy between engineering sciences, chemistry and biology to overcome a medical challenge currently not addressed in a specific manner.

References

1. "Flower Bouquet" nanoclusters strengthen titanium implant attachments http://www.gizmag.com/flower-boquet-nanoclusters-strengthen-titanium-implant-attachments/16082/ (accessed Nov 26, 2015).

2. Chen, Q.; Thouas, G. A. Metallic implant biomaterials. *Mater. Sci. Eng. R Reports* **2015**, *87*, 1–57.

3. Bauer, S.; Schmuki, P.; von der Mark, K.; Park, J. Engineering biocompatible implant surfaces. *Prog. Mater. Sci.* **2013**, *58*, 261–326.

4. Rocas, P.; Hoyos-Nogués, M.; Rocas, J.; Manero, J. M.; Gil, J.; Albericio, F.; Mas-Moruno, C. Installing Multifunctionality on Titanium with RGD-Decorated Polyurethane-Polyurea Roxithromycin Loaded Nanoparticles: Toward New Osseointegrative Therapies. *Adv. Healthc. Mater.* **2015**.

5. Lee, S. W.; Lee, H. J.; Lee, J. W.; Kim, K.-H.; Kang, J.-H.; Lee, M. H.; Lee, S. C. Surface functionalization of microgrooved titanium with dual growth factor-releasing nanoparticles for synergistic osteogenic differentiation of human mesenchymal stem cells. *Colloids Surf. B. Biointerfaces* **2015**, *135*, 565–574.

6. Siebers, M. C.; ter Brugge, P. J.; Walboomers, X. F.; Jansen, J. A. Integrins as linker proteins between osteoblasts and bone replacing materials. A critical review. *Biomaterials* **2005**, *26*, 137–46.

7. Mas-Moruno, C.; Fraioli, R.; Albericio, F.; Manero, J. M.; Gil, F. J. Novel peptide-based platform for the dual presentation of biologically active peptide motifs on biomaterials. *ACS Appl. Mater. Interfaces* **2014**, *6*, 6525–36.

8. Lee, D.-W.; Yun, Y.-P.; Park, K.; Kim, S. E. Gentamicin and bone morphogenic protein-2 (BMP-2)-delivering heparinized-titanium implant with enhanced antibacterial activity and osteointegration. *Bone* **2012**, *50*, 974–82.

9. Schliephake, H.; Scharnweber, D.; Dard, M.; Rossler, S.; Sewing, A.; Meyer, J.; Hoogestraat, D. Effect of RGD peptide coating of titanium implants on periimplant bone formation in the alveolar crest. An experimental pilot study in dogs. *Clin. Oral Implants Res.* **2002**, *13*, 312–319.

10. Ferris, D. RGD-coated titanium implants stimulate increased bone formation in vivo. *Biomaterials* **1999**, *20*, 2323–2331.

11. Zhao, P.; Liu, H.; Deng, H.; Xiao, L.; Qin, C.; Du, Y.; Shi, X. A study of chitosan hydrogel with embedded mesoporous silica nanoparticles loaded by ibuprofen as a dual stimuli-responsive drug release system for surface coating of titanium implants. *Colloids Surf. B. Biointerfaces* **2014**, *123*, 657–63.

12. Mattioli-Belmonte, M.; Cometa, S.; Ferretti, C.; Iatta, R.; Trapani, A.; Ceci, E.; Falconi, M.; De Giglio, E. Characterization and cytocompatibility of an antibiotic/chitosan/cyclodextrins nanocoating on titanium implants. *Carbohydr. Polym.* **2014**, *110*, 173–82.

13. Guelcher, S. A.; Srinivasan, A.; Dumas, J. E.; Didier, J. E.; McBride, S.; Hollinger, J. O. Synthesis, mechanical properties, biocompatibility, and biodegradation of polyurethane networks from lysine polyisocyanates. *Biomaterials* **2008**, *29*, 1762–75.

14. Guelcher, S. A.; Gallagher, K. M.; Didier, J. E.; Klinedinst, D. B.; Doctor, J. S.; Goldstein, A. S.; Wilkes, G. L.; Beckman, E. J.; Hollinger, J. O. Synthesis of biocompatible segmented polyurethanes from aliphatic diisocyanates and diurea diol chain extenders. *Acta Biomater.* **2005**, *1*, 471–84.

15. Bachelder, E. M.; Beaudette, T. T.; Broaders, K. E.; Paramonov, S. E.; Dashe, J.; Fréchet, J. M. J. Acid-Degradable Polyurethane Particles for Protein-Based Vaccines: Biological Evaluation and in Vitro Analysis of Particle Degradation Products. *Mol. Pharm.* **2008**, *5*, 876–884.

16. Engels, H.-W.; Pirkl, H.-G.; Albers, R.; Albach, R. W.; Krause, J.; Hoffmann, A.; Casselmann, H.; Dormish, J. Polyurethanes: versatile materials and sustainable problem solvers for today's challenges. *Angew. Chem. Int. Ed. Engl.* **2013**, *52*, 9422–41.

17. Chattopadhyay, D. K.; Raju, K. V. S. N. Structural engineering of polyurethane coatings for high performance applications. *Prog. Polym. Sci.* **2007**, *32*, 352–418.

18. Delebecq, E.; Pascault, J.-P.; Boutevin, B.; Ganachaud, F. On the Versatility of Urethane/Urea Bonds: Reversibility, Blocked Isocyanate, and Non-isocyanate Polyurethane. *Chem. Rev.* **2013**, *113*, 80–118.

19. Hetrick, E. M.; Schoenfisch, M. H. Reducing implant-related infections: active release strategies. *Chem. Soc. Rev.* **2006**, *35,* 780–9.

20. Zilberman, M.; Elsner, J. J. Antibiotic-eluting medical devices for various applications. *J. Control. Release* **2008**, *130*, 202–15.

21. Geurts, J.; Chris Arts, J. J.; Walenkamp, G. H. I. M. Bone graft substitutes in active or suspected infection. Contra-indicated or not? *Injury* **2011**, *42 Suppl 2*, S82–6.

22. Kolenbrander, P. E.; Palmer, R. J.; Periasamy, S.; Jakubovics, N. S. Oral multispecies biofilm development and the key role of cell-cell distance. *Nat. Rev. Microbiol.* **2010**, *8*, 471–80.

23. Rocas Alonso, P.; Rocas Sorolla, J. Method for producing a microencapsulate and corresponding reactive amphiphilic compound, microencapsulate and composition. 2014, Ecopol Tech, S.L.

Chapter II. Publication 4

PUUa Nanoparticles for Bone Regeneration and

Bacterial Infection Prevention.

In vitro experiments

COMMUNICATION

Installing Multifunctionality on Titanium with RGD-Decorated Polyurethane-Polyurea Roxithromycin Loaded Nanoparticles: Toward New Osseointegrative Therapies

Pau Rocas,* Mireia Hoyos-Nogués, Josep Rocas, José M. Manero, Javier Gil, Fernando Albericio, and Carlos Mas-Moruno*

Metallic biomaterials such as titanium (Ti) and its alloys have long been used for applications in bone fixation and regeneration owing to their excellent biocompatibility and mechanical properties.[1] However, their use is not exempt from limitations, which still today may compromise the long-term performance of these materials. In the first place, the high degree of "bioinertness" displayed by such metals may, in some clinical scenarios, translate into poor rates of osseointegration (i.e., insufficient implant-bone interactions) and inadequate mechanical fixation.[1] Moreover, bacterial infection and subsequent inflammation (i.e., peri-implantitis) has been described as another major cause of implant failure.[2] To address these drawbacks surface biofunctionalization with bioactive motifs has extensively been

P. Rocas, Prof. F. Albericio
Institute for Research in Biomedicine (IRB Barcelona)
08028 Barcelona, Spain
E-mail: pau.rocas@irbbarcelona.org
M. Hoyos-Nogués, Dr. J. M. Manero,
Prof. J. Gil, Dr. C. Mas-Moruno
Biomaterials, Biomechanics and Tissue Engineering Group
Department of Materials Science and Metallurgical Engineering
and Centre for Research in NanoEngineering (CRNE)
Technical University of Catalonia (UPC)
08028 Barcelona, Spain
E-mail: carles.mas.moruno@upc.edu
M. Hoyos-Nogués, Dr. J. M. Manero, Prof. J. Gil,
Prof. F. Albericio, Dr. C. Mas-Moruno
Biomedical Research Networking Centre in Bioengineering
Biomaterials and Nanomedicine (CIBER-BBN)
08028 Barcelona, Spain
Dr. J. Rocas
Nanobiotechnological Polymers Division
Ecopol Tech S.L., 43720 L'Arboç, Tarragona, Spain
Prof. F. Albericio
Department of Organic Chemistry
University of Barcelona
08028 Barcelona, Spain
Prof. F. Albericio
School of Chemistry & Physics
University of Kwazulu-Natal
Durban 4001, South Africa
Prof. F. Albericio
School of Chemistry
Yachay Tech
Yachay City of Knowledge
100119 Urcuquí, Ecuador

investigated.[1,3] Thus, cell adhesive peptides and proteins from the extracellular matrix (ECM) have been immobilized aiming at increasing the material's capacity to improve the adhesion of osteoblast cells.[4] Alternatively, antimicrobial coatings including antifouling polymers, drug releasing matrices or bactericidal peptide sequences, have also been developed.[5]

As evidenced by recent research and debate in the literature, it is expected that the combination of distinct biological functions on the surface may improve the biological performance of classical biomaterials.[6] However, the majority of current strategies only focus on either improving cell adhesion or reducing bacterial adherence. Thus, the aim of the present study was to exploit the novel concept of multifunctionality by simultaneously installing cell adhesive and antimicrobial properties on the surface of Ti.

Herein, we present a new class of shell-stratified amphiphilic polyurethane-polyurea nanoparticles (PUUa NPs, **Figure 1**A).[7] These innovative nanopolymeric systems display the following unique features:

(i) NPs shell decorated with an $\alpha v\beta3$-selective cyclic RGD peptide, which provides cell specificity.
(ii) High capacity to encapsulate hydrophobic drugs in the NPs oily core.

The RGD peptide motif, an integrin-binding sequence present in natural ECM proteins, such as fibronectin and vitronectin,[8] is a common cell adhesive motif used to enhance biointegrative effects on biomaterials.[9] In particular, the cyclic RGD peptide cRGDfK, designed and developed by Kessler and co-workers,[10] has gained increasing interest over the last years due to its much higher specificity toward integrins $\alpha v\beta3$ and $\alpha v\beta5$, which are widely expressed by osteoblasts and bone precursors, and capacity to effectively promote osseointegrative events.[11] Moreover, encapsulation of an antibiotic drug in the PUUa NPs would tackle another recurrent problem: bacterial infection associated with orthopedic and dental implants surgery. In this regard, the drug roxithromycin (Rx) was considered a promising candidate due to its potent antibacterial and anti-inflammatory effects.[12] Moreover, the lipophilicity of this drug (log P 2.9) ensured its effective encapsulation into PUUa NPs via hydrophobic interactions.[13] Thus, PUUa NPs represent an unprecedented dual approach to improve the osseointegration of implant materials: accelerated osteoblast adhesion and inhibition of bacterial infection (Figure 1B). To functionalize Ti materials, in this work we will focus on a novel approach we
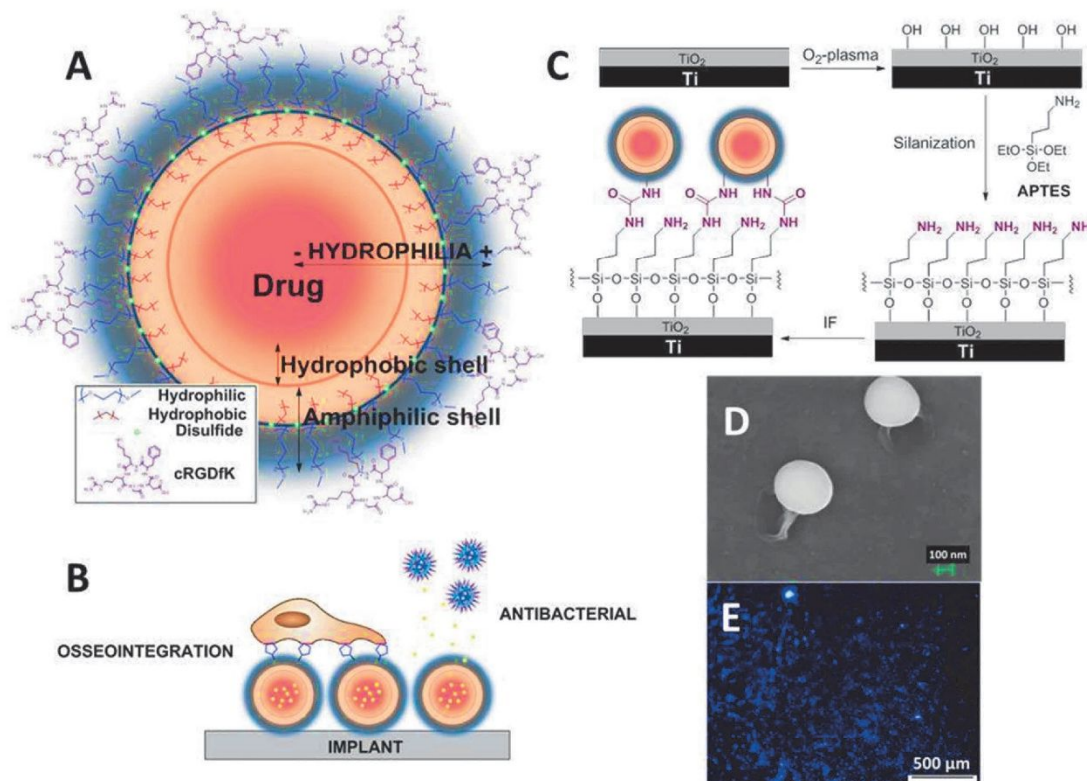
COMMUNICATION

Figure 1. Installing multifunctionality on Ti. A) Schematic representation of the stratified structure of PUUa NPs. B) A dual biological activity on Ti implants. C) Methodology to immobilize PUUa NPs on Ti by means of interfacial functionalization. D) Morphology of EDA-crosslinked PUUa NPs by scanning electron microscopy. E) Ti surfaces coated with fluorescently labeled EDA-crosslinked PUUa NPs.

described as interfacial functionalization (IF), where PUUa NPs bearing isocyanate reactivity and Ti surfaces containing superficial amino groups react to create highly stable urea bonds in the metal-nanocoating interface (Figure 1C). Significantly, one of the major advantages of this technique relies on the efficient and well established polyurethane and polyurea chemistry in the field of industrial coatings and biomedical devices.[14] Another key point of this methodology with respect to other approaches is the wide range of molecules that can be either hydrophobically encapsulated or covalently conjugated via quantitative urethane and/or urea bonds in the polymer backbone.

The production of PUUa NPs was based on the synthesis and self-assembly of a reactive amphiphilic prepolymer designated as Amphil (Figure S1, Supporting Information). This prepolymer bears two terminal isocyanate groups and multiple pendant hydrophilic and hydrophobic chains, which represent key structural features to mediate the stratification of the PUUa shell in the oil–water interface. Given the fact that the hydrophilic dangling chains of Amphil self-orient toward the water phase, while hydrophobic chains orient into the oily core, an increasing gradient of hydrophilicity is created from the hydrophobic core to the outer shell. This process stabilizes the structure of PUUa NPs in water and encapsulates the hydrophobic

shell with the drug in the inner core. Hence, such emulsification process yields a hydrophobically stratified PUUa NP with high encapsulation efficiency and capacity (see the Supporting Information for details).

Emulsification in water of the reactive prepolymers was followed by a precrosslinking step to fix the amphiphilic structure of the PUUa NPs. To this end, a diamino molecule was added to crosslink 50% of the total amount of free isocyanate functional groups of the shell (Figure S3, Supporting Information). This methodology ensured that PUUa NPs still contained accessible reactive isocyanate groups for further functionalization.

As schematized in Figure 1C, Ti surfaces were activated by oxygen plasma treatment followed by amino-silanization with (3-aminopropyl)triethoxysilane (APTES) to obtain an accessible monolayer of amino groups. Next, amino-activated Ti disks were immersed in reactive PUUa NPs and left to react during either 1 h or overnight (ON) both at 5 °C to prevent reaction of isocyanate groups with water. After such time, the remaining unreacted isocyanate groups in the NP shell were totally crosslinked adding the 100% of the crosslinking diamine.

To characterize the presence and distribution of PUUa NPs on Ti as well as to optimize the process of surface biofunctionalization, the fluorophore Clear Blue DFSB-C0 was encapsulated

Materials
Views

ADVANCED
HEALTHCARE
MATERIALS

COMMUNICATION

into the PUUa NPs and the fluorescence intensity on the NP-coated surfaces quantified by microscopy. Two crosslinking diamines of different hydrophilicity were used, L-lysine (Lys) or ethylenediamine (EDA). Moreover, two surface immobilization times were studied, 1 h and ON. As shown in Figure S4, Supporting Information, statistically significant higher densities of PUUa NPs were achieved at longer incubation times and when using EDA as crosslinker. Based on these data, the use of EDA and 1 h of incubation seemed to be optimal conditions for surface biofunctionalization.

Fluorescence analysis also revealed a very homogenous distribution of the PUUa NPs under all conditions (Figure 1E and Figure S5, Supporting Information). Moreover, scanning electron microscopy corroborated the presence of the PUUa NPs, which showed a well-defined spherical shape and suggested the formation of "root-like" polymeric linkages with the metallic surface (Figure 1D and Figure S6, Supporting Information).

The stability of the coatings was also analyzed with PUUa NPs that contained the fluorophore cadaverine-Oregon Green 488 covalently anchored via urea bonds. These NPs were immobilized on Ti surfaces and their stability analyzed after one and two weeks of incubation in phosphate-buffered saline (PBS) under orbital agitation. The binding of PUUa NPs onto Ti was proven stable under these conditions (Figure S7, Supporting Information).

As previously introduced, PUUa NPs were decorated with the integrin selective cRGDfK peptide to convey osseointegrative properties to the surfaces. For such purpose, the free primary amine of the Lys residue of cRGDfK was the cornerstone of our experimental design because represented the functionalization point between the polymeric shell and the peptide. Thus, the hydrophilic polyisocyanate linker Bayhydur 3100 (B3100)[15] was bounded to cRGDfK without affecting its bioactivity and capacity to mediate the specific interaction with $\alpha v \beta 3$ integrin receptors[10b] (Figure S1B, Supporting Information).

As monitored by MALDI-TOF MS and HPLC techniques (Figure S10 and Table S2, Supporting Information), B3100 reacted in a quantitative manner via urea linkage with cRGDfK peptide in PBS. At this point, the resulting hydrophilic B3100-cRGDfK reactive conjugate was added to the prepolymers mixture, homogenized and coemulsified leading to PUUa NPs encompassing the cRGDfK functionality in the outer shell (Figure S2, Supporting Information).

To determine the capacity of these functionalized biomaterials to trigger osteoblast-like cell adhesion, PUUa NPs-coated materials, and their controls, were incubated with sarcoma osteogenic (Saos-2) cells for 4 h and the number and area of adherent cells analyzed (**Figure 2**). Noteworthy, the presence of RGD-decorated PUUa NPs (Lys RGD or EDA RGD) yielded an outstanding increase in both cell attachment and spreading compared to uncoated (Ctrol) or aminosilanized (APTES) Ti ($p < 0.05$) (Figure 2A,B). In particular, cells seeded on surfaces coated with RGD-containing NPs developed clear actin filaments, and a well-defined cytoskeleton with some nascent focal adhesions (see Figure 2C). PUUa NPs not expressing the RGD motif (Lys or EDA) also enhanced cell binding compared to plain Ti, however these values were statistically lower ($p < 0.05$) than those achieved for RGD-decorated NPs. Moreover, PUUa NPs without the RGD motif failed to stimulate an adequate cell spreading and cytoskeleton (Figure 2), thus indicating that integrin binding and activation is required to successfully support cell adhesion.[16] Interestingly, the highest efficiency in cell adhesion was observed when EDA was used as crosslinking diamine, which is in agreement with previous surface characterization data (see Figure S4, Supporting Information). To demonstrate the long-term biological functionality of these coatings, cell proliferation studies were also performed for one and two weeks of incubation (Figure S11, Supporting Information). Of note, surfaces biofunctionalized with EDA RGD supported and promoted the growth of Saos-2 cells with
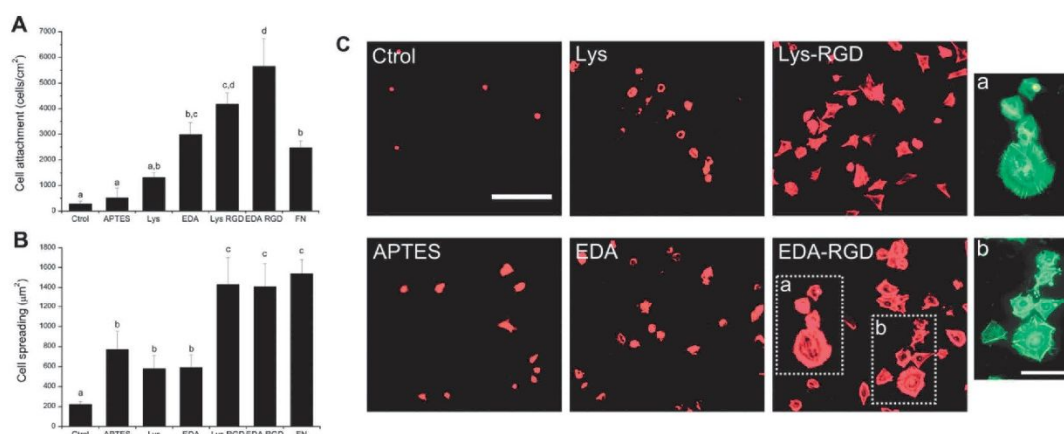
Figure 2. Adhesion of Saos-2 cells on biofunctionalized Ti surfaces after 4 h of incubation in serum free medium. A) Cell attachment (cells cm^{-2}). B) Cell spreading (averaged cell area, μm^2). Cell numbers and spreading were analyzed by immunostaining and fluorescence microscopy. Distinct letters denote statistically significant differences ($p < 0.05$) between groups. C) Visualization of actin filaments with phalloidin-rhodamine staining (scale bars: 200 μm). Visualization of vinculin on Ti surfaces functionalized with EDA-RGD was done with mouse anti-vinculin and anti-mouse Alexa 488 at a higher magnification (images a and b, scale bar: 100 μm).

COMMUNICATION

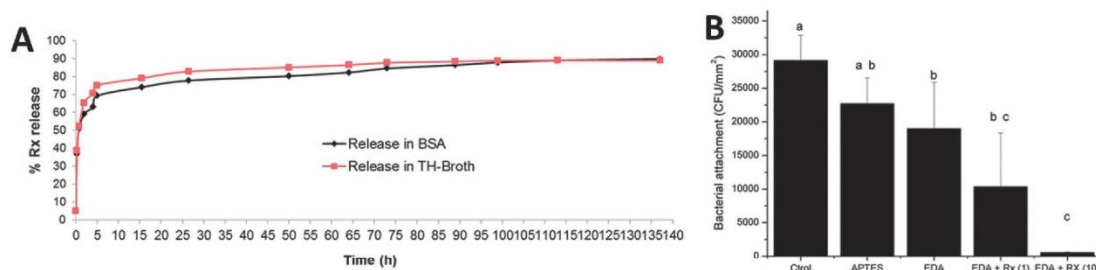**Figure 3.** A) Cumulative release profiles of Rx in Todd-Hewitt (TH) broth (red) and in BSA-liposomes (black). B) Bacterial adhesion of *S. sanguinis* on biofunctionalized Ti surfaces after 4 h of incubation in TH broth. Distinct letters denote statistically significant differences ($p < 0.05$) between groups.

proliferation rates statistically comparable to those obtained with the ECM protein fibronectin.

Incorporation of antibacterial properties to the Ti surface was the final step of our studies. In this regard, the antibiotic drug Rx was selected and encapsulated in our system. The encapsulation efficiency (EE) and drug loading (DL) of Rx into PUUa NPs was of 95% ± 1% and 9.5% ± 0.1%, respectively, as proved by HPLC analysis. Moreover, its in vitro drug release was monitored by mixing Rx-loaded PUUa NPs with either bacterial growth medium or a protein and lipid-rich buffer, which aims to mimic physiological conditions (**Figure 3**A).

Interestingly, crosslinked PUUa NPs released 60%–70% of the encapsulated drug during the first 4–6 h of incubation. Such initial burst release would respond to the elevated risk of bacterial infection described for implant materials during the 6 h post-implantation period,[17] followed by a prolonged and sustained antibacterial effect.

Thus, as a final proof of concept study, Ti surfaces were functionalized with PUUa NPs loaded with Rx, and bacterial adhesion to these surfaces investigated after 4 h of incubation. *Streptococcus sanguinis* was chosen as model bacteria because this oral strain is commonly involved in peri-implantitis and other implant-related pathologies.[18] The susceptibility of this bacterial strain to Rx was demonstrated in preliminary assays (Figures S12 and S13, Supporting Information). As illustrated in Figure 3B, PUUa NPs containing Rx were able to strongly suppress *S. sanguinis* adhesion in a concentration-dependent manner. The efficacy of our coating system after the initial burst release of the drug was also investigated. To this end, biofunctionalized samples were first incubated in TH broth for 20 h (i.e., a time point where more than the 70% of the drug is released, see Figure 3A) and bacterial adhesion checked afterward. Noteworthy, biofunctionalized surfaces were still able to significantly inhibit bacterial adhesion on Ti substrates (inhibition rate of 76%, see Figure S14, Supporting Information). Therefore, PUUa NPs are not only effective in preventing initial bacterial colonization but also reducing the risk of repetitive or late bacterial infection. Furthermore, the presence of Rx did not affect the positive effects previously observed on Saos-2 cell adhesion (Figure S15, Supporting Information), thereby proving the feasibility of our strategy to confer multifunctionality to Ti-based materials.

To conclude, we have described a novel methodology to produce PUUa NPs and their immobilization on Ti surfaces. These

systems combine outstanding cell-adhesive and antibacterial properties and thus represent excellent candidates to install multifunctionality on metallic surfaces in order to develop new generation biomaterials for bone regeneration.

Supporting Information

Supporting Information is available from the Wiley Online Library or from the author.

Acknowledgements

[1] a) C. Mas-Moruno, M. Espanol, E. B. Montufar, G. Mestres, C. Aparicio, F. J. Gil, M. P. Ginebra, in *Biomaterials Surface Science* (Eds: A. Taubert, J. F. Mano, J. C. Rodríguez-Cabello), Wiley-VCH, Weinheim, Germany, **2013**, pp. 337–374; b) S. Bauer, P. Schmuki, K. von der Mark, J. Park, *Prog. Mater. Sci.* **2013**, *58*, 261.

[2] a) A. G. Gristina, *Science* **1987**, *237*, 1588; b) A. Lee, H.-L. Wang, *Implant Dent.* **2010**, *19*, 387; c) R. P. Darveau, *Nat. Rev. Microbiol.* **2010**, *8*, 481; d) P. A. Norowski, J. D. Bumgardner, *J. Biomed. Mater. Res. Part B: Appl. Biomater.* **2009**, *88*, 530.

[3] a) R. Tejero, E. Anitua, G. Orive, *Prog. Polym. Sci.* **2014**, *39*, 1406; b) M. A. Fernandez-Yague, S. A. Abbah, L. McNamara, D. I. Zeugolisa, A. Pandit, M. J. Biggs, *Adv. Drug Delivery Rev.* **2014**, 2015, 84, 1, DOI: 10.1016/j.addr.2014.09.005.

[4] a) A. Shekaran, A. J. García, *J. Biomed. Mater. Res. A.* **2011**, *96*, 261; b) K. von der Mark, J. Park, *Prog. Mater. Sci.* **2013**, *58*,

COMMUNICATION

327; c) R. Fraioli, F. Rechenmacher, S. Neubauer, J. M. Manero, J. Gil, H. Kessler, C. Mas-Moruno, *Colloid. Surf., B* **2015**, *128*, 191.

[5] a) I Banerjee, R. C. Pangule, R. S. Kane, *Adv. Mater.* **2011**, *23*, 690; b) K. Glinel, P. Thebault, V. Humblot, C.M. Pradier, T. Jouenne, *Acta Biomater.* **2012**, *8*, 1670; c) M. Godoy-Gallardo, C. Mas-Moruno, M. C. Fernández-Calderón, C. Pérez-Giraldo, J. M. Manero, F. Albericio, F. J. Gil, *Acta Biomater.* **2014**, *10*, 3522; d) L. Zhang, C. Ning, T. Zhou, X. Liu, K. W. K. Yeung, T. Zhang, Z. Xu, X. Wang, S. Wu, P. K. Chu, *ACS Appl. Mater. Interfaces* **2014**, *6*, 17323; e) M. Godoy-Gallardo, C. Mas-Moruno, K. Yu, J. M. Manero, F. J. Gil, J. N. Kizhakkedathu, D. Rodriguez, *Biomacromolecules* **2015**, *16*, 483; f) E. M. Hetrick, M. H. Schoenfisch, *Chem. Soc. Rev.* **2006**, *35*, 780.

[6] a) D. F. Williams, *Biomaterials* **2011**, *32*, 4195; b) C. Mas-Moruno, R. Fraioli, F. Albericio, J. M. Manero, F. J. Gil, *ACS Appl. Mater. Interfaces* **2014**, *6*, 6525; c) W. Lin, C. Junjian, C. Chengzhi, S. Lin, L. Sa, R. Li, W. Yingjun, *J. Mater. Chem. B* **2015**, *3*, 30; d) W.-N. Yin, F.-Y. Cao, K. Han, X. Zeng, R.-X. Zhuo, X.-Z. Zhang, *J. Mater. Chem. B* **2014**, *2*, 8434.

[7] a) J. Rocas Sorolla, P. Rocas Alonso, (Ecopol Tech S.L.) WO 2014114838 A3, **2014**; b) P. Rocas, Y. Fernández, S. Schwartz, I. Abasolo, J. Rocas, F. Albericio, unpublished.

[8] a) M. D. Pierschbacher, E. Ruoslahti, *Nature* **1984**, *309*, 30; b) E. Ruoslahti, M. D. Pierschbacher, *Science* **1987**, *238*, 491.

[9] U. Hersel, C. Dahmen, H. Kessler, *Biomaterials* **2003**, *24*, 4385.

[10] a) M. Aumailley, M. Gurrath, G. Müller, J. Calvete, R. Timpl, H. Kessler, *FEBS Lett.* **1991**, *291*, 50; b) R. Haubner, R. Gratias, B. Diefenbach, S. L. Goodman, A. Jonczyk, H. Kessler, *J. Am. Chem. Soc.* **1996**, *118*, 7461.

[11] a) J. Auernheimer, D. Zukowski, C. Dahmen, M. Kantlehner, A. Enderle, S. L. Goodman, H. Kessler, *ChemBioChem* **2005**, *6*, 2034; b) B. Elmengaard, J. E. Bechtold, K. Soballe, *Biomaterials* **2005**, *26*, 3521; c) K. A. Kilian, M. Mrksich, *Angew. Chem.* **2012**, *124*, 4975; d) C. Mas-Moruno, P. M. Dorfner, F. Manzenrieder, S. Neubauer, U. Reuning, R. Burgkart, H. Kessler, *J. Biomed. Mater. Res. A.* **2013**, *101*, 87.

[12] K. V Rolston, D. H. Ho, B. LeBlanc, G. P. Bodey, *Eur. J. Clin. Microbiol. Infect. Dis.* **1990**, *9*, 30.

[13] A. Chen, US20050049209 A1, **2005**.

[14] a) N. M. K. Lamba, K. A. Woodhouse, S. L. Cooper, *Polyurethanes in Biomedical Applications*, CRC Press, Florida, **1997**; b) S. J. Stachelek, C. Song, I. Alferiev, S. Defelice, X. Cui, J. M. Connolly, R. W. Bianco, R. J. Levy, *Gene Ther.* **2004**, *11*, 15.

[15] H. J. Laas, T Hassel, W Kubitza, K. Noll, (Bayer AG) US5252696 A, **1993.**

[16] M. C. Siebers, P. J. ter Brugge, X. F. Walboomers, *Biomaterials* **2005**, *26*, 137.

[17] a) E. M. Hetrick, M. H. Schoenfisch, *Chem. Soc. Rev.* **2006**, *35*, 780; b) M. Zilberman, J. J. Elsner, *J. Controlled Release* **2008**, *130*, 202; c) J. Geurts, J. J. Chris Arts, G. H. Walenkamp, *Injury* **2011**, *42*, S82.

[18] P. E. Kolenbrander, R. J. Palmer, S. Periasamy, N. S. Jakubovics, *Nat. Rev. Microbiol.* **2010**, *8*, 471.

wileyonlinelibrary.com 5

Supporting Information

Installing Multifunctionality on Titanium with RGD-decorated Polyurethane-Polyurea Roxithromycin Loaded Nanoparticles: Towards New Osseointegrative Therapies**

Pau Rocas*, Mireia Hoyos-Nogués, Josep Rocas, José M. Manero, Javier Gil, Fernando Albericio, Carlos Mas-Moruno*

TABLE OF CONTENTS

1. Chemicals
2. Experimental section
3. Analytical techniques
4. Cell adhesion studies
5. Antibacterial studies
6. Statistical analysis

1. Chemicals

Cyclo(-Arg-Gly-Asp-D-Phe-Lys) (cRGDfK) was synthesized in house according to previously reported protocols[1]. YMER N-120 was kindly provided by Perstorp (Perstorp, Sweden) and N-Coco-1,3-propylenediamine (TAP 100D) by Clariant (Barcelona, Spain). Capric/caprylic triglyceride mixture (Crodamol GTCC) was obtained from Croda (Barcelona, Spain) and Bayhydur 3100 was purchased from Bayer (Leverkusen, Germany). Clear Blue DFSB-C0 was kindly provided from Risk Reactor Inc. (Santa Ana, CA, USA). Oregon Green 488 Cadaverine was purchased from Life Technologies (Grand Island, NY, USA). If not indicated otherwise, all other reagents were purchased from Sigma-Aldrich (St Louis, MO, USA). Extra dry grade acetone was used in every step of the polymers syntheses.

2. Experimental methods

2.1. Preparation of titanium disks

Titanium (Ti) disks (2 mm thick, 10 mm diameter) were obtained from commercially pure (c.p.) cylindrical Ti bars (Technalloy S.A., Sant Cugat del Vallès, Spain). After turning, Ti surfaces were sequentially grinded with abrasive silicon carbide papers (Neuertek S.A., Eibar, Spain; Beortek S.A., Asua-Erandio, Spain) of decreasing grit size (from P800, P1200 and P2500 - European P-grade standard). Smooth surfaces (Ra ≤ 40 nm) were finally achieved by polishing with suspensions of alumina particles (1 μm and 0.05 μm particle size) on cotton clothes. After polishing, mirror-like samples were ultrasonically cleaned with ciclohexane, isopropanol, distilled water, ethanol and acetone (3 x 2 min), and stored dry under vacuum. The average roughness of each sample after this process was assessed by white light interferometry using a Wyko NT9300 Optical Profiler (Veeco Instruments, New York, NY, USA).

2.2. Surface activation and silanization

Prior to silanization, samples were activated by oxygen plasma treatment. To this end, Ti samples were placed in a low-pressure plasma Femto reactor (Diener electronic, Ebhausen, Germany) and treated with oxygen plasma at 100 W and 0.5 mbar for 5 min. These conditions were optimized to yield highly hydrophilic surfaces, as indicated by wettability measurements (not shown). After this treatment, samples were immediately immersed in anhydrous toluene and silanized with (3-aminopropyl)triethoxysilane (APTES) (2 %, v/v) for 1 h at 70 °C under nitrogen atmosphere. Samples were then subjected to ultrasonication in toluene (5 min) to remove non-covalently bound silanes, and extensively rinsed with toluene, distilled water, ethanol and acetone. Samples were finally dried with nitrogen and the silane layer cured at 120 °C for 5 min. This method was adapted, with some modifications, from previously reported protocols[2].

2.3. Preparation of prepolymers

2.3.1 Preparation of the reactive amphiphilic prepolymer (Amphil).

The synthesis of the Amphil prepolymer was conducted on a 500 mL reaction vessel, which was initially pre-heated at 50 °C and purged with nitrogen. Then, YMER N-120 (5.50 g, 5.5 mmol), DEDS (0.30 g, 2.0 mmol), IPDI (3.38 g, 15 mmol), Crodamol GTCC (0.75 g) as oily core and DBTL (3 mg, 4,65 µmol) as catalyst were added to the reaction vessel under mechanical stirring to synthesize Hyfil, a reactive polyurethane prepolymer. The polyaddition reaction was followed by FT-IR, automatic titration and the final prepolymer characterized by NMR (Figure S8 and Figure S9 respectively)[3]. After 4 h of reaction, the vessel was cooled to 40 °C and TAP 100D (1.375 g, 4.28 mmol), dissolved in 10 g acetone as co-solvent, was added under constant agitation and kept under these conditions for 30 min to form Amphil, a reactive polyurethane-polyurea prepolymer. See Figure S1 A.

2.3.2 Preparation of Bayhydur 3100-cRGDfK conjugate (B3100-cRGDfK). The peptide cRGDfK (36 mg, 0.0596 mmol) was dissolved in phosphate buffered saline (PBS) (1 mL, 5ºC) and 10 µL of pure triethylamine were added to the solution. Then, this solution was mixed with the linker Bayhydur 3100 (125 mg, 0.167 mmol) and left to react for 2 h at 5 ºC under constant agitation. See Figure S1 B.

2.4. Synthesis of PUUa NPs

2.4.1. Synthesis of Clear Blue fluorescent PUUa NPs. Lysine (Lys) as crosslinker.
IPDI (0.485 g, 2.18 mmol) was added to the Amphil reaction vessel (see section 2.3.1) (mass ratio Amphil 21.75:1 IPDI) and were readily mixed during 10 min and purged with N_2. Then, an aliquot of this Amphil+IPDI mixture (1.785 g) was homogenized in another round-bottom flask with B3100 (125 mg, 0.167 mmol) and the lipophilic fluorophore Clear Blue DFSB-C0 (5 mg, 11.61 µmol). This organic mixture was emulsified in PBS (16.5 mL, pH 7.4, 5 ºC) with a magnetic stirrer under an ice bath to prevent isocyanate reaction with water. Once emulsified, Lys (152 mg, 1.04 mmol) was either added to crosslink 100 % of the total amount of free isocyanate groups or added to crosslink just 50 % of free isocyanate groups (Lys amount needed= 76 mg, 0.52 mmol) and left for 30 min. The reaction was followed by FT-IR. After this time, 100 % crosslinked PUUa NPs were used for characterization studies, and 50 % crosslinked reactive PUUa NPs to functionalize Ti surfaces (see below).

2.4.2. Synthesis of RGD-functionalized PUUa NPs. Lys as crosslinker. An aliquot consisting of a mixture of Amphil and IPDI (1.785 g) was prepared as previously described and mixed with the Bayhydur B3100-cRGDfK conjugate solution (16.1 % w/w) (see section 2.3), followed by emulsification in PBS and crosslinking with Lys as previously detailed (see section 2.4.1).

2.4.3. Synthesis of Clear Blue fluorescent PUUa NPs. Ethylene diamine (EDA) as crosslinker. The synthesis of these NPs was conducted as described above (see section 2.4.1) using EDA as crosslinking amine instead of Lys.

2.4.4. Synthesis of RGD-functionalized PUUa NPs. EDA as crosslinker. The synthesis of these NPs was done as detailed in section 2.4.2 but using EDA instead of Lys as crosslinking unit.

2.4.5. Synthesis of Oregon Green 488 Cadaverine fluorescent PUUa NPs. EDA as crosslinker. IPDI (0.485 g, 2.18 mmol) was added to the Amphil reaction vessel (see section 2.3.1) (mass ratio Amphil 21.75:1 IPDI) and were readily mixed during 10 min and purged with N_2. Then, an aliquot of this Amphil+IPDI mixture (0.87 g) was homogenized in another round-bottom flask with B3100 (62 mg, 0.084 mmol) and the fluorophore Oregon Green 488 Cadaverine (3.2 mg, 6.47 μmol), which contains a free primary amine that quantitatively reacts with isocyanate groups. Thus, Oregon Green 488 Cadaverine was left to react for 30 min with an excess of isocyanate-reactive species at 5 ºC in nitrogen atmosphere and magnetic stirring (278.75 mg polymer per mg of dye). At this point, the prepolymers were emulsified in water and the synthesis of these NPs was conducted as described above (see section 2.4.1) using EDA as crosslinking amine instead of Lys.

2.4.6. Synthesis of all-in PUUa NPs (NP-cRGDfK-roxithromycin). IPDI (0.485 g, 2.18 mmol) was added to the Amphil reaction vessel (see section 2.3.1) (mass ratio Amphil 21.75:1 IPDI) and were readily mixed during 10 min and purged purged with N_2. Then, an aliquot of this Amphil+IPDI mixture (1.785 g) was added to another round-bottom flask containing roxithromycin (220 mg, 0.26 mmol). As detailed in section 2.4.2, B3100-cRGDfK conjugate (16.1 % w/w) was added to this organic mixture under constant agitation followed by emulsification with PBS (16.5 mL, pH

7.4, 5 ºC) using a magnetic stirrer under an ice bath to prevent isocyanate reaction with water. Once emulsified, EDA (62.5 mg, 1.04 mmol) was either added to crosslink 100 % of the total amount of free isocyanate groups or added to crosslink just 50 % of free isocyanate groups (EDA amount needed=31.25 mg, 0.52 mmol) and left for 30 min. The reaction was followed by FT-IR. After this time, 100 % crosslinked PUUa NPs were used for MIC assays (see Figure S12) and roxithromycin encapsulation quantification. Alternatively, 50 % crosslinked reactive PUUa NPs were used to functionalize Ti surfaces (see below).

2.5. Functionalization of Ti surfaces with PUUa NPs

Aminosilanized Ti disks were immersed in a 20 mL emulsion containing 50 % crosslinked PUUa NPs (still bearing reactive isocyanate groups in the surface) and left to react for 1 h or overnight (ON) at 5 ºC under magnetic stirring. After this time, the remaining 50 % of crosslinker, either Lys (76 mg, 0.52 mmol) or EDA (31.25 mg, 0.52 mmol), was added and the non-reacted isocyanate groups were crosslinked forming urea bonds by interfacial polyaddition as proved by FT-IR. After the immobilization of the NPs, Ti samples were rinsed in milliQ water, air dried and stored under vacuum. The resulting surfaces functionalized with PUUa NPs, and their controls, are encoded as follows:

Ctrol: Ti surfaces non-functionalized
APTES: Ti surfaces silanized with APTES
FN: Ti surfaces functionalized with fibronectin (50 µg/mL)
EDA / EDA 1h: Ti surfaces silanized with APTES and functionalized with PUUa NPs for 1h crosslinked with ethylenediamine.

EDA ON: Ti surfaces silanized with APTES and functionalized with PUUa NPs overnight crosslinked with ethylenediamine.
EDA RGD: Ti surfaces silanized with APTES and functionalized with RGD-decorated PUUa NPs for 1h crosslinked with ethylenediamine.
Lys / Lys 1h: Ti surfaces silanized with APTES and functionalized with PUUa NPs for 1h crosslinked with L-Lysine.
Lys ON: Ti surfaces silanized with APTES and functionalized with PUUa NPs overnight crosslinked with L-Lysine.
Lys RGD: Ti surfaces silanized with APTES and functionalized with RGD-decorated PUUa NPs for 1h crosslinked with L-Lysine
EDA-RGD + Rx: Ti surfaces silanized with APTES and functionalized with RGD-decorated PUUa NPs encapsulating Rx crosslinked with ethylenediamine.

3. Analytical techniques

3.1. Chemical characterization

3.1.1. Quantification of conjugated cRGDfK peptide to PUUa NPs. To quantify the total amount of bound peptide to PUUa NPs, a calibration curve was performed by preparing standard solutions of cRGDfK peptide containing L-phenylalanine amide as internal standard for quantitative HPLC analysis. Analytical HPLC runs of the NP-RGD were performed in a WATERS 2998 HPLC (Milford, MA, USA) using a X-Bridge BEH130, C18, 3.5 µm, 4.6 X 100 mm reverse phase column with the following gradient: 5 to 30 % of B in 9 min at a flow rate of 1 mL/min; eluent A: H_2O with 0.045 % trifluoroacetic acid (TFA) (v/v); eluent B: CH_3CN with 0.036 % TFA (v/v) with UV detection at 220 nm.

3.1.2. Drug loading (DL) and encapsulation efficiency (EE) of Rx into PUUa NPs.

To quantify the total amount of encapsulated Rx into PUUa NPs, a calibration curve was performed by preparing standard solutions of Rx in $CH_3CN:KH_2PO_4$ buffer (30:70 v/v) adjusted to pH 5.3 with dilute ammonia for HPLC analysis. A volume of 0.5 mL of PUUa NPs 10 % (w/w) was placed into a centrifugal 3 KDa filter unit (Microcon, Carrigtwohill, Ireland) and centrifuged at 14000 g for 45 min. Analytical HPLC runs of the filtrate were performed by triplicate in a WATERS 2998 HPLC using a X-Bridge BEH130, C18, 3.5 μm, 4.6 X 100 mm reverse phase column with the following gradient: 5 to 100 % of B in 8 min at a flow rate of 1 mL/min; eluent A: H_2O with 0.045 % TFA (v/v); eluent B: CH_3CN with 0.036 % TFA (v/v) with UV detection at 205 nm.

3.1.3 In vitro RX cumulative release. The release kinetics of Rx from PUUa NPs was determined using two different release media: i) Todd-Hewitt (TH) broth medium (Scharlab SL, Sentmenat, Spain), a common medium for bacterial growth, or ii) PBS containing 4 % (w/w) of bovine serum albumin (BSA) and 1 mM phosphatidylcholine-cholesterol (4:1 mol %) liposomes, which mimic in vivo physiological conditions. To determine the amount of Rx released from PUUa NPs, 2 mL of PBS-BSA-Liposomes or TH broth medium were mixed with 0.5 mL of PUUa NP-Rx (10 % w/w). Mixtures were incubated at 37 ºC during 137 h and centri-filtrated at appropriate time intervals with centrifugal 30 KDa filter units (Vivaspin 6, Sartorius, Göttingen, Germany) at 4000 g for 30 min. The filtrates were analysed by HPLC following the same protocol used for DL and EE analysis. The supernatant (non-filtered) was refilled either with fresh TH broth medium or 1 mM liposomes.

3.1.4. Infrared spectra (FT-IR). IR spectra were performed using a FT-IR Nexus Termo Nicolet 760 (Waltham, MA, USA) by depositing a drop of the previously dissolved prepolymers at 1 % in acetone (v/v) on a NaCl disk.

3.1.5. MALDI-TOF MS. To characterize the coupling reaction between c-RGDfK peptide and Bayhydur 3100 linker a MALDI-TOF analysis was carried out on an Applied Biosystems Voyager-DETMRP mass spectrometer (Waltham, MA, USA) using α-cyano-4-hydroxycinnamic acid (ACH) as matrix.

3.1.6. NMR analysis. ^{1}H, ^{13}C and HSQC NMR spectra were recorded on a Varian Mercury, 400 MHz (Agilent, Santa Clara, CA, USA). Reactive PUUa prepolymer (Amphil) was dissolved in $CDCl_3$ (285 mg/mL).

3.2. Characterization of Ti surfaces

The size (particle diameter) and distribution of the PUUa-NPs onto Ti surfaces was studied by means of scanning electron microscopy (SEM) and fluorescence microscopy.

3.2.1. Scanning electron microscopy. SEM analysis was conducted on a Zeiss Neon40 microscope (Carl Zeiss, Jena, Germany). For each sample, five images were taken at a working distance of 7 mm and a potential of 5 kV. Samples were analyzed by triplicate.

3.2.2. Fluorescence microscopy. Functionalized Ti with fluorescent NPs was then analyzed by fluorescence microscopy on a Nikon E600 (Nikon, Tokyo, Japan). The average intensity of five images per sample was measured by triplicate using ImageJ 1.46R software (NIH, Bethesda, MD, USA).

3.3. Stability of the coatings

Ti surfaces were coated with PUUa-NPs crosslinked with EDA, containing the fluorophore cadaverine-Oregon Green 488 covalently attached (see section 2.4.5) as explained in section 2.5. Non-functionalized Ti disks were used as negative controls. Next, samples were immersed in 500 μL of PBS and left under orbital agitation

protected from light. After 1 week and 2 weeks, the intensity of fluorescence of each

sample (five images per sample, three disks per condition) was analyzed via

fluorescence microscopy on a Nikon E600 and processed using ImageJ 1.46R software.

4. Cell studies

4.1. Cell culture

The human osteogenic sarcoma (Saos-2) cell line was chosen as osteoblast-like cellular

model. Saos-2 cells were cultured in McCoy's 5A medium (Sigma-Aldrich)

supplemented with 10% (v/v) fetal bovine serum (FBS), 1 M 4-(2-hydroxyethyl)-1-

piperazineethanesulfonic acid (HEPES), 1% (w/v) sodium pyruvate, 50 U/mL

penicillin, 50 μg/mL streptomycin and 1% (w/v) L-glutamine (all cell culture

supplements from Aldrich). Cells were cultured at 37 ^{0}C in a humidified incubator at

5% (v/v) CO_2, changing culture medium every 2-3 days. Subconfluent cells were

detached by trypsin-EDTA and subcultured into a new flask. All experiments were

performed using cells at passages between 25 and 35.

4.2. Analysis of cell adhesion by immunofluorescence

The analysis of short-term cell adhesion events on Ti surfaces biofunctionalized with

PUUa-NPs was conducted by means of immuno-staining of nuclei, actin fibers and

vinculin. To this end, Ti substrates were transferred into 48-well plates and blocked

with 1% (w/v) BSA in PBS for 30 min at room temperature. Next, Saos-2 cells were

seeded at a density of 25,000 cells/disk (50,000 cells/mL) and allowed to attach in

serum free medium at 37 ºC. After 4 h of incubation, samples were rinsed twice with

PBS to remove non-adherent cells and attached cells were fixed with 4% (w/v)

paraformaldehyde for 30 min. Cells were then permeabilized with 0.05% (w/v) triton X-

100 in PBS for 20 min and blocked with 1 % BSA (w/v) in PBS for 30 min. Washings

between all steps were performed with PBS-Gly (PBS containing 20 mM of glycine) for

3 x 5 min. Next, samples were incubated 1 h with mouse anti-vinculin primary antibody (1:100 in 1 % (w/v) BSA in PBS), and then with anti-mouse Alexa 488 (1:2000) and phalloidin-rodhamine (1:300) (both in triton 0.05 % (w/v) in PBS for 1 h in the dark). Finally, samples were incubated with 4',6-diamidino-2-phenylindole (DAPI) (1:1000) in PBS-Gly for 2 min in the dark and mounted on microscope slides. Cells were examined by fluorescence microscopy (Nikon E600) and images processed with ImageJ 1.46R software. The number of cells attached was measured by counting stained nuclei (five fields per disk, three disks per condition). Cell spreading was calculated by measuring the area of at least 10 cells for each sample and averaged for three samples for each condition. Cellular studies were done using triplicates and repeated at least in three independent assays to ensure reproducibility.

4.3. Analysis of cell proliferation

The capacity of the biofunctionalized samples to support cell proliferation was analyzed after 1 and 2 weeks of incubation using the indicator of cell viability Alamar Blue (Invitrogen Life Technologies, Merelbeke, Belgium). Thus, surfaces were functionalized, rinsed and blocked with BSA as previously explained, and Saos-2 cells seeded at a density of 10,000 cells/disk (20,000 cells/mL) in serum free medium. After 4 h of incubation, the medium was aspired and replaced with complete medium supplemented with FBS. On days 7 and 15, culture medium was replaced with fresh medium containing 10 % (v/v) of Alamar Blue and further incubated for 2.5 h. After this time, fluorescence of the dye was quantified (λ_{ex}= 560 nm; λ_{em}= 590 nm) using a multimode microplate reader (Infinite M200 PRO, Tecan Group Ltd., Männedorf, Switzerland) and cell numbers calculated with a standard curve.

5. Antibacterial studies

5.1. Bacterial strains, media and growth conditions

Bacterial assays were done with the bacterial strain *Streptococcus sanguinis* (CECT 480, *Colección Española de Cultivos Tipo (CECT)*, Spain), a well known early colonizer critically involved in oral biofilm formation and the onset of periodontitis[4] *S. sanguinis* was growth and maintained in TH broth (Scharlab SL). Cultures were incubated overnight at 37 ºC before each assay. Bacterial suspensions were adjusted by measuring optical density (0.2 ± 0.01 at 600 nm), giving approximately $1 \cdot 10^8$ colony forming units (CFU)/mL. All assays were performed using three replicates for each condition. Bacterial numbers were confirmed by a colony forming units (CFUs) count.

5.2. Analysis of bacterial adhesion on functionalized samples

Functionalized and sterilized (UV treatment for 5 min at 254 nm) Ti samples were placed into 48-well plates and incubated with 1 mL of bacterial suspensions ($1 \cdot 10^8$ CFU/mL) for 4 h at 37 ºC. After this incubation period, substrates were rinsed twice with sterile PBS to remove non-adherent bacteria. Then samples were transferred to graduated centrifuge tubes containing 1 mL of PBS and vortexed for 5 min to detach adherent bacteria. Serial dilutions of these bacteria were seeded on TH agar plates (Scharlab SL) and CFUs counted after 48 h of incubation at 37 ºC.

To determine the efficacy of our coating system after the initial burst release of roxithromycin (ca. 70%) observed within the initial 4-5 h, biofunctionalized samples were first sterilized with UV for 5 min and incubated in TH broth for 20 h at 37 ºC as explained for the drug release experiments (see section 3.1.3). After this treatment, samples were washed with sterile PBS and bacterial adhesion assays performed as detailed above.

5.3. Determination of the minimal inhibitory concentration (MIC)

Bacterial cell numbers were adjusted to approximately $1 \cdot 10^6$ CFU/mL and these solutions incubated with PUUa-NPs loaded with increasing concentrations of

roxithromycin (Rx) (0.48, 0.24, 0.12, 0.06, 0.03, 0.015, 0.0075 and 0.00375 µg/mL). In detail, 100 µL of each bacterial suspension were added to a 96-well plate already containing 100 µL/well of each Rx concentration by triplicate. The final volume in each well was 200 µL. Controls were prepared using only culture medium, bacterial suspensions or PUUa-NPs loaded with Rx. To monitor bacterial growth, the plate was incubated at 37 ºC for 16 hours and every 15 min, with prior mixing for 5 s, the absorbance was measured at 600 nm using a microplate reader (Infinite M200 PRO, Tecan Group Ltd., Männedorf, Switzerland).

6. Statistical analysis

Data presented in this study are given as mean values ± standard deviations. Significant differences between group means were analyzed either by ANOVA test followed by post-hoc pairwise comparisons using Tukey's test, or by Kruskal-Wallis non-parametric test followed by Mann-Whitney test. Confidence levels were set with $p < 0.05$ unless otherwise stated.
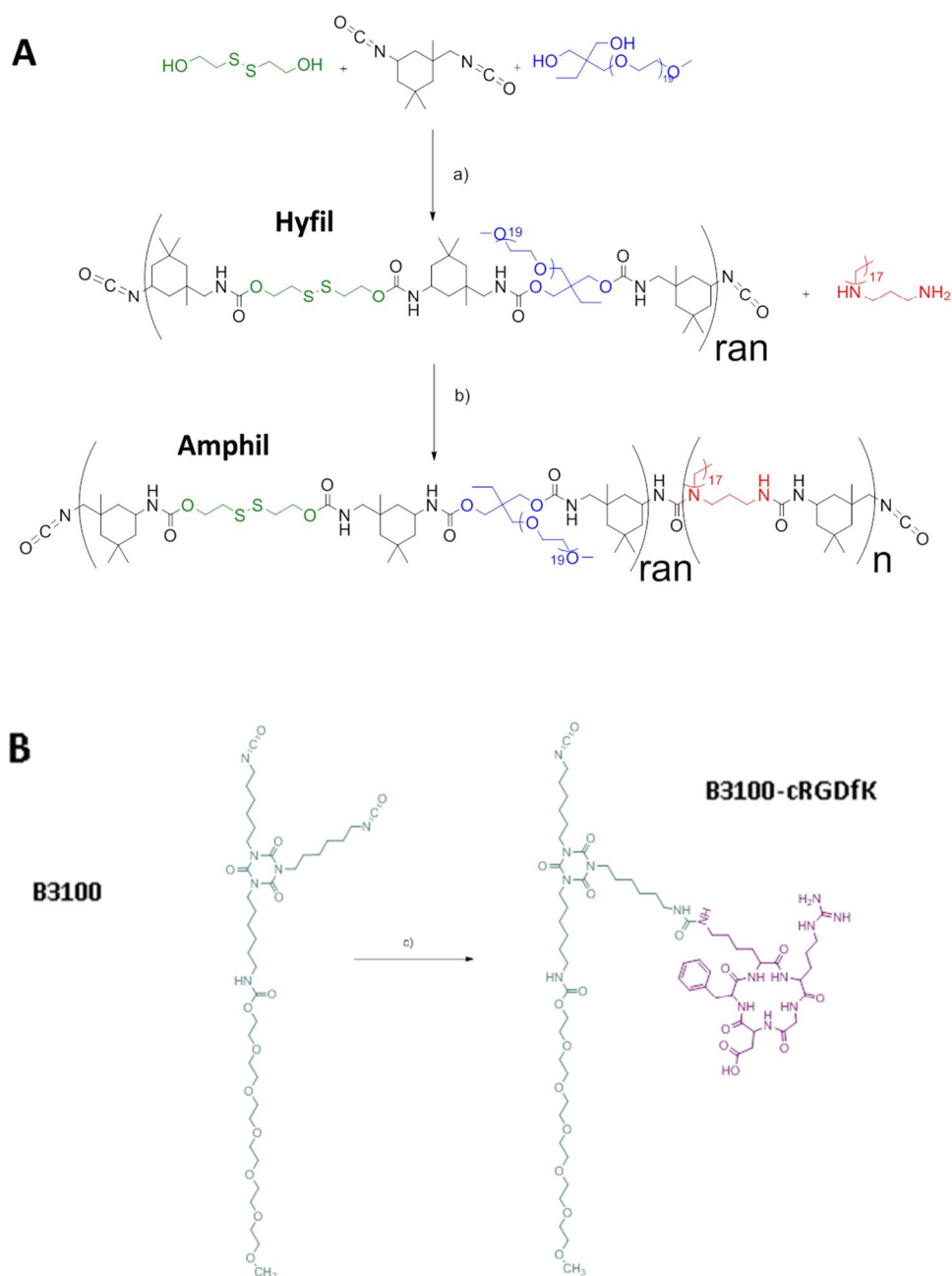
FIGURE S1

Figure S1. Synthesis of the reactive prepolymers Amphil (A) and B3100-cRGDfK (B). Reaction conditions for A: (a) DBTL (cat), Crodamol GTCC, N2, 50 ºC, 4 h (ran means random polymerization). b) Acetone, N2, 40 ºC, 30 min. For B: c) PBS, Et₃N (cat), 5ºC, 2 h.
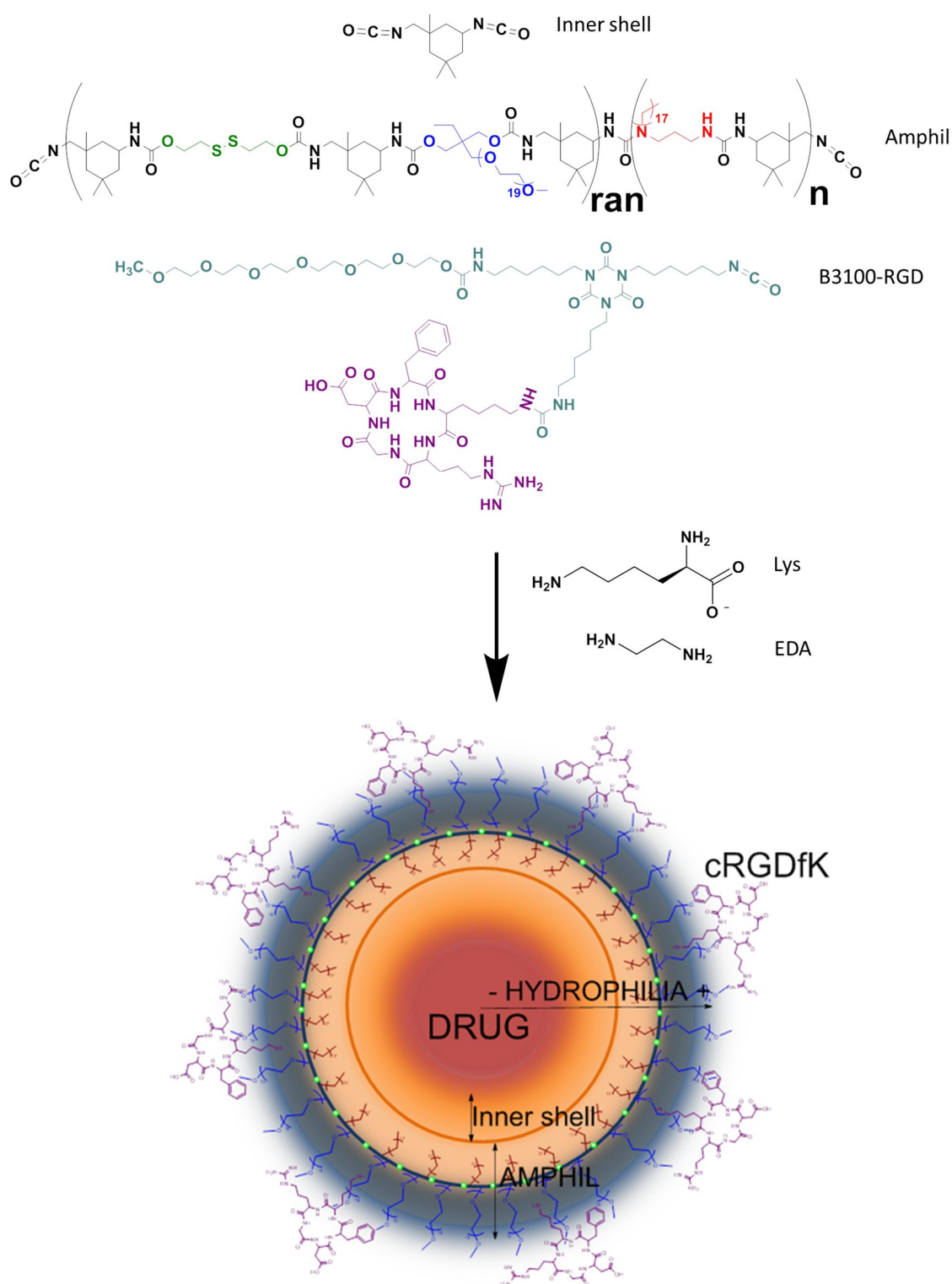
FIGURE S2

Figure S2. Schematic synthesis and stratified structure of a PUUa NP. Amphil, IPDI and B3100-RGD form the amphiphilic shell, inner shell and conjugated targeting peptide respectively. Crosslinking with Lys or EDA strengthens PUUa NP shell.
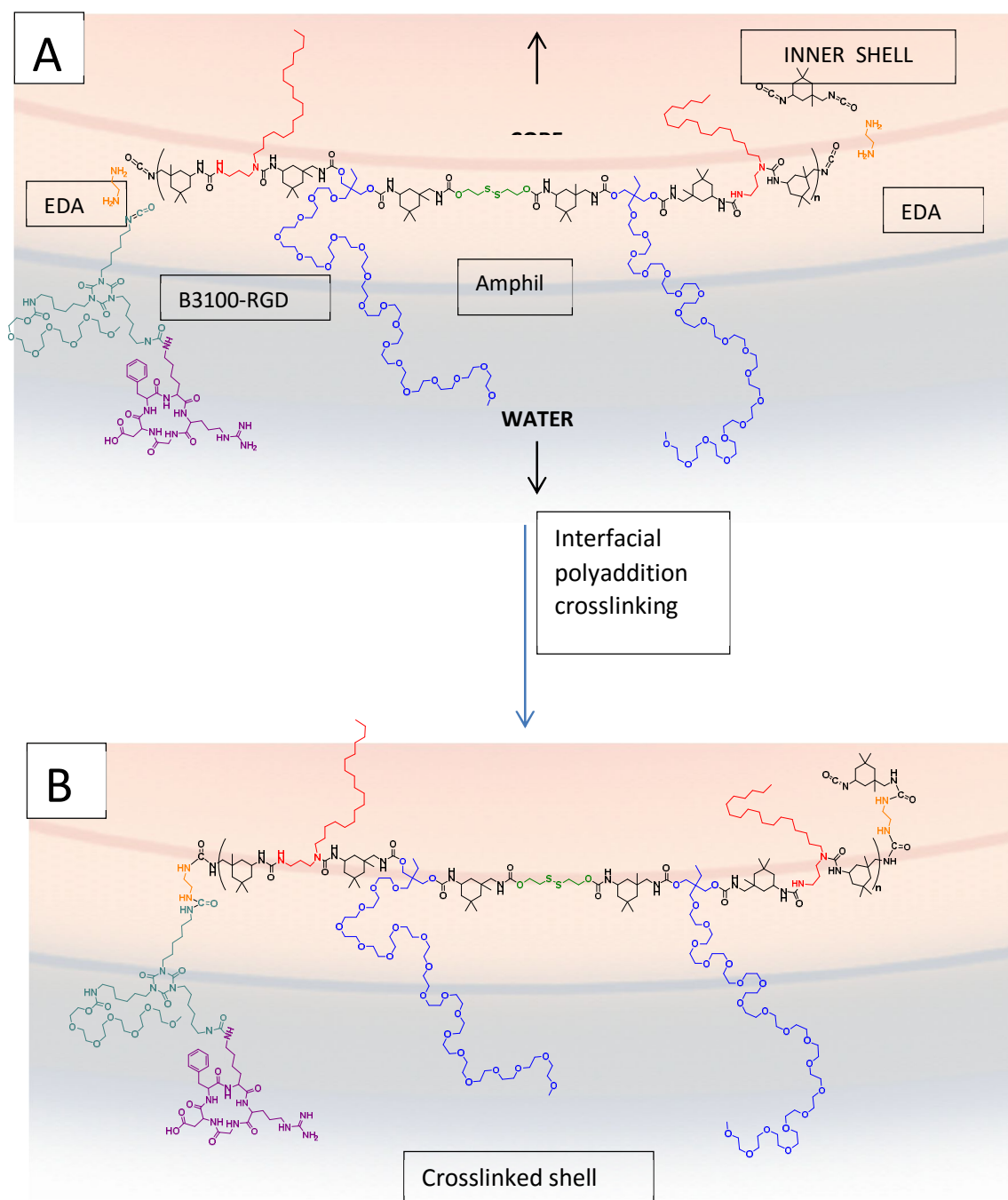
FIGURE S3

Figure S3. A) Crosslinking process of the PUUa NP shell. Amphil, IPDI and B3100-RGD self-stratify forming the shell after emulsification with water. B) After addition of EDA, interfacial polyaddition between the crosslinker and the reactive prepolymers occurs to form the crosslinked shell. EDA will fix the prepolymers by urea bonds creating a single structured shell.
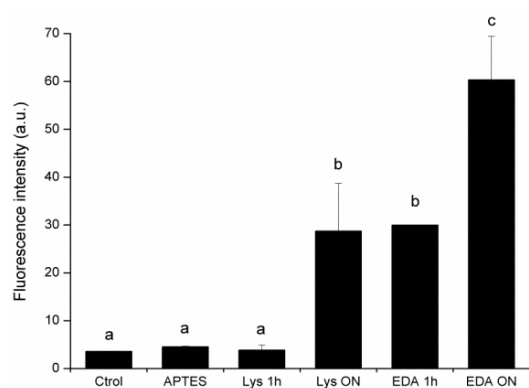
FIGURE S4

Figure S4. Fluorescence intensity of Ti samples functionalized with Clear Blue DFSB-C0-loaded PUUa-NPs and controls. Letters (a-c) denote statistically significant differences ($p < 0.05$) between groups. Values are expressed as mean ± standard deviation.

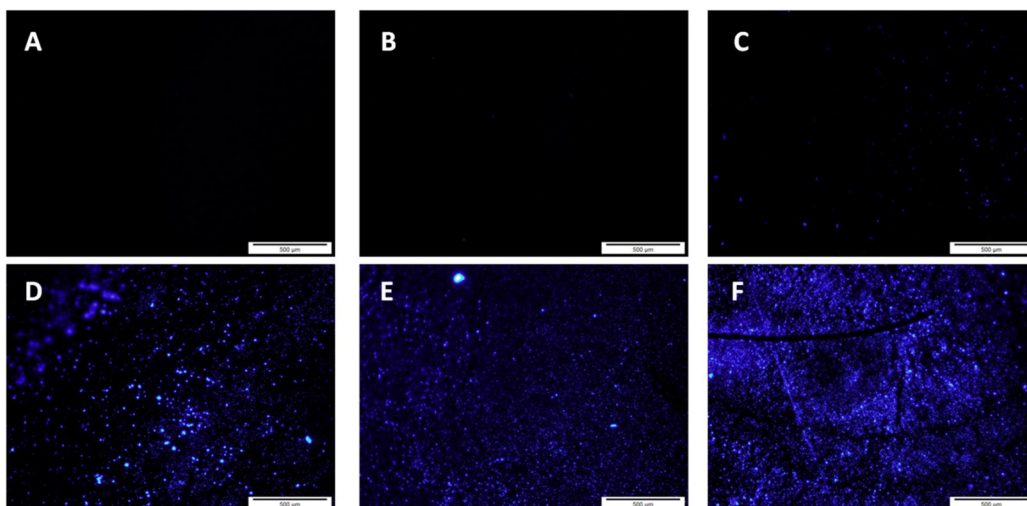**FIGURE S5**

Figure S5. Fluorescence images of Ti samples functionalized with Clear Blue DFSB-C0-loaded PUUa NPs and controls. (**A**) Ctrol; (**B**) APTES; (**C**) Lys 1h; (**D**) Lys ON; (**E**) EDA 1h; and (**F**) EDA ON.
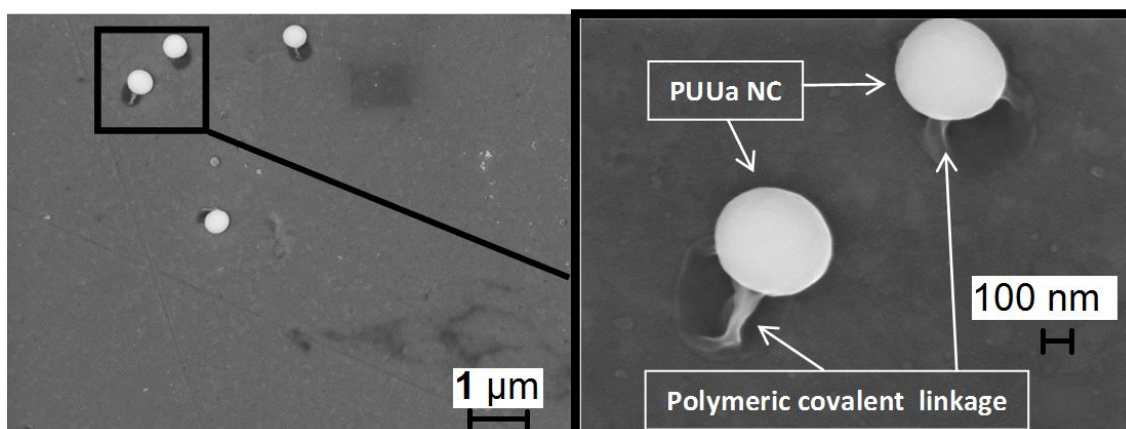
FIGURE S6

Figure S6. In the above cut-out can be observed a specific area of Ti functionalized with EDA NPs for 1 h. EDA NPs show a spherical shaped morphology. Moreover, the largest EDA NPs suggested polyurethane-polyurea roots between them and Ti aminosilanized surface.
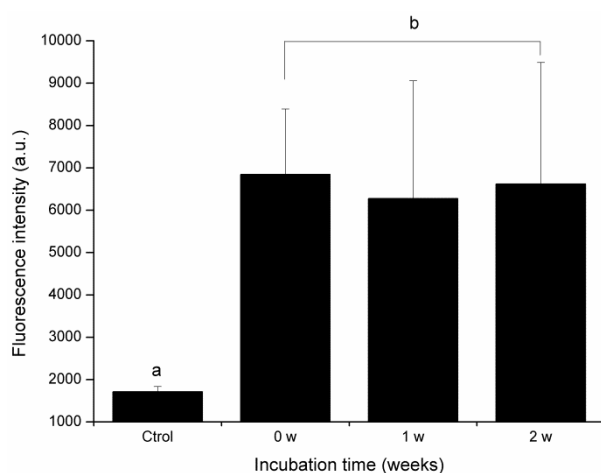
FIGURE S7

Figure S7. Fluorescence intensity of Ti samples functionalized with Oregon Green 488 Cadaverine fluorescent PUUa-NPs and controls. Samples were immersed in PBS and left under orbital agitation for 2 weeks. Fluorescence intensity was analyzed after 1 week and 2 weeks of incubation. Letters (a,b) denote statistically significant differences ($p<0.05$) between groups. Values are expressed as mean ± standard deviation.

TABLE S1

	Diameter (nm)	PDI
EDA	101.3	0.22
EDA RGD	127.4	0.32

Table S1. Particle size (diameter) of PUUa NPs was statistically analyzed on 5 different zones for each sample. The polydispersity index (PDI) was calculated as PDI = (Standard Deviation/Mean Diameter)^2
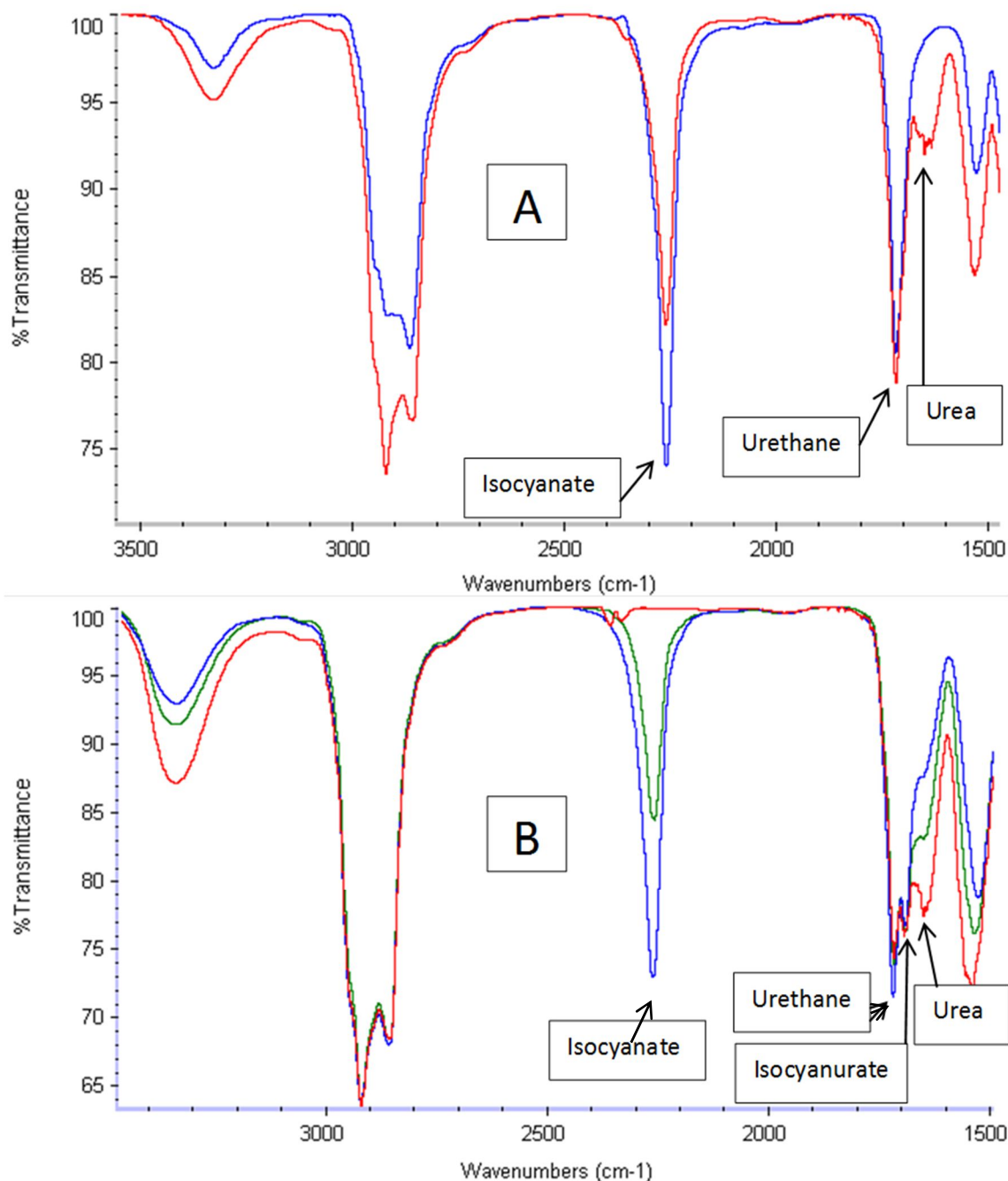
FIGURE S8

Figure S8. A) IR spectra of Amphil polymerization process. Blue spectrum corresponds to polyurethane prepolymer formation. The addition of TAP 100D results in the appearance of a polyurea band at 1650 cm^{-1}, concomitant with the proportional decrease of the isocyanate band (Red). B) IR spectra of the emulsified PUUa NPs before the addition of 50 % EDA (Blue); 30 min after EDA addition (green); and 10 min after 100 % addition of EDA (Red). The isocyanate band clearly decreases over time as the diamino crosslinker is added. The IR band at 2270 cm^{-1} corresponds to the stretching of the –N=C=O functional group. The sharp band at 1715 cm^{-1} is ascribed to urethane C=O stretching. At 1690 cm^{-1} appears the isocyanurate C=O stretching band corresponding to the B3100 linker. The increasing band at 1653 cm^{-1} is attributed to the urea C=O stretching and the one at 1520 cm^{-1} to urethane N-H deformations.
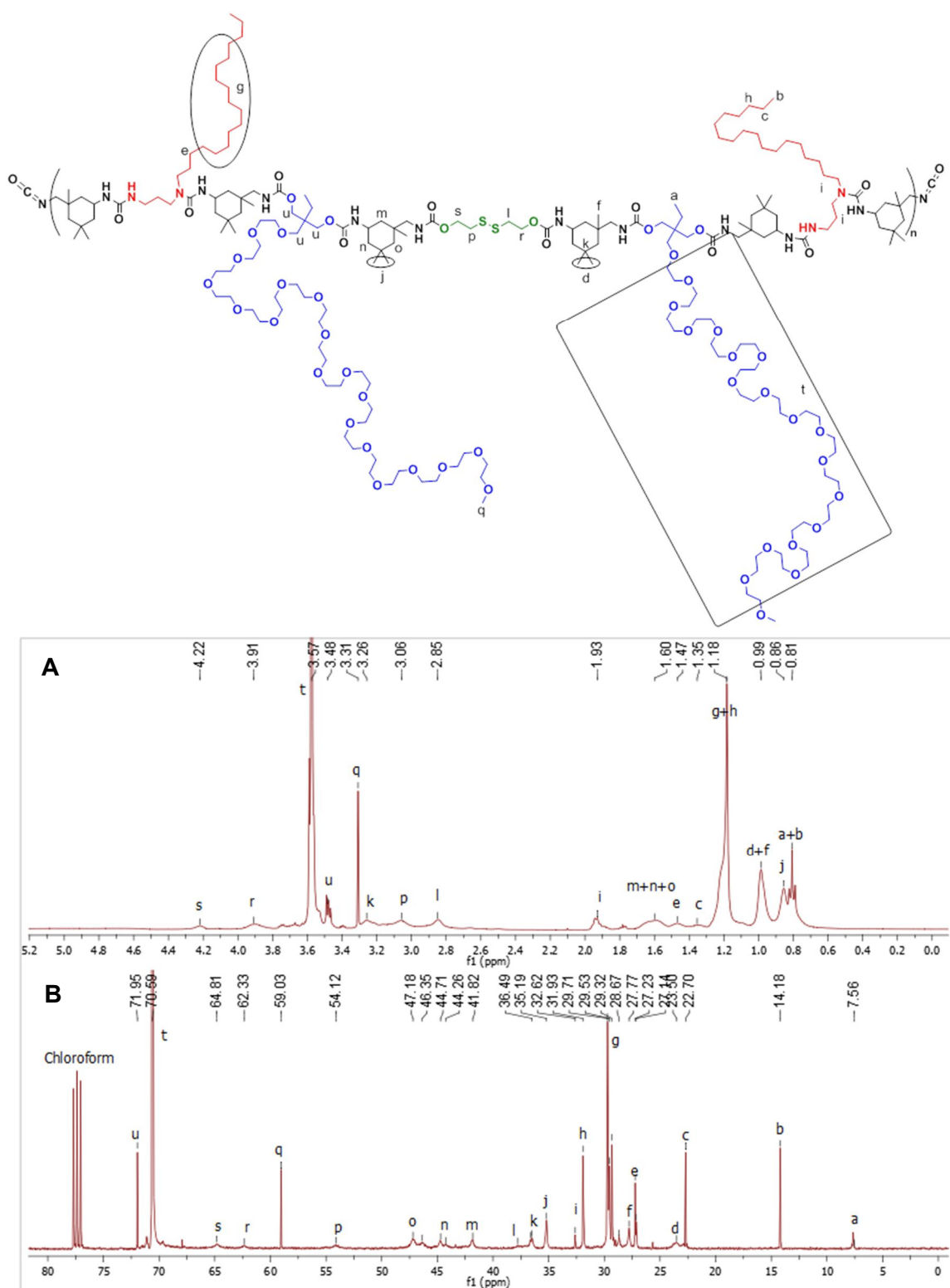
FIGURE S9

Figure S9 400 MHz ^{1}H NMR spectra (A) and 400 MHz ^{13}C NMR spectra (B) of reactive prepolymer Amphil in CDCl$_3$. All peaks have been assigned according to previous ^{13}C and ^{1}H NMR and HSQC analysis of each monomer (spectra not shown) and bibliographic data[5].

FIGURE S10
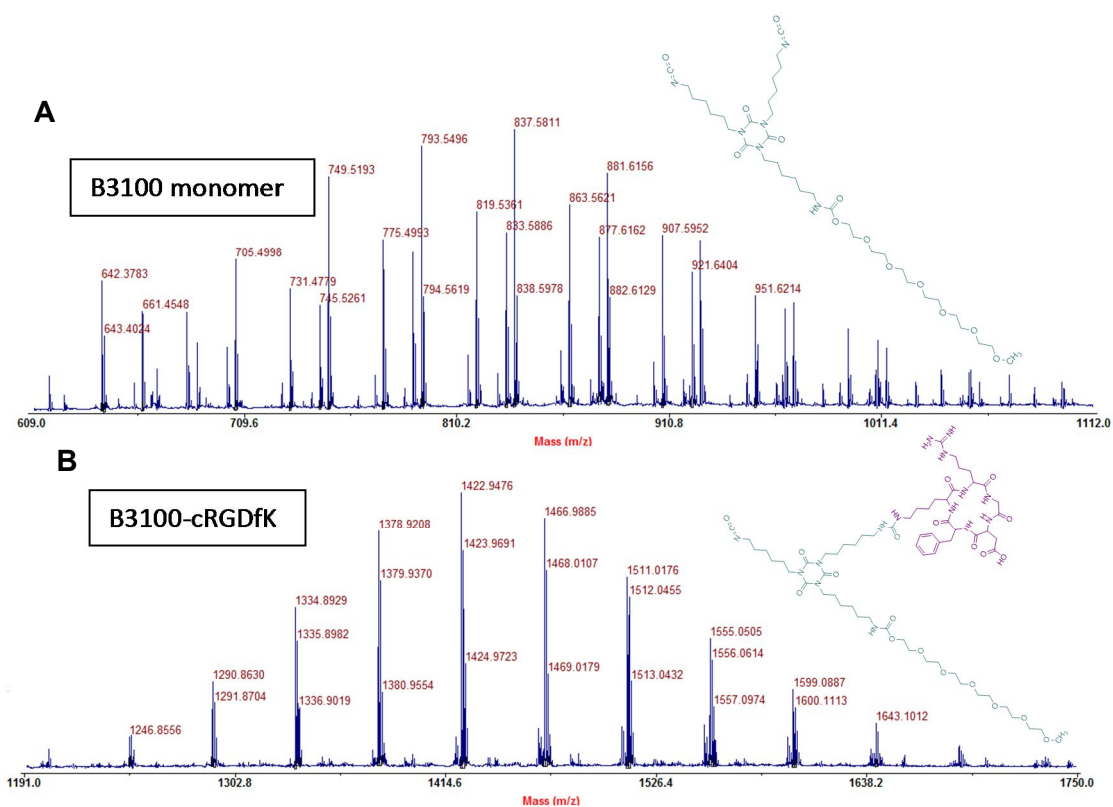
Figure S10. As seen in the MALDI-TOF experiment, the free monomer Bayhydur 3100 (hydrophilic polyisocyanate) has a mass distribution of 700-900 g/mol (A) After 2h of reaction a new mass distribution appears centred on 1400 (800+603.68 (cRGDfK)), which is consistent with the mass of the B3100-cRGDfK conjugate (B)

TABLE S2

	FREE RGD (mM)	FREE RGD (mg/mL)	**Conjugated RGD (mg/mL)**	**Yield (%)**
EDA RGD	NQ	NQ	**1.95**	**100**

Table S2. A calibration curve of standard cRGDfK solutions was performed to obtain the total amount of conjugated cRGDfK peptide in the PUUa NP-RGD sample. NQ = non conjugated cRGDfK concentration was below 1.5 µg/mL (below HPLC detection limit)

FIGURE S11
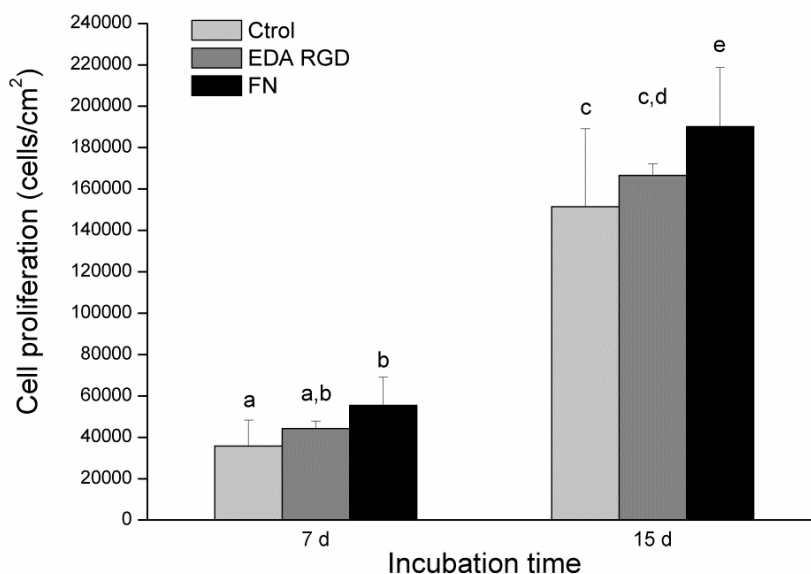
Figure S11. Proliferation (cells/cm^2) of Saos-2 cells on biofunctionalized Ti surfaces after 7 and 15 days of incubation. Quantification of cell numbers was done using the indicator of cell viability Alamar Blue. Distinct letters denote statistically significant differences (p<0.05) between groups. Values are expressed as mean ± standard deviation.

FIGURE S12

Figure S12. Growth curves of planktonic S. *sanguinis* were performed to obtain minimum inhibitory concentration (MIC) values of EDA + Rx. The curves show an initial growth inhibition at the lowest concentration of Rx (0.001875 mg/L).

FIGURE S13
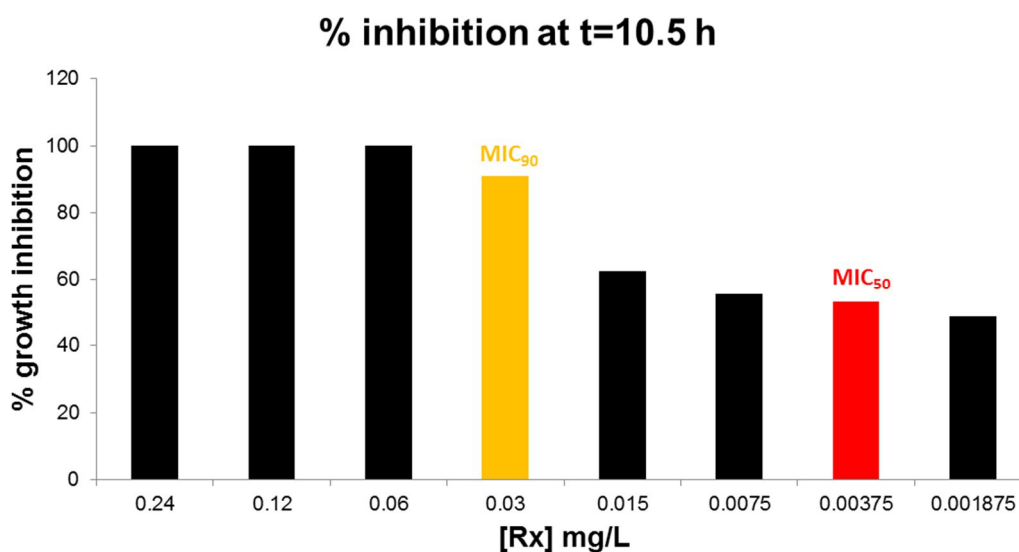
Figure S13. Growth inhibition rates were determined after 10.5 h of incubation from MIC curves. MIC_{50} is defined as MIC at which 50% of isolates were inhibited. In this case, MIC_{50} was reached at $[Rx] = 0.00375$ mg/L. MIC_{90} is defined as MIC at which 90% of isolates were inhibited by a specific antimicrobial. MIC_{90} appears at $[Rx] = 0.03$ mg/L values. Concretely, EDA + Rx MIC50 and MIC90 values show 16 and 133 fold decrease in comparison with free Rx values[6].

FIGURE S14
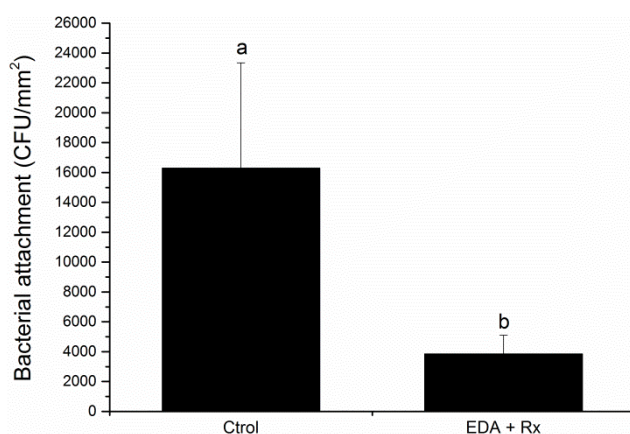
Figure S14. Bacterial adhesion of *S. Sanguinis* on biofunctionalized Ti surfaces after 4 h of incubation in TH broth. Prior to conducting this assay, surfaces were immersed in TH broth and incubated during 20h to ensure the release of $\geq 70\%$ of the drug Roxithromycin. Distinct letters denote statistically significant differences (p<0.05) between groups. Values are expressed as mean ± standard deviation.
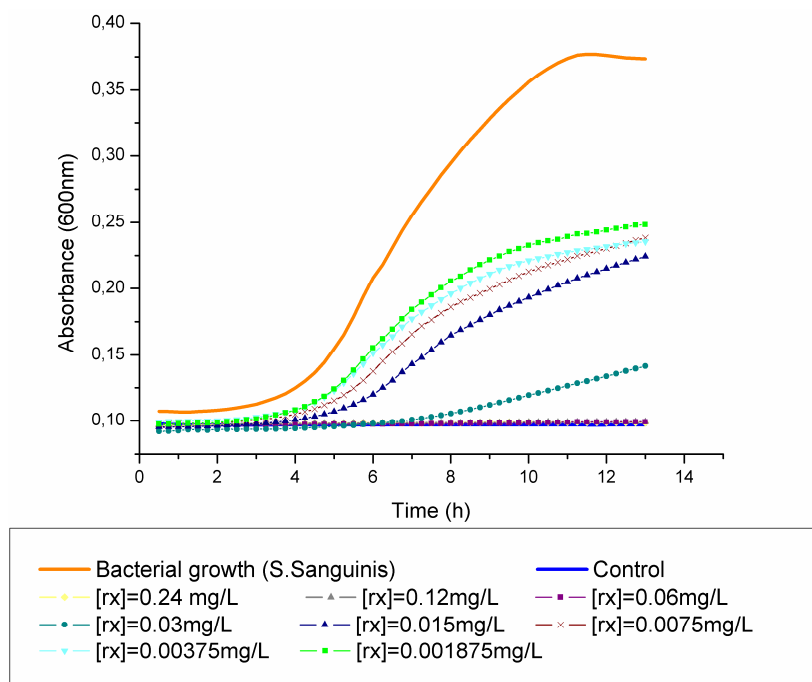
FIGURE S15
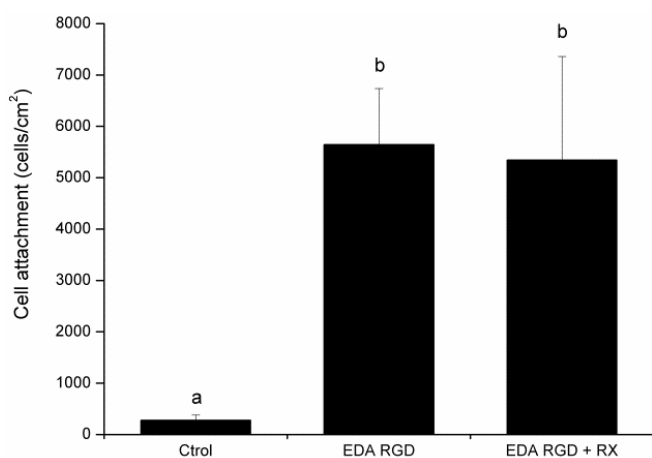
Figure S15. Attachment of Saos-2 cells (cells/cm^2) on biofunctionalized Ti surfaces after 4h of incubation in serum free medium. Cell numbers were analyzed by immunostaining and fluorescence microscopy. Letters (a,b) denote statistically significant differences (p<0.05) between groups. Values are expressed as mean $\pm$ standard deviation.

References

[1]   R. Haubner, R. Gratias, B. Diefenbach, S. L. Goodman, A. Jonczyk, H. Kessler, *J. Am. Chem. Soc.* **1996**, *118*, 7461.
[2]   M. Zhu, M. Z. Lerum, W. Chen, *Langmuir* **2012**, *28*, 416.
[3]   I. R. Clemitson, I. R. Clemitson, *Castable Polyurethane Elastomers*; CRC Press, 2008.
[4]   P. E. Kolenbrander, R. J. Palmer, S. Periasamy, N. S. Jakubovics, *Nat. Rev. Microbiol.* **2010**, *8*, 471.
[5]   A. Prabhakar, D. K. Chattopadhyay, B. Jagadeesh, K. V. S. N. Raju, *J. Polym. Sci. Part A Polym. Chem.* **2005**, *43*, 1196.
[6]   K. V Rolston, D. H. Ho, B. LeBlanc, G. P. Bodey, *Eur. J. Clin. Microbiol. Infect. Dis.* **1990**, *9*, 30.

Chapter III.

Nanoimmunotherapy for

Tolerance Induction

Chapter III.

Chapter III. Introduction

Polyurethane-Polyurea Nanoparticles

for Autoimmune Diseases Therapy

Introduction 3. Polyurethane-Polyurea Nanoparticles for Autoimmune Diseases

Autoimmune diseases therapy

Autoimmune diseases (AD) affect up to 50 million people in the United States, according to the American Autoimmune Related Diseases Association (AARDA) and 75% of those affected are women. Moreover this increasing incidence of autoimmune diseases is generalized through developed countries. The approximate cost per year of treating autoimmune diseases is $100 billion dollars, however, the standard therapies are not effective enough and frequently invoke numerous undesirable side effects[1]. The current standard of therapy for autoimmune diseases seeks to broadly suppress the immune system, however the nonspecific nature of these treatments may result in enhanced patient susceptibility to opportunistic infections. Clearly, new strategies focused on the induction of long-term antigen-specific tolerance, rather than unspecific immunosuppression, need to be further investigated for the treatment of human immune-mediated diseases.

Autoimmune diseases arise from an exacerbate immune response against autologous proteins, which ends with the attack and destruction of healthy tissues. By now, most of them are still poorly understood and chronic. Concretely, in autoimmune diseases, certain immune cells subsets contribute to the loss of tolerance towards self-antigens that are presented as foreign antigens initiating an immune response which involves autoantibodies production as well as inflammation and tissue damage. Most of autoimmune diseases are directly associated to autoinflammation, where antigen presenting cells (APC) such as dendritic cells (DC), macrophages and B lymphocytes uptake and process self-proteins and present them to T-cells that are specific for this autoantigen. The immune system, structured in innate (rapid response of the organism) and adaptive (cellular and humoral response) components, defends the body. It is mainly involved in the recognition and elimination of externally acquired antigens such as virus and bacteria as well as being responsible of immunologic memory and tolerance to self-antigens. Tolerance to self-antigens is maintained by negative selection processes that prevent the existence of some self-antigen-specific lymphocytes by induction of anergy. Loss of self-tolerance (which provokes an autoimmune disease) may happen if autoreactive lymphocytes are not deleted or inactivated during their maturation and self-antigens are presented to the immune system in an activated manner.

Although advances have been achieved, current therapies still have limitations in the routes of administration, high drug doses over long time periods, low specificity for the desired target, side-effects and thus, patient dissatisfaction. In this regard, nanotechnologies offer promising solutions to current limitations of immunosuppressive and biological treatments.

Dendritic cells

From the group of APC together with macrophages and B lymphocytes, DCs are particularly interesting as they play a key role in linking both primary and secondary immune responses and also determine if the immune response will perform immunity or tolerance depending on the stimuli they have previously received (Figure 1).
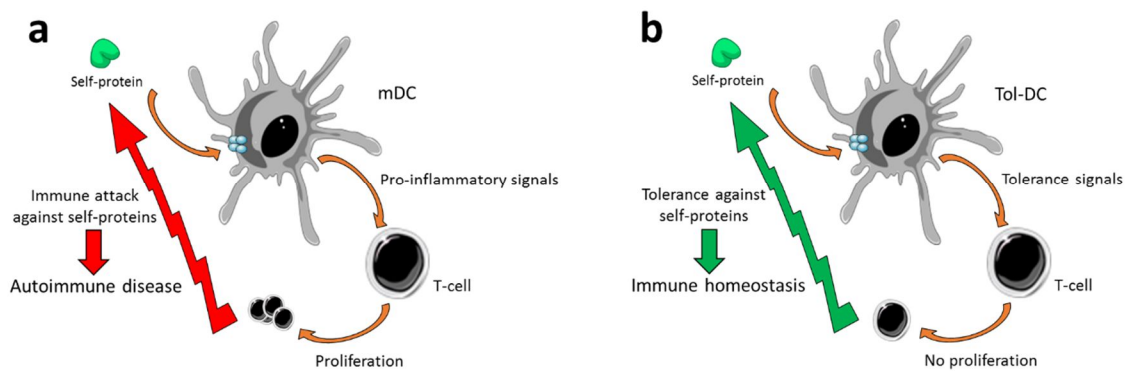
Figure 1. a) Autoimmune disease produced by an autologous autoimmune response against healthy self-proteins. b) Immune homeostasis induced by a tolerogenic response against self-proteins.

Specifically, DCs are a group of cells derived from bone-marrow that are found in the blood, epithelia and lymphoid tissues and are commonly referred as professional APCs as their main function is to present antigens in its cell surface along with the appropriate co-stimulatory molecules. They are highly specialized to capture and process antigens *in vivo*, having the key ability to digest macromolecules and present them as smaller entities on major histocompatibility complex (MHC) molecules and later recognized by T cells[2]. In consequence, their molecular sensors and antigen processing machinery self-classify them as critical in the establishment of immunological memory. When DCs don´t have the ability to recognize foreign entities are named immature DCs (iDCs). In contrast to mature DCs their primary function is to find and capture foreign bodies and antigens in their home tissue. Once they recognize pathogens through pattern recognition receptors (PPRs) they start a maturation process in order to acquire the capacity to simulate T cells, converting themselves to

mature DCs (mDCs). This T cell stimulation is done through co-stimulatory molecules such as CD40, CD80, CD83, MHCII as well as the secretion of pro or anti-inflammatory cytokines like interleukin (Il)-6, IL-12p70, IL-23 TNFα or IL-10. Cytokine secretion pattern strongly defines the resulting T cell lymphocyte polarization to balance the response to immunity or tolerance against the presented antigen.

Tolerogenic dendritic cells

Tolerance is the ability of the immune system to ignore specific antigens. Central tolerance occurs in the thymus for T cells and the bone marrow for B cells. Antigens can be derived endogenously from the host cells or externally from foreign entities, the immune system has to be able to distinguish between innocuous and harmful antigens to avoid autoimmune diseases or undesired immune responses. Dendritic cells also play a key role in maintaining immune tolerance. Tolerogenic DCs (Tol-DCs) generated with corticosteroids and a maturation cocktail, which is a combination of cytokines (IL-1β, IL-6, TNFα) and Prostaglandin E2 (PGE2), present impaired up-regulation of costimulatory molecules such as CD80, CD83, MHCII compared with mature DCs (mDCs). Moreover, Tol-DCs present higher production of the anti-inflammatory cytokine IL-10 meanwhile the inflammatory cytokines IL-12p70 and IL-23 remain undetectable[3]. In fact, Tol-DCs keep the ability to produce high levels of IL-10 after a secondary stimulation with lipopolysaccharide (LPS)[4]. Tol-DCs induced lower proliferative allo-response compared to mDCs. Furthermore, recently Mertk has been described as a positive marker for Tol-DCs generated with corticosteroids[5]. Therefore, Tol-DCs generated *ex vivo* show a great potential for immunotherapy applications in autoimmunity, acquired immune diseases and transplantation.

Nanoparticles based immunotherapy

Immunotherapy is a strategy that is based on the stimulation of the immune system to help fight the body against a disease attack for example cancer or allergy[6–8]. To date, immunotherapeutic strategies involve *ex vivo* loading of DCs associated antigens and adjuvants. This technique requires autologous cells and is extensive and costly due to its human-personalized nature[9,10]. Apart from that it limits standardization of DC-based treatment protocols[11]. Therefore, manipulation of DCs using nanoparticles could be a useful therapy to treat human autoimmune diseases *in vivo*[12,13]. To date few kinds of nanoparticles have been used to target DCs and deliver specifically their cargo (e.g. drugs, antigens, antibodies, etc.). Moreover, most of these few systems are

not fully stable under *in vivo* conditions leading to sub-optimal therapeutic effects[14–16]. Thus, new nano-based strategies ensuring long blood circulation, targeted behaviour and controlled release pattern are needed in the demanding field of immunotherapy.

Targeting dendritic cells by nanoparticles

As DCs have a natural talent to kidnap foreign bodies in the blood, in principle, the directionalization of drug delivery systems towards them should be more easily accomplished in comparison with other cell subsets[17–19]. In the present chapter, we evaluate a novel corticosteroid loaded-nanosystem for the effective in vitro generation of Tolerogenic-DCs (Tol-DCs). Accordingly, encapsulated budesonide (BDS) in multiwalled polyurethane-polyurea nanoparticles (PUUa NPs) based on self-stratified polymers by hydrophobic interactions in the oil-water interface were developed. DCs generated with encapsulated BDS presented better tolerogenic profile compared with the ones generated from free BDS. A significant reduction of cell surface costimulatory molecules as well as secretion of large amounts of IL-10, an anti-inflammatory cytokine, crucial to induce tolerance in the organism were observed, giving to the encapsulated BDS a great potential to the in vivo generation of Tol-DCs (Figure 2).
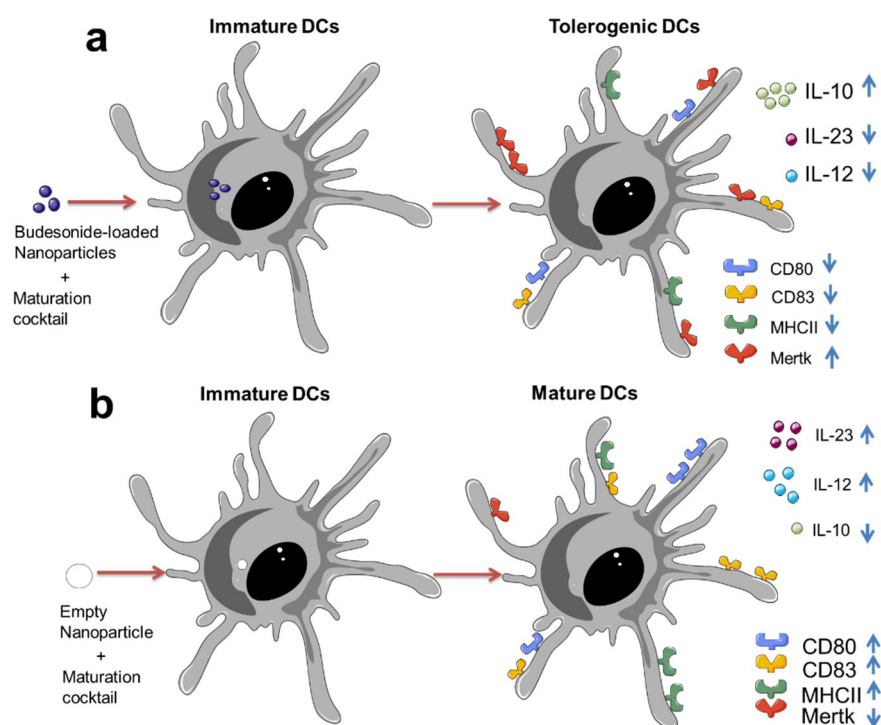

Figure 2. a) Schematic process for the generation of Tol-DCs from PUUa NP-BDS with a better tolerogenic profile for tolerance induction. b) Schematic process for the generation of mDCs with an immunogenic profile.

In addition, in multicellular human samples of T lymphocytes, B-lymphocytes and DCs progenitors PUUa NPs showed a specific quantitative internalization only into DCs (CD14 positive monocytes) proving the targeted behavior of our NPs.

References

1. Autoimmune Statistics - AARDAAARDA http://www.aarda.org/autoimmune-information/autoimmune-statistics/ (accessed Nov 27, 2015).

2. Steinman, R. M.; Banchereau, J. Taking dendritic cells into medicine. *Nature* **2007**, *449*, 419–426.

3. Collin, M.; McGovern, N.; Haniffa, M. Human dendritic cell subsets. *Immunology* **2013**, *140*, 22–30.

4. Lutz, M. B.; Schuler, G. Immature, semi-mature and fully mature dendritic cells: which signals induce tolerance or immunity? *Trends Immunol.* **2002**, *23*, 445–449.

5. Cabezón, R.; Carrera-Silva, E. A.; Flórez-Grau, G.; Errasti, A. E.; Calderón-Gómez, E.; Lozano, J. J.; España, C.; Ricart, E.; Panés, J.; Rothlin, C. V.; Benítez-Ribas, D. MERTK as negative regulator of human T cell activation. *J. Leukoc. Biol.* **2015**, jlb.3A0714–334R–.

6. Tacken, P. J.; de Vries, I. J. M.; Torensma, R.; Figdor, C. G. Dendritic-cell immunotherapy: from ex vivo loading to in vivo targeting. *Nat. Rev. Immunol.* **2007**, 7, 790–802.

7. de la Fuente, M.; Langer, R.; Alonso, M. J. *Nano-Oncologicals*; Alonso, M. J.; Garcia-Fuentes, M., Eds.; Advances in Delivery Science and Technology; Springer International Publishing: Cham, 2014.

8. Cheung, A. S.; Mooney, D. J. Engineered materials for cancer immunotherapy. *Nano Today* **2015**.

9. Tacken, P. J.; Figdor, C. G. Targeted antigen delivery and activation of dendritic cells in vivo: steps towards cost effective vaccines. *Semin. Immunol.* **2011**, *23*, 12–20.

10. Palucka, K.; Banchereau, J. Cancer immunotherapy via dendritic cells. *Nat. Rev. Cancer* **2012**, *12*, 265–77.

11. Eggermont, L. J.; Paulis, L. E.; Tel, J.; Figdor, C. G. Towards efficient cancer immunotherapy: advances in developing artificial antigen-presenting cells. *Trends*

Biotechnol. **2014**, *32*, 456–65.

12. Cho, N.-H.; Cheong, T.-C.; Min, J. H.; Wu, J. H.; Lee, S. J.; Kim, D.; Yang, J.-S.; Kim, S.; Kim, Y. K.; Seong, S.-Y. A multifunctional core-shell nanoparticle for dendritic cell-based cancer immunotherapy. *Nat. Nanotechnol.* **2011**, *6*, 675–82.

13. Ali, H.; Weigmann, B.; Neurath, M. F.; Collnot, E. M.; Windbergs, M.; Lehr, C. Budesonide loaded nanoparticles with pH-sensitive coating for improved mucosal targeting in mouse models of in fl ammatory bowel diseases. *J. Control. Release* **2014**, *183*, 167–177.

14. Zou, P.; Chen, H.; Paholak, H. J.; Sun, D. Noninvasive fluorescence resonance energy transfer imaging of in vivo premature drug release from polymeric nanoparticles. *Mol. Pharm.* **2013**, *10*, 4185–94.

15. Chen, H.; Kim, S.; Li, L.; Wang, S.; Park, K.; Cheng, J.-X. Release of hydrophobic molecules from polymer micelles into cell membranes revealed by Förster resonance energy transfer imaging. *Proc. Natl. Acad. Sci.* **2008**, *105* , 6596–6601.

16. Xu, P.; Gullotti, E.; Tong, L.; Highley, C. B.; Errabelli, D. R.; Hasan, T.; Cheng, J.-X.; Kohane, D. S.; Yeo, Y. Intracellular drug delivery by poly(lactic-co-glycolic acid) nanoparticles, revisited. *Mol. Pharm.* **2009**, *6*, 190–201.

17. Anselmo, A. C.; Mitragotri, S. Cell-mediated delivery of nanoparticles: taking advantage of circulatory cells to target nanoparticles. *J. Control. Release* **2014**, *190*, 531–41.

18. Albert, M. L.; Pearce, S. F. A.; Francisco, L. M.; Sauter, B.; Roy, P.; Silverstein, R. L.; Bhardwaj, N. Immature Dendritic Cells Phagocytose Apoptotic Cells via v 5 and CD36, and Cross-present Antigens to Cytotoxic T Lymphocytes. *J. Exp. Med.* **1998**, *188*, 1359–1368.

19. Akagi, T.; Wang, X.; Uto, T.; Baba, M.; Akashi, M. Protein direct delivery to dendritic cells using nanoparticles based on amphiphilic poly(amino acid) derivatives. *Biomaterials* **2007**, *28*, 3427–36.

Chapter III. Publication 5

PUUa Nanoparticles for tol-Dendritic Cells Generation.

In vitro experiments

TABLE OF CONTENTS (TOC)

Nanoencapsulation of Budesonide in self-stratified polyurethane-polyurea nanoparticles induces powerful Human Tolerogenic Dendritic Cells

Georgina Flórez-Grau, Pau Rocas, Raquel Cabezón, Carolina España, Josep Rocas, Julián Panés, Fernando Albericio*, Daniel Benítez-Ribas*
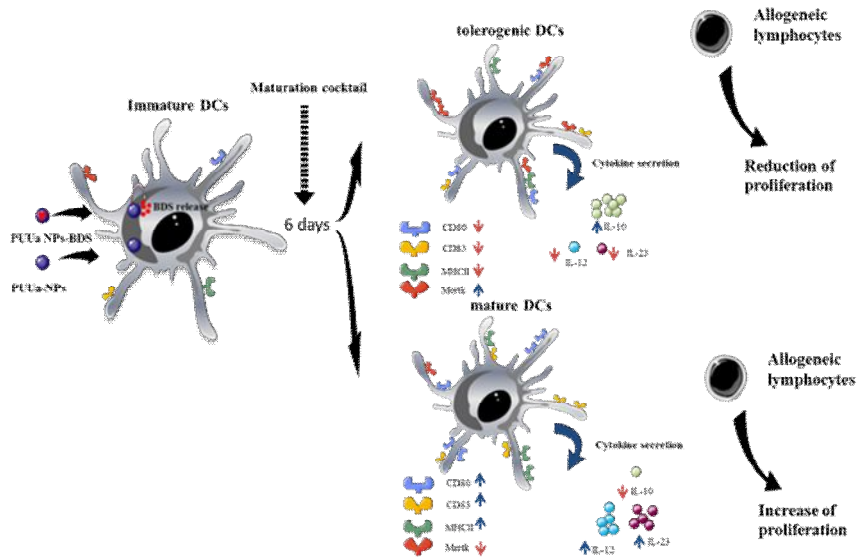
Budesonide-loaded polyurethane-polyurea nanoparticles (PUUa NPs) are used to induce specific tolerogenic dendritic cells and. This strategy represents a powerful potential therapeutic approach for autoimmune diseases.

Author 1, website 1
Author 2, website 2

Nanoencapsulation of Budesonide in Self-stratified Polyurethane-polyurea Nanoparticles Induces Powerful Human Tolerogenic Dendritic Cells

Georgina Flórez-Grau[1§], Pau Rocas[2§], Raquel Cabezón[1], Carolina España[3], Julián Panés[1,3], Josep Rocas[4], Fernando Albericio[2,5,6,7](✉), Daniel Benítez-Ribas[8](✉)

[1]*Institut d'Investigacions Biomèdiques August Pi i Sunyer (IDIBAPS), Barcelona, Spain*

[2]*Institute for Research in Biomedicine (IRB Barcelona), Barcelona, Spain*

[3]*Fundació Clínic per la Recerca Biomèdica, Barcelona, Spain*

[4]*Nanobiotechnological Polymers Division, Ecopol Tech S.L., Tarragona, Spain*

[5]*Department of Organic Chemistry, University of Barcelona, Barcelona, Spain*

[6]*School of Chemistry & Physics, University of Kwazulu-Natal, Durban, South Africa*

[7]*Networking Centre on Bioengineering Biomaterials and Nanomedicine (CIBER-BBN), Barcelona, Spain*

[8]*Centro de Investigación Biomédica en Red, Enfermedades Hepáticas y Digestivas (CIBERehd),Barcelona, Spain*

[§]*This authors contributed equally to this work.*

ABSTRACT

The design of novel strategies that efficiently target specific components of the immune system and in particular dendritic cells (DCs) *in vivo* to induce a tissue specific immune tolerance is gaining in importance and interest for the treatment of autoimmune diseases and for transplantation.

A novel corticosteroid loaded-nanosystem for the effective targeting of human DCs was evaluated in order to avoid the need to generate tolerogenic DCs (tol-DCs) *ex vivo*. Accordingly, budesonide (BDS) was encapsulated in multiwalled polyurethane-polyurea nanoparticles (PUUa NPs-BDS). This nanosystem was based on self-stratified polymers by hydrophobic interactions in the oil-water interface. DCs generated with encapsulated BDS presented a higher downregulation of costimulatory molecules (CD80, CD83, MHCII) and a more potent upregulation of inhibitory receptors than those produced from free BDS. Moreover, tol-DCs generated with encapsulated BDS secreted large amounts of IL-10, an anti-inflammatory cytokine that is crucial to induce tolerance in the organism. Altogether, conferred a better tolerogenic profile to tol-DCs generated with encapsulated BDS than tol-DCs generated with free drug   In addition, tol-DCs generated with PUUa NPs-BDS inhibited T lymphocytes activation, proliferation and IFN-γ production. Interestingly, these nanoparticles were specifically targeted to phagocytic cells in primary mononuclear cells. Thereby, the results showed here provided stunning evidence of the potential of PUUa NPs as drug carrier system to induce cells with a tolerogenic phenotype avoiding *ex vivo* cell isolation and culture.

1. Introduction

In the last decade, nanoimmunotherapy has emerged as a novel strategy to help the immune system fight diseases, ranging from cancer to autoimmune conditions[1–3]. Several studies have demonstrated the great therapeutic potential of manipulating and unleashing our own immune system to tackle cancer or infectious diseases[4]. In this regard, deregulated functions of immune system can lead to autoimmune diseases, where healthy tissues are attacked and destroyed by the immune system in the absence of a pathogenic situation[5]. Dendritic cells (DCs) are a heterogeneous subset of immune cells recognized as highly potent antigen-presenting cells (APCs) linking innate and adaptive immune responses. DCs are crucial in inducing immunogenic or tolerogenic responses to pathogens or harmless antigens respectively[6,7]. DCs are highly specialized in capturing and processing antigens in order to convert proteins into small peptides. These peptides are then presented to T-cells by major histocompatibility complexes (MHC) to initiate immune responses[8,9]. Once immature DCs have recognized pathogens through specialized receptors, such as pattern recognition receptors (PRRs), they mature to acquire the capacity to stimulate T-cells. T-cell activation and polarization is induced through costimulatory molecules such as CD40, CD80, CD83 and CD86, which are up-regulated on mature DCs (mDCs) membrane, as well as through the secretion of pro- or anti-inflammatory cytokines such as interleukinIl-6, IL-12p70, IL-23 TNF-α or IL-10 among others. The cytokine secretion pattern strongly defines the resulting polarization of T-cells in order to determine the type of immune response; either effector Th1 or Th17 immunity (IL-12p70, IL-23 and TNF-α) or tolerance induction through T regulatory cells or Tr1 (IL-10)[10].

Due to their physiological properties and the availability of clinical grade reagents, immunogenic DCs have been safely and successfully used in clinical trials aiming to generate an efficient immune response against tumors or infectious diseases[11–13]. Furthermore, as DCs play a key role in maintaining immune tolerance, the generation of tolerogenic DCs (tol-DCs) has great potential for immunotherapy applications in several immune-based diseases and transplantation, namely diabetes, rheumatoid arthritis, multiple sclerosis or Crohn's disease[14–18]. In this regard, there is evidence that DCs treated with immunosuppressive drugs can dampen inflammatory autoimmune responses, at least *in vitro*[19,20].

Several protocols, including the generation of DCs in the presence of corticosteroids, have been used to produce tol-DCs *in vitro*. These cells present a semi-mature phenotype, a pronounced shift towards anti-inflammatory versus inflammatory cytokine production and low T-cell stimulatory properties. The increased secretion of IL-10 by these cells is considered as a crucial factor to induce tolerance[21].

To date, immunotherapeutic strategies for the treatment of human diseases involve the isolation and *ex vivo* generation of DCs.[22,23] These approaches require the isolation and preparation of individualized autologous cells and thus call for costly culture protocols in certified GMP laboratories[24]. Moreover, this autologous requirement limits standardization among laboratories. An alternative to *ex vivo* cell generation is the *in vivo* targeting of specific immune cells in order to manipulate and modulate their function. Several approaches to deliver immunogenic or regulatory agents have been explored, including nanopolymeric systems as PLGA, PLA, and liposomes, among others[25]. Nanoparticle systems improve DC-targeted delivery of tumor antigens,

amplify immune activation via the use of new stimuli-responsive or immunostimulatory materials, and increase the efficacy of adoptive cell therapies[26,27]. Interestingly, the possibility to target DCs *in vivo* paves the way for immunotherapeutic approaches to treat human diseases by modifying immune responses without the need to culture cells. Recent studies have shown that nanoencapsulated corticosteroids in polymeric systems enhance the therapeutic properties of DCs[28–30]. However, these delivery systems tend to suffer limited performance as most show insufficient stability under *in vivo* conditions and limited encapsulation capacity[31]. We have recently demonstrated that common approaches based on drug encapsulation with monowalled nanostructures are not stable upon interaction with amphiphilic and hydrophobic cell membrane molecules (*e.g.* phospholipids, cholesterol)[32]. Thus, the cargo is non-specifically released from the nanoparticle core, poorly internalized by cancer cell lines, and less bioactive[33]. Hence, we envisaged that a disulfide-rich nanopolymeric system based on hydrophobically stratified polymers creating robust multiwalled nanostructures would be an interesting approach to improve encapsulation stability and maintain in-target redox biodegradation and drug release. However, the effect of these multiwalled nanostructures on human cells remains to be determined. Neither is it known whether human DCs are an appropriate target

Here we evaluated the performance of our previously described redox-sensitive self-stratified multiwalled nanoparticles [32,34,35] to quantitatively encapsulate various concentrations of budesonide (BDS) and analyzed the specific internalization of these particles by primary human monocyte-derived DCs **(Figure 1)**.
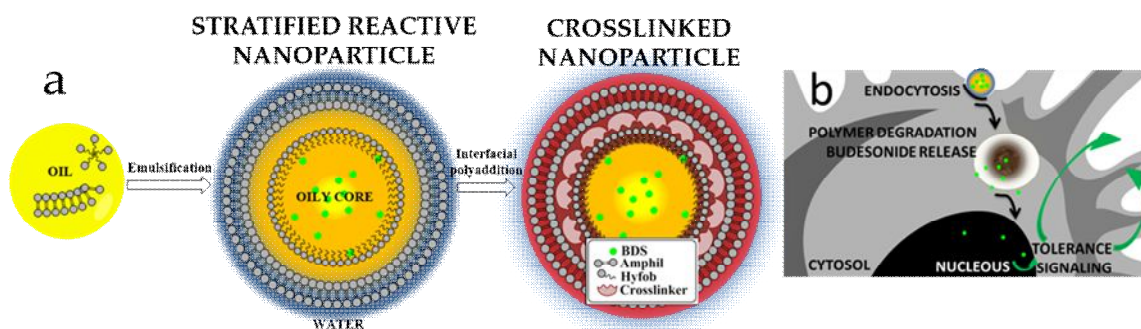

Figure 1. Nanoparticles synthetic strategy and cell internalization. (a) Emulsification of Hyfob and Amphil leads to reactive nanostructures that are further crosslinked in the o/w interface. (b) Dendritic cell internalization, drug release in the cytosol and tolerance signaling scheme.

In addition, we studied the generation of tol-DCs *in vitro*, comparing equal doses of encapsulated to soluble BDS. For this purpose, polyurethane-polyurea nanoparticles (PUUa NPs) carrying different doses of BDS were incubated with human monocyte-derived DCs. The toxicity of these particles was then measured by cell viability determination and their internalization was monitored over time. In addition, to validate PUUa NPs as an appropriate carrier for immunosuppressive drugs, we measured the expression of costimulatory molecules and production of cytokines after DC activation by LPS stimulation and the capacity of DCs NP-treated to activate T-cells.

2. Experimental

2.1. Materials

YMER N-120 was provided by Perstorp (Perstorp, Sweden) and N-Coco-1,3-propylenediamine (Genamin TAP 100D) by Clariant (Barcelona, Spain). Capric/caprylic triglyceride mixture (Crodamol GTCC) was obtained

from Croda (Barcelona, Spain) and Bayhydur 3100 was purchased from Bayer (Leverkusen, Germany). If not indicated otherwise, all other reagents were purchased from Sigma-Aldrich (St Louis, MO, USA). Extra dry acetone was used during the syntheses.

2.2. Experimental methods

2.2.1. Synthesis of reactive prepolymers for multiwalled PUUa NP preparation.

2.2.1.1. Preparation of the reactive amphiphilic prepolymer (Amphil). A 500-mL four-necked reaction vessel was pre-heated at 50ºC and purged with nitrogen. YMER N-120 (5.50 g, 5.5 mmol), 2-Hydroxyethyl disulfide (DEDS) (0.15 g, 1.0 mmol), Crodamol GTCC (0.75 g) and Isophorone diisocyanate (IPDI) (3.38 g, 15 mmol) were then added to the reaction vessel under mechanical stirring in the presence of dibutyltin dilaurate (DBTL) as catalyst (3 mg, 4.65 µmol). The polyaddition reaction was maintained in these conditions until DEDS and YMER reacted quantitatively with IPDI, as determined by FT-IR and the automatic titration[36]. At this point, the vessel was cooled to 40ºC, and Genamin TAP 100D (1.45 g, 4.44 mmol) dissolved in 10 g of acetone was added under constant stirring and left to react for 30 min. The formation of polyurethane and polyurethane-polyurea prepolymers was followed by FT-IR and characterized by NMR[37].

2.2.1.2. Preparation of the reactive hydrophobic prepolymer (Hyfob). To synthesize the hydrophobic prepolymer, a 20-mL Schlenk flask was pre-heated to 50ºC and purged with nitrogen. DEDS (0.15 g, 1.0 mmol) and IPDI (0.485 g, 2.18 mmol) in acetone (7 g) were then added with DBTL as catalyst (0.24 mg, 0.37 µmol) and left to react for 1 h with magnetic stirring. At this point, the Schlenk flask was cooled to 40ºC, and a solution of Genamin TAP 100D (0.15 g, 0.5 mmol) in 3.0 g acetone was added under constant stirring. The reaction left to react for 30 min. The formation of polyurethane and polyurethane-polyurea prepolymers was followed by FT-IR and characterized by NMR[37].

2.2.2. Synthesis of multiwalled PUUa nanoparticles.

2.2.2.1. Synthesis of PUUa NPs. A previously homogenized aliquot of Amphil+Hyfob (1.69 g, mass ratio Amphil 13.35:1 Hyfob) (see section 2.2.1.) was added to a round-bottom flask containing B3100 (125 mg, 0.167 mmol) under nitrogen atmosphere. This organic mixture was then emulsified in pure water (16 mL, 5 ºC) in a magnetic stirrer under an ice bath to prevent isocyanate reaction with water. Once the mixture was emulsified, L-lysine was added (68.56 mg, 0.47 mmol). The interfacial polyaddition reaction was controlled by FT-IR. After 30 min, DETA (32.18 mg, 0.31 mmol) was added, and the crosslinked nanoparticles were formed by a second interfacial polyaddition, as shown by FT-IR. Acetone was removed gently under reduced pressure. PUUa NPs were dialysed (100000 MWCO, Spectrum Laboratories, California, USA) against pure water during 72 h for Zeta potential experiments. For *in vitro* experiments, PUUa NPs were dialysed against PBS for 72 h.

2.2.2.2. Synthesis of PUUa DiI-loaded NPs (PUUa NPs-DiI). These NPs were synthesized as previously described (see section 2.2.2.1.) adding Amphil+Hyfob in a round bottom flask containing DiI (2.5 mg, 2.67 µmol) as lipophilic fluorophore. The organic mixture was homogenized and subsequently, section 2.2.2.1 followed without modifications.

2.2.2.3. Synthesis of PUUa Oregon Green 488 Cadaverine-conjugated NPs (PUUa NPs-cad). An aliquot of this Amphil+Hyfob mixture (0.87 g, mass ratio Amphil 13.35:1 Hyfob) was homogenized in another round-bottom flask with the amine reactive fluorophore Oregon Green 488 Cadaverine (3.2 mg, 6.47 µmol) and B3100 (62 mg, 0.084 mmol). The amino-reactive Oregon Green 488 Cadaverine was left to react for 30 min with excess isocyanate-reactive species at 5ºC under a nitrogen atmosphere and magnetic stirring (273 mg of polymer/mg of dye). At this point, the prepolymers were emulsified in water (8 mL, 5 ºC), and L-lysine was added (34.2 mg,

0.24 mmol) to the solution. The interfacial polyaddition reaction was followed by FT-IR. After 30 min, DETA (16.1 mg, 0.16 mmol) was added, and the crosslinked nanoparticles were formed by a second interfacial polyaddition, as shown by FT-IR. Acetone was removed gently under reduced pressure.

2.2.2.4. Synthesis of 0.5% (*w/w*) BDS-loaded PUUa NPs (PUUa NPs-BDS 0.5%). These PUUa NPs were synthesized as previously described (see section 2.2.2.1.) using BDS as encapsulated molecule. The polymeric organic mixture was homogenized with BDS (10 mg, 23.22 μmol), followed by emulsification in PBS (16 mL, 5ºC) in a magnetic stirrer under an ice bath to prevent isocyanate reaction with water. At this point, section 2.2.2.1. was followed without further modifications.

2.2.2.5. Synthesis of 10% (*w/w*) BDS-loaded PUUa NPs (PUUa NPs-BDS 10%). These PUUa NPs were synthesized as previously described (see section 2.2.2.1.) using BDS as encapsulated molecule. The polymeric organic mixture was homogenized with BDS (200 mg, 0.46 mmol), followed by emulsification in PBS (16 mL, 5ºC) in a magnetic stirrer under an ice bath to prevent isocyanate reaction with water. At this point, section 2.2.2.1. was followed without further modifications.

2.3. Analytical techniques

Transmission electron microscopy. Nanoparticle morphology was studied in a Jeol JEM 1010 (Peabody, MA, USA). A 200 mesh copper grid coated with 0.75% FORMVAR was deposited on a drop of 10 mg/mL of nanoparticles in water for 1 min. Excess nanoparticles were removed by washing in fresh MilliQ water for 1 min. The grid was then deposited on a drop of uranyl acetate 2% *w/w* in water for 30 sec. Excess uranyl acetate was blotted off, and the grid was air-dried before measurement.

BDS drug loading (DL) and encapsulation efficiency (EE). To quantify the total amount of encapsulated BDS in PUUa NPs, a calibration curve was performed by preparing standard solutions of BDS in EtOH:H2O (1:1 v/v) for HPLC analysis. Lyophilized PUUa NP-BDS 0.5% (*w/w*, 5 mg) or PUUa NP-BDS 10% (*w/w*, 250 μg) to maintain the same final BDS concentration, were emulsified in EtOH:H2O (1:1 v/v) and placed in a centrifugal 3 KDa filter unit (Microcon, Carrigtwohill, Ireland) and centrifuged at 14000 *g* for 30 min. Analytical HPLC runs of the filtrate were performed in triplicate in a WATERS 2998 HPLC using a X-Bridge BEH130, C18, 3.5 μm, 4.6 X 100-mm reverse-phase column with the following gradient: 5 to 100% of B in 8 min at a flow rate of 1 mL/min; eluent A: H2O with 0.045% TFA (v/v); eluent B: CH3CN with 0.036% TFA (v/v) and UV detection at 220 nm.

Size distribution by DLS. 0.5% PUUa NPs and 10% PUUa NPs were analysed on a Malvern Zetasizer Nano-ZS90 (Malvern, UK) at 1 mg/mL in pure water at 37ºC.

Lyophilization and redispersion procedures.

Previously dialysed samples (100 mg/mL) were lyophilized and directly redispersed at the desired concentration by overnight stirring at 1500 rpm. They were then examined by TEM and DLS to ratify optimal size and morphology characteristics.

2.4. Biological studies

2.4.1. Generation of human DCs. Peripheral blood mononuclear cells (PBMCs) were isolated from whole blood of healthy donors after ficoll separation and cultured for 2 h at 37°C to allow monocytes to adhere to the flask. Non-adherent cells, namely Peripheral Blood Lymphocytes (PBLs), were washed and cryopreserved. Monocytes adhered to the plate were cultured in X-VIVO 15 medium (BioWhittaker, Lonza, Belgium) supplemented with 2% AB human serum (Sigma-Aldrich,Spain), IL-4 (300U/ml), and GM-CSF (450U/ml) (both from Miltenyi Biotec, Madrid, Spain) for 6 days to obtain immature DCs (iDCs). Maturation cocktail (MC) composed by IL-1β, IL-6 (both at 1000 U/ml) TNF-α (500U/ml) (CellGenix, Freiburg, Germany) and PGE$_2$ (10µg/ml) (Sigma-Aldrich, Spain) was added on day 6 for 24 h. To generate tol-DCs, BDS (10^{-6} M) (AstraZeneca Farmaceutica, Spain) was added at day 3. Nanoparticles with BDS (PUUa NPs-BDS 0.05, 0.1 and 1 µM) and empty nanoparticles control (PUUa NPs) were also added at day 3 to compare their effect to those carrying soluble BDS.

For DC stimulation, 100 ng/ml of LPS (Sigma-Aldrich, Spain) was added at day 7 and incubated for 24 h. After stimulation, DC supernatant was collected for cytokine detection.

2.4.2. Flow cytometry analysis. In order to evaluate the DC phenotype, flow cytometry was performed. Monoclonal antibodies (mAbs) or their appropriate isotype control were used: Anti-CD80, CD83 and MHCII PE-labeled (BD-pharmigen), anti-hMer APC labeled (R&D systems). Flow cytometry was performed using FACSCanto II, and data were analyzed with BD FACSdiva 6.1™ software.

To confirm PUUa NP internalization by DCs, DiI-fluorescently labeled NPs were added to iDCs and incubated for 10, 30 or 120 min at 37°C. iDCs positive for DiI-NP were measured and quantified by flow cytometry (BD LSRFortessa™ cell analyzer).

2.4.3. Fluorescence microscopy. In order to confirm NP internalization by DCs, cells were incubated with PUUa DiI-loaded NPs for 120 min, and then washed, fixed, stained with MHC II-FITC, and adhered to a cover slip previously treated with poly L-lysine (Sigma-Aldrich, Spain). Images were obtained with a fluorescence microscope Olympus BX51.

2.4.4. T-cell proliferation. A mixed lymphocyte reaction (MLR) was used to test the immunogenicity of DCs. DCs were co-cultured with T-cells from a different donor at a ratio of 1:20 (10^5 T-cells) in 96 round-bottom well plates. T-cell proliferation was measured using tritiated thymidine (1 µCi/well, Amersham, UK), which was added at day 6. Incorporation was measured after 16 h. Supernatant was collected at day 6 for IFNγ analysis.

2.4.5. Cytokine production. IL-10, IL-12p70 and IL-23 production by DCs was analyzed by ELISA (eBioscience), following the manufacturer's guidelines. Supernatant from T-cell cultures was collected after 6 days of allogeneic response, and IFN-γ (eBioscience) was analyzed by ELISA following the manufacturer's guidelines.

2.4.6. Statistical analysis. Results are shown as the mean ± SD. To determine statistical differences between the means, the paired or independent sample ANOVA test was used. Bonferroni post-test was applied to determine differences between two data sets. Statistical significant differences were set at $p < 0.05$ (*), $p < 0.01$ (**) or $p < 0.001$ (***).

3. Results and discussion

3.1.1. PUUa NP characterization

Multiwalled PUUa NPs have been extensively characterized by FT-IR, automatic titration, NMR and fluorescence spectroscopy in a previous proof-of-principle study[32]. In the present study, both PUUa NPs and PUUa NPs-BDS 0.5% were found to be monodisperse (PDI<0.1), with sizes between 24.4 ± 6.1 (PDI=0.06) and 28.2 ± 8.1 (PDI=0.08) nm respectively (**Figure 2**). Our system allowed almost 100% of encapsulation efficiency at a drug loading of 5.2 μg BDS per mg PUUa NPs. BDS encapsulation at 0.5% (*w/w*) did not significantly affect the size distribution of nanoparticles. However, a slight increase of ± SD was observed for the 0.5% BDS-loaded nanosystem. This observation may be attributable to minimal hydrophobic interactions of the drug with the stratified prepolymers during NP emulsification. Of note, the morphology of 10% BDS-loaded PUUa NPs, which contained 106 μg BDS per g PUUa NPs, changed as the core mass was increased 20 times. This led to NP sizes of around 170 ± 52 nm (PDI=0.09), as confirmed by TEM and DLS.
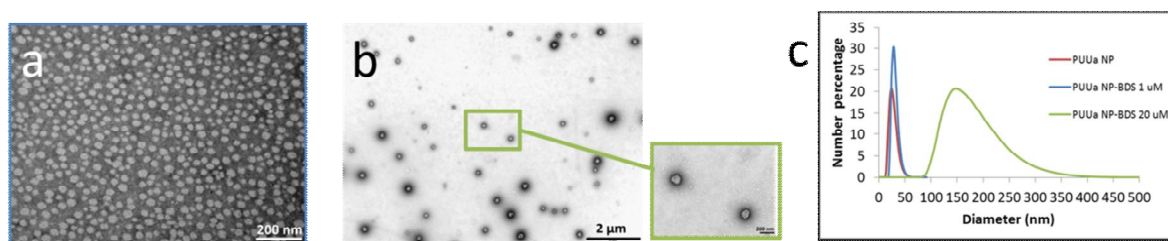

Figure 2. Nanoparticles characterization. (a) TEM micrograph of PUUa NP-BDS 0.5%.(b) TEM micrograph of PUUa NP-BDS 10%. (c) DLS plot of hydrodynamic diameters of our case study formulations.

Several strategies have been developed to target specific cell subsets *in vivo* to achieve improved control over the function and phenotype of immune cells. In particular, DCs are used to modify the immune response to tumors or autoimmune diseases. Therapeutic strategies are based on cell isolation and culture to obtain mature or tolerogenic DCs. *In vivo* targeting strategies would circumvent the costly and time-consuming procedures required for *ex vivo* generation of human DCs for immunotherapy of human diseases The present study is the first to address polyurethane-polyurea NP (PUUa-NP) delivery into phagocytic cells using BDS as a model immunosuppressive drug to generate tol-DCs. This innovative drug delivery system consists mainly of a self-stratified nanostructure formed by hydrophobic interactions between an amphiphilic and a hydrophobic prepolymer. Moreover, their stratified nanostructure is further stabilized by chemical crosslinking, which translates into a greater capacity to encapsulate hydrophobic drugs in the core. Finally, the disulfide-rich shell provides the nanosystem with glutathione-triggered drug release, thereby preventing the release of the drug before PUUa NPs are internalized into the cell. Interestingly, PUUa NPs did not contain any external surfactant, and cryoprotectants were not required for lyophilization or redispersion procedures. We propose that this behavior is due to the combination of the PEG-like structure of YMER N-120, which retains water molecules, and the robustness conferred to the NPs during crosslinking, a process that allows the NP shell to maintain its nanostructure during freeze-drying, thereby conserving dangling hydrophilic chains on the surface of the polymeric shell[38]. These characteristics will be clear advantages for the future translation of this nanosystem to *in vivo* preclinical experiment.

3.1.2. Drug loading (DL) and encapsulation efficiency (EE).

BDS was encapsulated at 0.5 and 10% (*w/w*) in PUUa NPs. As expected, both nanosytems exhibited excellent encapsulation efficiency (above 95%), as quantified by the HPLC calibration method explained above. DLs of 0.48 ± 0.06% and 9.9 ± 0.1% were achieved respectively. EE was 99.7 ± 0.2% for NP-BDS 0.5% and 99 ± 0.1% for NP-BDS 10%.)

3.2 Generation of tol-DCs using PUUa NPs-BDS 0.5%

3.2.1. DCs internalize PUUa NPs.

DCs are highly specialized in capturing soluble and particulate antigens To establish whether NPs were internalized by human DCs, we analyzed DCs incubated with DiI-loaded PUUa NPs for 10, 30 and 120 min. Internalization efficiency was measured using flow cytometry. DCs incubated with NPs-DiI presented the highest ratio of internalization at 120 min, with about 70% (± 14.4 SD) of DCs positive for DiI staining (**Figure 3a**). Moreover, in order to confirm that the PUUa NPs were indeed internalized and not merely bound to the membrane, fluorescence microscopy was used to visualize the distribution of PUUa NPs-DiI. Most of the NPs-DiI internalized by DCs was located inside the cytoplasm as they did not co-localize with membrane MHC class II (**Figure 3b**). We previously described that the structure of PUUa NPs is stable under physiological media and that the cargo is specifically delivered into the cells and not passively diffused like other NPs such as liposomes or PLGA[31,33]. To demonstrate that PUUa NPs are internalized by active phagocytes and not passively incorporated by other cells, we incubated freshly isolated PBMCs with Cadaverine-labeled PUUa NPs. NP internalization was analyzed by flow cytometry in T-lymphocytes (CD3+), B-lymphocytes (CD19+) and monocytes (CD14+). As expected, PUUa NPs were internalized efficiently only by phagocytic cells, CD14+ monocytes (**Figure 1S a**).

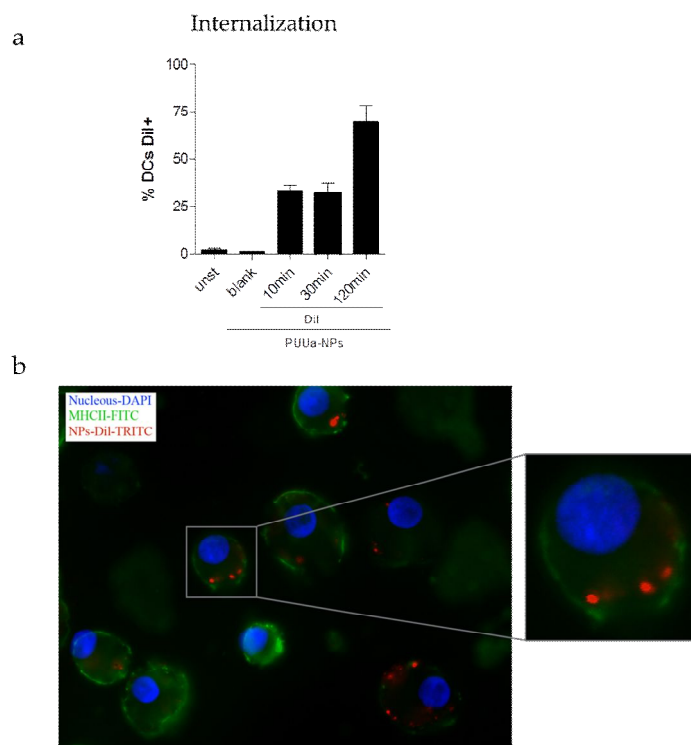**Figure 3. NPs internalization by DCs.** (a) DCs were incubated with PUUa NPs-DiI loaded for 10, 30 or 120 min. Incorporation of DiI was measured by flow cytometry. Percentage of DiI+ cells is presented as mean ± SD of n=2 independently performed experiments. (b) Fluorescence microscopy images (20X) of DCs incubated with PUUa NPs-DiI for 120 min. Picture shows membrane MHCII-FITC (in green), PUUa NPs-DiI (in red), and nucleus (in blue).

3.2.2. Incorporation of NPS-BDS 0.5% efficiently generates tol-DCs.

As shown above, PUUa NPs were efficiently internalized by human DCs. To rule out toxicity of NPs in human primary cells, we analysed DCs viability after 4 days in culture with PUUa NPs-BDS (Figure S1b). We observed that the viability of DCs treated with PUUa NPs-BDS at maximum dose (1μM) was over 85%.

It has been previously described that tol-DCs generated with glucocorticoids are characterized by low expression of costimulatory molecules compared to mature DCs. In addition, MERTK was recently described to be up-regulated in tol-DCs and may be involved in tolerance induction.

We evaluated the efficiency of generating tol-DCs using PUUa NPS-BDS 0.5% as a tolerogenic agent instead of free BDS treatment. To assess the tolerogenic properties of DCs treated with different BDS concentrations of PUUa NP-BDS 0.5% (0.05, 0.1 and 1μM) or free BDS (1μM)the expression of activation surface markers was analysed by flow cytometry and cytokine secretion profile by ELISA.

Our results showed that the addition of PUUa NPs-BDS 0.5% at 1.0 μM impaired the upregulation of CD80, CD83 and MHCII (18.8%, 37.6% and 25.7% reduction, respectively)compared to mDCs as expected of corticosteroid treated-DCs. Moreover the low expression of costimulatory molecules was significantly higher than free BDS at 1.0 μM (**Figure 4a**).

Interestingly, these significant differences in the upregulation of maturation markers compared with free BDS indicate that PUUa NP-encapsulated corticosteroid is more efficient than free BDS in inducing a tolerogenic phenotype on DCs. To confirm the generation of tolerogenic signals, the expression of MERTK, a recently described tolerogenic-related molecule expressed on human tol-DCs[39] was analyzed. As expected, MERTK was up-regulated in tol-DCs and its expression in PUUa NP-BDS 0.5% treated DCs showed a directly proportional dose-dependent positive effect (**Figure 4a**).
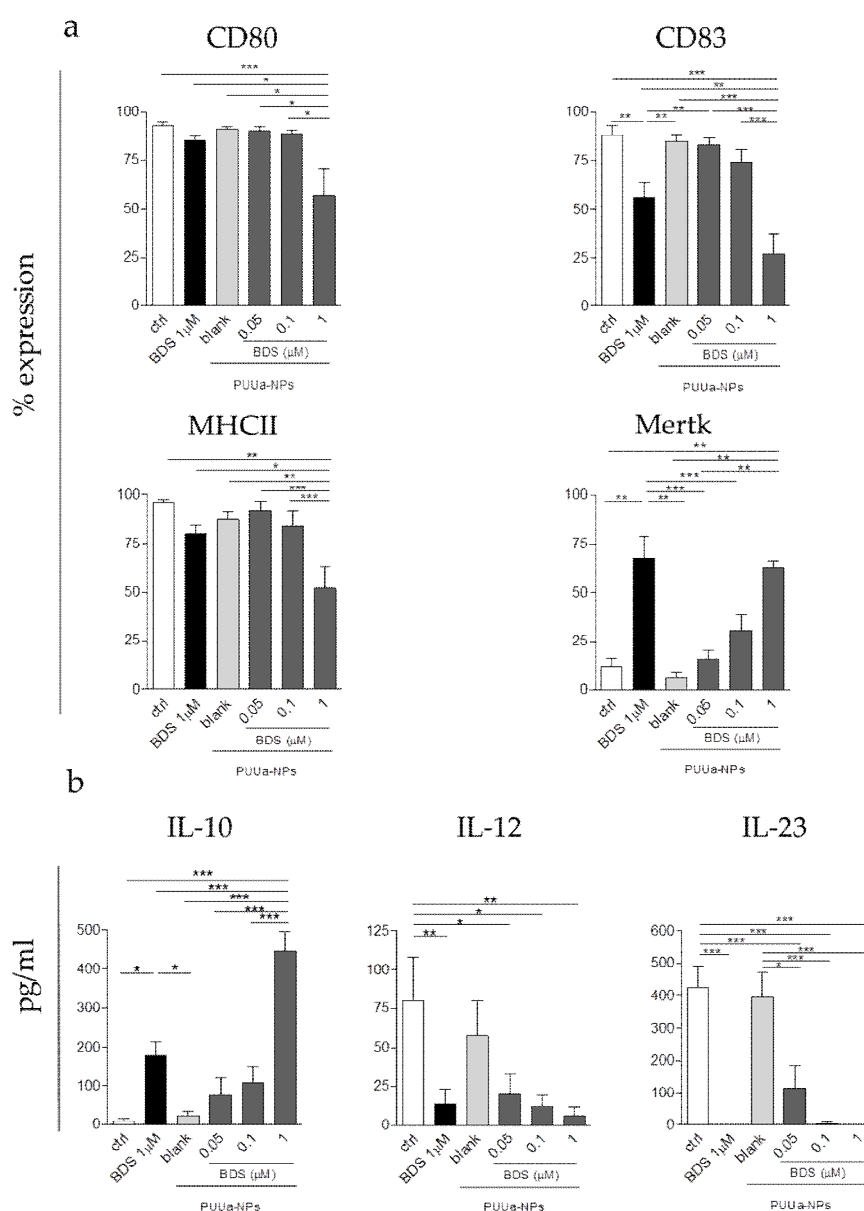
Figure 4. Characterization of tol-DCs generation using PUUa NPs-BDS 0.5%. (a) tol-DCs were generated with PUUa NPs-BDS 0.5% at different BDS doses (0.05, 0.1 and 1μM) and compared to soluble BDS (1μM). Expression of surface costimulatory molecules was analysed by flow cytometry.. Results are presented as the mean ± SD of n=6 independently performed experiments.**(b) Cytokine production by DCs stimulated with LPS (100ng/mL) for 24 h.** IL-10, IL-12 and IL-23 levels were analysed in the supernatants of DC culture by ELISA.Results are presented as the mean ± SD of n=6 independently performed experiments.

To determine the influence of PUUa NP-treated DCs on cytokine production, DCs were stimulated with 100 ng/ml of LPS for 24 h at day 7. Interestingly, those cells treated with PUUa NPs-BDS 0.5%produced higher levels of IL-10 compared to mDCs.Surprisingly Il-10 produced by DCs treated with PUUa NPs-BDS 0.5% 1μM were significantly higher (about 60% more) than DCs treated with free BDS at the same concentration

(**Figure 4b**) (180 ± 88 pg/ml versus 420 ± 120 pg/ml; p=0.0007). These results are in agreement with the semi-mature phenotype shown in **Figure 4a**nd indicate a more specific anti-inflammatory effect induced by encapsulated BDS compared to the free form. The expression of pro-inflammatory cytokines IL-12p70 and IL-23 was efficiently reduced in DCs treated with free BDS and in DCs treated with PUUa NPs-BDS 0.5% compared with control DCs and DCs treated with blank PUUa NPs. Furthermore, a BDS dose-response reduction of both IL-12 and IL-23 secretion was observed (**Figure 4b**).

In order to check a possible difference in BDS encapsulation, BDS was encapsulated using two different concentrations(0.5% versus 10%) were assessed. Howevernon differences in regulation of the phenotype of costimulatory molecules were detected (**Figure 2S**).

PUUa NPs-BDS 0.5% were efficiently targeted into phagocytic cells both in circulating monocytes when co-cultured with PBMCs and in *in vitro*-derived DCs, and the NPs were located in the cytoplasm. DCs have an endogenous capacity to degrade internalized pathogens and show a high constitutive concentration of reduced glutathione (GSH) compared to other immune cells[40]. PUUa NPs 0.5% combine fundamental properties for drug delivery such as high encapsulation stability, redox degradability, and very small sizes (< 30 nm) as they exhibited a superior cell internalization and only intracellular localization. We can attribute these effects to the full digestion of PUUa NPs-BDS 0.5% upon endocytosis and considerable intracellular drug release, as we also observed a high rate of PUUa NPs 0.5% internalization in phagocytic cell populations of the immune system.

DCs incubation with PUUa NPs-BDS caused a profound effect on the phenotype and on the production of the immunosuppressive cytokine IL-10. It is tempting to speculatethat the encapsulation of BDS provides each DC with a full dose of the drug, while DC treatment with the free drug leads to a lower final concentration per cell because BDS shows poor solubility and it is diluted in the extracellular media. Consequently, DCs expressed lower amounts of surface costimulatory molecules and also secreted large amounts of IL-10, a crucial anti-inflammatory cytokine. In contrast, the production of pro-inflammatory cytokines like IL-12 and IL-23 in response to LPS was reduced or absent.

3.2.3. Kinetics of IL-10 production by tol-DCs

As shown in our previously results, the release of BDS inside DCs is crucial to induce the production of IL-10 by tol-DCs. Therefore, we studied the connection between the amount of encapsulated BDS and DC anti-inflammatory response by examining IL-10 secretion kinetics. In this regard, secreted IL-10 was analyzed 4, 8, 12, 24 and 48 h after addition of LPS to DCs incubated with free BDS, PUUa NP-BDS 0.5%, and PUUa NP-BDS 10%, and the blank PUUa NPs control. Interestingly, tol-DCs treated with PUUa NP-BDS 0.5% initiated IL-10 production at 12 h and the highest secretion of this cytokine was at 48 h. However PUUa NPs-BDS 10% did not produce the same amounts of IL-10. For that reason we considered PUUa-BDS 0.5% the best option for tolerance induction in DCs.Morevoer, these results indicates that there is a release of the drug and it is likely to affirm that the release should be done inside the cell. (**Figure 2S B**).

3.2.4. DCs treated with PUUa NPs-BDS 0.5% show tolerogenic function.

To study the functional consequences of tol-DCs generated by PUUa NPs-BDS 0.5% incubation, we set up an assay to evaluate the T-cell stimulatory properties of DCs. Mixed Leukocyte Response (MLR) consists of

DCs co-cultured with allogeneic T-cells to induce T-cell activation. tol-DCs generated with free BDS or PUUa NPs-BDS 0.5% (1 μM) showed less capacity to induce T-cell proliferation (measured by Tritiated thymidine incorporation and IFN-γ production) than mDCs or DCs incubated with blank PUUa NPs. In this case, we did not observe statistically significant differences between free and encapsulated BDS (p = 0.33) (**Figure 5**), although the proliferative response induced by PUUa NPs-BDS 0.5% was lower than the proliferation induced by free BDS.

To confirm that PUUa NPs-BDS 0.5% were active only upon specific cell internalization, total PBMCs were subjected to free or encapsulated BDS, and T-cell proliferation was polyclonally induced using αCD3αCD28 stimulation. Our results showed that both encapsulated BDS and free BDS reduced drastically lymphocyte proliferation (**Figure 2S C**).
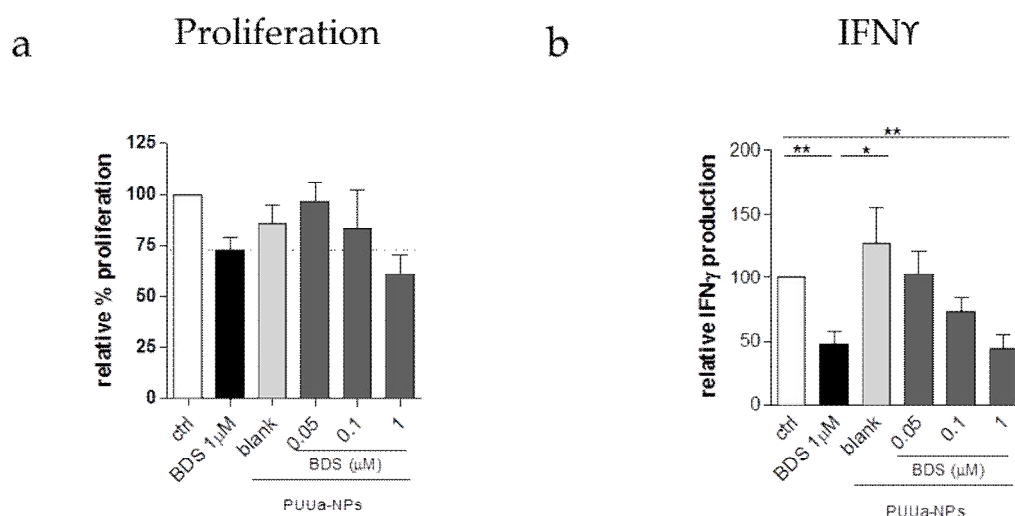

Figure 5. Lymphocyte activation. (a) Mixed lymphocyte reaction (MLR) .DCs treated with PUUa NPs-BDS 0.5% using diffenrent BDS doses (0.05,0.1 and 1μM) and with free BDS 1μM were co-cultured with allogenic PBLs for 7 days.. Results are presented as the mean ±SD of n=5 independently performed experiments (b) IFN-γ production was analyzed from the supernatant by ELISA.. Results are presented as the mean ±SD of n=5 independently performed experiments.

These results indicate that the release of BDS is achieved upon PUUa NPs 0'5% internalization into the cytoplasm of phagocytic cells and not passively diffused, as tol-DCs were carefuly washed before co-culturing with PBLs, all together suggest the specificity of the cargo delivery.

In agreement with the tolerogenic phenotype, DCs generated with PUUa NPs-BDS were unable to activate T-cell proliferation and IFN-γ production, thus revealing strong tolerogenic properties. Interestingly, the effect of PUUa NPs-BDS was restricted to phagocytic cells (monocytes or DCs), as it was not observed in other immune cells like T- or B-lymphocytes.

Taken together, these results reveal that PUUa NPs efficiently deliver their cargo once internalized by DCs and modify the cell phenotype to a tolerogenic status. Moreover this results open new possibilities to encapsulated different drugs to modulate the response of DCs.

4. Conclusions

In summary, herein we report that self-stratified PUUa NPs boost the effect of lipophilic corticosteroids in human DCs. Specifically, PUUa NP-BDS 0.5%exhibited a profound encapsulation ability which allowed the simultaneous internalization of the drug-loaded nanosystem as observed by flow citometry and fluorescence microscopy. Moreover, this internalization and release of the drug translated into a better tolerogenic profile of DCs. Furthermore, PUUa NPs exhibited a specific targeting to dendritic cells and their precursors without affecting other immune cell subsets, which provided stunning evidence of their potential as smart drug delivery system for autoimmune diseases treatment. Nowadays, more research is underway to actively target DCs in *in vivo* animal models of human diseases like autoimmunity or chronic inflammatory diseases.

References

[1] Tacken, P. J.; de Vries, I. J. M.; Torensma, R.; Figdor, C. G. Dendritic-cell immunotherapy: from ex vivo loading to in vivo targeting. *Nat. Rev. Immunol.* **2007**, *7*, 790–802

[2] de la Fuente, M.; Langer, R.; Alonso, M. J. *Nano-Oncologicals*; Alonso, M. J.; Garcia-Fuentes, M., Eds.; Advances in Delivery Science and Technology; Springer International Publishing: Cham, 2014

[3] Cheung, A. S.; Mooney, D. J. Engineered materials for cancer immunotherapy. *Nano Today* **2015**

[4] Waldmann, T. A. Immunotherapy: past, present and future. *Nat. Med.* **2003**, *9*, 269–77

[5] Granucci, F.; Zanoni, I.; Ricciardi-Castagnoli, P. Central role of dendritic cells in the regulation and deregulation of immune responses. *Cell. Mol. Life Sci.* **2008**, *65*, 1683–97

[6] Shao, K.; Singha, S.; Clemente-Casares, X.; Tsai, S.; Yang, Y.; Santamaria, P. Nanoparticle-Based Immunotherapy for Cancer. *ACS Nano* **2014**, *9*, 16–30

[7] Gharagozloo, M.; Majewski, S.; Foldvari, M. Therapeutic applications of nanomedicine in autoimmune diseases: From immunosuppression to tolerance induction. *Nanomedicine* **2015**, *11*, 1003–1018

[8] Banchereau, J.; Steinman, R. M. Dendritic cells and the control of immunity. *Nature* **1998**, *392*, 245–252

[9] Steinman, R. M.; Banchereau, J. Taking dendritic cells into medicine. *Nature* **2007**, *449*, 419–426

[10] Collin, M.; McGovern, N.; Haniffa, M. Human dendritic cell subsets. *Immunology* **2013**, *140*, 22–30

[11] Butterfield, L. H. Dendritic cells in cancer immunotherapy clinical trials: are we making progress? *Front. Immunol.* **2013**, *4*, 454

[12] Anguille, S.; Smits, E. L.; Lion, E.; van Tendeloo, V. F.; Berneman, Z. N. Clinical use of dendritic cells for cancer therapy. *Lancet. Oncol.* **2014**, *15*, e257–67

[13] Banchereau, J.; Briere, F.; Caux, C.; Davoust, J.; Lebecque, S.; Liu, Y.; Pulendran, B.; Palucka, K. Mmunobiology of. **2000**, 767–811

[14] Pulendran, B.; Tang, H.; Manicassamy, S. Programming dendritic cells to induce T(H)2 and tolerogenic responses. *Nat. Immunol.* **2010**, *11*, 647–55

[15] Steinman, R. M.; Hawiger, D.; Nussenzweig, M. C. Tolerogenic dendritic cells. *Annu. Rev. Immunol.* **2003**, *21*, 685–711

[16] Cabezón, R.; Benítez-Ribas, D. Therapeutic potential of tolerogenic dendritic cells in IBD: from animal models to clinical

application. *Clin. Dev. Immunol.* **2013**, *2013*, 789814

[17] Hu, J.; Wan, Y. Tolerogenic dendritic cells and their potential applications. *Immunology* **2011**, *132*, 307–14

[18] Benham, H.; Nel, H. J.; Law, S. C.; Mehdi, A. M.; Street, S.; Ramnoruth, N.; Pahau, H.; Lee, B. T.; Ng, J.; G. Brunck, M. E.; Hyde, C.; Trouw, L. A.; Dudek, N. L.; Purcell, A. W.; O'Sullivan, B. J.; Connolly, J. E.; Paul, S. K.; Le Cao, K.-A.; Thomas, R. Citrullinated peptide dendritic cell immunotherapy in HLA risk genotype-positive rheumatoid arthritis patients. *Sci. Transl. Med.* **2015**, *7*, 290ra87–290ra87

[19] Hackstein, H.; Thomson, A. W. Dendritic cells: emerging pharmacological targets of immunosuppressive drugs. *Nat. Rev. Immunol.* **2004**, *4*, 24–34

[20] Kooten, C. Van; Stax, A. S.; Woltman, A. M.; Gelderman, K. A. Handbook of Experimental Pharmacology " Dendritic Cells " The Use of Dexamethasone in the Induction of Tolerogenic DCs. **2009**, 233–250

[21] Cabezón, R.; Ricart, E.; España, C.; Panés, J.; Benitez-Ribas, D. Gram-negative enterobacteria induce tolerogenic maturation in dexamethasone conditioned dendritic cells. *PLoS One* **2012**, *7*, e52456

[22] Jauregui-Amezaga, A.; Cabezón, R.; Ramírez-Morros, A.; España, C.; Rimola, J.; Bru, C.; Pinó-Donnay, S.; Gallego, M.; Masamunt, M. C.; Ordás, I.; Lozano, M.; Cid, J.; Panés, J.; Benítez-Ribas, D.; Ricart, E. Intraperitoneal Administration of Autologous Tolerogenic Dendritic Cells for Refractory Crohn's Disease: A Phase I Study. *J. Crohns. Colitis* **2015**

[23] Suwandi, J. S.; Toes, R. E. M.; Nikolic, T.; Roep, B. O. Inducing tissue specific tolerance in autoimmune disease with tolerogenic dendritic cells. *Clin. Exp. Rheumatol.* *33*, 97–103

[24] Naranjo-Gómez, M.; Raïch-Regué, D.; Oñate, C.; Grau-López, L.; Ramo-Tello, C.; Pujol-Borrell, R.; Martínez-Cáceres, E.; Borràs, F. E. Comparative study of clinical grade human tolerogenic dendritic cells. *J. Transl. Med.* **2011**, *9*, 89

[25] Park, Y.-M.; Lee, S. J.; Kim, Y. S.; Lee, M. H.; Cha, G. S.; Jung, I. D.; Kang, T. H.; Han, H. D. Nanoparticle-based vaccine delivery for cancer immunotherapy. *Immune Netw.* **2013**, *13*, 177–83

[26] Cho, N.-H.; Cheong, T.-C.; Min, J. H.; Wu, J. H.; Lee, S. J.; Kim, D.; Yang, J.-S.; Kim, S.; Kim, Y. K.; Seong, S.-Y. A multifunctional core-shell nanoparticle for dendritic cell-based cancer immunotherapy. *Nat. Nanotechnol.* **2011**, *6*, 675–82

[27] Fang, R. H.; Hu, C.-M. J.; Luk, B. T.; Gao, W.; Copp, J. A.; Tai, Y.; O'Connor, D. E.; Zhang, L. Cancer Cell Membrane-Coated Nanoparticles for Anticancer Vaccination and Drug Delivery. *Nano Lett.* **2014**, *14*, 2181–2188

[28] Leonard, F.; Ali, H.; Collnot, E.-M.; Crielaard, B. J.; Lammers, T.; Storm, G.; Lehr, C.-M. Screening of budesonide nanoformulations for treatment of inflammatory bowel disease in an inflamed 3D cell-culture model. *ALTEX* **2012**, *29*, 275–85

[29] Ali, H.; Weigmann, B.; Neurath, M. F.; Collnot, E. M.; Windbergs, M.; Lehr, C.-M. Budesonide loaded nanoparticles with pH-sensitive coating for improved mucosal targeting in mouse models of inflammatory bowel diseases. *J. Control. Release* **2014**, *183*, 167–77

[30] Beloqui, A.; Coco, R.; Alhouayek, M.; Solinís, M. Á.; Rodríguez-Gascón, A.; Muccioli, G. G.; Préat, V. Budesonide-loaded nanostructured lipid carriers reduce inflammation in murine DSS-induced colitis. *Int. J. Pharm.* **2013**, *454*, 775–83

[31] Zou, P.; Chen, H.; Paholak, H. J.; Sun, D. Noninvasive fluorescence resonance energy transfer imaging of in vivo premature drug release from polymeric nanoparticles. *Mol. Pharm.* **2013**, *10*, 4185–94

[32] Rocas, P.; Fernández, Y.; Schwartz, S.; Abasolo, I.; Rocas, J.; Albericio, F. Multifunctionalized polyurethane–polyurea nanoparticles: hydrophobically driven self-stratification at the o/w interface modulates encapsulation stability. *J. Mater. Chem. B* **2015**, *3*, 7604–7613

[33] Chen, H.; Kim, S.; Li, L.; Wang, S.; Park, K.; Cheng, J.-X. Release of hydrophobic molecules from polymer micelles into cell membranes revealed by Förster resonance energy transfer imaging. *Proc. Natl. Acad. Sci.* **2008**, *105* , 6596–6601

[34] Rocas Sorolla, J.; Rocas Alonso, P. Process for the manufacture of a microencapsulated and reactive amphiphilic compound, and corresponding microencapsulated composition 2014

[35] Rocas, P.; Hoyos-Nogués, M.; Rocas, J.; Manero, J. M.; Gil, J.; Albericio, F.; Mas-Moruno, C. Installing Multifunctionality on Titanium with RGD-Decorated Polyurethane-Polyurea Roxithromycin Loaded Nanoparticles: Toward New Osseointegrative Therapies. *Adv. Healthc. Mater.* **2015**

[36] Clemitson, I. R. *Castable Polyurethane Elastomers*; CRC Press, 2008

[37] Prabhakar, A.; Chattopadhyay, D. K.; Jagadeesh, B.; Raju, K. V. S. N. Structural investigations of polypropylene glycol (PPG) and isophorone diisocyanate (IPDI)-based polyurethane prepolymer by 1D and 2D NMR spectroscopy. *J. Polym. Sci. Part A Polym. Chem.* **2005**, *43*, 1196–1209

[38] Moyano, D. F.; Ray, M.; Rotello, V. M. Nanoparticle – protein interactions : Water is the key. **2014**, *39*, 1069–1073

[39] Cabezón, R.; Carrera-Silva, E. A.; Flórez-Grau, G; Errasti, A. E.; Calderón-Gómez, E.; Lozano, J. J.; España, C.; Ricart, E.; Panés, J.; Rothlin, C. V.; Benítez-Ribas, D. MERTK as negative regulator of human T cell activation. *J. Leukoc. Biol.* **2015**, jlb.3A0714–334R–

[40] Kamide, Y.; Utsugi, M.; Dobashi, K.; Ono, A.; Ishizuka, T.; Hisada, T.; Koga, Y.; Uno, K.; Hamuro, J.; Mori, M. Intracellular glutathione redox status in human dendritic cells regulates IL-27 production and T-cell polarization. *Allergy* **2011**, *66*, 1183–92

Electronic Supplementary Material

Nanoencapsulated Budesonide Efficiently Induces the Generation of Human Tolerogenic Dendritic Cells

Georgina Flórez-Grau[1][§], Pau Rocas[2][§], Raquel Cabezón[1], Carolina España[3], Julián Panés[1,3], Josep Rocas[4], Fernando Albericio[2,5,6,7](✉), Daniel Benítez-Ribas[8](✉)

[1]*Institut d'Investigacions Biomèdiques August Pi i Sunyer (IDIBAPS), Barcelona, Spain*

[2]*Institute for Research in Biomedicine (IRB Barcelona), Barcelona, Spain*

[3]*Fundació Clínic per la Recerca Biomèdica, Barcelona, Spain*

[4]*Nanobiotechnological Polymers Division, Ecopol Tech S.L., Tarragona, Spain*

[5]*Department of Organic Chemistry, University of Barcelona, Barcelona, Spain*

[6]*School of Chemistry & Physics, University of Kwazulu-Natal, Durban, South Africa*

[7]*Networking Centre on Bioengineering Biomaterials and Nanomedicine (CIBER-BBN), Barcelona, Spain*

[8]*Centro de Investigación Biomedica en Red, Enfermedades Hepáticas y Digestivas (CIBERehd),Barcelona, Spain*

[§]*This authors contributed equally to this work.*

a

NPs internalization

b

Figure 1s: NPs internalization by PBMCs and DCs viability. (a) PBMCs were isolated from whole blood and incubated with NPs-Cadaverine after 120 minutes of incubation. Results are presented as the mean ± SD of n=3 independently performed experiments. **(b)** Viability of DCs incubated with PUUa NPs was assessed. PUUa NPs did not cause any effect on DCs viability . Results are presented as the mean ± SD of n=5 independently performed experiments PUUa NPs-Cadaverine for 120 min**.** About 90% of monocytes incorporates
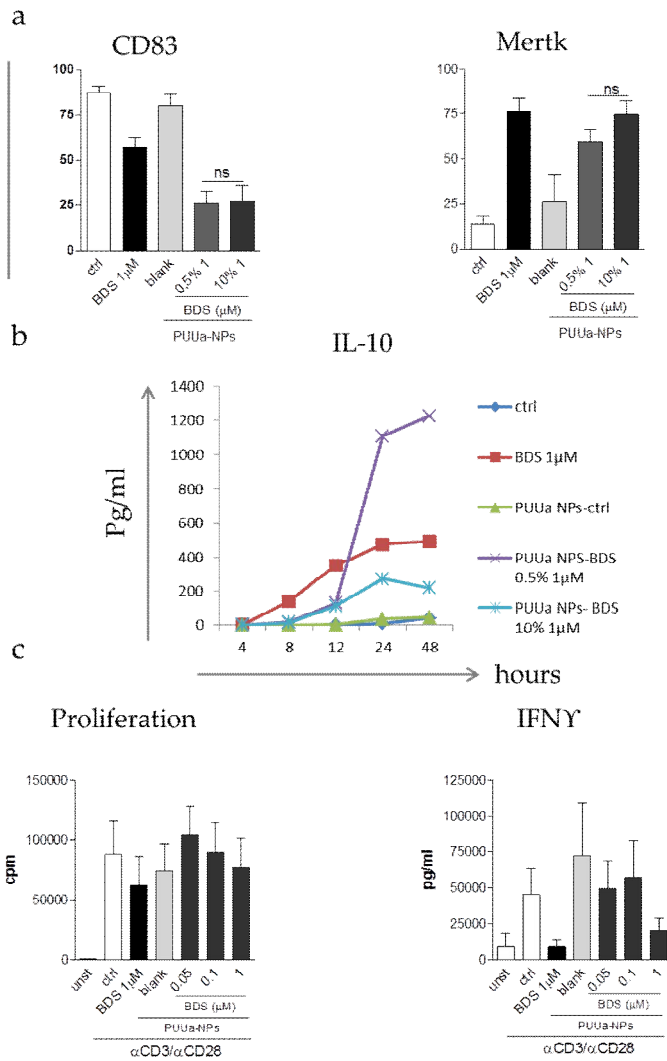
Figure 2S: assessment of BDS loading and PPUa tested in T-cells (a) CD80 and CD83 were evaluated using two different BDS loadings 0.5 and 10 % respectively. Results are presented as the mean ± SD of n=3 independently performed experiments **(b)** Kinetics of IL-10 production by tol-DCs **(c)** PBMCs incubated with PUUa NPs-BDS. Results show that encapsulated BDS did not reduced. (c) Activation of Peripheral blood Lymphocytes (PBLs) with anti-CD3/CD28. PBLs where incubated with anti-CD3/CD28 after 2 hours PUUa NPs-BDS were added

General Conclusions

General Conclusions

As plotted in this thesis, we have showed the fitting of choice of polyurethane-polyurea polymers to create hydrophobically stratified nanosystems to achieve a controlled drug delivery. Taking advantage of the well-established isocyanate chemistry, a robust and scalable methodology for the synthesis of PUUa NPs has been developed. The research covered herein has therefore contributed to the development of straightforward synthetic tools for the manufacturing of multifunctional NPs for the pharmaceutical industry. From the methodology established here, a broad range of possibilities arise for the creation of bioactive nanostructured nanoassemblies.

According to the proposed objectives, the main conclusions of this thesis are:

Chapter 1

Multiple PUUa NPs have been engineered with tailored core volume, shell width, stratification, crosslinking degree, surface charge, HLB value, lyophilization and redispersion ease, encapsulation stability, biodegradability and targeting moieties. In addition we have proved the larger encapsulation stability when using self-stratified multiwalled PUUa NPs compared with their monowalled counterparts.

Thanks to the free amino group of the lysine residue we have developed a novel approach to conjugate the cRGDfK peptide to a hydrophilic polyisocyanate linker via urea bonds formation in a quantitative (yield >95 %), rapid (2 h) and green (aqueous buffer as solvent) chemistry to further decorate our PUUa NPs via an interfacial polyaddition crosslinking step.

The targeting conjugate was proved to be active to guide faster and more efficiently both *in vitro* and *in vivo* the PUUa NPs to the desired tumor cells. In addition PUUa NPs encapsulating plitidepsin exhibited better toxicity profile, pharmacokinetics and biodistribution in mice than that observed for out reference cremophor-plitidepsin formulation.

Chapter 2

The robust synthetic methodology opened new areas of application with incredibly encouraging results in the creation of multifnctional titanium implants. PUUa NPs were innovatively covalently anchored to the titanium surface by the here presented method Interfacial Functionalization. At the optimized conditions, this coating resulted to be homogeneous as characterized by SEM and fluorescnece microscopy. Bioactivated

titanium surfaces with cRGDfK-decorated PUUa NPs loaded with roxithromycin antibiotic drug translated into a tremendous enhancement of osteoblastic cells adhesion to accelerate bone formation and profound inhibition of *Streptococcus Sanguinis* bacteria adhesion for bacterial infections prevention.

Chapter 3

PUUa NPs loaded with budesonide immunosuppressive drug induced tolerogenicity to dendritic cells much more efficiently than the free drug. Concretely, PUUa NPs, which were not cytotoxic to DCs, were endocytosed just in phagocytic cells in a multicellular sample of peripheral blood mononuclear cells. BDS-loaded PUUa NPs reduced significantly costimulatory molecules expression as well as significantly higher amounts of IL-10 immunosuppressive cytokine were secreted compared to free BDS. In addition, tolerogenic dendritic cells reduced significantly lymphocytes proliferation.

Resum de la Tesi

Capítol I. Nanopartícules de poliuretà i poliurea per a la teràpia i visualització del càncer

1. Introducció

2. Síntesi de polímers reactius de poliuretà-poliurea autoestratificables en emulsions oli en aigua.

3. Multifuncionalització de la paret de la nanopartícula amb molècules bioactives per obtenir biodegradabilitat, alliberament controlat de l'encapsulat i direccionalització activa a cèl·lules cancerígenes que sobreexpressen αvβ3 integrina a la seva membrana.

4. Encapsulació i alliberament del fàrmac anticancerigen plitidepsina i de fluoròfors lipofílics.

5. Estudis in vitro en cèl·lules cancerígenes i estudis *in vivo* de toxicitat, farmacocinètica i biodistribució.

Capítol II. Nanobiomaterials antibacterians per regeneració òssia

1. Introducció

2. Estratègia pel recobriment d'implants metàl·lics. Funcionalització Interfacial.

3. Encapsulació i alliberament del fàrmac antibacterià i antiinflamatori roxitromicina.

4. Estudis *in vitro* d'adhesió d'osteoblasts i d'adhesió bacteriana.

Capítol III. Nanopartícules de poliuretà i poliurea per la teràpia de malalties autoimmunològiques

1. Introducció

2. Encapsulació del fàrmac immunosupressor budesonida.

3. Estudis *in vitro* funcionals en cèl·lules dendrítiques

Capítol I. Nanopartícules de poliuretà i poliurea per a la teràpia i visualització del càncer

1. Introducció

Avui dia és ben sabut que les teràpies convencionals del càncer, com la quimio- i radioteràpia s'estan quedant obsoletes davant de l'augment de la incidència d'aquesta malaltia en les societats més desenvolupades. Així doncs, nous tractaments farmacològics s'han erigit com a una alternativa de futur per millorar les prespectives de curació del càncer. Entre elles ha aparegut la nanotecnologia que pretén millorar l'eficàcia de fàrmacs citotòxics tant en fases d'investigació com clíniques. Per tal de millorar l'eficàcia, els sistemes nanotecnològics fan servei de la seva capacitat d'encapsulació i multifuncionalitat per a millorar aspectes negatius comuns de la majoria de fàrmacs d'ús global. Aquests són entre d'altres, poca solubilitat aquosa, falta d'especificitat per la cèl·lula cancerígena i com a resultat, baixa biodisponibilitat.

Entre els sistemes nanotecnològics més emprats s'hi troben els que estan fets de polímers, ja que aquests permeten la inclusió de multiples funcionalitats en la seva estructura per mitjà de tècniques d'allò més variades. Tant és així, que actualment els sistemes fets de polímers de PLGA, PLA, PCL, etc. Són els ques es troben en fases clíniques de desenvolupament més avançades. No obstant això, cap d'aquestes nanopartícules polimèriques en fase clínica estan direccionalitzades específicament per alliberar el fàrmac a la zona tumoral. Entre d'altres raons, això és així degut principalment a tres factors, la seva falta de grups reactius per biofuncionalitzar-los, la seva complexa metodologia sintètica i les costoses etapes de purificació dels productes dels subproductes/monòmers.

Per aquesta raó el desenvolupament de nous sistemes aptes per a ser fàcilment funcionalitzats, sintetitzats i a més, de forma curosa amb el medi ambient, desperten un gran interès industrial. En aquest sentit la química dels poliuretans i poliurees s'ajusta molt bé a les característiques prèviament esmentades. La seva adaptabilitat química està altament comprovada a nivell industrial, així com ho està la netedat de les seves reaccions en baix contingut de solvents. No menys important és la seva biocompatibilitat que ha estat ampliament contrastada durant la seva utilització com a biomaterials referència en la industria dels catèters, implants, etc. Endemés, recentment, estudis focalitzats en la seva citotoxicitat, hemocompatibilitat i biodegradabilitat com a sistema nanoparticulat han estat també clau en l'hora de despertar finalment l'interès de la comunitat científica per aquests versàtils nanosistemes.

2. Síntesi de polímers reactius de poliuretà-poliurea autoestratificables en emulsions oli en aigua.

Per a la preparació de nanopartícules polimèriques amb una estructura ordenada, controlada, funcionalitzada i amb la capacitat de contenir actius (com ara cosmètics o medicaments) en un alt rendiment, manca un procés sintètic ben definit. Com he comentat abans, els sistemes polimèrics existents per crear nanopartícules no sempre són fàcilment funcionalitzats i menys encara, de manera específica i directa. A més, els monòmers i polímers utilitzats com a precursors, en molts casos no estan dissenyats per a participar de forma activa en la nanoestructuració de la paret de la nanopartícula, donant lloc a nanoestructures poc definides a nivell interfacial que han de ser estabilitzades amb emulsionants externs.

La idea de crear nanopartícules arquitectònicament controlades sorgeix del desig d'obtenir materials amb estructures ben definides prèviament preconcebudes. Per exemple, alguns investigadors en el camp de la nanomedicina polimèrica han emprès el desafiament de crear materials estructurats a nivell nanomètric aprofitant interaccions electrostàtiques entre les espècies carregades contràriament tot creant nano i micropartícules amb diverses capes i múltiples funcionalitats mitjançant la tècnica coneguda com Layer-by-Layer (LbL).

No obstant, aqui proposem una metodologia alternativa, escalable basada en un meticulós disseny de nanopartícules de Poliuretà-poliurea mostrant una estructura multifuncional per millorar la capacitat d'encapsulació de compostos lipofílics i controlar l'alliberament en el lloc desitjat. Així doncs, s'han sintetitzat prepolímers reactius de diferent hidrofòbia amb grups isocianat terminals i cadenes laterals penjants hidrofòbiques i/o hidrofíliques.

En la part exterior de la paret s'hi localitza el polímer amfifílic (Amphil) que està constituït per cadenes penjants hidrofíliques i hidrofòbiques, i enllaços disulfur. La cadena hidrofílica és un diol polietoxilat (YMER™ N120) amb els dos grups hidroxil molt a prop lun de l'altre. Alhora, la cadena polietoxilada lateral queda ortogonal a la cadena principal del polímer. És també important tenir en compte la curta distància entre els enllaços uretà que es formen per reacció de YMER™ N120 amb diissocianat d'isoforona (IPDI), que promou una compactació de l'estructura polimèrica obtenint una paret més densa amb més efecte barrera comparat amb els polímers formats per PEG, on els grups hidroxil disten molts enllaços i donen lloc a estructures menys barrera. Seguint el mateix raonament, la cadena hidrofòbica, que és una diamina alquílica de cadena llarga (C18) forma en aquest cas enllaços urea amb IPDI i queda penjant ortogonalment de la cadena

polimèrica principal. Com abans, els grups d'urea formen part de la cadena principal i la cadena penjant alquílica (C12 o C18) queda ortogonal. Els enllaços disulfur, és a dir, disulfur de 2-hidroxietil (DEDS), s'incorporen per reacció uretànica amb l'IPDI amb la finalitat d'obtenir una paret biodegradable intracel·lularment enfront del tripèptid glutatió que es troba altament sobreexpressat en el citosol de la gran majoria de cèl·lules cancerígenes. Per tal d'obtenir un prepolímer amb grups isocianat reactius per a l'últim pas de reticulació, és important dir que s'afegeix sempre excés de IPDI respecte DEDS, YMER™ N120 i diamines hidrofòbiques (Figura 1).

A més, un segon compost hidrofòbic (Hyfob, un monòmer hidrofòbic o un prepolímer hidrofòbic) amb grups isocianat reactius s'agrega a la mescla abans d'emulsionar. L'objectiu de l'addició d'un compost hidròfob amb grups isocianats és el promoure una primera estratificació dels prepolímers per interaccions hidrofòbiques en medi aquós i en segon lloc, permetre que aquesta estructura estratificada preformada i reactiva es pugui fixar mitjançant el reticulació amb poliamines com dietilentriamina o L-lisina (Figura 1).
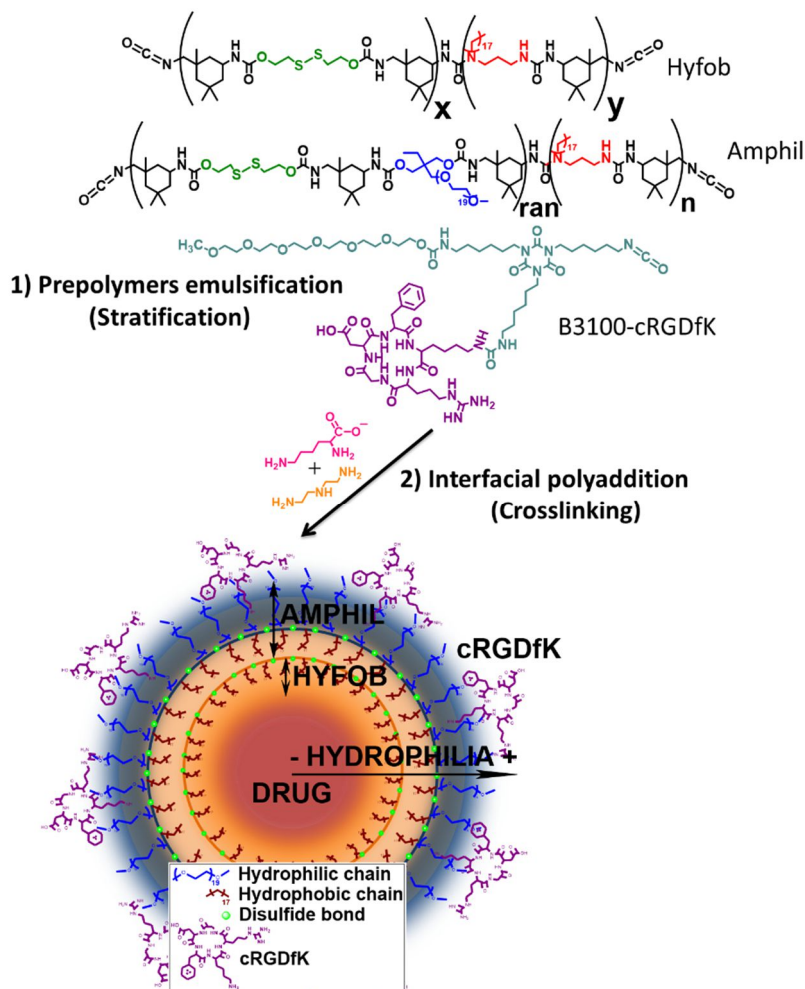

Figura 1. Esquema de formació de PUUa NPs autoestratificables

Cal dir que el fet d'haver seleccionat els isocianats com a grup reactiu en els prepolímers és a causa de les reaccions quantitatives que tenen lloc amb amines i poliamines, fins i tot en medis aquosos i a baixa temperatura.

3. Multifuncionalització de la paret de la nanopartícula amb molècules bioactives per obtenir biodegradabilitat, alliberament controlat de l'encapsulat i direccionalització activa a cèl·lules cancerígenes que sobreexpressen αvβ3 integrina a la seva membrana.

Tal i com s'ha dit abans, la introducció de grups disulfur a la paret de la nanopartícula va permetre que les PUUa NPs fossin biodegradables enfront al glutatió sobreexpressat cel·lularment. Concretament, se sap que hi ha una diferencia aproximada de 3 ordres de magnitud més de glutatió a l'interior (10 mM) de les cèl·lules que a l'exterior (10 µM). A més, intracel·lularment, hi ha 4 cops més glutatió en cèl·lules cancerígenes que en cèl·lules sanes. D'aquesta manera, hem demostrat que les nanopartícules es degraden quan són exposades a glutatió 10 mM, donant lloc a canvis morfològics i inestabilitat en medi aquós. A més hem pogut demostrar mitjançant diverses tècniques que aquesta biodegradació dóna lloc a un alliberament controlat de la molècula encapsulada. Tant es així que hem vist que en condicions que simulen el reg sanguini (alt contingut proteic, fosfolípids i colesterol) no s'ha produït alliberació de l'encapsulat, tot demostrant l'especificitat de tal alliberament.

A més, per a bioactivar les nostres nanopartícules perque interactuin específicament amb integrines αvβ3 sobreexpressades en la superfície de les cèl·lules tumorals, el grup amino de L-lisina del pèptid cRGDfK el vàrem fer reaccionar amb un linker poliisocianat. El resultant conjugat mantenia reactivitat isocianat i alhora el pèptid direccionalitzador. Per tal d'incloure el conjugat bioactiu a la nanopartícula, es van mesclar el Hyfob, Amphil i el conjugat i es van emulsionar en medi aquós per propiciar l'estratificació de la paret de les nanopartícules. Aquesta paret, es podria dir que és metaestable, doncs els prepolimers tot i està en medi aquós contenen els grups reactius isocianat. Per tant, per tal d'estabilitzar-la de forma definitiva se li van afegir poliamines provocant un reticulació de la mateixa i un augment de l'estabilitat i l'efecte barrera. Gràcies a a aquesta nova metodologia relativament senzilla s'obté de forma escalable i industrial una paret polimèrica que conté cada molècula en una posició més superficial o més interior en funció del seu HLB (Figura 2).
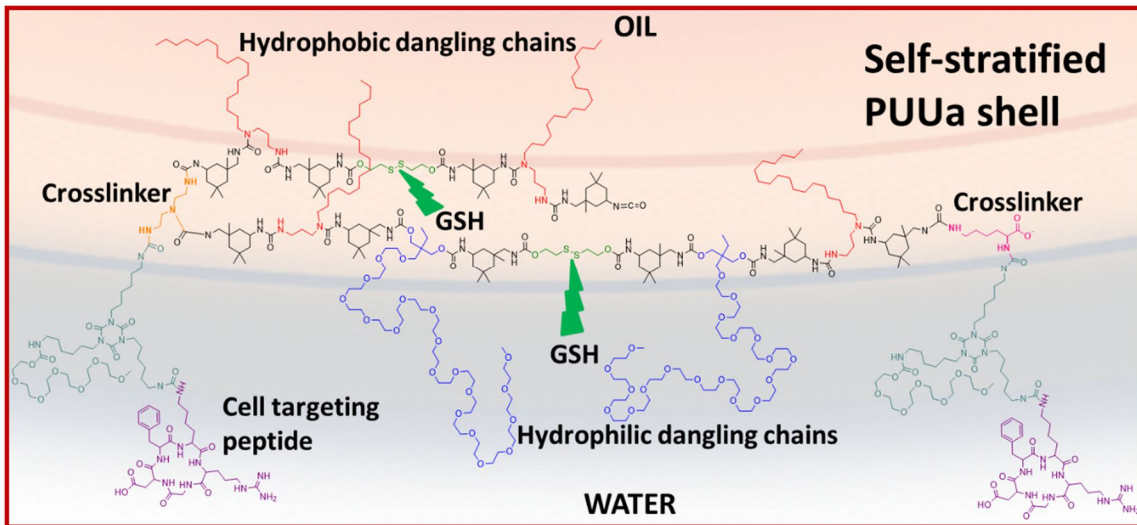
Figura 2. Nanoestructura autoestratificada i reticulada ideal de la paret polimèrica les PUUa NP.

Aquesta tecnologia permet noves formes de teràpia, diagnòstic i visualització per lluitar contra diverses malalties de manera més selectiva, especialment per al tractament del càncer, on els efectes secundaris del fàrmac antitumoral en les cèl·lules sanes són altament devastadors per l'organisme. Aquesta nova plataforma nanotecnològica pot ser també molt útil per a moltes altres aplicacions industrials, no només en el camp farmacèutic, ja que utilitza intermedis industrials econòmics, les reaccions són controlades, quantitatives i no es necessiten costoses etapes de purificació. Definitivament, és un sistema versàtil i escalable.

4. Encapsulació i alliberament del fàrmac anticancerigen plitidepsina i de fluoròfors lipofílics.

Com a fàrmac model, vam utilitzar plitidepsina, un fàrmac d'origen marí originalment comercialitzat per PharmaMar S.A. (Aplidin®), actualment en fase clínica III pel tractament de mieloma. Tot i que inicialment es va obtenir d'Aplidium Albicans, avui dia es sintetitza artificialment al laboratori. Té un caràcter altament hidrofòbic i una molt alta activitat anticancerígena enfront de gran varietat de línies tumorals, però una baixa biodisponibilitat i biodistribució, que li dónen una finestra terapèutica molt minsa.

El nostre sistema d'encapsulació ha mostrat resultats gairebé quantitatius d'encapsulació de plitidepsina, obtenint rendiments superiors al 95 % amb un contingut de fàrmac del 2 % i del 7 % d'oli + fàrmac respecte nanopartícula. L'alliberament de plitidepsina de les nanopartícules es va estudiar per HPLC i es va observar que no

s'alliberava en un medi sense glutatió mentres que si que ho feia en un medi 10 mM de glutatió, alliberant un 70 % de fàrmac en una setmana. A la vegada també es va estudiar l'alliberament de fluoròfors lipofílics en un estudi preliminar tot arribant a les mateixes conclusions.

5. Estudis *in vitro* en cèl·lules cancerígenes i estudis *in vivo* de toxicitat, farmacocinètica i biodistribució.

Com a prova de concepte, en primer lloc vàrem provar la biocompatibilitat de les PUUa NP, tot comprovant que no eren citotòxiques en divereses línies cel·lulars. A més es va demostrar mitjançant citometria de flux i microscòpia de fluorescència que les PUUa NP-RGD iternalitzaven via endocítica de receptor de membrana a les cèl·lules cancerígenes que sobreexpressaven la integrina αvβ3 més ràpidament i en major grau que no pas en cèl·lules que no la sobreexpressaven. Imatges de microscopia confocal varen ajudar a provar que la internalització propiciava també una localització al lisosoma/endosoma de les PUUa NP. Finalment, els experiments cel·lulars també varen suggerir que les nanopartícules eren capaces d'escapar del lisosoma i arribar al citosol, on es produeix la degradació de les PUUa NP i l'alliberament del seu contingut, en aquest cas DiI, un fluoròfor lipofílic. Paral·lelament, en assajos *in vitro* de toxicitat cel·lular es va revelar que les PUUa NP també deixaren anar la plitidepsina encapsulada, doncs els valors de IC50 eren similars als de la plitidepsina lliure.

Posteriorment, passant a estudis *in vivo* amb ratolins immunodeprimits es va constatar que la dosi màxima tolerada (MTD), passava de 0,9 mg/kg a 3 mg/kg quan el fàrmac estava encapsulat en el nostre sistema. D'altra banda, els paràmetres farmacocinètics, com la concentració màxima (Cmax), àrea sota la corba (AUC) i els temps de vida mitjana en plasma eren molt majors, i per tant millors, per la plitidepsina encapsulada en PUUa NP que no pas lliure. Estudis de fluorescència *in vivo* van provar que les PUUa NP-RGD tendien a acumular menys en el fetge que la versió no decorada. Per corroborar-ho l'anàlisi *ex vivo* de contingut de plitidepsina i fluoròfor DiR concordaren, tot confirmant que les nanopartícules RGD-direccionalitzades a integrines tenien menor acumulació en fetge i melsa, la qual cosa suggeria que les nanopartícules conseguien evitar segrest pels macròfags del sistema reticuloendotelial.

En general doncs, els nostres resultats amb diferents tipus de PUUa NPs representen una plataforma robusta i fiable per l'alliberació controlada de molècules lipofíliques, tals com la plitidepsina. Ja que l'encapsulen eficientment i de forma estable, no modifiquen la seva activitat citotòxica i millora els perfils toxicològics, farmacocinètics i la biodistribució del fàrmac. A més, la funcionalización de la superfície de les PUUa NP

amb el pèptid direccionalitzador i zwitteriònic cRGDfK sembla millorar les propietats de llarga circulació en sang del sistema.

Capítol II. Nanobiomaterials antibacterians per regeneració òssia

1. Introducció

Biomaterials metàl·lics tals com el titani (Ti) i els seus aliatges han estat utilitzats clàssicament en fixació i regeneració òssia a causa de la seva excel·lent biocompatibilitat i propietats mecàniques. No obstant això, el seu ús no està exempt de limitacions, que encara avui poden comprometre el rendiment a llarg termini d'aquests materials. En primer lloc, el fet que el titani sigui tan inert, es pot traduir en poca osteointegració (és a dir, mínima invasió de cèl·lules òssies sobre l'implant de titani) i fixació inadequada mecànicament. D'altra banda, la infecció bacteriana i la conseqüent inflamació (és a dir, peri-implantitis) estan descrites com una de les principals causes de fracàs de l'implant post-operació. Així doncs, per fer front a aquests inconvenients, la biofuncionalització d'implants metàl·lics amb espècies bioactives és una de les estratègies més investigades com a alternativa de futur a aquest problema. En aquest sentit pèptids i proteïnes que contenen la seqüència peptidica L-Arginina-Glicina-L-Aspartic acid s'han usat per funcionalitzar superfícies i així millorar la biocompatibilitat i adhesió cel·lular via interacció amb integrines expressades a la membrana de la cèl·lula, encaregades de les interaccions entre cèl·lules i d'aquestes amb la matriu extracel·lular (ECM). D'altra banda, també s'han desenvolupat recobriments antimicrobians per mitjà de polímers anti-incrustants, sistemes d'alliberació de fàrmacs o seqüències de pèptids bactericides.

Tal i com ho demostren estudis científics recents i debats encapçalats per experts d'aquest camp, la combinació de diferents funcions biològiques en la superfície està destinada a millorar el comportament biològic dels biomaterials clàssics en el camp de la medicina regenerativa. [6] No obstant això, la majoria de les estratègies actuals només se centren en millorar l'adherència cel·lular o bé reduir l'adherència bacteriana. Així, l'objectiu del present estudi va ser explotar el concepte de multifuncionaliat instal·lant simultàniament capacitat d'adhesió cel·lular i propietats antibacterianes en la superfície del titani (Figura 3).
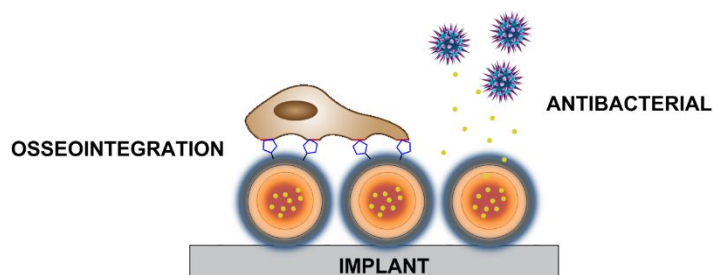

Figura 3. Estratègia general de multifuncionalitat en implants metàlics recoberts amb PUUa NPs.

2. Estratègia pel recobriment d'implants metàl·lics. Funcionalització Interfacial.

L'objectiu principal del present estudi no era només desenvolupar materials multifuncionals per regeneració òssia sino també fer-ho de forma fàcilment escalable, amb una química eficient i sostenible amb el medi ambient. D'aquesta forma, es va procedir a activar químicament la superfície del titani amb grups amina. Llavors s'hi va afegir una emulsió de nanopartícules amb grups reactius isocianat a la seva superfície per tal de crear enllaços urea entre les nanopartícules polimèriques i els grups amina del titani. A aquest procés el vàrem anomenar Funcionalització Interfacial (IF), ja que els enllaços urea es produeixen a la interfase entre el metall, l'aigua i la paret amfifílica de la PUUa NP. La resta de grups isocianat de la PUUa NP que no havien reaccionat amb el Ti es van reticular afegint etilendiamina com a agent reticulant.

La qualitat del recobriment del Ti amb PUUa NP es va optimitzar utilitzant diferents agents reticulants, temps de IF i temperatura, essent etilendiamina, 1 h i 5 ºC les condicions adients per a obtenir biomaterials multifuncionals. Per arribar a aquesta conclusió es van fer servir tècniques com microscòpia electrònica de rastreig (SEM) i microscòpia de fluorescència que ens van ajudar a assegurar la homogeneïtat del recobriment així com la morfologia de les PUUa NP post-funcionalització.
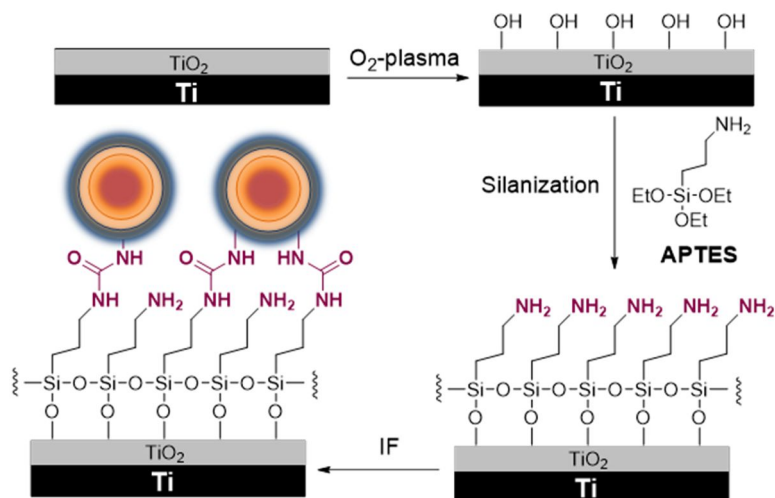

Figura 4. Procediment per al recobriment de Ti amb PUUa NPs amb grups isocianat reactius.

3. Encapsulació i alliberament del fàrmac antibacterià i antiinflamatori roxitromicina.

L'encapsulació de la roxitromicina en PUUa NP la vàrem dur a terme al 10 % de càrrega de fàrmac respecte PUUa NP. El rendiment resultant de tal encapsulació va ser altament eficient, donant lloc a un 95 % de fàrmac encapsulat. Per tal d'evitar el procés infecciós

després de l'inserció del implant metàlic és clau el període de temps que transcorre durant les següents 6 hores. Per tant, es necessita un sistema que alliberi una quantitat important de l'antibiòtic en aquest període de temps per així prevenir possibles infeccions. El nostre sistema ha demostrat al voltant d'un 60-70 % d'alliberació de roxitromicina just en les primeres 4-6 h d'incubació del titani funcionalitzat amb PUUa NP en medi biològic. Seguidament segueix un alliberament constant i més lent fins al 85 % de roxitromicina en 6 dies en medi biològic per prolongar l'efecte antibacterià en el temps.

4. Estudis *in vitro* d'adhesió d'osteoblasts i d'adhesió bacteriana.

A l'hora de determinar la capacitat d'aquests nanobiomaterials per adherir osteoblasts, es van incubar peces de titani funcionalitzades amb PUUa NPs durant 4 h amb cèl·lules osteogèniques de sarcoma (Saos-2) i es van analitzar el nombre i l'àrea de les cèl·lules adherides. Interessantment, les superfícies recobertes de PUUa NP-RGD van donar valors molt més alts en l'àrea i el nombre de cèl·lules adherides que no pas els controls sense PUUa NP i amb PUUa NP però sense RGD. A més les superfícies que contenien RGD varen donar lloc a l'adhesió de cèl·lules amb clars filaments d'actina i adhesions focals. Els millors resultats es van obtenir per les superfícies de Ti recobertes amb PUUa NP-RGD reticulades amb etilenediamina, fet que concorda amb els millors resultats obtinguts quant a qualitat i homogeneïtat del recobriment durant la caracterització fisico-química del nostre mètode. Alhora vam assegurar que la qualitat de l'adhesió de Saos-2 no empitjorava quan les superfícies de PUUa NP contenien roxitromicina encapsulada a més de RGD. Per acabar, per tal de demostrar l'adequació del nostre approach per a implants de llarga durada, es va testar l'estabilitat biològica dels recobriments i estudiar la proliferació de Saos-2 durant dues setmanes. Els resultats conclogueren que la proliferació era equivalent a l'obtinguda per la fibronectina, proteïna de la matriu extracel·lular.

En resum, hem demostrat la capacitat de les PUUa NP per actuar com a entitats multifuncionalitzadores i bioactivadores de superfícies inerts de titani per a crear materials d'última generació per medicina regenerativa, tot obtenint-ho de forma eficient i relativament fàcil d'industrialitzar.

Capítol III. Nanopartícules de poliuretà i poliurea per la teràpia de malalties autoimmunològiques

1. Introducció

La nanoimmunoteràpia és una disciplina relativament nova dins la immunoteràpia i alguns dels últims resultats publicats dins aquest camp han demostrat que el seu potencial per tractar tant malalties autoimmunològiques, adquirides i transplantaments, és real i viable. A l'any 2004, aproximadament 1 de cada 31 persones patia una malaltia autoimmunològica als EUA, o el que és el mateix, 8.5 milions de persones estaven afectats.

El cost aproximat per any del tractament de malalties autoimmunològiques és de 100 bilions de dòlars, no obstant això, els tractaments estàndard no són prou eficaços i provoquen amb freqüència nombrosos efectes secundaris inadequats. L'actual mètode de tractament per a malalties autoimmunològiques busca suprimir el sistema immune de forma general, donant lloc a rebrots violents de la malaltia quan es deixa el tractament i facilitant les infeccions per agents externs. Clarament, noves estratègies dirigides a immunosuprimir el sistema immunològic de forma específica a llarg termini, en lloc d'immunosupressió inespecífica, necessiten investigar-se més a fons per al tractament de malalties autoimmunològiques tan comuns com la psoriasi, malaltia de Crohn, esclerosi múltiple, etc.

En aquest capítol ens centrem en estudis fets amb cèl·lules dendrítiques (DCs) humanes, doncs són unes de les principals responsables de les reaccions immunològiques que esdevenen dins el nostre organisme. La majoria de malalties autoimmunològiques estan directament associades a una autoinflamació d'un teixit del nostre cos, on un antigen propi és reconegut per les cèl·lules presentadores d'antígens (APC), ja siguin macròfags, cèl·lules B o DCs, com un cos estrany i foraster que ha de ser atacat i eliminat. Si aquest procés es cronifica, el coneixem com a malaltia autoimmunològica. Encara que s'han aconseguit importants avanços, les teràpies actuals pateixen encara remarcables limitacions en les vies d'administració, grans dosis de fàrmacs durant períodes de temps llargs, baixa especificitat per a la diana terapèutica, efectes secundaris i per tant, insatisfacció del pacient. En aquest sentit, la nanotecnologia ofereix solucions prometedores a les limitacions actuals dels tractaments amb immunosupressors i actius biològics. Concretament, la manipulació de DCs usant nanopartícules podria ser una teràpia útil per al tractament de malalties autoimmunològiques humanes *in vivo*. Fins avui poques classes de nanopartícules s'han utilitzat per a direccionalitzar-les a DCs i lliurar-hi específicament la seva càrrega (per

exemple medicaments, antígens, anticossos, etc.). A més, la majoria de les nanopartícules usades en aquests assajos mostren problemes d'estabilitat sota condicions *in vivo* que duen a problemes en la biodistribució i eficàcia del tractament. D'acord amb això, noves estratègies nanofarmacològiques que permetin una llarga circulació en sang, direccionalització específica per la diana immunològica del fàrmac i tinguin un patró d'alliberament controlat són necessaris en l'exigent camp de la immunoteràpia. En aquest capítol, les PUUa NP utilitzades tenien una doble paret autoestratificada amb disulfurs tant a la paret interior com a l'externa, per tal d'afavorir l'alliberament del seu contingut un cop es biodegradin els polímers per reacció amb el glutatió sobreexpressat intracel·lularment (Figura 5). En aquest sentit, com ja hem anat explicant en els dos capítols anteriors, les PUUa NP representen una plataforma potencialment perfecta per a conseguir tractaments holístics en favor del pacient.
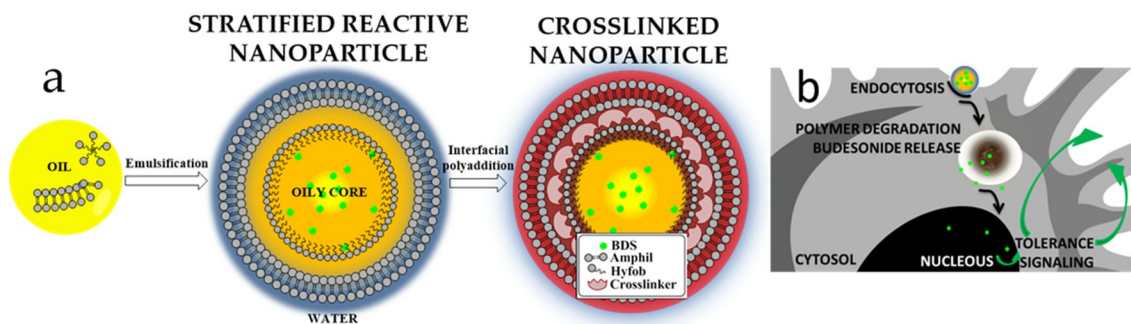

Figura 5. a) Procediment sintètic de les PUUa NP autoestratificables per interaccions hidrofòbiques. b) Esquema d'internalizació de PUUa NP, degradació i alliberament del fàrmac i senyalització de tolerància.

2. Encapsulació del fàrmac immunosupressor budesonida.

Les DCs Tolerogèniques (Tol-DCs) es generen amb corticoesteroides i un còctel de maduració, que és una combinació de citocines (IL-1β, IL-6, TNFα) i prostaglandina E2 (PGE2), donant alts nivells de molècules coestimuladores com CD80, CD83 i MHCII en comparació amb DCs madures (mDCs). D'altra banda, les Tol-DCs presenten una major producció de la citocina antiinflamatòria crucial IL-10 mentre que les citocines inflamatòries IL-12p70 i IL-23 romanen indetectables. L'encapsulació de budesonida en el nostre sistema es va dur a terme per tal d'estandarditzar un mètode per generar Tol-DCs de forma més efectiva i eficient, que no pas els corticosteroids lliures molt inespecífics amb múltiples efectes secundaris, i que potencialment sigui capaç d'arribar a les DCs circulants de l'organisme de forma específica i direccionalitzada (Figura 6).
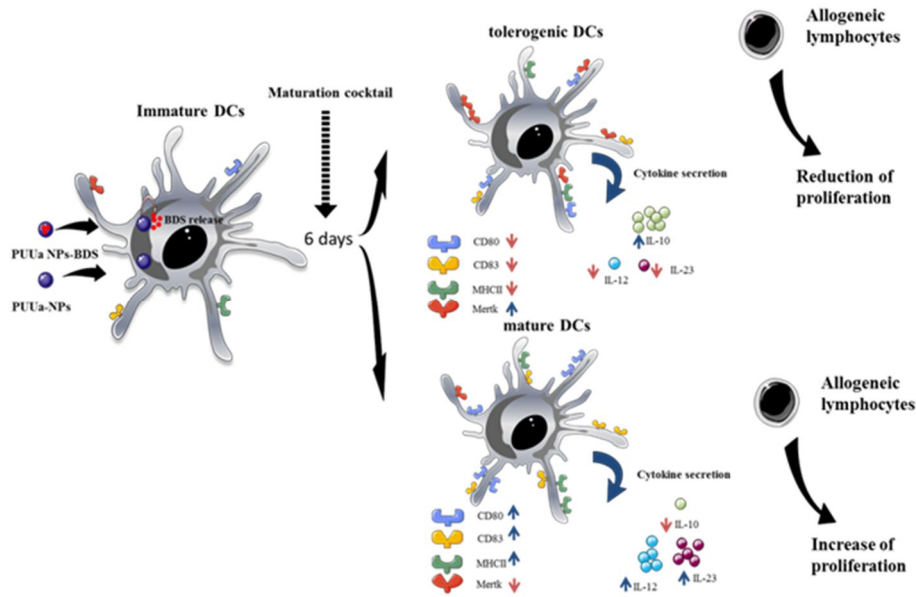
Figura 6. Procediment de formació de Tol-DCs a partir de PUUa NP-BDS i les característiques biològiques diferenciadores de les Tol-DCs resultants.

L'encapsulació de budesonida (BDS), un corticosteoroid immunosupressor altament hidrofòbic, es va produir en un rendiment superior al 95 % amb una càrrega de fàrmac sobre PUUa NP del 0.5 % en un cas i del 10 % en l'altre. D'aquesta manera es va voler comprovar com variava l'efecte terapèutic del fàrmac segons la càrrega dins la PUUa NP. El que es va observar des d'un primer moment és que ambdues formulacions mostraven mides de partícula i morfologia diferents, doncs la carregada al 0.5 % contenia 20 cops menys budesonida que la del 10 %. Les PUUa NP 0.5 % tenien unes mides de 30 nm, com les PUUa NP sense fàrmac. En canvi, les PUUa NP 10 % varen mostrar unes mides més grosses, al voltant de 170 nm. De la mateixa manera que moltes cèl·lules cancerígenes, les DCs tenen una gran capacitat per degradar qualsevol compost que internalitzen, gràcies a això tenen un alt contingut citoplasmàtic de glutatió, ideal per a biodegradar les nostres PUUa NP amb enllaços disulfur a la seva nanoestructura.

3. Estudis *in vitro* funcionals en cèl·lules dendrítiques

El comportament de PUUa NPs amb i sense budesonida es va estudiar a fons biològicament *in vitro* usant DCs obtingudes de diferents pacients, entre ells jo mateix.

Primer de tot es va comprovar la toxicitat de les PUUa NP amb i sense budesonida i es va concloure que cap formulació era tòxica a les concentracions d'interès terapèutic. Seguidament es va encapsular un fluoròfor lipofílic per tal d'estudiar el procés

d'internalització cel·lular per microscòpia de fluorescència i citometria de flux. Els assajos corroboraren que després de 2 h un 70 % de les cèl·lules incorporaven les PUUa NP. Tot seguit vam demostrar que en una mostra de cèl·lules mononuclears de sang perifèrica (PBMC) que contenia cèl·lules T, cèl·lules B i DCs, les PUUa NPs entraven gairebé de forma exclusiva a les cèl·lules dendrítiques. Per tal de caracteritzar el fenotip de les Tol-DCs generades a partir de BDS nanoencapsulada, es van quantificar les molècules de membrana CD80, CD83 i MHCII, i en els tres casos es van veure reduïdes respecte els valors obtinguts amb BDS sense encapsular. A la vegada, els nivells de MERTK, una proteïna de membrana inhibidora es mostrava tant elevada com en les Tol-DCs obtingudes a partir de BDS lliure. Alhora la citocina IL-10, que és clau donant senyals de tolerància al seu voltant, va ser secretada 3 cops més en les Tol-DCs incubades amb PUUa NP-BDS que no pas amb BDS liure. A més per tal de decantar-nos per les PUUa NP 0.5 % o les 10 % vam decidir seguir la secreció de IL-10 fins a 48 h. Curiosament, tot incubar les Tol-DC a la mateixa concentració final de BDS (1 μM) les carregades al 0.5 % van ser les que van donar nivells més alts d'aquesta citocina inductora de tolerància. Això suggereix que les PUUa NP 0.5 % són més adequades per immunoteràpia degut a la seva mida de 30 nm i a una millor distribució del fàrmac a l'interior de les DCs. D'acord amb el fenotip de tolerància, Tol-DCs generades amb PUUa NPs-BDS no van promoure l'activació ni proliferació de cèl·lules T d'un altre donant. Revelant així les propietats fortament tolerogèniques de les Tol-DCs generades a partir de PUUa NP-BDS 0.5 %.